AD NUMBER

AD884140

LIMITATION CHANGES

TO:

Approved for public release; distribution is unlimited.

FROM:

Distribution authorized to U.S. Gov't. agencies and their contractors; Critical Technology; MAY 1971. Other requests shall be referred to Air Force Materials Laboratory, LIM, Wright-Patterson AFB, OH 45433. This document contains export-controlled technical data.

AUTHORITY

afml ltr, 7 dec 1972

AFML-TR-69-67
Volume IV

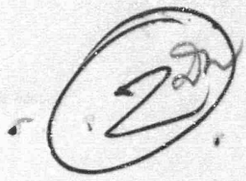

IMPROVED GRAPHITE MATERIALS FOR RE-ENTRY VEHICLES

E. R. STOVER

GENERAL ELECTRIC COMPANY

TECHNICAL REPORT AFML-TR-69-67, Vol. IV

MAY, 1971

Air Force Materials Laboratory
Air Force Systems Command
Wright-Patterson Air Force Base, Ohio

UNCLASSIFIED

Security Classification

DOCUMENT CONTROL DATA - R & D

(Security classification of title, body of abstract and indexing annotation must be entered when the overall report is classified)

1. ORIGINATING ACTIVITY *(Corporate author)*
General Electric Company
Re-Entry and Environmental Systems Division
P.O. Box 8555, Philadelphia, Pennsylvania 19101

2a. REPORT SECURITY CLASSIFICATION
UNCLASSIFIED

2b. GROUP

3. REPORT TITLE
IMPROVED GRAPHITE MATERIALS FOR RE-ENTRY VEHICLES - VOLUME IV

4. DESCRIPTIVE NOTES *(Type of report and inclusive dates)*
Final Report January 1, 1970 to October 31, 1970

5. AUTHOR(S) *(First name, middle initial, last name)*
Edward R. Stover

6. REPORT DATE	7a. TOTAL NO. OF PAGES	7b. NO. OF REFS
May, 1971	175	13

8a. CONTRACT OR GRANT NO.	9a. ORIGINATOR'S REPORT NUMBER(S)
F33615-68-C-1283	
b. PROJECT NO. 7350	
c.	9b. OTHER REPORT NO(S) *(Any other numbers that may be assigned this report)*
d. Task No. 735002	AFML-TR-69-67, Vol. IV

10. DISTRIBUTION STATEMENT
This report is subject to special export controls and each transmittal to foreign governments or foreign nationals may be made only with prior approval of the Air Force Materials Laboratory (LLM), Wright-Patterson Air Force Base, Ohio 45433

11. SUPPLEMENTARY NOTES	12. SPONSORING MILITARY ACTIVITY
	Air Force Materials Laboratory (LLM) Wright-Patterson Air Force Base, Ohio

13. ABSTRACT

Several types of carbon-carbon composites have been developed, in which either high or low modulus carbon fiber bundles extend continuously in several directions in three dimensions. Ablation screening tests at 90 atm. stagnation pressure have shown that 3-directional reinforced graphites, having a high proportion of fibers in the axial direction can have ablation rates similar to ATJ-S with proper matrix processing. Fine-textured, cubic, 7-directional-reinforced composites have shown performance similar to 3-directional samples with similar processing. Comparison ablation data on the 3-D Mod. 3 C/C composite and IP fibrous graphite are also included. Preliminary flexure and plate slap screening tests on "7-D reinforced graphite" indicate a pot ntial for a tough composite with isotropic properties, and further development of this concept is recommended for future work. Preliminary thermal-mechanical properties and plate slap screening data have been obtained on CVD infiltrated 4-directional Omniweave reinforced carbons, suitable for thermal shields, in which composite fiber bundles are packed in 4-directions with close-to-cubic symmetry. When high modulus filaments are used, this material shows high impact resistance and high strain to failure (1.5-2.5% elongation) at maximum load in tension at room temperature, in addition to high surface hardness (requiring diamond grinding) and uniform recession in simulated thermal shield ablation tests.

DD FORM 1 NOV 68 1473

UNCLASSIFIED

Security Classification

14 KEY WORDS	LINK A		LINK B		LINK C	
	ROLE	WT	ROLE	WT	ROLE	WT
Composite materials						
Carbon/graphite						
Carbon Processing						
Chemical Vapor Deposition						
Three dimensional reinforcement						
Omniweave						
Mechanical Properties						
Tensile Stress-Strain						
Thermal Expansion						
Plate Slap Testing						
Failure Mechanisms						
Ablation Testing						
Scanning Electron Microscopy						
Nose Tips						
Heat Shields						
High Modulus Graphite Fibers						

IMPROVED GRAPHITE MATERIALS FOR RE-ENTRY VEHICLES

E. R. STOVER

GENERAL ELECTRIC COMPANY

FOREWORD

This volume is the final report prepared in partial fulfillment of the requirements of Contract F33615-68-C-1283, Project No. 7350, Task 735002, with the Ceramics and Graphite Branch, Metals and Ceramics Division, of the Air Force Materials Laboratory. Mr. J. D. Latva, LLM, is the AFML project engineer and program monitor.

A portion of the funding for this effort was from the AFML Laboratory Director's Discretionary Fund.

The work has been conducted within the Technology Engineering Laboratory of the Research and Engineering Department, Re-Entry and Environmental Systems Division, General Electric Company, P. O. Box 8555, Philadelphia, PA 19101. The principal investigator, project manager and author of this report is Dr. E. R. Stover of the Metallurgy and Ceramics Laboratory. The principal contributors from GE-RESD were as follows: M. Wexler and W. C. Marx, Omniweave fabrication; P. Bolinger, W. Mueller, B. Gorowitz, Dr. J. J. Gebhardt and J. Yodsnukis, CVD infiltration, impregnation and heat treating; P. Magin, III, electron microscopy; W. Connell and J. P. Brazel, property determinations; J. Roetling, ultrasonic evaluation; A. Oaks, radiography; P. Ritter, plate slap testing; and A. R. Saydah, ablation testing. W. A. Holmwood of the General Electric Research and Development Center, Schenectady, NY, operated the scanning electron microscope, and Dr. E. Feingold of the Space Sciences Laboratory supervised the X-ray analysis. J. R. Henson, of the Arnold Engineering Development Center, supervised the ablation test operations. The first series of ablation tests was conducted through the cooperation of Dr. M. Minges, LLS, of the Air Force Materials Laboratory. Experimental processing of certain samples for test under this project was conducted at the request of the AFML project engineer by J. L. Cook of the Y-12 Plant, Union Carbide Nuclear Corporation, Oak Ridge, Tennessee. Other processing was provided by Dr. D. H. Petersen at the LTV Research Center, Dallas, Texas, without cost to this project. W. L. Lachman of Fiber Materials, Inc., Graniteville, Mass., supervised the 3D and 7D weave fabrication.

Many of the items compared in this report were commercial items that were not developed or manufactured to meet Government specifications, to withstand the tests to which they were subjected, or to operate as applied during this study. Any failure to meet the objectives of this study is no reflection on any of the commercial items discussed herein or on any manufacturer.

This report covers work conducted during the period January 1, 1970, through October 31, 1970. The report was submitted for approval March, 1971.

This technical report has been reviewed and is approved.

W. G. RAMKE
Chief, Ceramics and Graphite Branch
Metals and Ceramics Division
Air Force Materials Laboratory

ABSTRACT

Several types of carbon-carbon composites have been developed, in which either high or low modulus carbon fiber bundles extend continuously in several directions in three dimensions. Ablation screening tests at 90 atm. stagnation pressure have shown that 3-directional reinforced graphites, having a high proportion of fibers in the axial direction can have ablation rates similar to ATJ-S with proper matrix processing. Fine-textured, cubic, 7-directional-reinforced composites have shown performance similar to 3-directional samples with similar processing. Comparison ablation data on the 3-D Mod. 3 C-C composite and IP fibrous graphite are also included. Preliminary flexure and plate slap screening tests on "7-D reinforced graphite" indicate a potential for a tough composite with isotropic properties, and further development of this concept is recommended for future work. Preliminary thermal-mechanical properties and plate slap screening data have been obtained on CVD infiltrated 4-directional Omniweave reinforced carbons, suitable for thermal shields, in which composite fiber bundles are packed in 4-directions with close-to-cubic symmetry. When high modulus filaments are used, this material shows high impact resistance and high strain to failure (1.5-2.5% elongation) at maximum load in tension at room temperature, in addition to high surface hardness (requiring diamond grinding) and uniform recession in simulated thermal shield ablation tests.

TABLE OF CONTENTS

TABLE OF CONTENTS (CONT'D)

ILLUSTRATIONS

ILLUSTRATIONS (CONT'D)

ILLUSTRATIONS (CONT'D)

ILLUSTRATIONS (CONT'D)

ILLUSTRATIONS (CONT'D)

ILLUSTRATIONS (CONT'D)

ILLUSTRATIONS (CONT'D)

ILLUSTRATIONS (CONT'D)

ILLUSTRATIONS (CONT'D)

TABLES

SECTION I

INTRODUCTION

This three-year program has been concerned with exploratory development of "multi-dimensional reinforced" graphite materials having improved performance for re-entry applications where hardening is a requirement. The initial objectives, guidelines for the development, and studies related to the use of metallic additives in the materials, were described in AFML TR-69-67, Vol. I (SFRD). Processing studies and material characterization, including ablation, plate slap and property comparisons, were described in Volumes II and III (U). Some observations and test data related to fundamental mechanisms affecting performance of carbon-carbon composites were presented at the Carbon Composite Technology Symposium held in January, 1970 (Ref. 1.).

The program has emphasized effects of constituent characteristics and microstructures which result from different processing techniques on the following: (a) resistance to ablation at high heat flux and high stagnation pressure, (b) mechanical behavior in flexure and tension, and (c) resistance to spall from flyer plate impact. Reinforced graphites for nose tips and candidates for carbon-carbon thermal shield frusta have both been considered.

The effort related to nose tip applications included an early exploration of CVD-infiltrated, carbonized felt and foam which were subsequently impregnated with pitch formulations and graphitized. Other than a higher ultrasonic attenuation, the needled rayon-precursor felt composites processed in this way showed no advantages over similar material densified entirely by CVD infiltration. Other types of composites (wool felt and reticulated foams) could not be filled to the high density required for this application. These materials have a relatively low resistance to crack propagation, similar to the bulk graphites, which was an additional reason for abandoning this type of reinforced graphite, in favor of composites made from three-dimensional weaves.

The work in 1969, reviewed in AFML TR-69-67 Vol. III, explored the application of 4-direction reinforcements, including GE-RESD "4-D Omniweave", to nose tip constructions. Although compaction of a woven cylinder to a cone with a highly unidirectional tip was demonstrated, the high anisotropy resulting from the use of high density PAN-precursor tow resulted in cracks in the graphitized composite. Ablation performance of a pitch-impregnated 4-D composite (made from 10,000 filament Type II tow) and of a CVD-infiltrated Thornel 40 braid composite were both inferior to CVD-infiltrated composites having a less unidirectional, closer-to-cubic reinforcement geometry. Test results also indicated the need for finer texture than had been obtained in the first samples, and the need to reduce the cracking at reinforcement bundle interfaces.

Consequently, work in 1970 directed towards nose tip development has included "4-D" composites having finer weave texture (small bundles), and close-to-cubic symmetry. The geometry of this reinforcement construction, discussed in detail in Volume III, is illustrated in Figure 1.

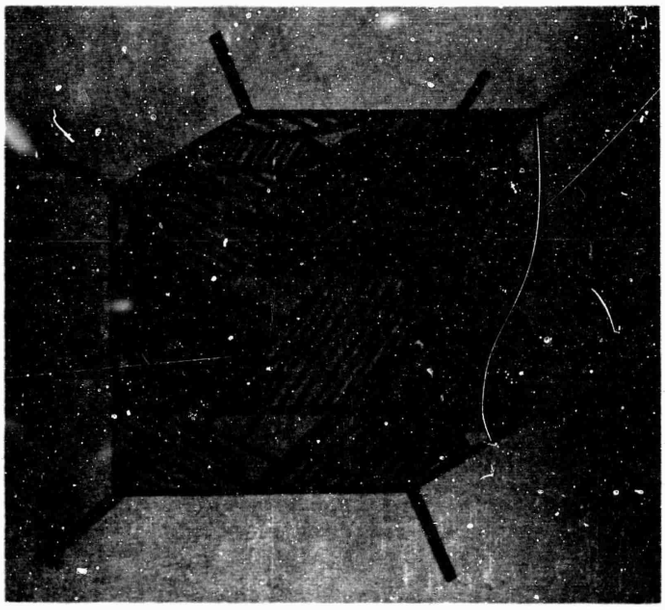

Figure 1 - Unit cell (smallest repeating unit of structure) for 4-D cubic packing; lines within hexagonal bundles represent fiber directions parallel to the cube diagonals. Note that the interstitial pores are connected, deformed tetrahedra which fill 25% of space.

Section II of this report describes the studies conducted during 1970 related to nose tip materials. In addition to the 4-D reinforcements, 3-D constructions having a high axial component of fibers, and 7-D cubic reinforcements (first described in Volume III) have been compared using both low-density low-anisotropy fibers and high-density, high-modulus fibers. Microscopic studies indicated that the latter should have improved resistance to oxidation and vaporization (Ref. 1).

Developments related to thermal shield frusta under this program include the early comparisons of felt, foam and three-dimensional weaves (made with conventional textile looms) and discussed in Volume II. The plate slap data on materials of this type (Volume III) indicated superiority of woven reinforcements with steeper fiber angles to the thickness direction. Ablation tests after plate slap showed the possibility of accepting partial damage (as in a 4-D reinforcement) without degrading surface ablation performance. Note also that data on carbonized wool felt (Volume II) suggests use of this material as a sub-shield insulation with significant compression strength.

During 1970 the concept of a 4-D, high-modulus fiber reinforced thermal shield with a CVD-infiltrated matrix was pursued. The characterization of 4-D with a graphitized pitch matrix (Volume III) showed that high-anisotropy reinforcements resulted in large property anisotropies when the 4-D geometry was deformed by large amounts; consequently, emphasis was placed on the tightly packed cubic symmetry illustrated in Figure 1. Studies by Gebhardt (Ref. 2) in 1969 for the AFML Advanced Development Program demonstrated feasibility of preparing CVD-infiltrated 4-D cylinders, and indicated benefits from the hard as-deposited matrix on mechanical properties. These studies are the basis of the developments reported in Section III of this report.

SECTION II

NOSE TIP MATERIAL DEVELOPMENT

1. OBJECTIVES AND PLAN OF EXPERIMENTS

a. Incentives for Development

Multi-dimensional reinforced graphites should provide a basis for improving several of the performance characteristics which limit the application of "polygraphites" (processed from particulate material) for atmospheric entry under severe environmental conditions. Such improvements are based on the assumption that certain observed types of mechanisms operate to affect the material properties, and that high-density, flaw-free materials are accomplished by optimized processing. The anticipated improvements are these:

(1) Reliable prevention of catastrophic failure from thermal stress which develops in the center of a solid nose tip, or at the inner wall of a thick shell: Although the generation of stress will depend on the combinations of thermal conductivity, thermal expansion and elastic constants in different orientations, ability of the material to relieve the stress by forming non-propagating microcracks (which account for some ductility in polygraphites) can be increased in certain directions by high-strength fiber reinforcement. The reinforcement geometry and dimensions, relative to the thermal stress gradient, strength of reinforcement relative to the matrix, and distribution of microcracks already present as a result of cooling during processing (an inevitable characteristic of all graphites) affect the ability to relieve such stress without complete fracture.

(2) Improved hardening capability: Reinforcement with high-modulus fibers in certain directions can increase strength in critical directions (as in bending a sharp tip), provide higher stress wave attenuation, and reduce crack propagation, thus raising the spall threshold.

(3) Reduced surface recession rate: Although texture of woven reinforcements may cause greater surface roughness than polygraphites, this may not occur if density uniformity is obtained throughout the composite and if fibers are well bonded to the matrix. Filaments oriented at high angles to an ablating surface may be less susceptible to mechanical removal than grains of polygraphite. High-strength fibers and matrix constituents may also be more resistant to particle erosion.

(4) More reliable detection of significant flaws: The regular lattice of a carefully prepared weave provides a basis for detecting irregularities with high sensitivity by radiography or ultrasonic measurements parallel to the reinforcement directions, which is not available with a "statistical" material like polygraphite.

b. Problems Requiring Study

It was recognized at the beginning of the program that the potential advantages of multidirectional reinforced graphites could be realized only if the selection of constituents and processing techniques were sufficiently optimized so that certain important material characteristics were achieved. Ideally, an arrangement of high-modulus, high-strength and high-density fiber reinforcements having a uniform packing geometry and fine texture (minimum possible dimension of reinforcement bundles) was a goal of reinforcement fabrication. The graphite matrix filling the interstices between filaments and filament bundles arranged in different directions should be similar to that of a bulk graphite suitable for nose tips, in having no large or continuous residual pores or cracks. Good bonding between reinforcements and matrix, and both strength and dimensional stability at high temperatures were also set as goals for the processing of these reinforced graphite composites.

Fundamental limitations to achieving all of these characteristics in a single material were encountered, however:

(1) Thermal expansion anisotropy inherent to carbon and graphite filaments results in residual stress and cracks at interfaces between bundles oriented in different directions, after cooling from a high temperature required to insure constituent thermal stability.

(2) Reinforcement packing geometries result in large cavities separated by smaller channels, which tend to plug before densification by infiltration and chemical vapor deposition (CVD) or impregnation and carbonization is completed.

Thermal expansion of unidirectional bundles showed significant differences between low and high modulus fibers (AFML TR-69-67 Vol. III pp 72-73.) Consequently, a "trade-off" was postulated between the benefits resulting from high-modulus, high-density filaments and the increased microcracking inherent to composites made from them. Differences in weave geometry affect both microcrack location and formation and the degree to which pores can be filled during processing; hence, this was also a variable requiring study.

Addtional trade-offs were postulated, based on the economic factor of greater time/cost to prepare high-quality fine-textured weaves and to fill completely the residual porosity by many repeated impregnation cycles. The technique of a single low-temperature infiltration without graphitization promised not only much more rapid processing, but a minimum of microscopic damage as a result of lower mismatch in thermal contraction of fiber bundles.

Finally, the trade-off between high temperature stability and high temperature strength of the matrix constituents was recognized as a problem area requiring a relatively empirical approach, since the "ease of graphitization" varies with carbon precursor as well as thermal history.

Consideration of these problem areas indicated need for comparison of samples covering a variety of material variables. Performance in nose-tip type of ablation environments was the primary basis for this comparison.

c. Comparisons in Ablation Screening Tests

Two series of tests in the AEDC 5MW arc at 90 atmospheres stagnation pressure were conducted at 6-month intervals. Samples were prepared with combinations of constituents and process histories which would provide answers to questions about effects of certain characteristics on ablation performance. Bulk density and microstructure were used to select the best specimens to fill the available test positions, and microscopic evaluation after test was used to assist interpretation of the test data.

In the first series, the questions asked were: (1) Can rapid CVD-infiltration of low-anisotropy-fiber weaves provide ablation performance similar to ATJ-S? (2) Does heat treatment to graphitization temperatures affect such materials? (3) Is fine texture (small bundle size) important? and (4) Does geometry (3 vs 4 direction reinforcement) make a difference with similar size, density, and other characteristics? Comparison samples of CVD-infiltrated and pitch + resin impregnated C-C composites with high-anisotropy fibers, as well as ATJ-S and 3-D Mod. 3 composite material were included for comparison. The differences in texture perpendicular to the axis are illustrated in Figure 2.

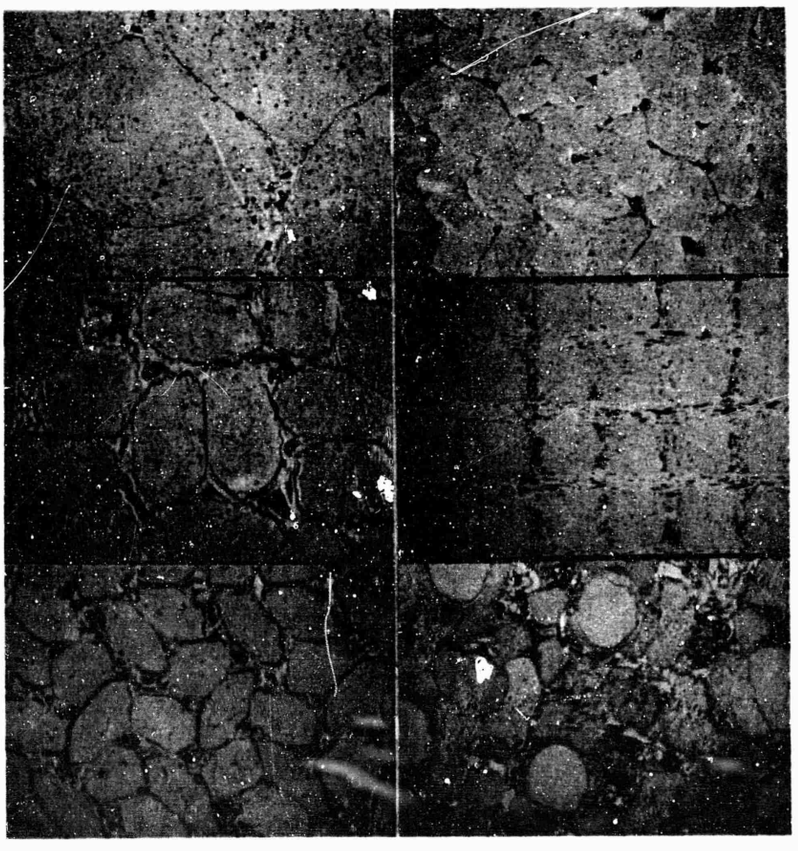

Figure 2 - Polished sections of composites in first series of ablation tests showing comparison of bundle sizes. 10 X.

The results of the first series of ablation tests indicated that coarse texture does degrade performance significantly; both the 32,400-filament low-anisotropy bundles and the 10,000-filament high-anisotropy bundles resulted in composites with higher recession rates than 2,160-filament low-anisotropy bundles with the same (4-D) geometry and an as-infiltrated CVD-carbon matrix. The 3-D and 4-D fine-textured materials were similar, with and without an anneal to over 2700°C, although this heat treatment did not produce the same degree of graphitization found in the resin-impregnated 3-D Mod. 3 or in ATJ-S. The highly graphitized 4-D composite made from Thornel-40 and pitch + resin impregnations was inferior to the CVD-infiltrated fine-textured composites. These results provided encouragement for the rapid infiltration as a technique in processing, although residual porosity was significant in the samples which were tested, and heat of ablation was not quite equal to the average for ATJ-S.

Consequently, the second series of tests was used to compare all-fine-textured reinforcements with either low-anisotropy, low-density or high-anisotropy, high-density filaments in the weave. CVD-infiltration was combined with graphitization and multiple impregnation processing, using both pitch and resin, in attempts to produce both maximum density and high temperature stability in the composite constituents. Several sequences of processing were conducted in parallel and both microstructure and ablation performance compared at similar density levels. Samples having 3-D, 4-D and 7-D geometries were compared, and a fairly large matrix of samples was made available for test. The final selection of samples to fill the available test slots was based not only on microstructure and density of the candidates, but to a limited extent, on the performance of the first few specimens tested, in order to answer the following questions:

(1) Can the high-density, high-anisotropy filaments in fine-textured weaves provide ablation performance comparable to or superior to that resulting from low-density, low-anisotropy filaments, with comparable densification and thermal history?

(2) Is there a significant difference in ablation performance due to weave geometry when 3-D, 4-D and 7-D composites have similar bundle dimensions and similar densification and thermal histories?

(3) Is there a difference in performance due to the type of matrix constituent in contact with filaments and the type used to fill the larger interstices, with comparable densification and thermal histories?

The results of these tests have permitted some specific recommendations regarding future development of these types of composites, and have shown that ablation performance comparable to the bulk graphite standards can be achieved. In the following portions of this section, the fabrication and processing of 3-D and 4-D composites will first be discussed, and this will be followed by a discussion of 7-D reinforced graphite development. Microstructures in the ablation comparison materials are compared with those of the experimental composites. Finally, in part 5, the detailed test results and post-test evaluation of the samples are presented.

2. 3-DIRECTIONAL AND 4-DIRECTIONAL REINFORCED COMPOSITES

a. Selection and Characteristics of Fiber Reinforcements

Post-ablation microscopy had previously shown that acrylic-precursor fibers ablated less rapidly than the lower density rayon-precursor fibers, in both oxidation and vaporization (AFML TR-69-67 Vol. III and Ref. 1.) The higher anisotropy of the high-modulus fibers aggravated the cracking around the bundles made from the 10,000 filament tow which was available. Consequently, a search was made (in January, 1970) for acrylic-type precursor tow having a smaller number of filaments, in order to make reinforcements with finer texture.

An initial sample of 3000 filament tow from Fiber Technology Inc., "SS-3000" (later termed C-3000) was found to be suitable for Omniweave fabrication of 4-D reinforcements, which was not the case with a 720-filament acrylic-type precursor yarn from another source. Consequently, high-anisotropy-fiber reinforcements were made from this material, and a yarn with approximately the same packing diameter was made from cellulose-type precursor material for low-anisotropy-fiber reinforcements having similar texture. Due to later delivery, the acrylic-type fibers could not be made into composites in time for the first series of ablation tests.

The acrylic-type-precursor fibers had a smaller diameter than the Modmore II PAN-precursor fibers studied previously, as shown in Figure 3. However, the properties provided by the vendors were similar, as indicated in Table I.

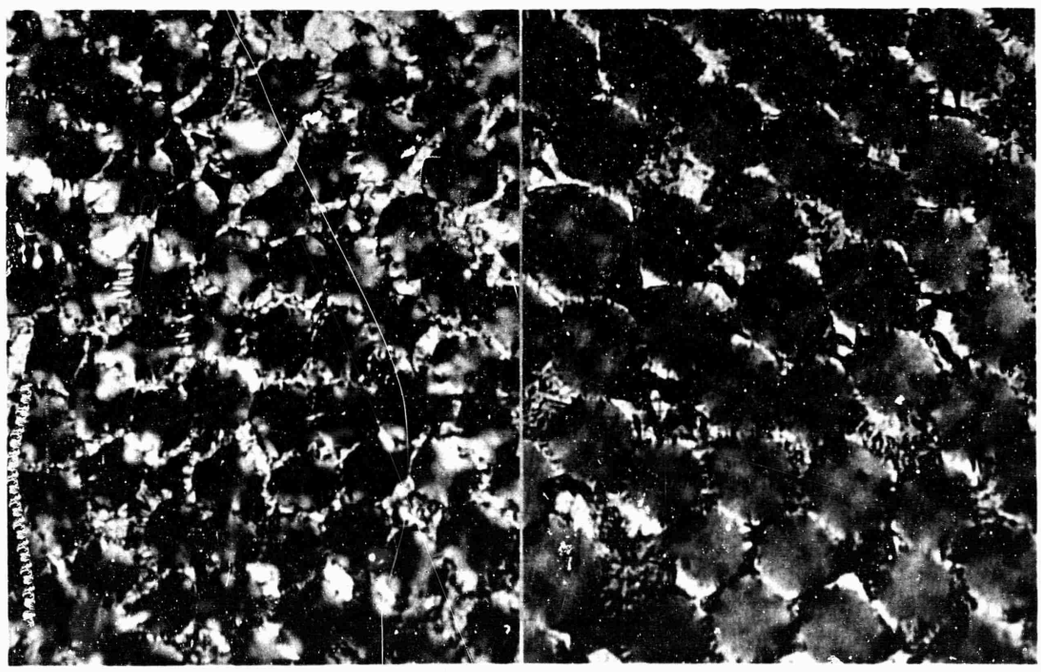

Figure 3 - Microstructure of acrylic-type precursor filaments from Fiber Technology, at left (impregnated with phenolic resin and heated to 2750°C) compared with Type II fibers in 2500°C graphitized pitch, right. Polarized light, 1390 X.

TABLE I

FILAMENT DATA FOR COMPOSITES TESTED IN ABLATION

Characteristic or Property	Fiber Technology			Whittaker	Union Carbide
	CXH	CXL	C-3000	Modmore II	Thornel 40
Carbon Content, Per Cent	99.0	88.0	99.0+	99.0	99.9
Immersion Density, g/cc	1.43	--	1.70-1.75	1.75	1.56
Cross Section Area, 10^{-7} in.^{2}	1.0	1.1	0.5 - 0.65[a]	0.7	0.6
Tensile Strength, 10^3 psi	163.4[b]	125.6[b]	330[b]	350-450	259[c]
Elastic Modulus, 10^6 psi	5.4	4.9	49	35 - 45	41.3[c]

Notes: a-Measurement of first batch was 0.65 x 10^{-7} in.^{2}, used for tensile data.
b-Tensile data is average of 15 measurements with 1-inch gage length.
c-Data reported in AFML-TR-69-67 Vol. II, p. 9.

The C-3000 was provided with a low twist of 1.2 turns per inch and a teflon coating of 3 to 4 per cent. The tow had been heat treated at a temperature in the range 2000° to 2400°C (Ref. 3.)

The cellulose-type precursor filaments were prepared with both a high final processing temperature (CXH) and a low temperature (CXL) with the differences shown in Table I. The CXL was used only to check effects of filament purity on ablation performance, and most composites were made from CXH, which has properties identical to the standard twisted 2-ply CX-2. For CX-3, three 720-filament precursor strands were combined to make a tow with 1.2 turns per inch, carbonized, and coated with 3 to 4 per cent teflon; the resulting 2160-filament tow closely matched the C-3000 in lateral dimensions. A small amount of 45-ply tow, with 1.0 turns per inch and teflon coating was also made from CXH, for fabrication as a coarse-textured 4-D composite with "CXH-45" bundles.

Strand breaking strengths determined by Fiber Technology Inc. showed that the specially prepared bundles had good mechanical properties. The average of 15 tests on CX-3 with treatment "H" was 18.1 pounds (4.84 grams per denier), while the average with treatment "L" was 16.5 pounds (the 45 ply CXH did not break at 200 pounds.) The C-3000 was impregnated with epoxy before test and broke at 61 pounds. The special preparation and teflon coating provided good handling characteristics during weaving and the resulting bundles did not show the regions of larger filament separation which had been found around separate plies of twisted 2-ply yarn in previous composites.

Table I also shows data on the fibers used in the composites included for comparison in ablation tests: Whittaker Corp. Modmore II and Union Carbide Corp. Thornel 40 (grade WYF.)

b. Omniweave Fabrication

The GE-RESD "Omniweave" fabrication techniques showed promise initially, because 4-directional reinforcements could be compacted to higher density and closer-to-cubic symmetry than had been obtained by another procedure (AFML-TR-69-67, Vol. II pp 9-11.) In exploring the potential of this type of reinforcement for composite nose tip materials, several problems were identified as critical to the successful development of the concept:

(1) Could fine-textured composites be prepared with uniform, tight packing and without lost yarns or other defects ?

(2) Could the more sensitive high-modulus fibers be fabricated as in (1) as well as low-anisotropy materials ?

(3) Could the process be scaled up to billet dimensions without loss of quality, or could coarse-textured constructions suffice without a serious degradation in ablation performance ?

The first two questions were studied under this program by preparing 31 x 31 element strips with both CX-3 and C-3000 fibers. The question of substituting coarse texture was studied with a 6 x 6 element strip of CX-45. The problem of scaling-up fine-textured tightly packed Omniweave to an 84 x 84 element construction was a more difficult undertaking, however, and was left for separate study under another program.

The answer to the first two questions was positive, although the strips were not quite as tightly packed as had been hoped, and there were some variations in packing density along the length, as different techniques of fabrication were employed. Radiographs of the 31 x 31 element weaves are shown in Figures 4 and 5.

Figure 4 - Radiograph of Omniweave #229, made from 31 x 31 C-3000 tows; Top: 0°; Bottom: 90°. 1 X.

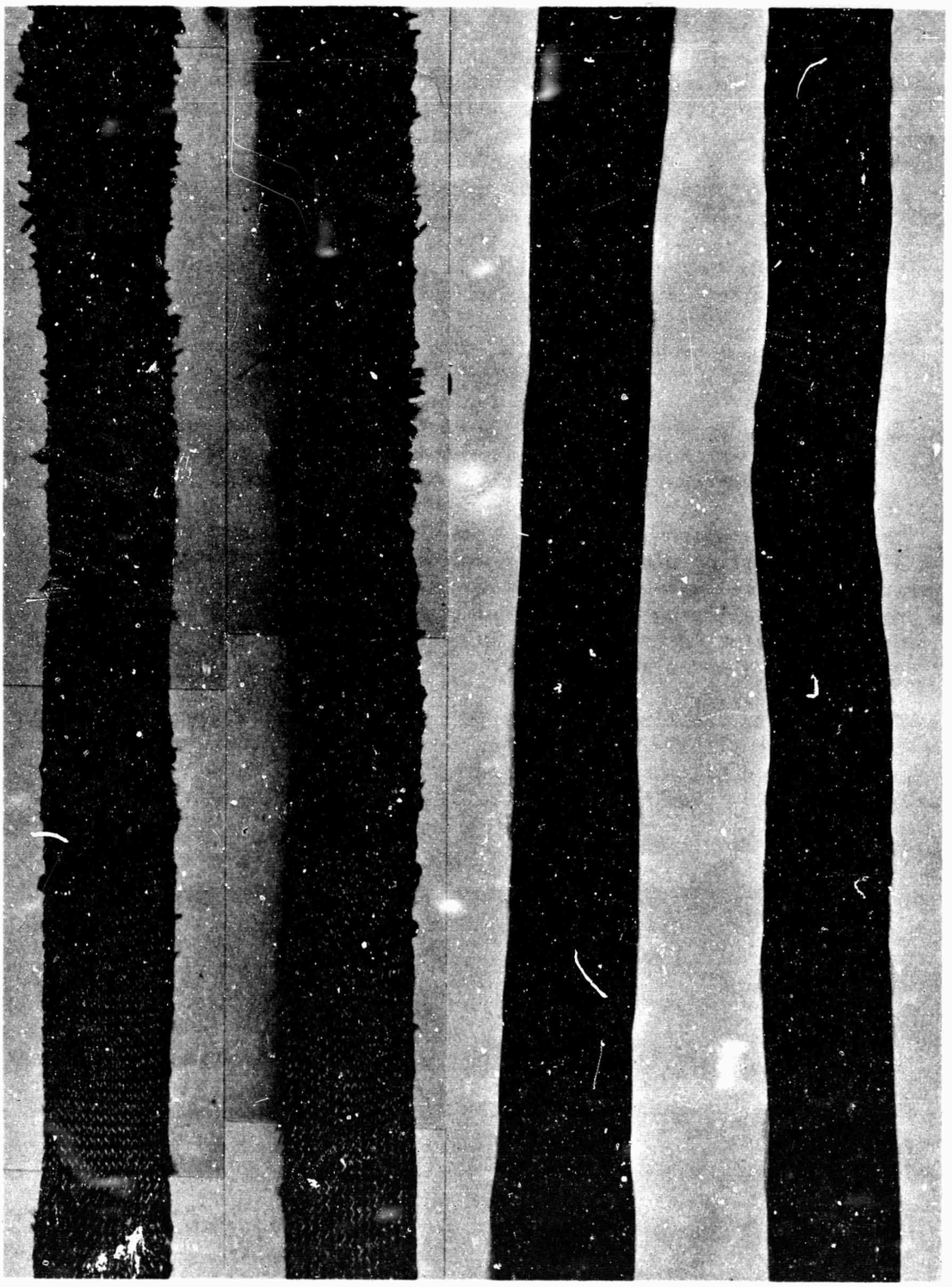

Figure 5 - Surface texture and radiographs of 31 x 31 element Omniweave strips made with CXH-3 fibers (#213 at right) and CXL-3 fibers (#214, at left;) note packing density variations along length. 1 X.

As shown by the radiographs, the CX-3 weaves were about 0.8 inch square as woven, while the C-3000 was 1.2 inch square. Bulk densities were about 0.65 g/cc average for the CXH-3 and CXL-3 (45% dense) and 0.7 g/cc for the C-3000 (40 % dense.) The surface projection of the fiber angle was the same on both sides of each weave and varied from 36° to 43° in the CX-3 weaves and from 34° to 44° in the C-3000. Compacting experiments on a low-density portion of the CXL-3 weave showed that a portion with 37.5° projected surface angle as woven (47.4° fiber to the weave direction) could be changed from 29.3° (38.5° fiber angle to weave direction) to 57.2° (65.5° fiber angle to weave direction) with increases in packing density of 33% and 25 % respectively. The more tightly packed portions were more resistant to such deformation. Total lengths woven were about 16 inches for the CX-3's and 14 inches for the C-3000 weave.

c. 3-Directional Weaving at Fiber Materials Inc. (FMI)

The weaves purchased from FMI were intended to provide a comparison of ablation performance with the same fibers and matrix constituents in the finest textured 3-D orthogonal construction which could be prepared by existing methods. Fiber Technology CX-2 yarn was used in the first of these and in the lateral direction of the second, while C-3000 tow was used for the axial oriented bundles in the second case.

The "standard" FMI 3-D billet was constructed with 1/8 inch spacing between axial fiber bundles, which left interstitial voids that were too large for successful processing to nose tip materials. Consequently, the FMI weave techniques were modified to prepare billets with 0.04 inch axial center-to-center spacing, as shown in Figure 6. Four ends of CX-2 yarn, or two ends of C-3000, were used in each axial bundle (vertical in Figure 6) while two ends of CX-2 (CXH-1 in the billet with C-3000) were used as laterals. A fibrous filler was added during weaving between each perpendicular lateral layer, and this fibrous filler accounted for 5.4 % of the weight of the first billet. Figure 7 illustrates the uniformity of the all-CXH reinforced billet.

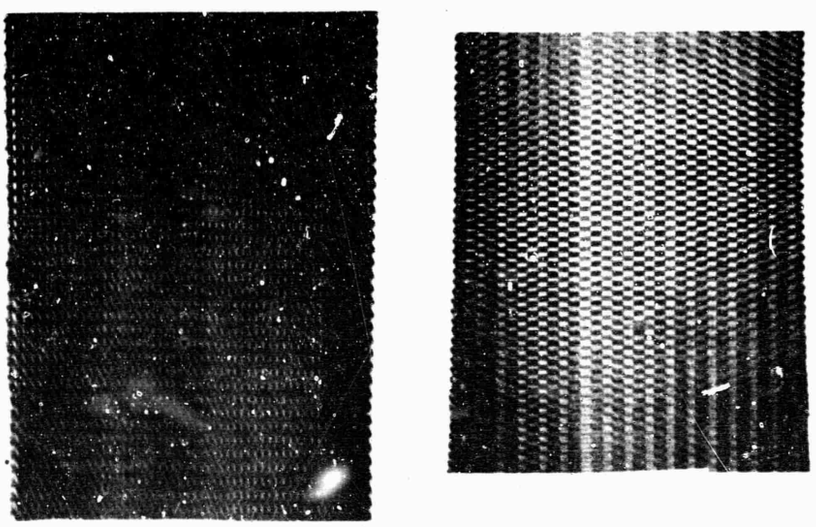

Figure 6 - Radiographs of FMI weaves with 0.03-inch bundles on 0.04-inch centers (left) and with 0.06-inch bundles on 0.125-inch centers (right). 1 X.

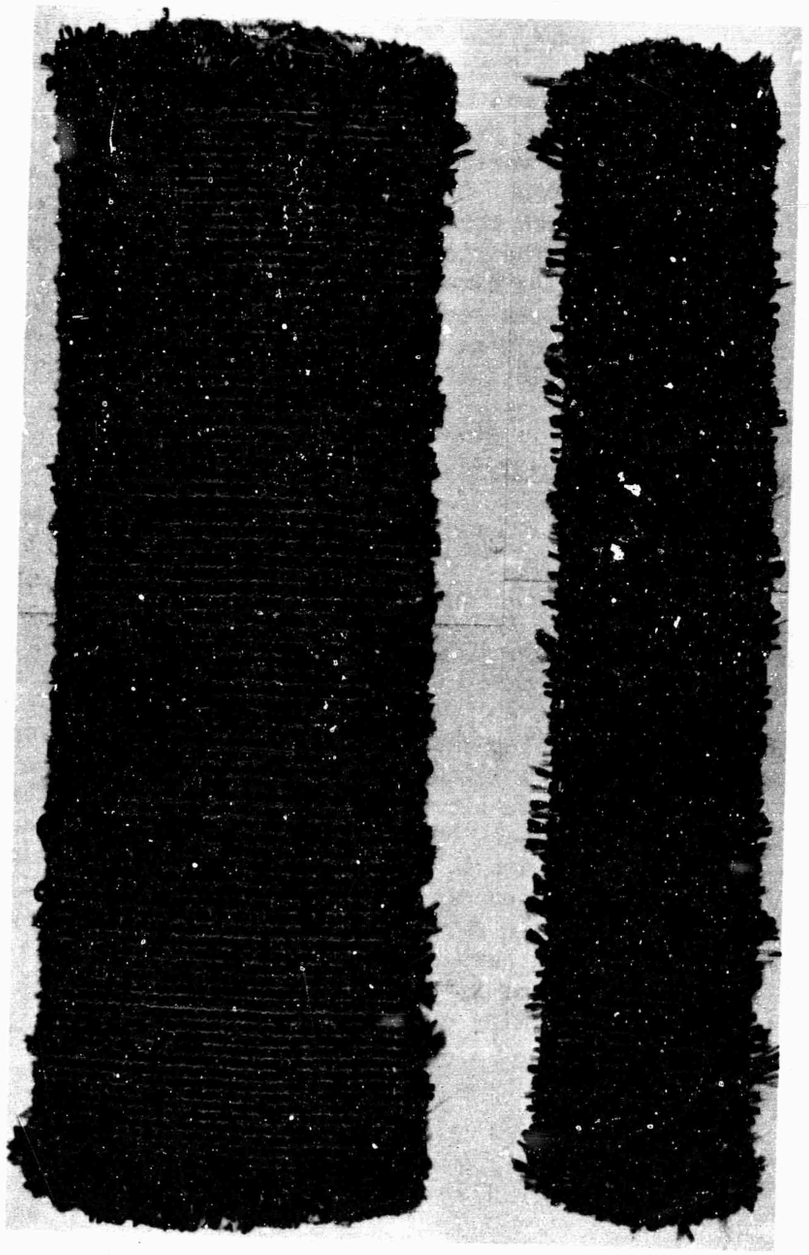

Figure 7 - FMI billet made from CXH yarn with 0.04 inch between axial (longitudinal) bundles and a fibrous filler added during weaving. 1 X

The second billet prepared by FMI was initially planned to have 720 filament acrylic-type precursor reinforcements in the lateral directions, but this yarn could not be handled with sufficient ease to permit efficient fabrication, so only a few layers (first 1/8 inch) were added, and CXH was used in the remainder. After the first 3 inches were woven, an attempt was made to add three times as much filler between each of the layers. However, as shown in Figure 8, this resulted in too much spreading between the lateral bundles. Although the whole billet was utilized in the tests, the portions of specimens subjected to ablation were all taken from the central region having uniform spacing of CXH laterals and filler corresponding to that in the first billet.

Figure 8 - Radiographs of FMI-woven 3-D billet with a high axial component of acrylic-precursor fibers on 0.04 inch centers; top half was a region in which a larger proportion of filler was added during weaving. 1 X.

d. Preparation of All-CVD-Infiltrated Composites

A technique for rapid infiltration of woven composites had been developed by GE-RESD under a separate program, and a major objective of the first series of ablation tests was the evaluation of this matrix when applied to the AFML reinforcements. Although neither the Omniweave nor the FMI weave made from C-3000 were available in time for processing before this test series, the CX reinforced materials in both geometries and with both coarse and fine constructions were processed for the experiment.

The technique, which has been described previously (Ref. 2, p. 202), is termed "direct r.f. infiltration", since it involves direct coupling of the field from an r.f. coil with the weave suspended in a rapidly moving gas stream at about 1 atm. pressure. The objective is creation of a temperature gradient in the material similar to that obtained by the heated-substrate temperature-gradient method, and deposit microstructures are similar to those obtained in the "1100°C PCTG" deposit discussed in Volumes II and III.

A preliminary experiment was conducted to ensure that this technique was capable of penetrating a block of nose tip dimensions. As shown in Figure 9, a two-inch cube was cut from the "standard" FMI weave purchased for this program, and suspended in the coil so that a temperature gradient was formed in a manner similar to that which would result if a billet were moved slowly through the coil. After sectioning, the block showed deposit at the center line about 1 inch from each of the surfaces, indicating that penetration was achieved. Since this billet contained no fibrous filler, the interstices were not filled and total bulk density was relatively low (below 1.5 g/cc.)

The samples for test were all infiltrated as 0.7 to 1.2 inch square portions of the weave. In most cases, the infiltrated blocks were ground to cylinders and infiltrated a second time, and in some cases a final infiltration was conducted on the ground tips. Such a procedure is consistent with the processing which could be applied to a nose tip.

The increases in density, which resulted from 14 to 40 hours of infiltration at temperatures estimated to be about 1100°C, were as follows:

CXH 3-D (FMI)	0.64 g/cc to 1.55 g/cc
CXH-45 4-D	0.77 g/cc to 1.59 g/cc
CXH-3 4-D	0.63 g/cc to 1.65 g/cc
CXL-3 4-D	0.59 g/cc to 1.61 g/cc

The initial densities were measured after an initial heat treatment in vacuum to 1700°C in all cases.

Cylinders of 3-D and 4-D CXH composites were heated in a Brew resistance furnace for 1 hour above 2400°C; power settings indicated at least 2750°C, and probably 2900°C was reached (deposition on the sight glass prevented accurate temperature measurement.) The 3-D sample expanded 1.8 % in length without any measurable change in diameter, but the 4-D sample expanded 2.8 % in length and 1.1 % in diameter. Both lost 0.2 % in weight. Afterwards, they were infiltrated 8 and 12 hours, respectively, with the following weight increases and densities: 3-D: 2.8 % (1.57 g/cc); 4-D: 8.9 % (1.61 g/cc).

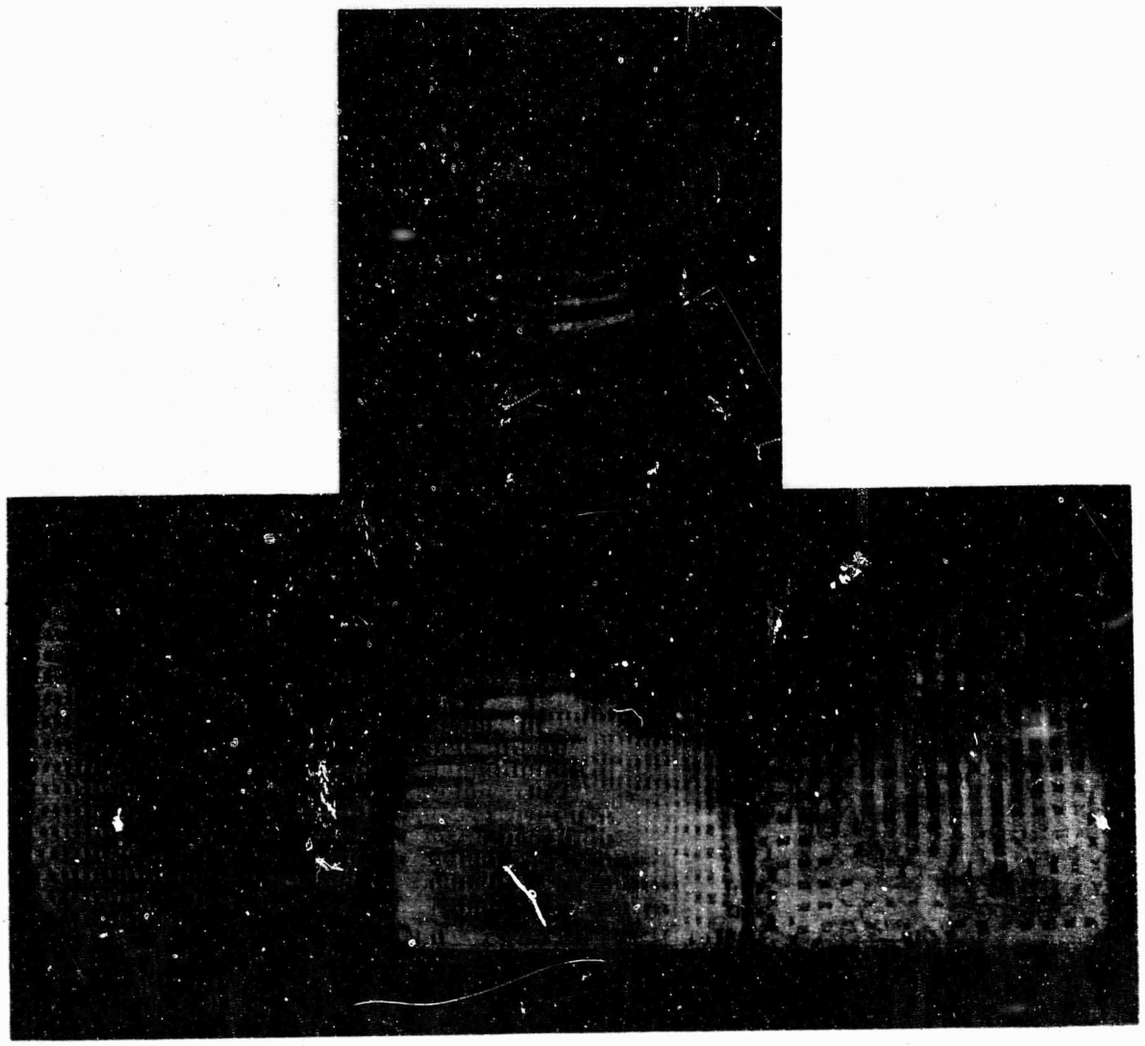

Figure 9 - Gradient-infiltrated cube of 3-D orthogonal weave, showing arrangement in coil and surface temperature profile (top) and shiny surfaces where deposit occurred on a section through the center (left) and two outer surfaces before sectioning (1 X.)

Microstructures resulting from the r.f. infiltration are illustrated in Figures 10 to 13. There was residual porosity in all of the fiber bundles as well as larger pores in the interstices between bundles. Note, however, in Figures 10 and 11, the tendency of deposition around the fibrous filler to fill much of the interstitial space in the 3-D weave. The open interstitial channels in the 4-D composites, for example Figure 13, resulted in a thick deposit of a more laminar material, in comparison with the fine-grained deposit (often with evidence of soot or whisker formation) in the filament bundles. The granular deposit showed no change resulting from the annealing while the laminar, thick deposits tended to crack and deform. As shown by post-ablation microscopic examination, discussed in Part 5 of this section, the fine grained deposit adhered well to the filaments in ablation.

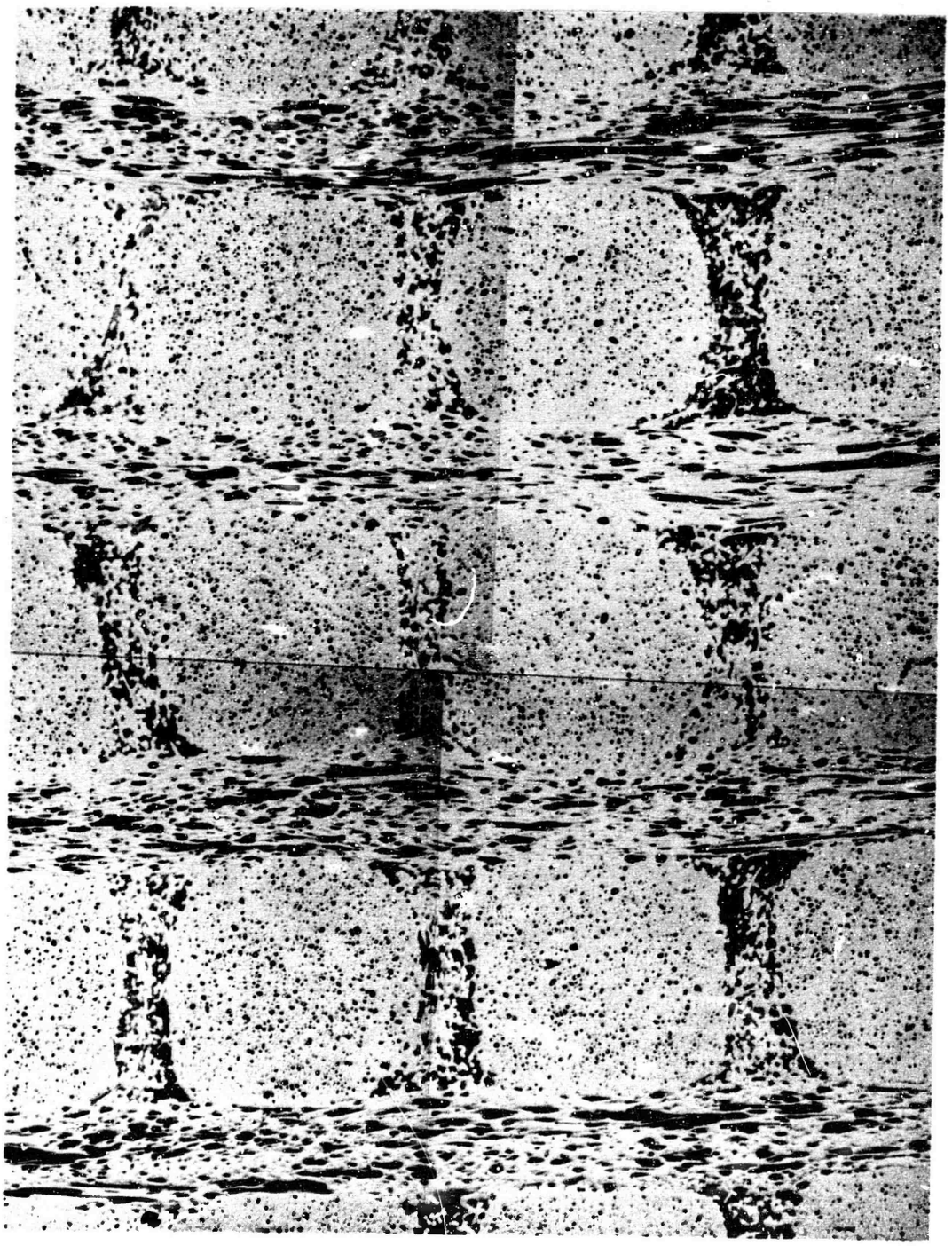

Figure 10 - Rapidly infiltrated CXH 3-D (FMI) composite having fibrous addition to interstitial voids; view of surface perpendicular to axial bundles having 0.04 inch spacing. Bright field, 50 X

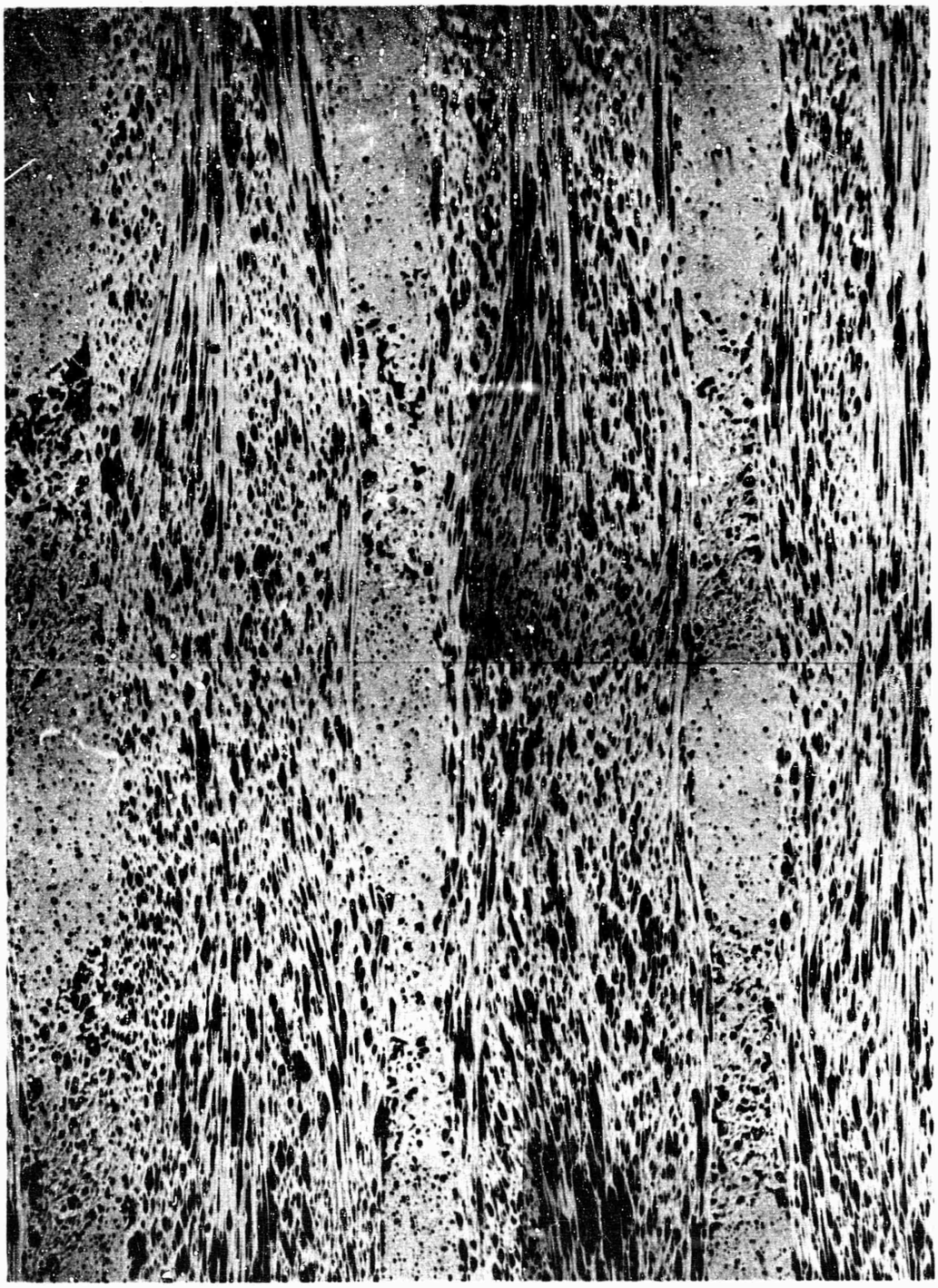

Figure 11 - Rapidly infiltrated CXH 3-D (FMI) composite having fibrous addition to interstitial voids; view of surface parallel to axial fiber bundles (vertical). 50 X.

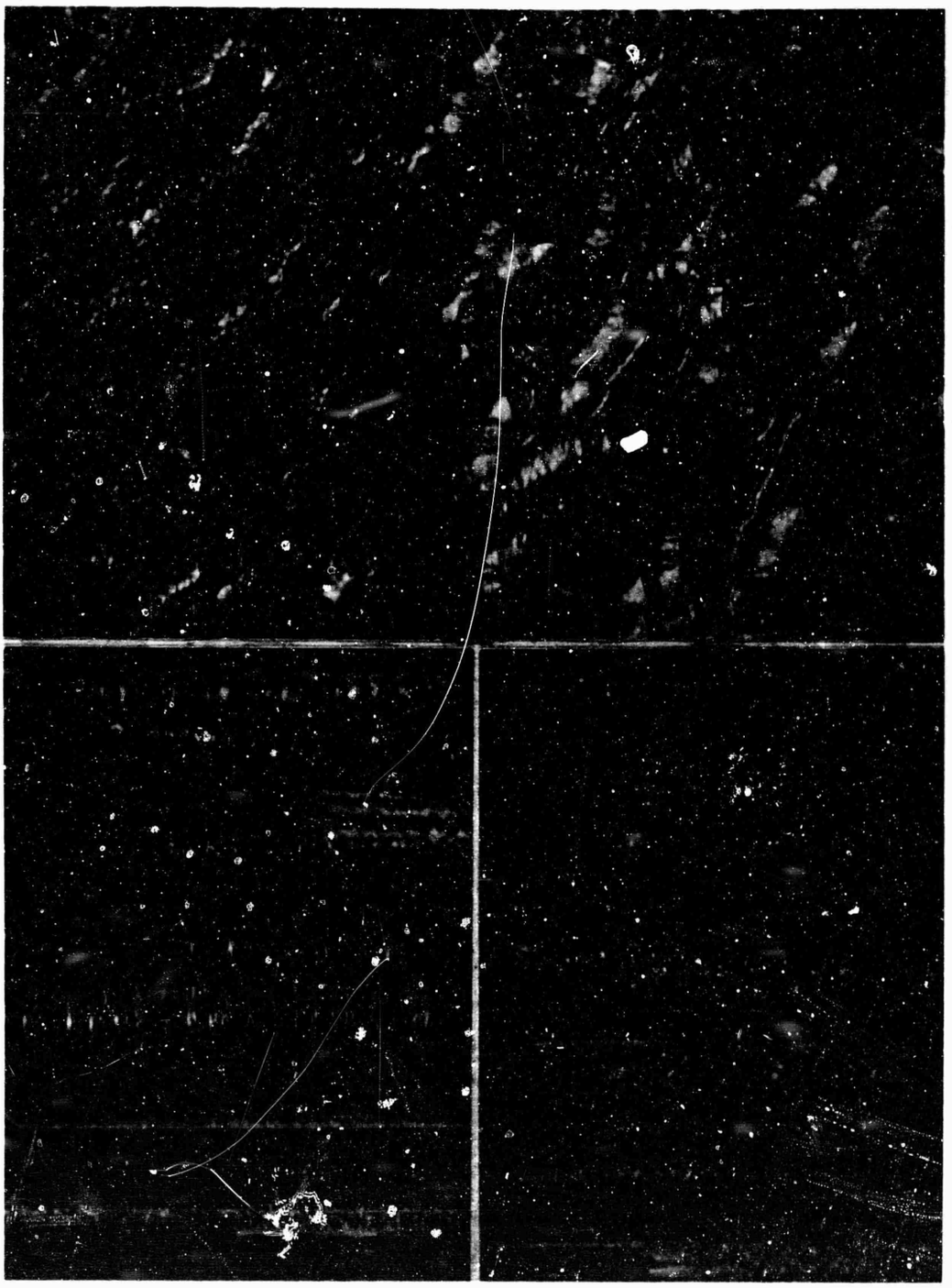

Figure 12 - Microstructures in rapidly infiltrated 3-D FMI CXH, graphitized and re-infiltrated. Top: gradient between CXH fiber bundle (left) and fibrous filler in interstice. Bottom: fine-grained CVD carbon between fibers. Polarized, 1590 X.

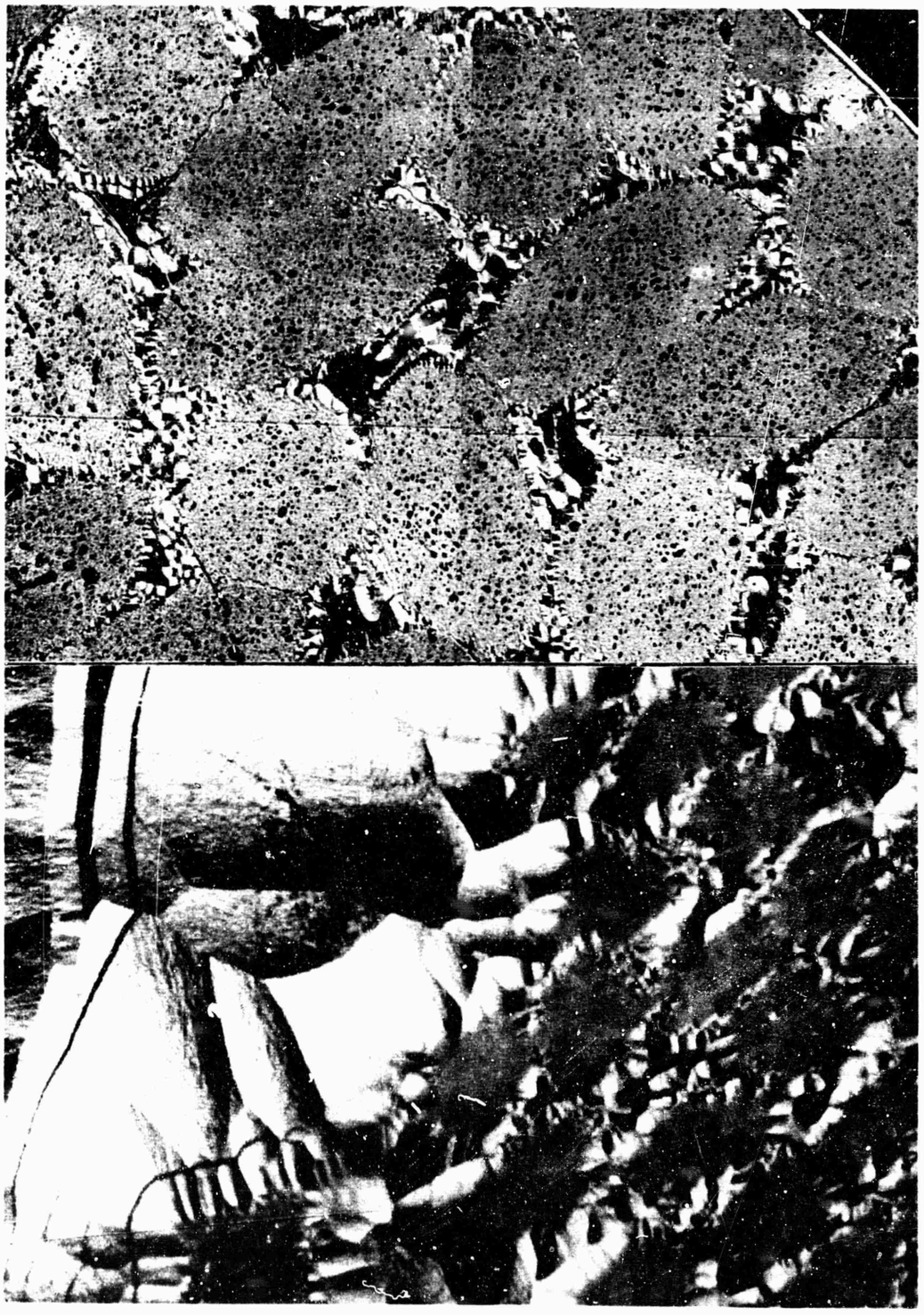

Figure 13 - Microstructures in rapidly infiltrated 4-D CXH, graphitized and re-infiltrated; top: 50 X; bottom: 1590 X (polarized.)

In addition to the microscopic studies of the samples tested in the first series, a qualitative comparison of the relative degree of graphitization was obtained using an XRD-5 X-ray spectrometer. Cylinders were cut from the stems used to hold the specimens during the ablation test, and these were mounted to expose the face perpendicular to the axis to a beam of Cu K_α radiation. The same cylinders were used for bulk density and porosity comparisons. A scintillation detector with pulse height analyser was used with the following set-up: 1° beam slit, medium resolution sollar slit, 0.1° detector slit, 4° take-off angle, and 50 kv peak at 15 ma beam current. Figures 14 and 15 illustrate the strip chart recorder traces of the (002) and (100)-(101) diffraction regions.

These line traces show that the constituents in the infiltrated composites had a relatively low degree of graphitization and the anneal, which may have reached 2900°C, did not produce a structure as graphitic as the constituents in ATJ-S or the 3-D Mod. 3 comparison. The graphitized high-modulus fiber bundles in the 3-D Mod. 3 were perpendicular to the surface exposed to the beam, so that these should not account for the sharp (002) line in Figure 14. Although more detailed studies of the peaks as a function of specimen orientation might permit some separation of the fibers and CVD carbon contributions to the patterns, which would be necessary before lattice parameter and "crystallite size" numbers would be meaningful, these curves demonstrate that the composites were farther from equilibrium graphite structure than most materials which have been considered for nose tips.

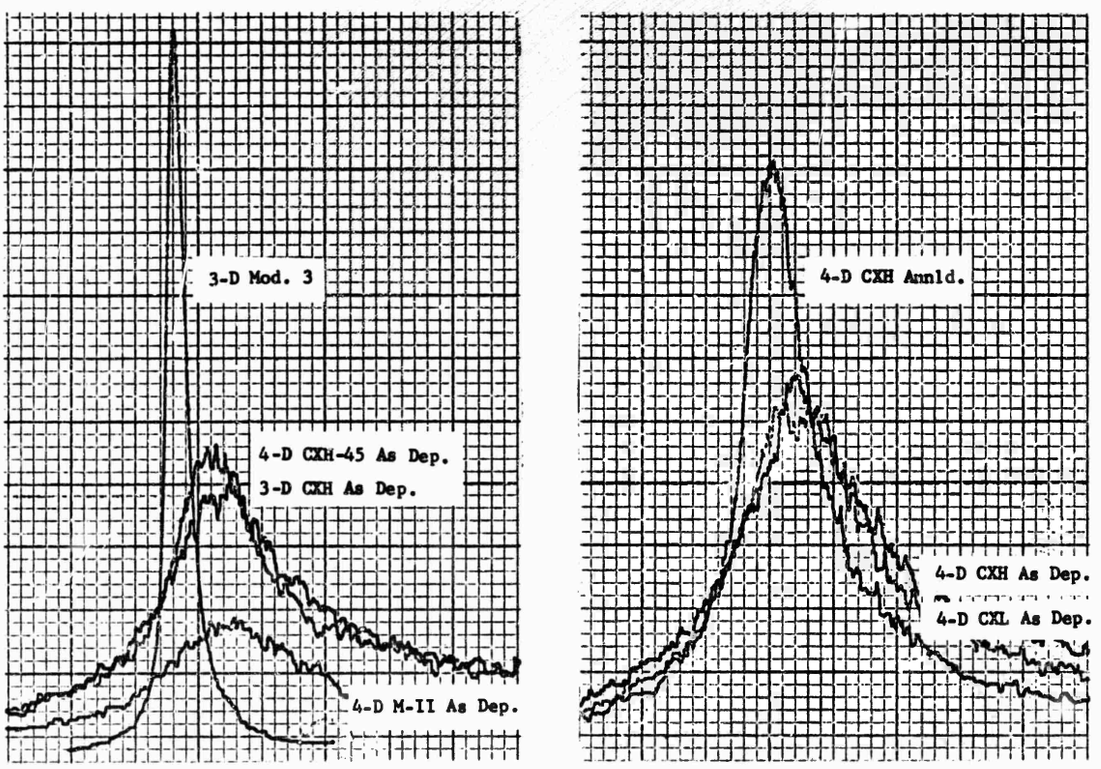

Figure 14 - Diffractometer traces of (002) diffraction line profiles.

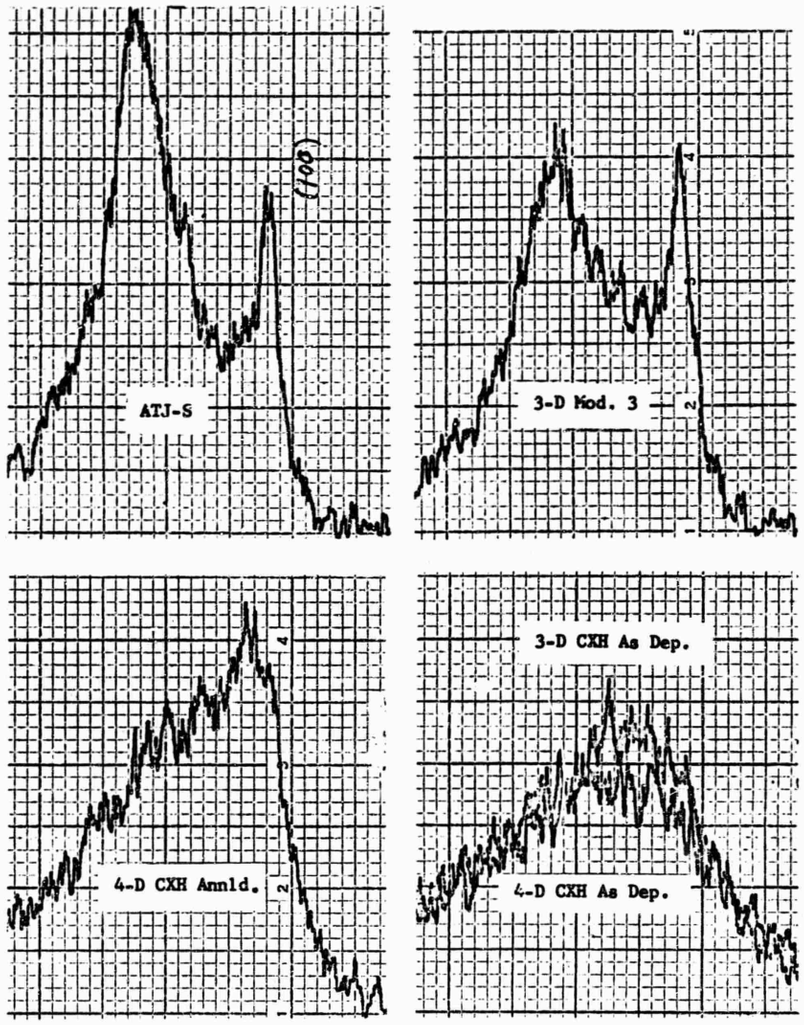

Figure 15 - Diffractometer traces of (100)-(101) bands (Cu-kα radiation.)

The comparison sample of Modmore II (M-II) 4-D had been r.f. infiltrated in a similar manner, and the low (002) peak in Figure 14 is probably the result of the high preferred orientation in the fiber bundles, which would orient more planes away from the face of the cylinder being irradiated. This composite had a bulk density of 1.83 g/cc; it had been prepared from a 4-D Omniweave having 0.45 g/cc and an angle of fibers to the axis of 34° (projected surface angles on the orthogonal faces were 25° and 26°.)

Open porosity as well as bulk density was compared in the cylinders cut from the stems of the ablation samples. Apparent density was obtained from immersion in naptha solvent (Fisher Catalogue No. N-3, Lot 750254), which had a specific gravity of 0.664 g/cc, measured by displacement of an aluminum block in the same manner as the samples, at the test temperature of 68°F ± 1°.

The cylinders were oven dried at 300°F for two hours before determining the dry weight. Then, they were placed in a beaker within a vacuum desiccator which was evacuated to below 100 microns. The beaker was then filled with the naptha. After immersion 16 hours at 1 atmosphere, immersed weight was determined using a wire basket and a balance without removing the samples from the liquid. Although measurements were then made of weight in air with the pores filled with naptha, evaporation introduced errors. Consequently, bulk density was calculated from weight in air (dry) and cylinder dimensions. The volume per cent open pores was thus calculated as:

$$\text{Per Cent Open porosity} = 100 \left(1 - \frac{\text{Bulk Density}}{\text{Apparent Density}} \right).$$

Results in Table II show a continuous porosity similar to the ATJ-S and 3-D Mod. 3 ablation comparison materials, which were measured at the same time.

TABLE II

BULK DENSITY AND OPEN POROSITY OF ABLATION SAMPLES

Type of Material	Code	Bulk Density g/cc	Open Porosity %
3-D, CXH + CVD	3XH11t11	1.55	4.9
3-D (annealed)	3XH11Gt11	(1.57)*	---
4-D, CXH + CVD	4XH11t11	1.63	3.0
4-D (annealed)	4XH11Gt11	1.61	7.6
4-D, 45 ply + CVD	4XH(45)11t11	1.55	4.4
4-D, CXL + CVD	4XL11t11	1.61	4.2
4-D, M-II + CVD	4MII11t	1.83	6.7
ATJ-S	ATJ-S cored	1.84	6.4
	ATJ-S #2	1.86	4.7
	ATJ-S #3	1.85	5.8
	ATJ-S #4	1.86	9.8
	ATJ-S #5	1.86	4.6
3-D Mod. 3	3-D Mod 3 a	1.69	5.6
	3-D Mod 3 b	1.67	6.8

* Sample lost during ablation test; blank density shown.

e. Comparison Samples of Pitch-Impregnated 4-D Composites

The first series of ablation tests included two composite samples which were impregnated by LTV Research without cost to the project. The objective was to compare ablation performance of two types of graphite matrices with high modulus fiber reinforcements, after processing to more complete pore filling than had been achieved in the earlier tests at Battelle Memorial Inst., in which the pitch-impregnated M-II 4-D material had performed poorly (Vol. III, pp 112-126).

Portions of the Thornel 40 braid strip described in AFML TR-69-67 Vol. II, pp 9-10, were sent to the LTV Research Center where the following processing was conducted (Ref. 4). The strips were compressed to 1 in. x 1.5 in. in cross section, so that projected fiber angle to the weave direction was about 14° (10° projected on each side of the strip). The strips were heated to 1000°C in vacuum and then subjected to several cycles of impregnation followed by carbonization to 1000°C and graphitization to 2500°C. The first strip was initially impregnated with Allied Chemical pitch grade 30 Med. coal tar pitch, which brought bulk density from 0.58 g/cc initial to 1.15 g/cc, after graphitizing. Several furfuryl alcohol impregnations were then used to bring density to 1.60 g/cc, after graphitizing. Finally, a series of impregnations with a petroleum-based LTV resin system resulted in a final bulk density of 1.75 g/cc. A second section of weave was impregnated entirely with the petroleum-base impregnant, from 0.70 g/cc to 1.69 g/cc after graphitizing. A sample of Omniweave 4-D strip made from Herculese Grafil HT 10,000 filament tow was also impregnated with the petroleum-based resin, from 0.78 g/cc initial to 1.77 g/cc. The fiber angle in the HT 4-D composite was about 27° (20° on each side) to the length.

The two samples which were included in the ablation series were both Thornel-40 reinforced. One of these, with the coal tar pitch impregnant, had a bulk density of 1.72 g/cc and an open porosity of 6.0 percent, measured on a cylinder cut from the stem after test. The second, impregnated entirely with the petroleum-derivitive, had a density of 1.67 g/cc and 13.2 percent open porosity. The X-ray diffraction patterns are shown in Figure 16.

Microstructures found in these samples are illustrated in Figures 17 to 19. The petroleum derivitive precursor produced relatively large mesophase grains in the interstices, although structure within filament bundles was similar to that resulting from the coal tar pitch. The interstitial porosity was not well filled, which probably was responsible for catastrophic failure in ablation. Glassy carbon, partially graphitized in some regions, resulted from the furfural impregnant. The microstructures showed severe cracking around filament bundles, probably due to "sissoring" of the 4-D structure with temperature changes.

Flexure tests on bars cut from these blocks were made as a check of relative strength of the different materials. As shown in Figures 20 and 21, the samples showed the resistance to crack propagation characteristic of most 4-D reinforced graphites. The data in Table III indicates significantly higher strength with the petroleum derivitive material, even though density was lower, in the same weave. The Grafil HT reinforcement was relatively weak, and it was not possible to machine suitable ablation specimens from this material, due to chipping of the matrix.

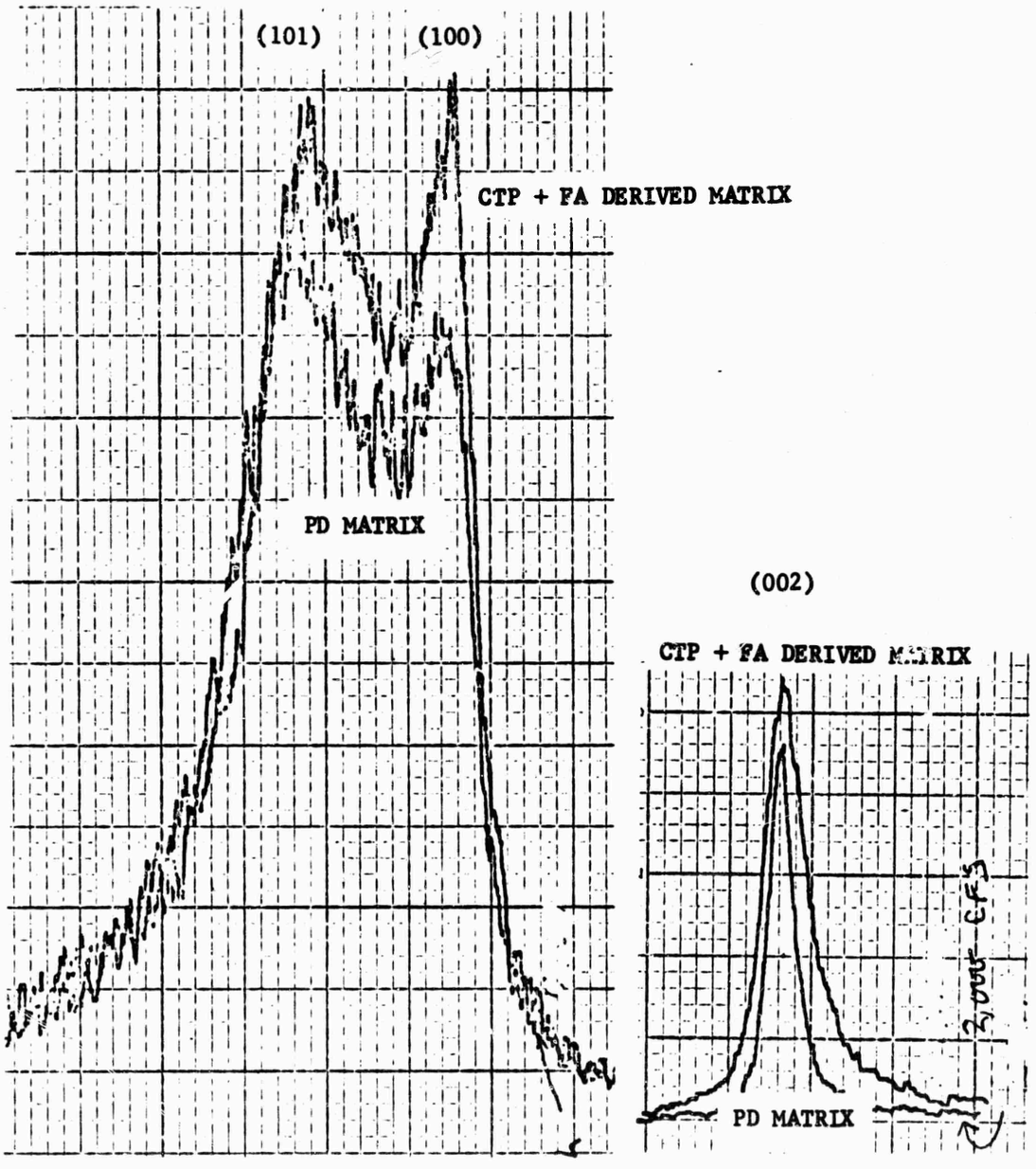

Figure 16 - X-ray diffractometer line profiles of pitch impregnated samples showing evidence of graphitization in (100)-(101) region, at left, and (002) relative line width at right; sample with "PD" matrix is more graphitic than that with CTP + FA derived matrix (Cu K radiation.)

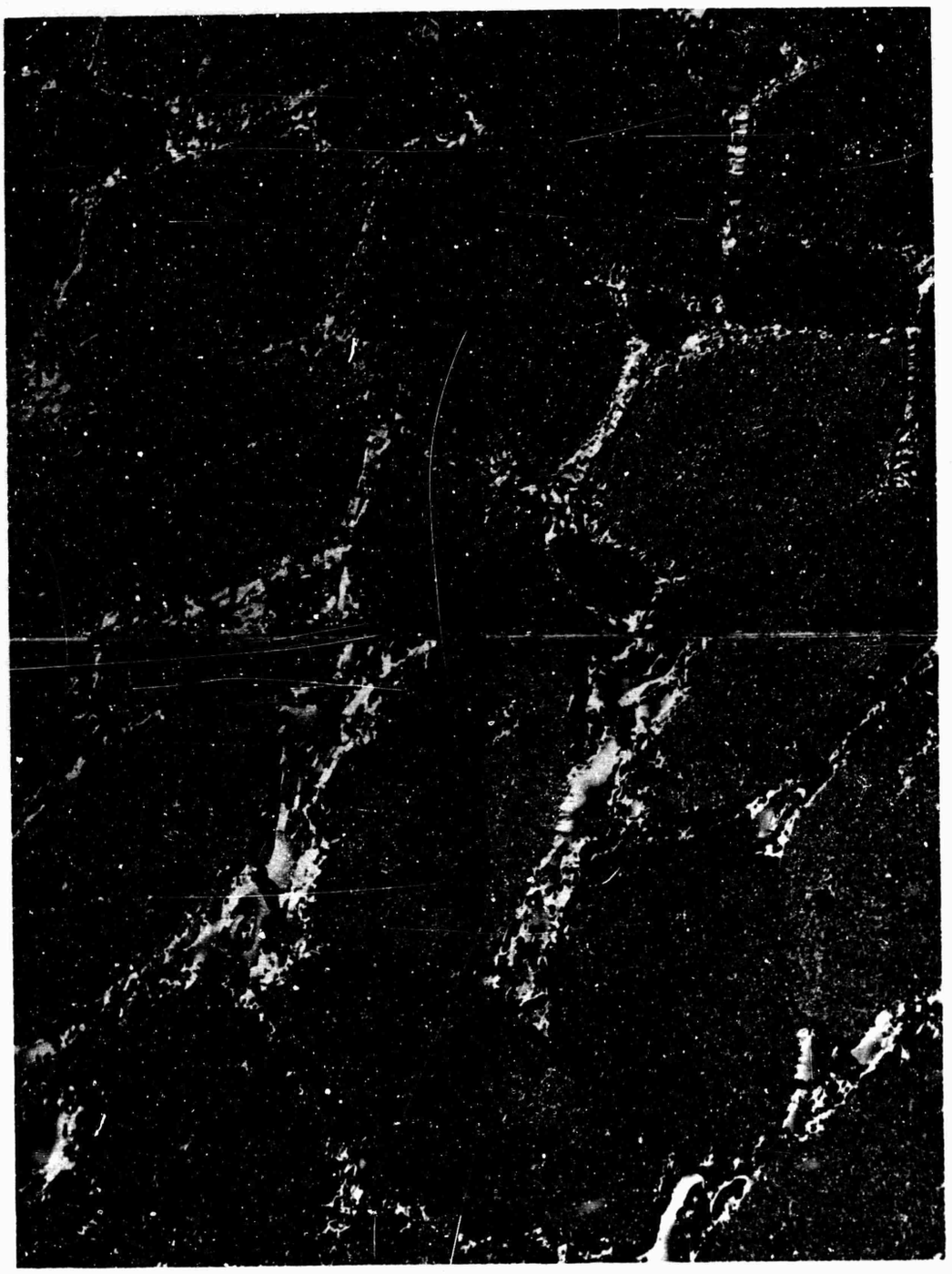

Figure 17 - Microstructures of Thornel 40 4-D composites ablation tested; "PD" matrix at top, graphitized CTP + FA matrix at bottom. Polarized light, 50 X.

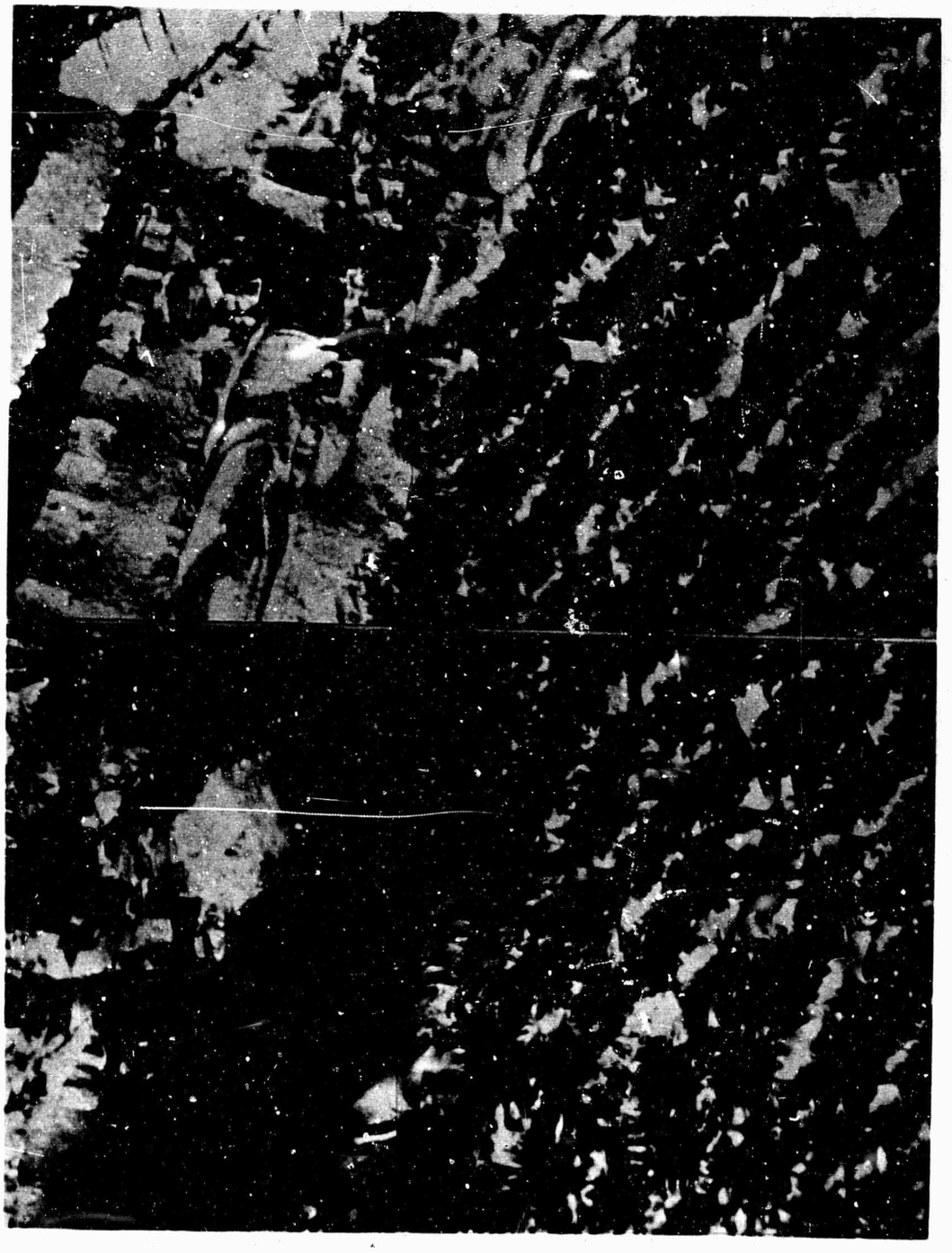

Figure 18 - Microstructures of Thornel 40 4-D composites showing matrix structure in filled void, left, and fiber bundle, at right. Top: "PD" matrix; bottom: graphitized CTP + FA matrix showing fine-grained CTP-derived material (top left) and partially transformed glassy carbon (bottom left.) Polarized light, 1590 X.

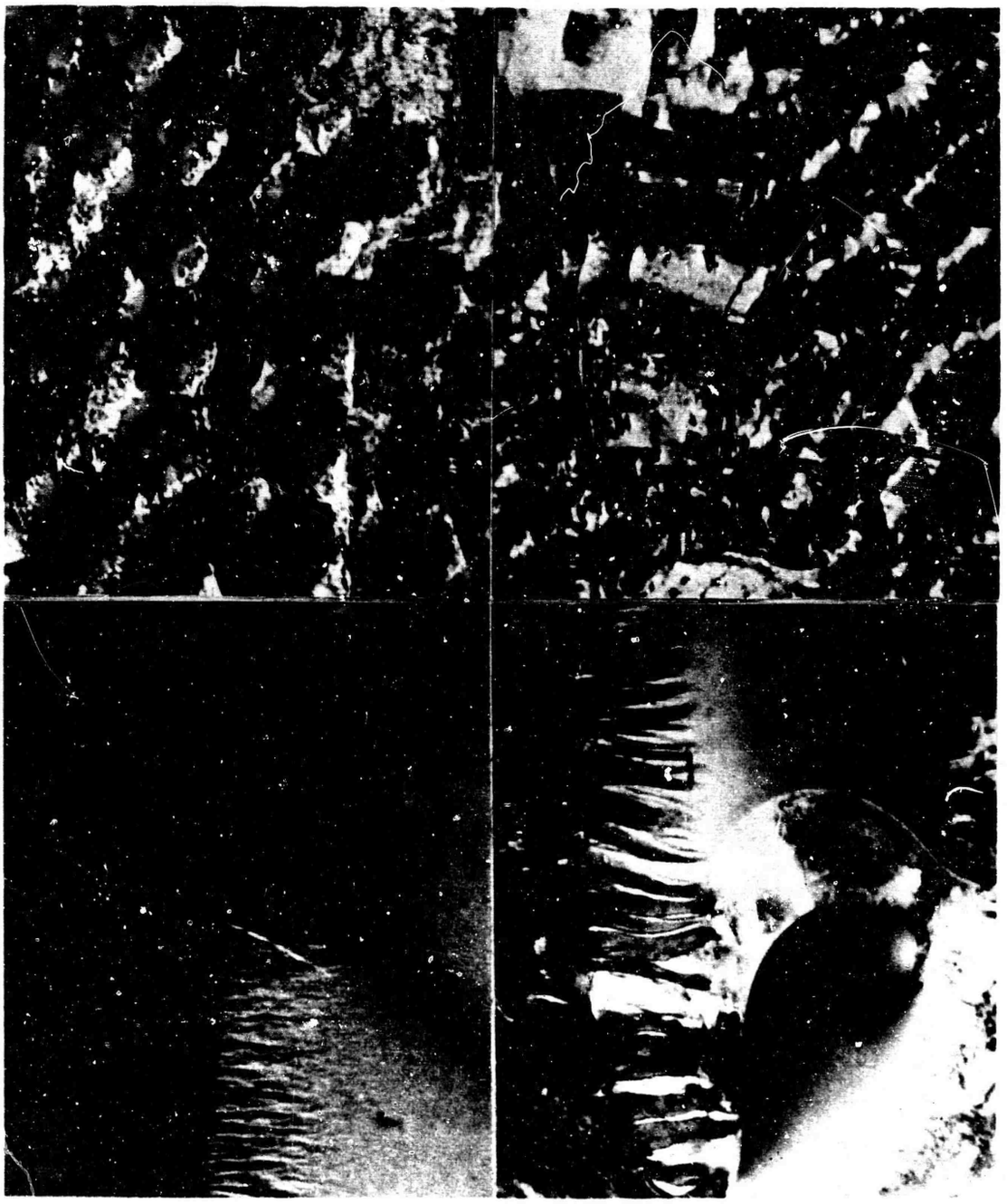

Figure 19 - Microstructures with petroleum-derivitive "PD" matrix, at top (Grafil HT filaments at left, Thornel 40 filaments at right); and areas of partially graphitized glasslike carbon resulting from the CTP + FA matrix, bottom. Polarized light, 1590 X.

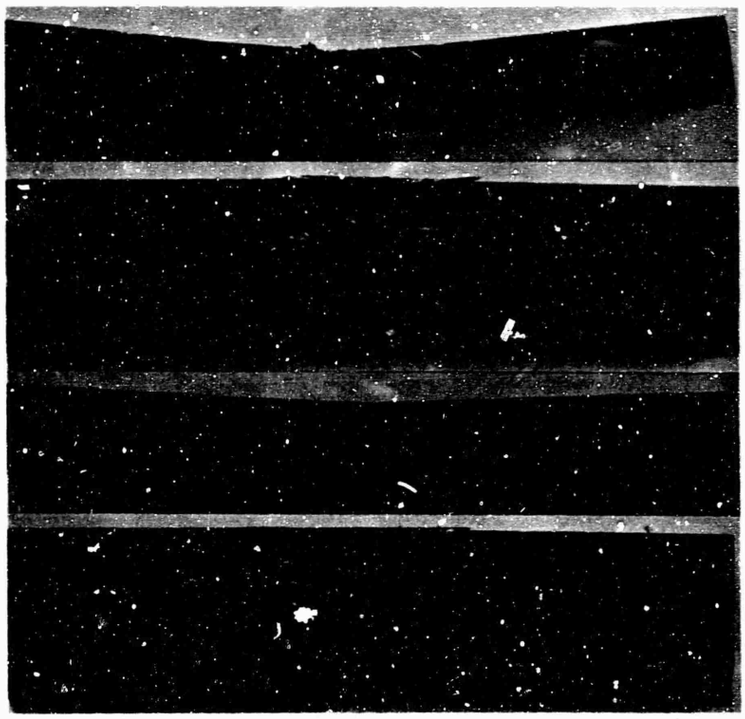

Figure 20 - Thornel-40 4-D bars after 3-point flexure test showing fiber angles; top: WYF # 5 (CTP + FA matrix, 7,970 psi strength); bottom: WYF # 7 (PD matrix, 28,250 psi strength). 1.85 X.

TABLE III

FLEXURE TEST RESULTS ON PITCH-IMPREGNATED 4-D COMPOSITES

Sample No.	Impregnant	D, g/cc	E, 10^6psi	FS, psi	Shear Stress, psi
WYF # 1	CTP + FA	1.75	2.3	7,450	458
WYF # 2	CTP + FA	1.75	2.3	7,630	476
WYF # 3	CTP + FA	1.75	2.4	7,720	477
WYF # 4	CTP + FA	1.75	2.6	7,970	498
WYF # 5	CTP + FA	1.73		7,480	
WYF # 6	PD	1.69	4.7	24,000	1500
WYF # 7	PD	1.69	5.5	28,250	1758
HT # 1	PD	1.77	0.3	3,920	245
HT # 2	PD	1.72	0.5	4,560	285

NOTES: WYF = Thornel 40 fibers; HT = Grafil HT (10,000 filament tow)
CTP + FA = Pitch followed by furfural impregnants (graphitized.)
E = Apparent elastic modulus calculated from calibrated movement between loading points in 3-point bend, on 2.00 inch span.
FS = Modulus of Rupture, calculated from simple elastic theory. Bars were all 0.50 inch wide and 0.25 inch thick.

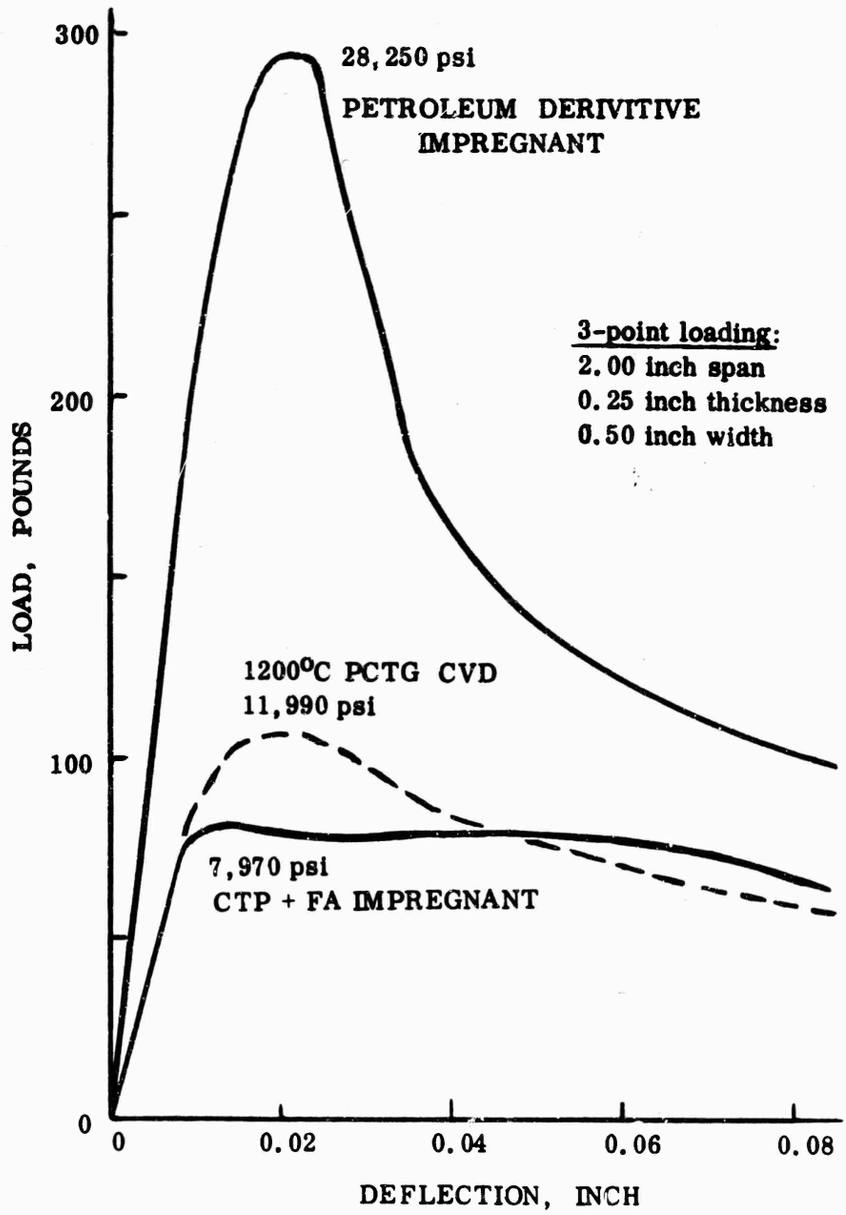

Figure 21 - Load-deflection diagrams of flexure tests on impregnated Thornel 40 4-D composites; test on CVD infiltrated composite from previous work shown for comparison (Vol. III p. 70.) The angle of fibers to tension direction, based on surface angles (Figure 20) are approximately 18° with the CTP + FA matrix and 14° with the petroleum-derivative (PD) matrix.

1. Preparation of Composites by Combinations of CVD Infiltration and Multiple Impregnation-Graphitization Cycles.

The composites processed for test in the second series were prepared using several combinations of infiltration, impregnation and heat treatment. The object was to prepare samples which had been subjected to high temperatures in which the microcracks resulting from thermal contraction were filled, as well as residual porosity, by repeated liquid impregnation and carbonization. The advantage of initial infiltration was intended to be a more rapid initial densification and creation of a matrix which might have higher strength and thermal stability than that resulting from liquid precursors. The experiment was designed to provide materials processed entirely by liquid impregnation for comparison, but the relatively long time for such processing required final densification by CVD infiltration of these samples in order to meet the test date.

Three types of processing were applied to reinforcements made from both low-anisotropy and high-anisotropy fibers. The increases in bulk density which resulted in the 3-D and 4-D composites are described in Figure 22.

Initially, all of the reinforcements were placed in a furnace, evacuated to ~1 torr, and heated to 1700°C for 1 hour; they were cooled under vacuum for 24 hours to a low temperature before the furnace was filled with nitrogen. This treatment resulted in the following weight losses:

4-D, C-3000:	- 1.9 %	3-D, C-3000 + CXH:	- 3.6 %
4-D, CXH:	- 4.7 %	3-D, CXH:	- 3.3 %
4-D, CXL:	-12.5 %		

The heat treated reinforcements were then cut into sections and subjected to either of three types of processing: (a) impregnation with coal tar pitch and carbonization at high pressure, followed by graphitization at 3000°C, (b) impregnation with phenolic resin and carbonization, followed by heating to 2700°C, or (c) CVD infiltration at 1 atm. pressure followed by a high temperature anneal and subsequent processing by either (a) or (b). In order to achieve a bulk density sufficient to qualify for test, many of the samples were given a final r.f. infiltration under the same conditions used for the samples in the first series of tests, after grinding to cylindrical blanks or tip configurations. All materials were heat treated at 2500°C or above as the final process step.

As indicated by the symbols in Figure 22, two techniques for initial CVD infiltration were employed. One of these was essentially identical to the r.f. procedure used for the first series of tests, except that the temperature was raised to approximately 1300°C, and the natural gas was diluted with hydrogen sufficiently to prevent sooting. Preliminary experiments indicated that this technique provided more rapid filling of the larger pores and produced a deposit which was as resistant to transformation during high temperature annealing as was the 1100°C r.f. deposit. Prior to the infiltration, the samples were heated one-half hour in hydrogen at the deposition temperature.

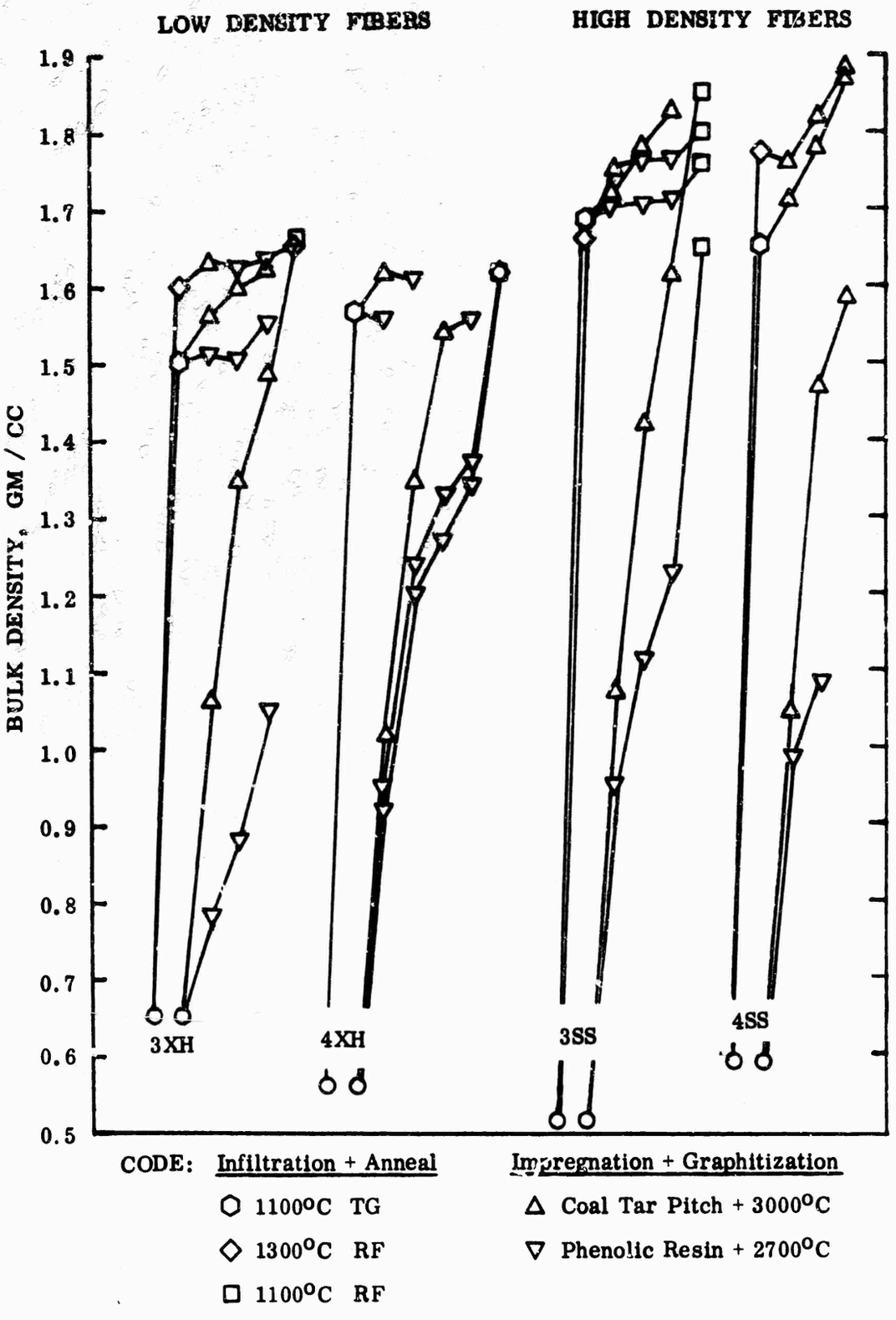

Figure 22 - Bulk density at successive process steps in 3-D and 4-D blocks.

The second procedure used for initial infiltration was a thermal gradient infiltration identical to that used to prepare the thermal shield composites discussed in Section III of this report. The procedure followed that developed by Gebhardt (Ref. 2, pp 184-194), and involved a long (167 hour) infiltration in natural gas at 1 atm. pressure with a substrate heated to a temperature estimated to be 1100°C throughout the infiltration (950°-1020°C monitored on a standard sight position). The strips were slit and packed in felt strapped to a graphite mandrel so that the cut surface was outermost and then covered with a layer of thin carbon felt. Sample thicknesses were 0.6 to 0.7 inch. The assembly was heated in hydrogen to the deposition temperature and held for one hour before deposition. The resulting deposit was similar to that created by the r.f. method, although the deposition temperature and rate were lower.

The infilitrated samples were annealed prior to further processing, primarily to remove residual gas and to generate thermal cracks which would permit better penetration of the impregnants. Then one set, together with a set of weaves which had not been infiltrated, was sent to the Y-12 plant of the Union Carbide Nuclear Corporation, Oak Ridge, Tennessee. The processing there was conducted without cost to the project by arrangement of the AFML project engineer, and was intended to explore the advantages of unique high-pressure impregnation and baking apparatus and techniques developed for discontinuous-fiber-reinforced composites (Ref. 5-6) in obtaining densification of the woven reinforcements.

The samples were all impregnated with Allied Chemical Corporation's CP-277-15V Grade coal-tar pitch. Three impregnation and baking cycles were conducted with a graphitization to 3000°C after each (some samples were included only in the third cycle). The density after each cycle is plotted in Figure 22. The exact procedure followed included the steps listed below (Ref. 7):

1. Samples were weighed, identified, and wrapped in carbon felt;
2. Evacuated to 200-500 microns for 4 - 8 hours;
3. Impregnated for 4 - 8 hours with coal-tar pitch at 200°C and an air overpressure of 50 psi;
4. Solidified pitch, and sealed parts and pitch in an evacuated stainless steel container;
5. Transferred assembly to autoclave and pressurized to 75 psi;
6. Heated autoclave to 200°C at 100° C/hour;
7. Pressurized autoclave to a pressure of 10,000 to 12,000 psi (required about one hour) and maintained temperature of 200°C;
8. Heated autoclave to 600° at 100° C/hour and maintained the pressure at 10,000 psi;
9. Heated from 600° to 700°C at same rate but reduced pressure to 9000 psi (this is to flush more argon through the container system);
10. Reduced pressure and temperature together to ambient conditions;
11. Removed, decanned, cleaned, and weighed samples;
12. Graphitized to 3000°C at 300°C/hour with a 1/2-hour hold at 3000°C, and weighed.

After the samples were returned from Y-12, the blocks which had been infiltrated and impregnated three times were sectioned, micropolished and examined for uniformity. Then a cylinder was ground from each, and samples were selected for nose tip specimens after a more accurate bulk density had been obtained.

The samples which had not been infiltrated first, or which had received only one cycle at Y-12, were not sufficiently dense to qualify for test without further processing. Some of these were infiltrated by the r.f. technique, and graphitized. Others were subjected to a series of phenolic resin impregnations (using Monsanto SC1008 resin) followed by carbonization in a 60 hour cycle to 1100°C and a graphitization. The results of these process steps, and the results on weaves which were subjected directly to phenolic resin impregnation and graphitization, are illustrated in Figure 22. All of the samples selected for test, except those having infiltration followed by three Y-12 impregnations, were infiltrated by the r.f. method as 0.5-inch diameter cylinders, and in some cases as finally ground nose tips, and given a final graphitization treatment to 2700°C.

In order to describe the rather complex process history, the samples were all coded to indicate the sequence of process steps. The abbreviations used are described in Table IV.

Microstructures are illustrated in Figures 23 through 28. The pitch produced a relatively fine-grained mesophase structure with the usual alignment parallel to fiber surface (Figure 23). The pitch and CVD carbon coated the surfaces of cracks which provided an indication of the stages of processing at which the cracks or phase separations had occurred (Figures 24 and 25). The pyrolytic carbon deposits were similar to those observed previously, except that soot was not found, and they showed the same resistance to change in structure during graphitization noted before.

The pattern of cracks which developed on cooling from the process temperatures probably has a significant effect on the thermal and mechanical properties and their dependence on orientation in these materials. Examples of the preferential location of these cracks, which originate from the anisotropy in thermal expansion coefficients inherent to the fiber bundles, are shown in Figures 26 through 28. A difference in patterns was particularly noted between samples impregnated directly and those subjected to an initial infiltration (Figure 26). The liquid impregnation apparently tended to rearrange the filaments, causing them to agglomerate, so that distribution was not as uniform as in the samples densified by CVD. Generally, cracks preferred to pass through fiber bundles rather than through the more random fiber-filled interstices or even at fiber bundle intersections.

TABLE IV

MATERIAL DESCRIPTION CODE

Characteristic	Abbreviation*	Detailed Explanation
Fiber Geometry	3	3-Directional Orthogonal (FMI Weave with 0.04-in. centers)
	4	4-Directional Omniweave or Braid
	7	7-Directional Orthogonal (FMI Weave with 0.1-in. unit cell)
Fiber Type (Refers to Axial Fibers in 3-D)	XH	Fiber Technology CX fiber with high temperature treatment (99 % carbon). Initial filament density = 1.43 g/cc
	XL	Fiber Technology CX fiber with low treatment temperature (88 % carbon)
	SS	Fiber Technology acrylic-type carbon tow (3000 or 2000 filament) Initial filament density = 1.75 g/cc
CVD Infiltration	11	Approximately 1100°C infiltration temperature.
	13	Approximately 1300°C infiltration temperature.
Liquid Impregnation	Y	High pressure impregnation and carbonization at Y-12 Plant, Oak Ridge, with 3000°C graphitization between cycles.
	R	Phenolic resin impregnation and carbonization at GE-RESD with 2500°C-2700°C graphitization between cycles.
Heat Treatment	A	Anneal at 2100°C - 2400°C.
	V	Vacuum anneal at 2100°C.
	G	Graphitization at 2500°C - 2700°C.

*Symbols are combined in order of processing; "t" refers to machining of tip.

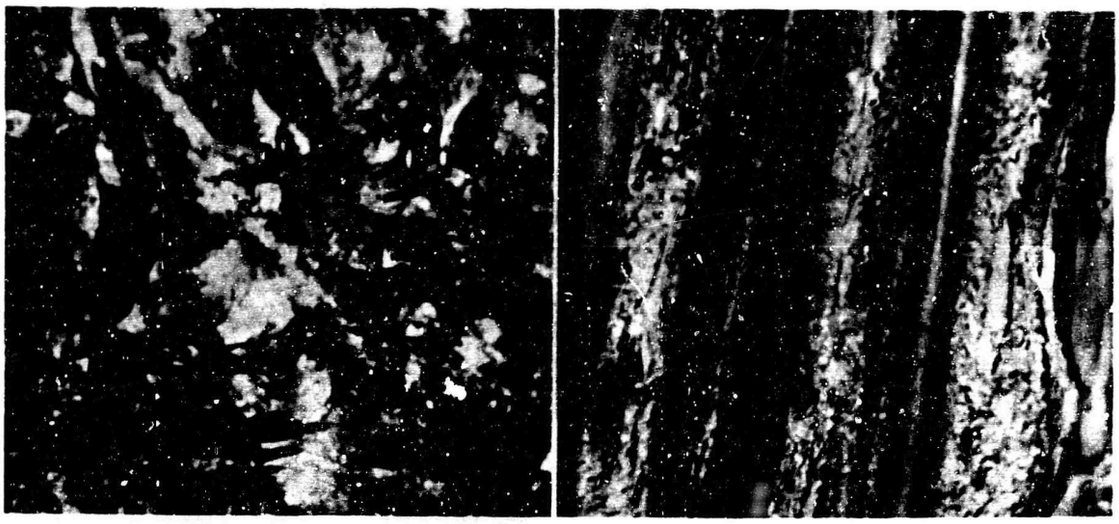

Figure 23 - Microstructure of graphitized 15V pitch in large pore (left) and in C-2000 bundle (right) of 3SSY11G. Polarized light, 1800 X.

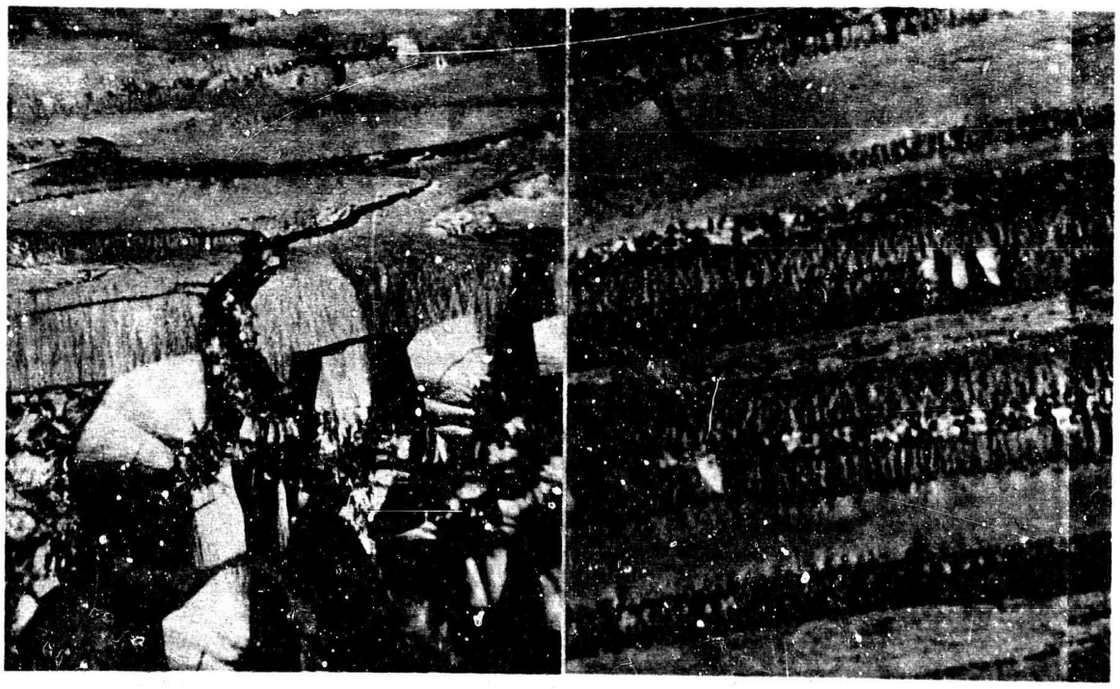

Figure 24 - Cracks in 3SS11AY: at left, crack through graphitized pitch which filled a previous crack in the CVD-infiltrated fibrous filler has penetrated the infiltrated axial C-2000 bundle (at top) and has been diverted by the fiber/CVD carbon interfaces (860 X); at right an initially cracked fiber (at top) has been partially coated by the 1100°C PCTG carbon (1800 X.) Polarized light, oil immersion.

Figure 25 - Cracks in 3-D composites: top left - crack in graphitized pitch and at graphitized pitch / fiber interface in a lateral (CXH) bundle in 3SSY11G; top right - graphitized pitch filled a prior fracture at fiber / CVD carbon interface in 3SS11AY, and then separated from both CVD carbon and fibers in the lateral bundle; bottom left,- a crack at C-2000 fiber and 1300°C r.f. infiltrated carbon is visible (center of view) in 3SS13AYRG11G; bottom right shows "glassy" 1100° deposit lining a crack in graphitized pitch which had penetrated a lateral bundle crack in 3SSi3AYRG11G. Polarized light, 1800 X.

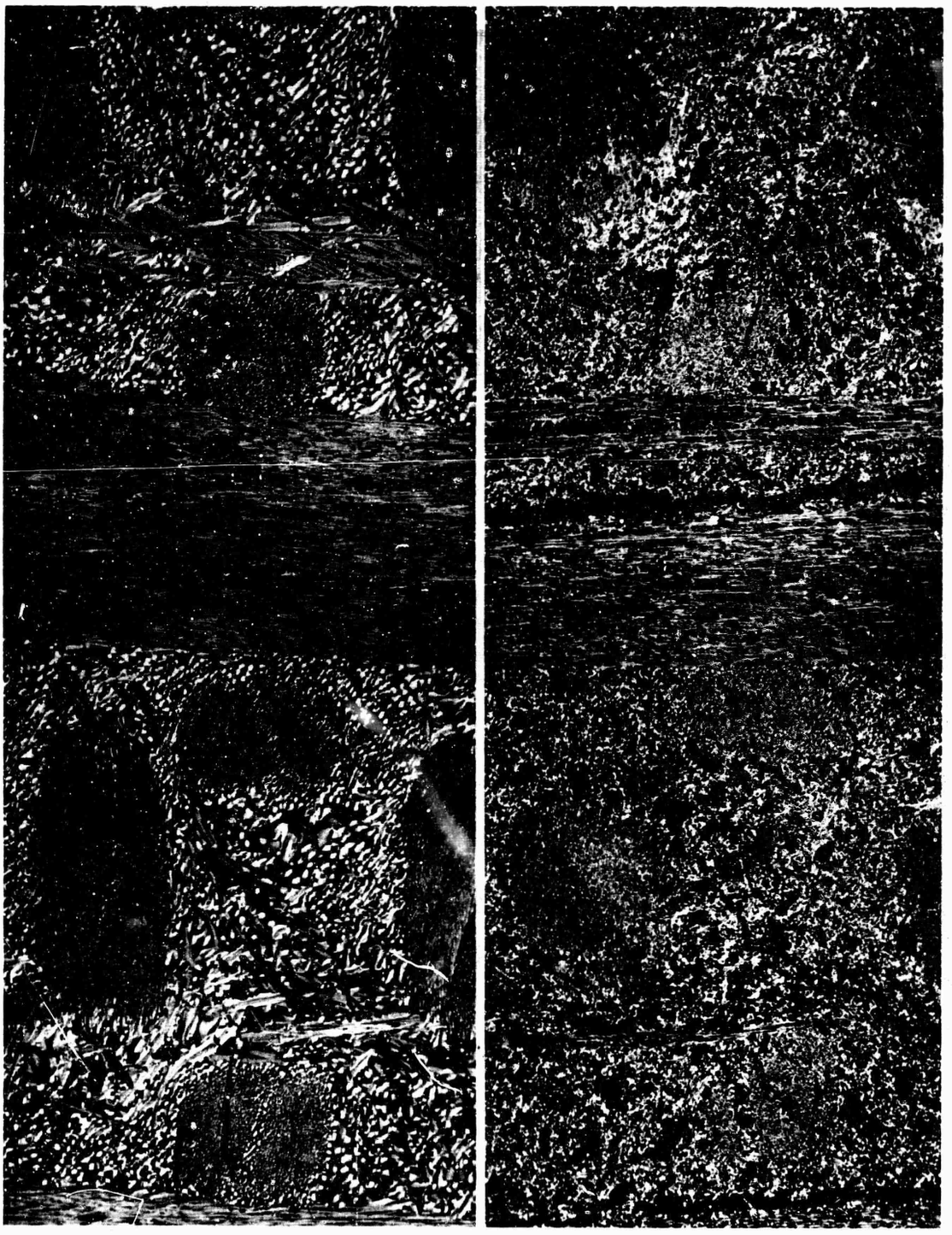

Figure 26 - Microstructures of models 3SS11VRGt11G, which was infiltrated and then impregnated with resin (left) and 3SSY11G. which was impregnated with pitch and then infiltrated (right) showing differences in cracks and porosity. Polarized light, 50 X.

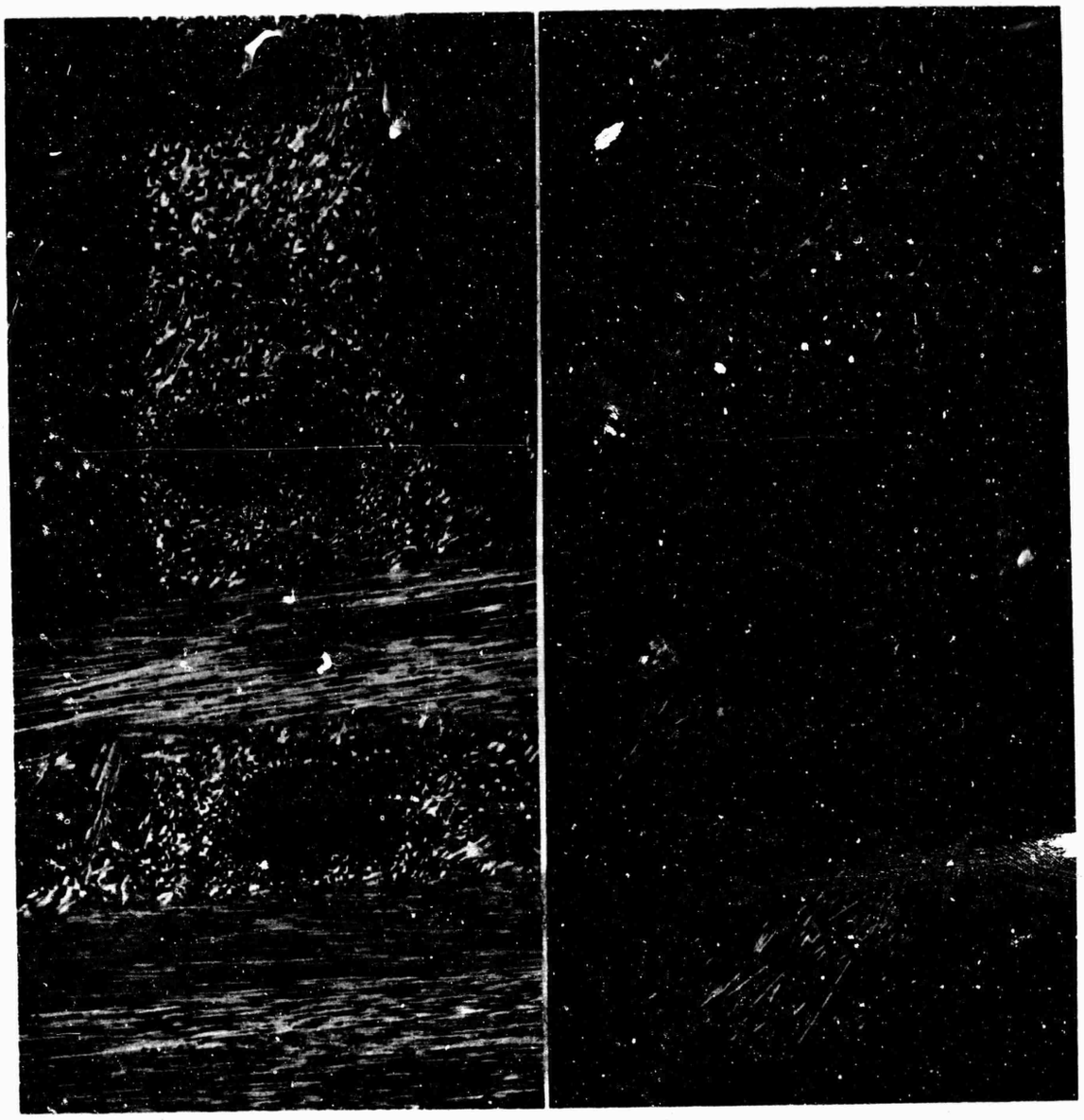

Figure 27 - Crack patterns in sample 3SS11VY (left) and 3XH11VY (right) with weaving direction horizontal. Polarized light, 50 X.

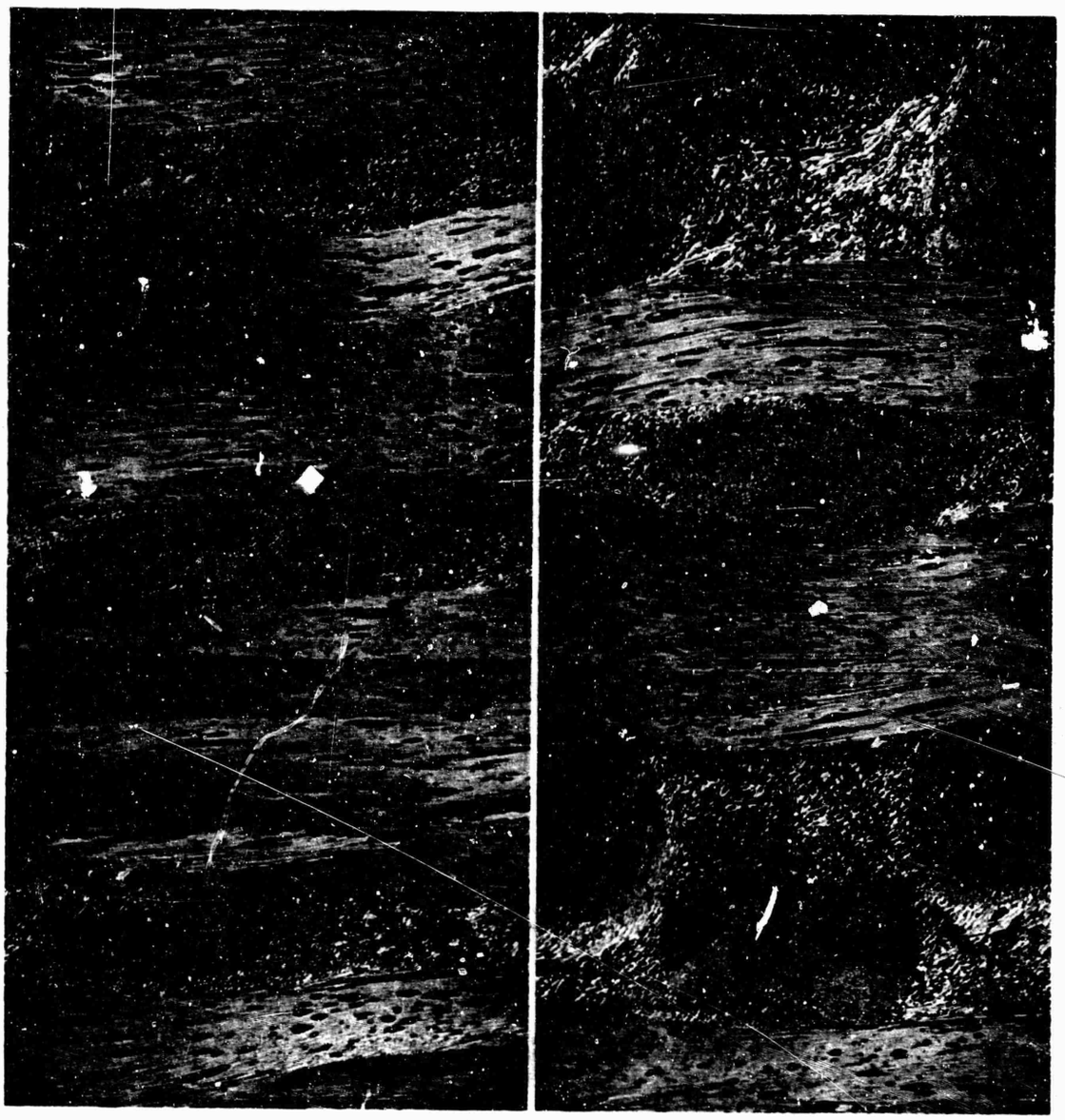

Figure 28 - Crack patterns in low-modulus fiber weave (3XH13GYRG) in slab, left, and in base of sample after ablation test (right.) Weaving direction is horizontal. Polarized light, 50 X.

Preliminary property evaluations were made on two of the composites, which had been CVD infiltrated and then impregnated three times at Y-12 with graphitization to 3000°C after each cycle. The blocks were sufficiently large that both a cylinder for ablation test and two bars, 0.25 x 0.4 x 2 inch in dimension, could be obtained from each. One bar was used for thermal expansion measurements, by intermittent heating in steps to 1900°F in the fused silica assembly of a Brinkman dilatometer. Then both bars from each composite were broken in flexure in 3-point loading on a 2.00 inch span, and the plot of load vs center-point deflection was obtained from the Instron chart record after correction for load cell deflection; rate was 0.02 in./min.

The thermal expansion data are presented in Figure 29. The coefficient at temperature, α_T, and the mean coefficient to temperature from 74°F are plotted as a function of temperature, as well as the linear expansion, to provide a basis for extrapolation to higher temperatures. The difference in coefficients between the composite with high-modulus acrylic-type precursor fibers in the direction of measurement, and the composite with low-modulus rayon-precursor fibers, is 0.8 x 10^{-6} /°F, which compares with 1 x 10^{-6}/°F for unidirectional bundles of similar fibers (AFML TR-69-57 Vol. III p. 73.) The bars changed dimension as a result of the heating, as follows:

Bar and Fiber Type	Length	Width	Thickness
3SS11VY (High Modulus)	- 0.25 %	+ 2.0 %	+ 0.8 %
3XH11VY (Low Modulus)	- 0.05 %	+ 0.8 %	+ 0.2 %

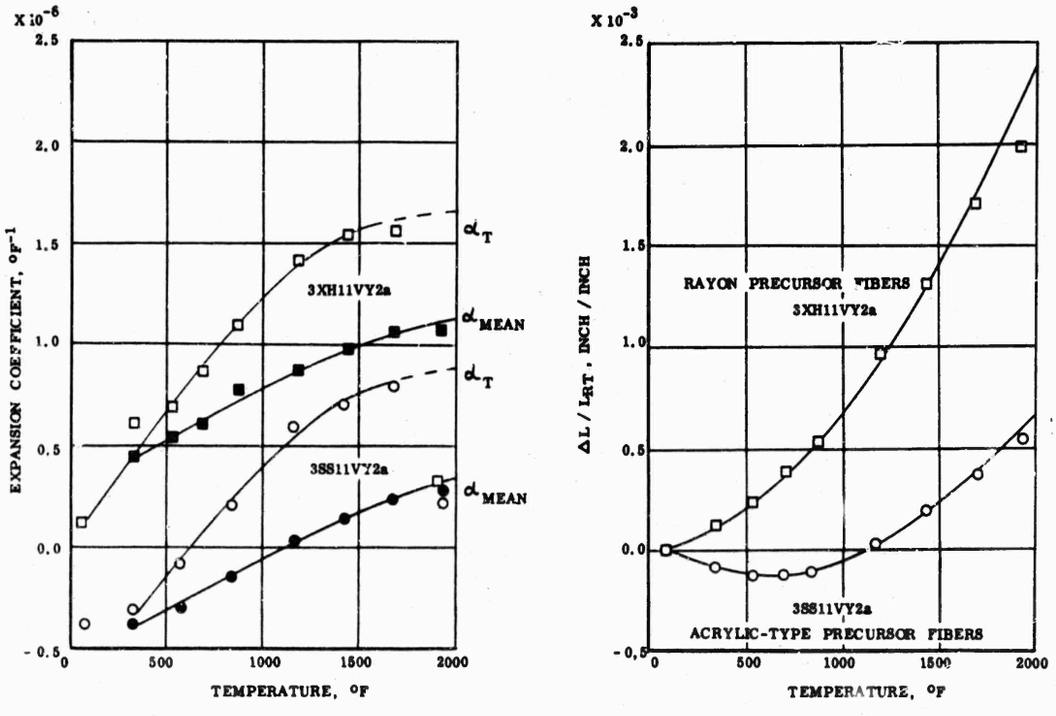

Figure 29 - Thermal expansion results on 3-D composites in the Z direction.

The flexure strength, apparent elastic modulus, and maximum shear stress were calculated assuming simple beam theory, and are presented in Table V The bars did not separate upon fracture, as would occur with a polygraphite when tested in this manner, and the crack propagation path on a side of the bar, which had been micropolished before machining, is illustrated in Figure 30. The load-deflection curves are shown in Figure 31. A test on a bar of fibrous graphite IP-50 used for ablation comparisons is shown for comparison; this bar, which had 0.376 inch width and 0.251 inch thickness, had been prepared with a similar pitch and processing heat treatment; it showed an apparent modulus of 1.1×10^6 psi and broke at 6,400 psi.

The load-deflection diagrams were plotted in order to compare relative toughness, or work to fracture, which is essentially the same as impact strength if there is no effect of loading rate. Because of the high strength and incomplete crack propagation, the area under the curves, normalized to uniform bar dimensions, is several times the area under the IP curve, which is representative of bulk graphites. In comparison with similar curves of 4-D composites (e.g. Figure 21 in this report and Vol. III, p. 70), however, the 3-D reinforced composites have much less toughness.

The low-modulus composite has a toughness similar to that of the high-modulus composite in spite of the lower strength. Based on the flexure data, modulus is only 37 % as great (in the Z direction) and strain to failure is 2.3 times as high. Since the difference in modulus is greater than the difference in thermal expansion coefficients, the high-modulus composite probably has a lower resistance to failure from thermal stress in the Z direction. The apparent moduli of elasticity are lower than data which would be obtained in tension; other comparisons of 3-D composites tested in tension and flexure suggest that tensile modulus may be estimated as 8×10^6 psi for 3SS11VY and 2×10^6 psi for 3XH11VY, based on the flexure tests.

Figure 30 - Micropolished sides of flexure bars after test, showing fracture paths; 3XH11VY-2b left (low-modulus axials), and 3SS11VY-2a right (high-modulus axials.) 10 X.

TABLE V

FLEXURE TEST RESULTS ON 3-D COMPOSITES

Sample No.	Section, in. Width	Height	Density g/cc	Apparent E, 10^5 psi	Flexure Strength psi	Shear Stress psi
3SS11VY2a	0.459	0.252	1.83	6.2	27,700	1,740
3SS11VY2b	0.480	0.250	1.82	6.35	27,400	1,710
3XH11VY2a	0.429	0.250	1.67	1.6	17,100	1,070
3XH11VY2b	0.471	0.250	1.65	1.75	19,250	1,205

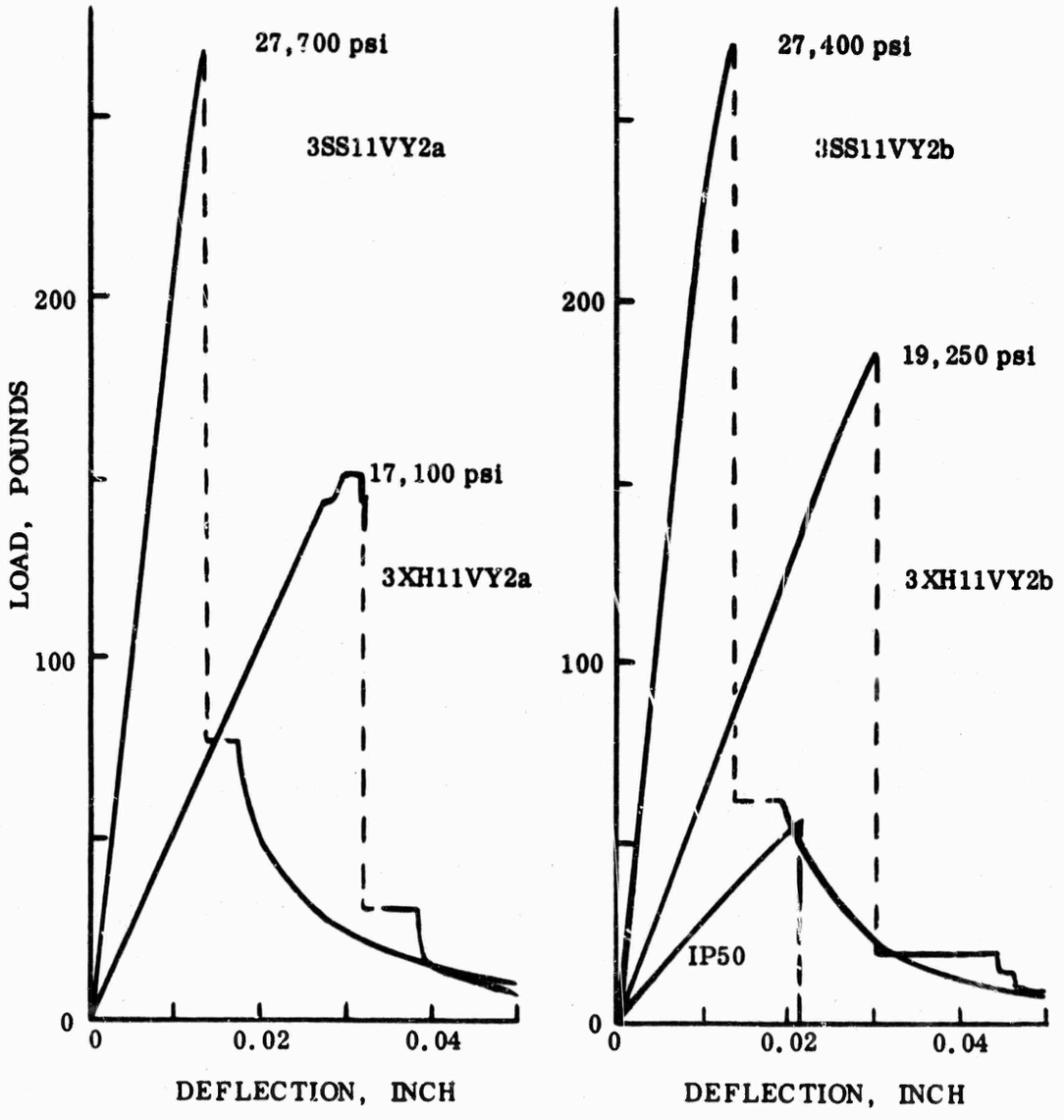

Figure 31 - Load-deflection curves for 3-D composites in 3-point bend.

3. 7-DIRECTIONAL REINFORCED MATERIAL DEVELOPMENT

a. Initial Feasibility Demonstration

In 1969 the first woven 7-directional reinforcement was prepared by Fiber Materials Inc., Graniteville Mass., and the structure was evaluated by radiography (see AFML TR 69-67 Vol. III - AD 868270, pp 15-18.) During 1970 preliminary properties were determined from a portion of this billet after densification by chemical vapor deposition. Subsequently, two fine-textured billets were prepared with different fibers and processed for a further evaluation of the potential of such materials for nose tips.

The 7-directional geometry, illustrated below, contains three 3-D orthogonal directions, which will be designated X, Y, and Z, where Z is the weaving direction. The other reinforcements, termed T, U, V, and W for the purposes of this discussion, are parallel to the corner-to-corner diagonals of a cube.

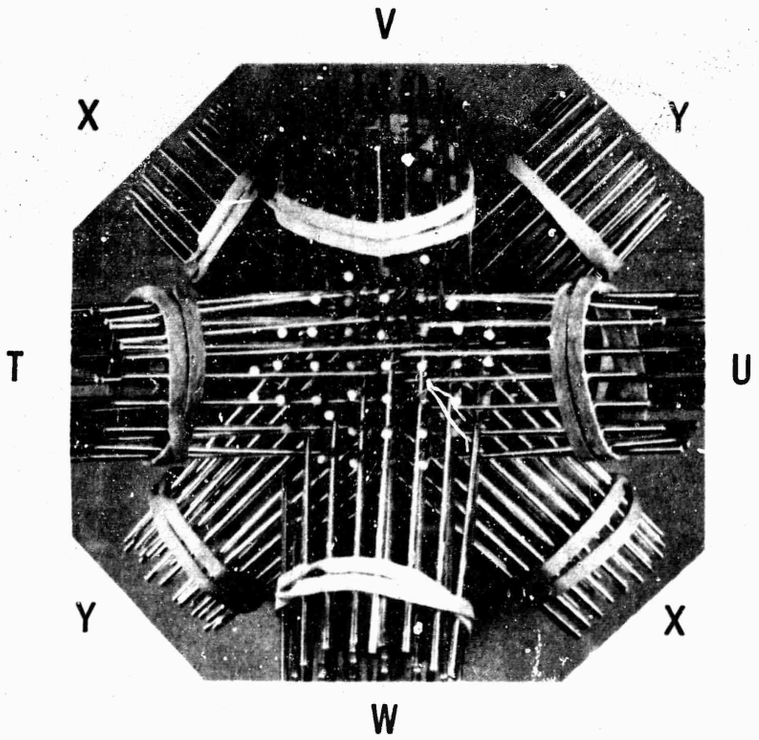

Figure 32 - Model of 7-Directional reinforcement, viewed parallel to "Z" direction; 3-D orthogonal directions are XYZ; 4-D diagonal directions are TUVW.

The original billet contained 16 ends of Fiber Technology Inc. CXH 2-ply carbon in each of the seven directions. The unit cell was a 0.25-inch cube, since the 3-D lattice points, half of which are filled in a checkerboard fashion, were 1/8 inch center-to-center.

From the 2-in. square billet, 4 inches long, a length slightly more than 1 inch was removed for processing to determine order-of-magnitude properties resulting from filling with a CVD-carbon matrix. The remainder of the billet was not processed because the coarse texture did not permit specimens of sufficient size for reliable mechanical property determinations. This material may be used in future comparisons of different types of matrix processing.

The block was first infiltrated to 1.5 g/cc bulk density (initial weave density was 0.53 g/cc) by inducing current directly in the weave while suspended in a stream of methane at 1 atmosphere; surface temperature was about 1100°C. The block was sectioned into two ½-inch pieces at this point, and one half was further infiltrated to about 1.6 g/cc. Both were then heated in argon to 2750°-2850°C, which resulted in an expansion of about 2 % in all dimensions and 0.25 % loss in weight. One of the blocks, which contained the billet end, was kept for display, and the other was reinfiltrated as before to a final density of 1.65 g/cc, as measured from weight and dimensions after grinding. A single flexure specimen and a plate-slap specimen were then machined from this block, with surfaces parallel to the X and Y lattice elements.

The flexure specimen was 0.431-in. wide, 0.364-in. thick (loading direction) and 2.004-in. long. It was tested in 3-point loading on a 2.00 inch span. Calibrated deflection between loading points indicated an apparent elastic modulus of 0.5 x 10^6 psi, assuming simple beam theory (as-deposited 3-D and 4-D samples made from the same fiber showed values of 1.5-2.0 x 10^6 psi and 0.8 x 10^6 psi in identical tests on bars with the same thickness/span ratio.) This indication of low elastic modulus is consistent with effects of graphitization on carbon composites generally.

The flexure strength, which, like apparent modulus, may deviate from tensile values by as much as 2X, was comparable with values obtained on 3-D and 4-D CVD infiltrated, CXH-reinforced samples with the same aspect ratio. The 8800 psi modulus of rupture corresponded to 820 psi shear stress (from simple beam theory) and fracture occurred on the tensile side. As shown in Figure 33, crack propagation was incomplete (the "Y" bundle in the center of the tensile surface did not fracture) and 20.6 % of the failure load was held before further deflection was imposed. This result indicates good crack propagation resistance, or fracture toughness, inherent to this reinforcement geometry.

The plate slap specimen was checked ultrasonically before test with longitudinal waves at 0.65 MHz, using a ½-inch diameter transducer. The block was 0.443 inch thick in the "Z" direction and 1.645 g/cc average bulk density. Five measurements showed an average of 4.18 mm/microsecond, or a sonic modulus of 4.2 $\pm$ 0.3 x 10^6 psi. Attenuation was 29 $\pm$ 3 db/ cm. Radiographs, Figure 34, showed some porosity remaining in the 7-D lattice interstices.

After test at 3000 taps with a 12 mil aluminum flyer, only superficial damage was apparent, as shown in Figure 35.

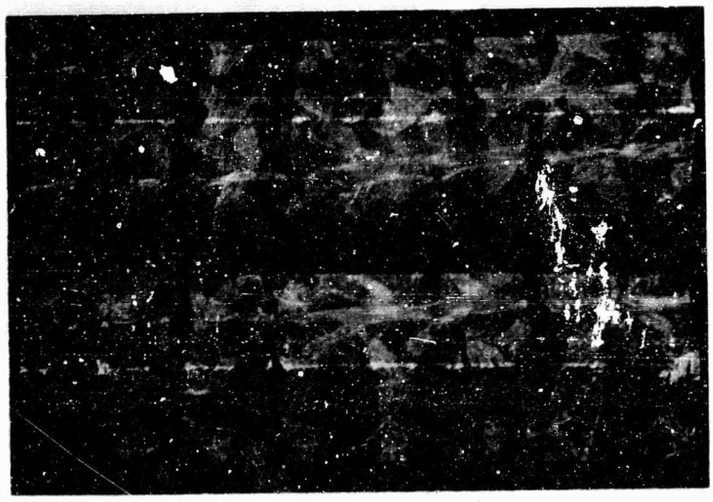

Figure 33 - Flexure specimen 7-D-1a after maximum load at 8,830 psi apparent maximum fiber stress; tensile surface (center) and two sides show incomplete crack propagation at boundaries between elements; 20.6 % of load was held after maximum. 1.85 X

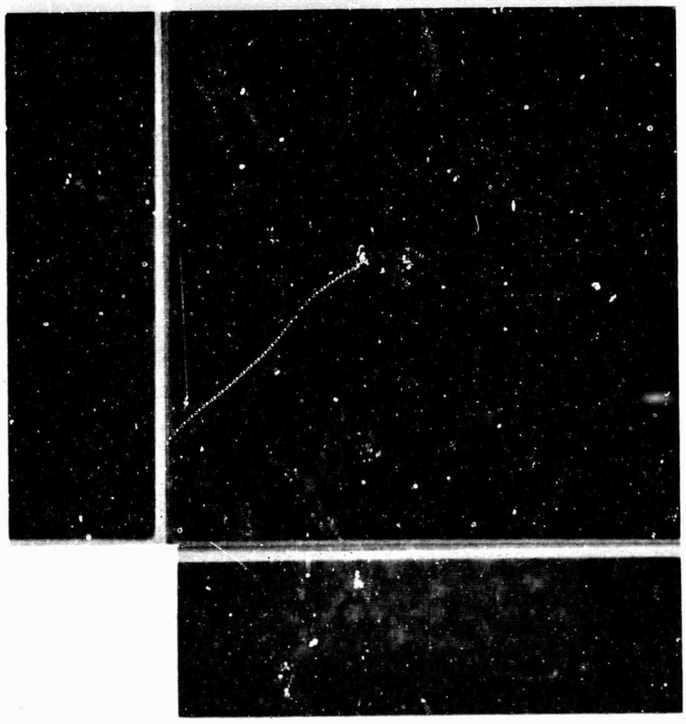

Figure 34 - Radiographs of specimen 7-D-1 before plate-slap test. 1.9 X

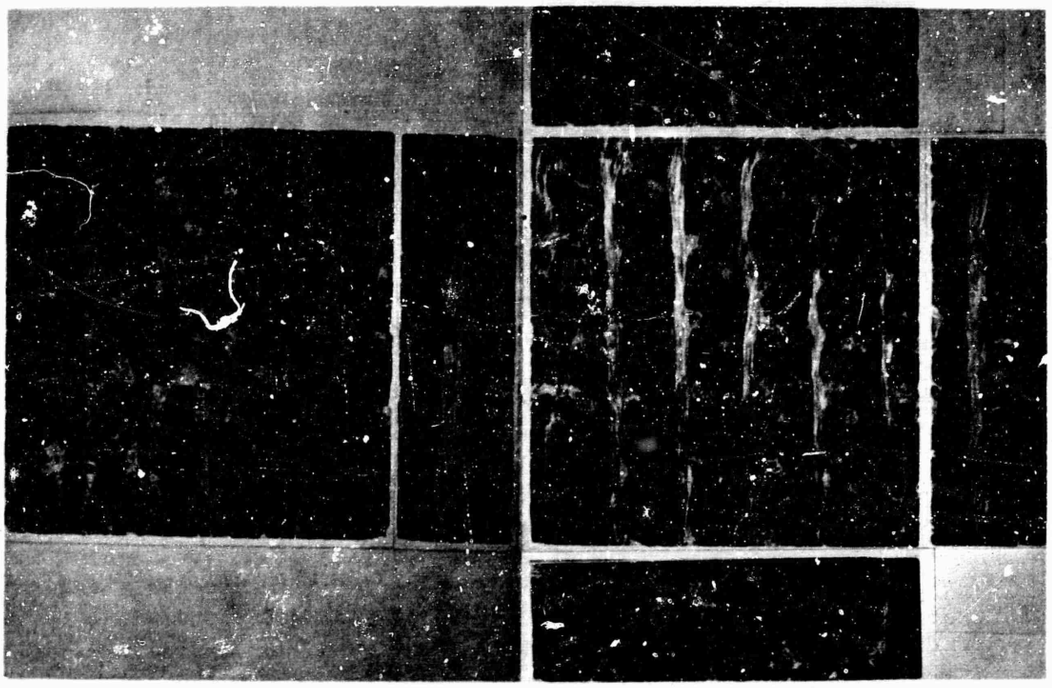

Figure 35 - Plate-slap sample 7-D-1 after impact at 3000 taps; no damage except for chipping of two 4-D elements from edge on impacted surface. 1X

These initial results on the coarse-textured billet indicated a general performance level sufficient to pursue the concept for hardened nose tips. A second stage of effort was thus defined with the following objectives:

(a) Demonstrate feasibility of fabricating the 7-D geometry with a fine texture (0.05-in. center-to-center spacing in the 3-D lattice), required for adequate ablation performance, with both low and high modulus fibers.

(b) Obtain high-shear ablation data in comparison with 3-D and 4-D geometries with similar fibers and process histories.

A third stage of effort would evaluate feasibility of scaling the fabrication process to dimensions suitable for nose tips (4 to 6 inch diameter), optimizing the matrix processing, and determining thermal-mechanical properties required for nose tip design. A final stage of effort would fabricate nose tips and verify the superior resistance to fracture which should result from such a rigid reinforcement network, in both thermal stress and impact.

b. Fabrication and Processing of Fine-Textured 7-D Billets

Two additional billets, nominally 1.1 inch square by 2.5 inch long, were fabricated by Fiber Materials Inc. The first of these was prepared from 2 ends of CXH 2-ply yarn in each direction, and Fiber Technology acrylic-precursor carbon C-2000 (2000 filament tow) was used in the second. Both were

prepared with a nominal 0.05 inch between centers in the 3-D lattice. Properties of the batch of C-2000 were 310,000 psi single-filament tensile strength and 45 x 10^6 psi modulus, with density by sink-float immersion of 1.70 to 1.75 g/cc and cross-sectional area of 0.5 to 0.6 x 10^{-7} in^2.

As received, the billets showed excellent uniformity and freedom from imperfections, as shown by the radiographs in Figures 36 and 37. Unlike the first billet, a hump resulted on the XZ and YZ sides. The bulk density was estimated by surrounding the billets with a thin plastic bag, partially evacuated so as to conform to the surface, and then immersing in water to determine volume. The billet "7XH" (made from CX-2) thus had 0.54 g/cc bulk density (120 cc volume), while "7SS" (made from C-2000) had 0.51 g/cc (93 cc volume).

The billets were heated to 1700°C in vacuum (about 1 torr) for 1 hour for surface purification. Weight losses were 5.34% for 7XH and 4.97% for 7SS. They were then infiltrated by induced heating to about 1300°C surface temperature in natural gas at 1 atmosphere and annealed in argon to 2200°C for 10 minutes. The heat treatment resulted in 0.40% weight loss in 7XH and 0.23% loss in 7SS (infiltrated), and both expanded 1.6% in length. After this treatment each billet was sectioned approximately in half in a plane close to XZ (or YZ). The polished surfaces were photographed to show lattice uniformity, illustrated in Figures 38 and 39. The two halves of each billet were then ground to blocks, and bulk densities were estimated from weight and dimensions as follows: 7XH13 A = 1.50 g/cc; and 7SS13 A = 1.60 g/cc.

The first half in each case was submitted to Y-12 for one impregnation and pressure baking with 15V coal tar pitch and graphitization to 3000°C. The second half was impregnated with SC1008 phenolic resin, after graphitization to 2500°C, baked and reimpregnated before final treatment. Subsequent processing by phenolic resin impregnation and graphitization was conducted exactly as with the 3-D blocks. The samples were ground to cylinders, r.f. infiltrated, graphitized and r.f. infiltrated and graphitized again. The final infiltration was conducted on samples after grinding to nose tips in one set, and not in another set. The changes in density with these process steps are shown in Figure 40. Expansion in volume during the graphitization tended to offset the weight pick-up. The composite with high-modulus fibers (7SS) generally expanded more than the other (7XH); in final graphitization of the tips for 1 hour at 2500°C, for example, volume based on stem dimensions increased an average of 0.59% for four 7XH models and 0.85% for four 7SS models.

Microstructures are illustrated in Figures 41 to 44. The difference between the pitch and resin structures was most noticeable in the larger interstices (Figure 41). As resin penetrated a crack, Figure 42, it developed a structure which graphitized close to the fibers, but remained as a "glassy carbon" in the larger volumes. The crack patterns, Figures 43 and 44, showed some separations at bundle intersections, with occasional cracking at certain orientations within bundles. These crack patterns should be studied more thoroughly in their relationship to mechanical and thermal properties.

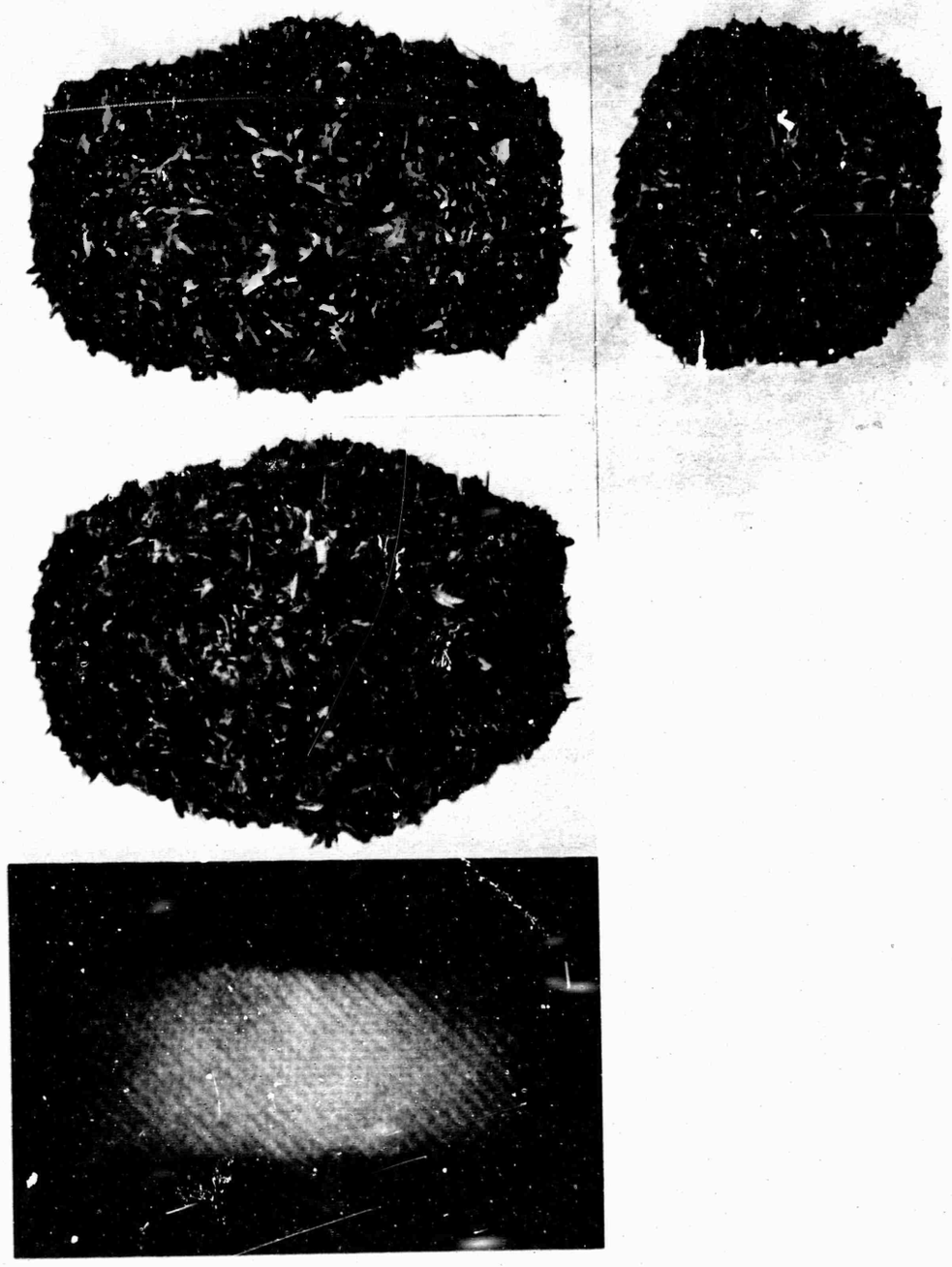

Figure 36 - 7-Directional Reinforced billet made from CXH fiber; top: Z direction (right) and direction bisecting X and Y (left); bottom: surface and radiograph in X or Y direction. 1 X

Figure 37 - Billet 7SS (C-2000 fiber) radiographed in X direction (left), X-Y bisection direction (center) and W (4-D) direction (right.)

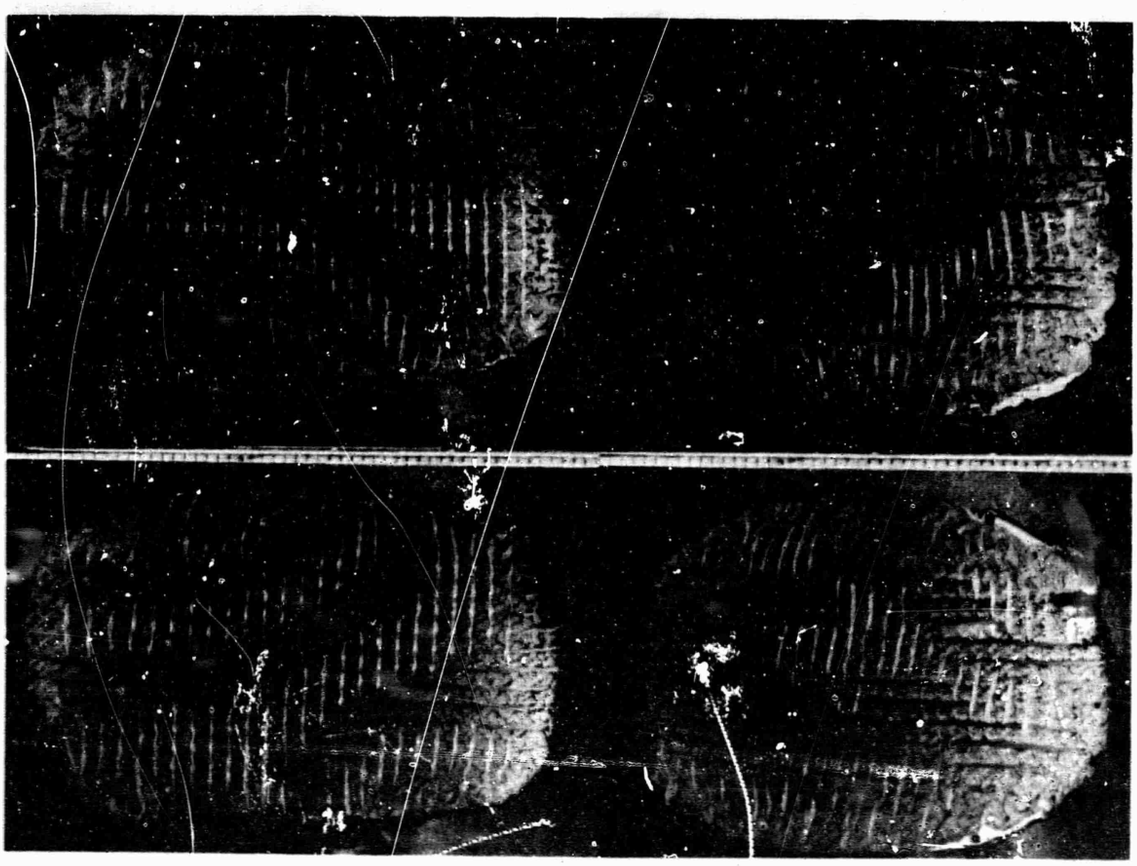

Figure 38 - Infiltrated and annealed billets sectioned to show structure; 7XH, left, 7SS, right. 1.0 X

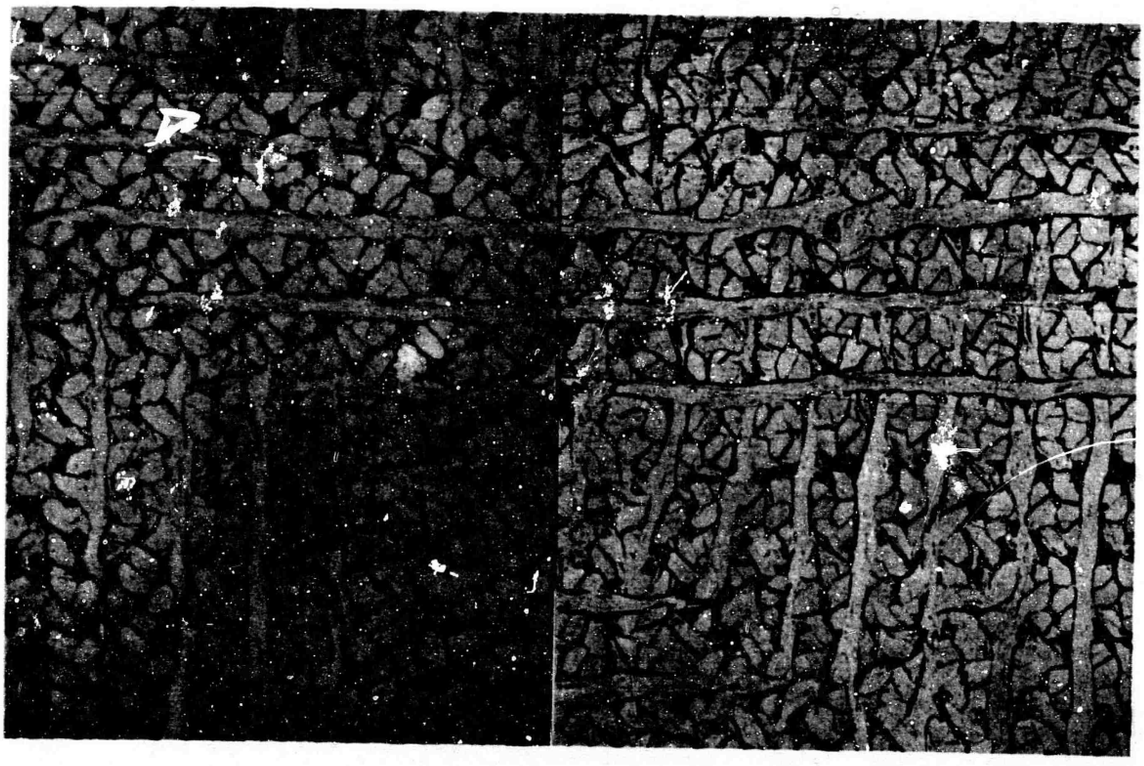

Figure 39 - Polished sections of 7XH13A (left) and 7SS13A (right) at 3.9 X.

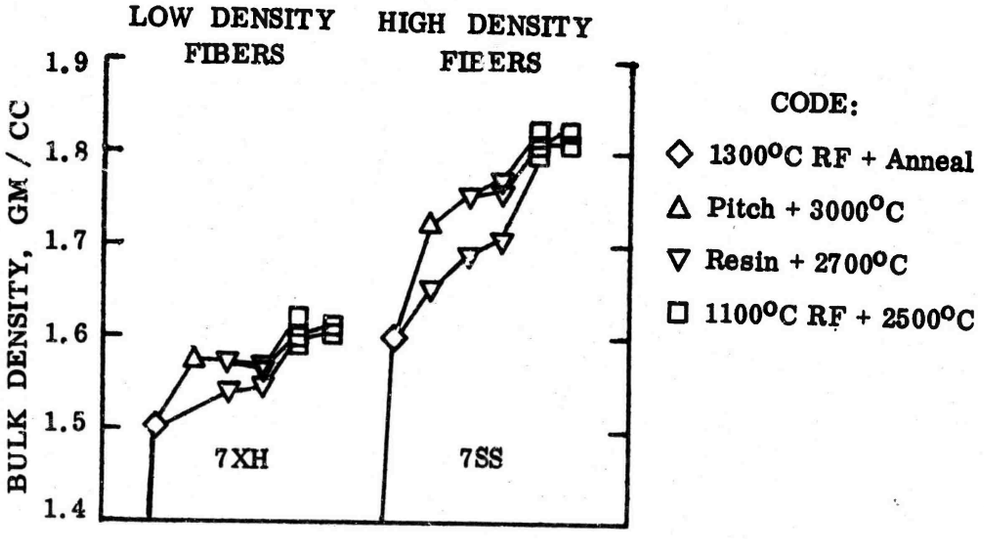

Figure 40 - Bulk density at successive process steps in 7-D composites.

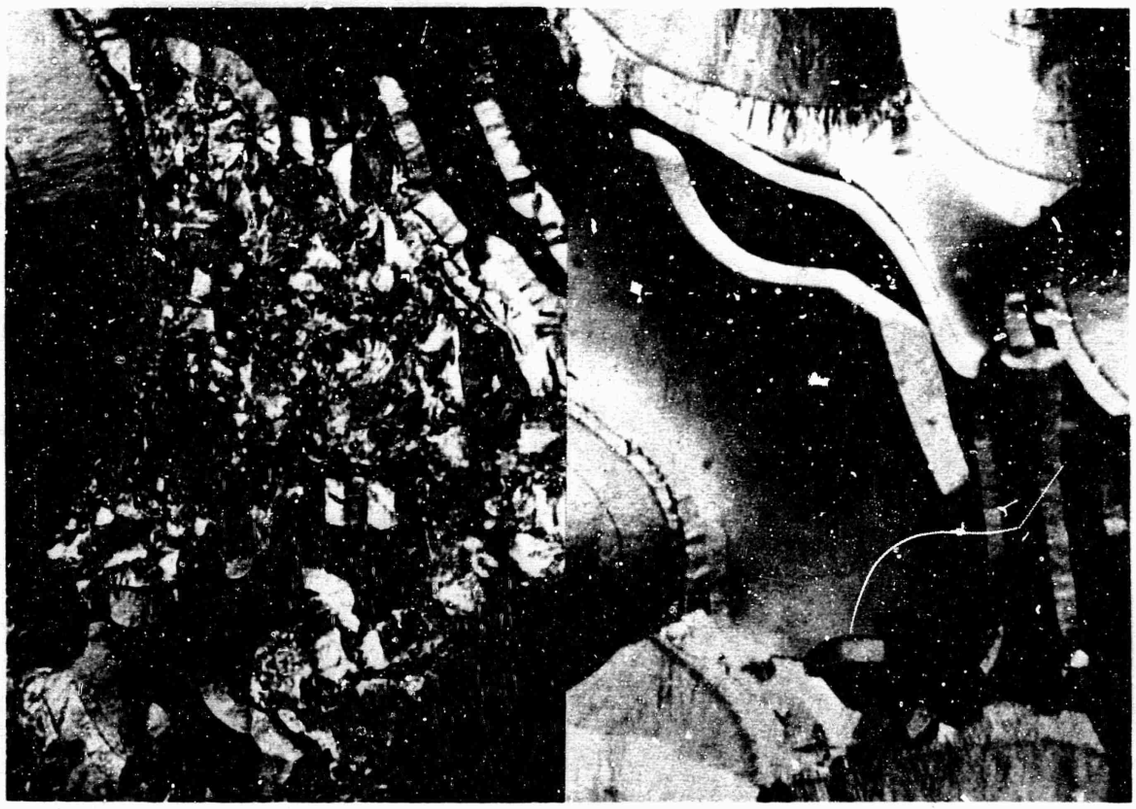

Figure 41 - Microstructure resulting from interstice filling in 7-D composites with 15V pitch (left) and phenolic resin (right); CVD infiltrated and graphitized (samples 7SS13AYRG(2)11 and 7SS13ARG(2)11). Polarized light, 1390 X.

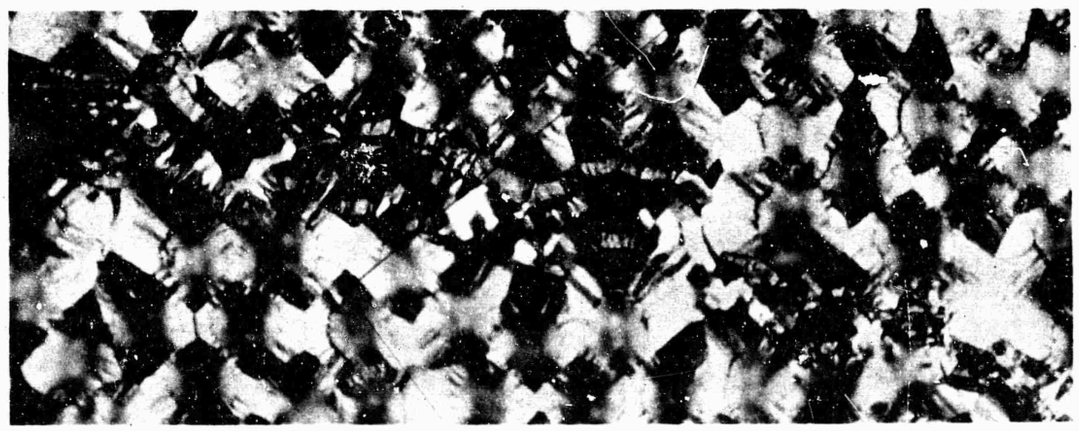

Figure 42 - Change in structure resulting from penetration of crack in fiber bundle with phenolic resin (from left); sample 7SS13ARG(2)11. Polarized light, 1390 X.

Figure 43 - Typical section in ~XY plane of 7-D composite with low-modulus fiber bundles (7XH13AYRG11G), showing pattern of cracks and residual porosity; "Z" bundles are triangular-section bundles in four corners and at center of figure. Polarized light, 50 X.

Figure 44 - Section in ~XY plane of high-modulus 7-D composite 7SS13AYRG11G; "Z" bundles, which are smaller than in low-modulus composites, are at center and four corners of the figure. Polarized, 50 X.

4. MATERIALS USED FOR ABLATION COMPARISONS

a. ATJ-S Comparison Standards

The ATJ-S standard models were obtained from two sources. The first was cut from a broken model which had been included in tests in the 50 MW arc at AFFDL. This came from a "cored" billet in which the center had been removed at a bulk density of 1.5 g/cc, before impregnating and graphitizing to 1.84 g/cc. This material was free of discontinuities observable by radiography and had only 0.001 weight per cent ash.

The other ATJ-S models (numbered 2 through 7) were cut from adjacent regions of a billet which had been used in other test programs at GE-RESD. Radiographs of these models showed spots of calcium concentration typical of ATJ and ATJ-S which is not specially treated (the ATJ model holders and pressure models also showed such spots). Rather large turbulent erosion pits developed in these models late in the runs. In one case, model #5, calcium oxide concentrations were found at the base of two of the pits; however, a definite correlation between these concentrations and the turbulent erosion was not established.

All of the ATJ-S models were cut with axes parallel to the across-grain orientation (parallel to billet molding direction) as shown by the relative heights of the X-ray diffraction peaks recorded by an X-ray spectrometer with the beam focussed on the base of the models after test.

b. Discontinuous Carbon-Carbon Composite Materials

The second series of ablation tests included samples of fibrous graphite prepared at the Y-12 plant, Union Carbide Nuclear Corporation, Oak Ridge, in addition to ATJ-S from the same billet used in the first series of tests. The samples were representative of materials characterized in terms of ablation performance and physical properties by the Sandia Corporation, and were taken from batches having two different density levels. These materials had been prepared with the same pitch impregnant and processing used in the experimental composites processed at Y-12 for AFML use in this program.

These comparison samples were taken from batches identified as IP50 (provided by I. Auerbach of the Sandia Corp.) and IP59 (provided by J. L. Cook of Y-12, Oak Ridge). The processing techniques and preliminary ablation data on this class of materials have been reported by these authors (Refs. 5-9). Both materials contained about 35 volume per cent of rayon-precursor fibers about 2 microns wide and 250 microns long. Approximately isotropic agglomerates of these fibers had been prepared by blending with coal tar pitch (15V) and compacting warm under isostatic pressure, then grinding to about 0.03 inch diameter granules. Billets were prepared by warm isostatic pressing and pressure carbonization and densified by several pressure impregnation-carbonization cycles with graphitization treatments at 3000°C. The resulting materials have low anisotropy, (1.1-1.2 radial/axial and radial/tangential thermal expansion ratios), and performance in nose tip ablation simulation tests and in predicted resistance to thermal stress failure which are similar or superior to ATJ-S (Refs. 5-9).

Microscopic structural characteristics are illustrated in Figures 45 - 48. Note the finer pores but larger "grains" compared with ATJ-S, and the presence of glassy carbon "lakes" in IP-59. Mercury porosimetry at Y-12 showed a smaller total porosity (10% compared with 14 %) in IP59 and a smaller channel size (over 90 % of channels below 0.3 micron equivalent diameter.) (Ref. 5 .)

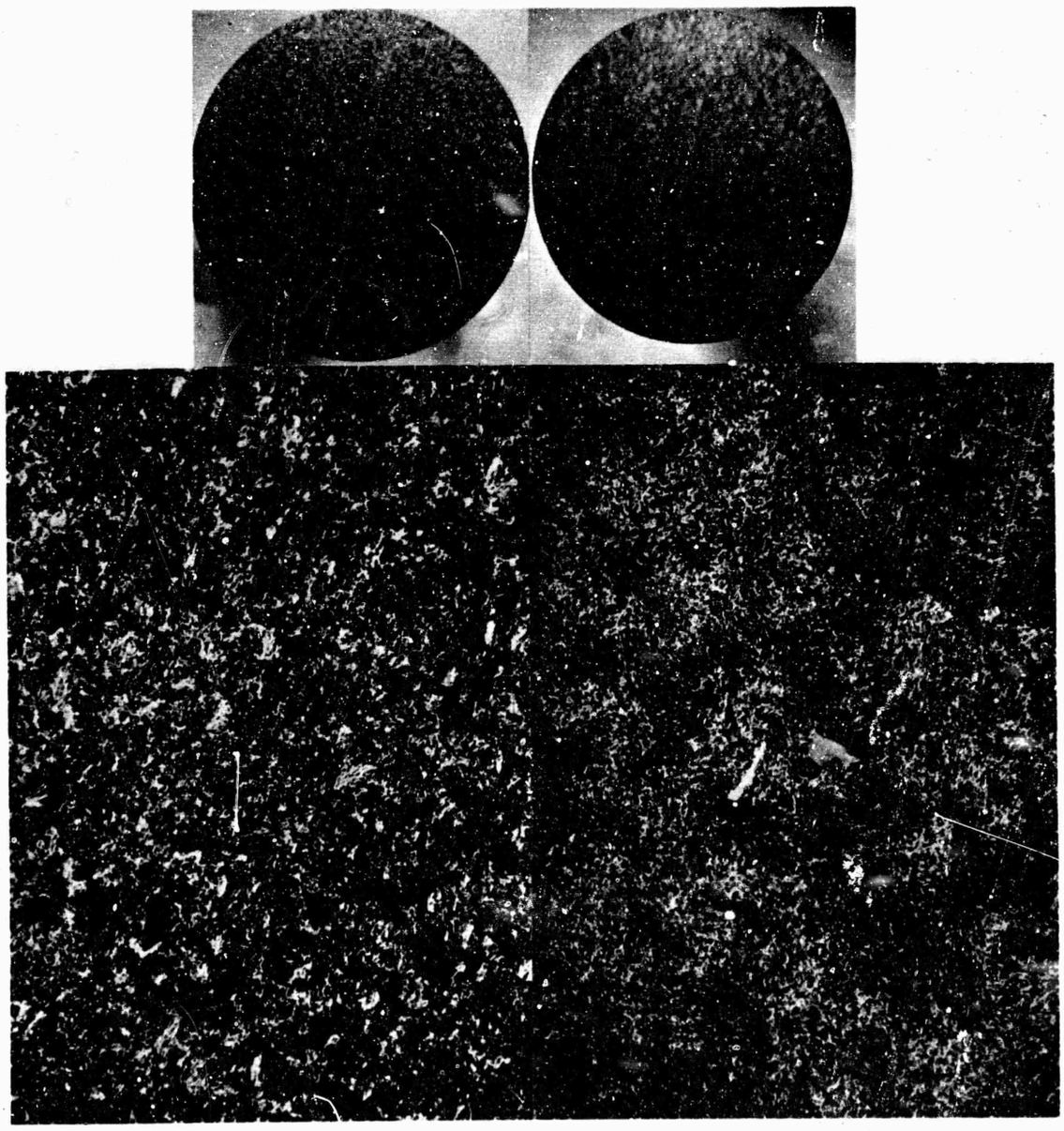

Figure 45 - Comparison of ATJ-S (left) and IP-59 (right); "grain" structure under oblique illumination at 3.9 X (top) and direct polarized light at 50 X (bottom).

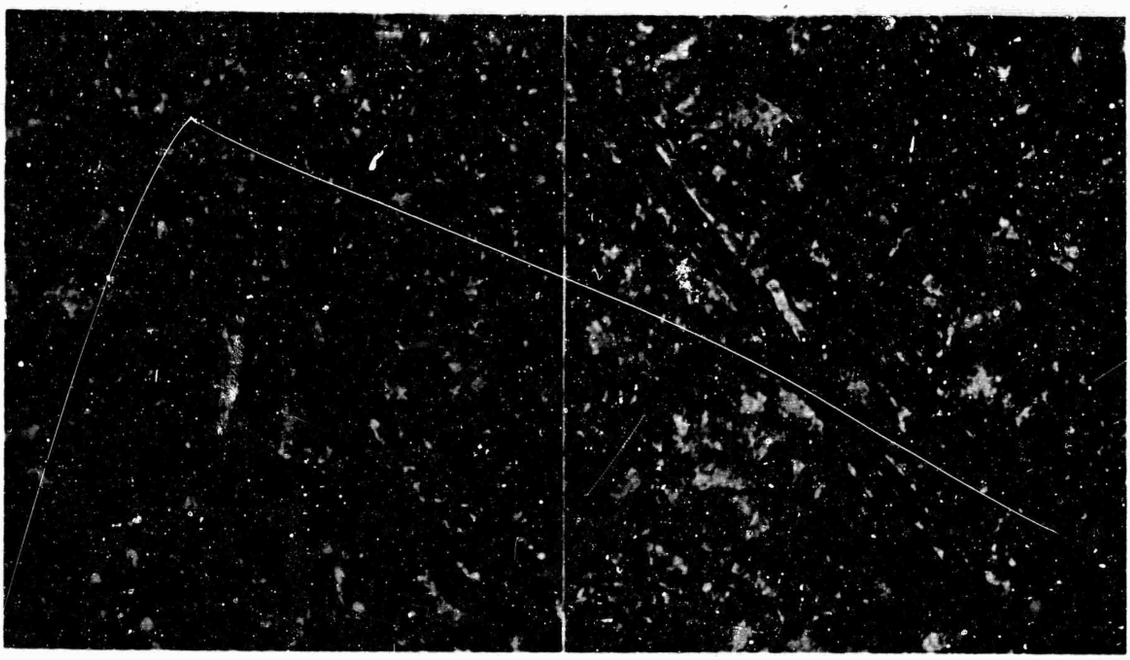

Figure 46 - Fibers and graphitized pitch matrix in IP59. Polarized, 1390 X.

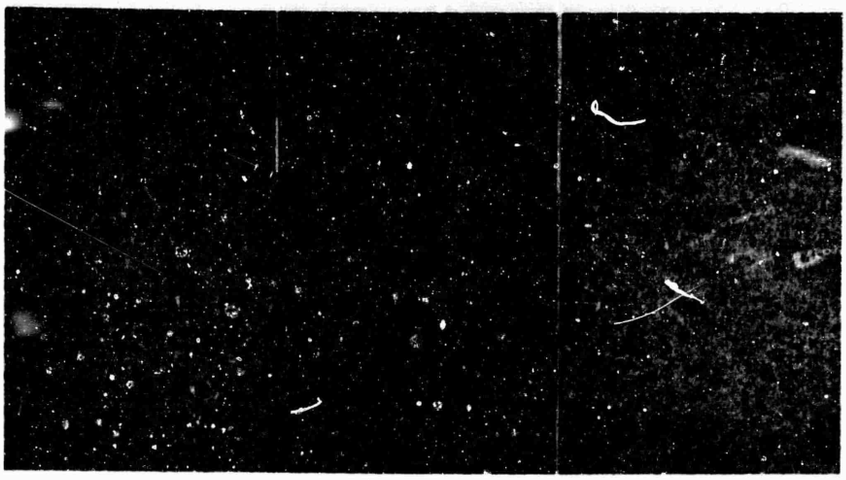

Figure 47 - Porosity on polished cross sections under direct illumination at 5 X; left: ATJ-S; center: IP50; right: IP59.

The two batches were similar in constituents and processing, except that the IP59 had the benefit of an improved agglomerating procedure and several more impregnations than IP50, with a resulting higher bulk density (1.87 g/cc for IP59, and 1.71 g/cc for IP50, for the samples tested). Both samples were oriented with the specimen axis parallel to the original billet axis. A specimen of IP50 was cut from a cylinder used to check thermal conductivity at RESD, and which had been evaluated ultrasonically at Sandia Laboratories. Two specimens were cut from block "C" of IP59 with the same orientation parallel to billet axis, and were cut so that a disc for metallography was removed adjacent to the two specimen tips.

Figure 48 - Matrix "lakes" in IP59 at 460 X; top: bright field, bottom: polarized light. View at left shows glassy carbon regions, which are not optically active, around an unusually large pore. View at right shows a region in which most of the "lake" has graphitized.

Some properties were determined by GE-RESD on samples of the IP50 which confirm the more extensive characterization for Auerbach at Sandia (Ref. 9):

Thermal conductivity (BTU/ft-sec-^{o}F) at: 150^{o}F = 0.0245 (like ATJ-S)
(axial, 1.71 g/cc) 670^{o}F = 0.0160
1250^{o}F = 0.0115

Thermal expansion: 3.1×10^{-3} in./in. from 80^{o}F to 2000^{o}F; radial direction.

At 1500^{o}F: $\frac{\Delta L}{L_{RT}\Delta T} = 1.9 \times 10^{-6}/^{o}F$ (heating), $2.1 \times 10^{-6}/^{o}F$ (cooling)

Flexure strength in 3 point bend (radial direction) = 6400 psi at 1.71 g/cc.

c. 3-D Mod. 3 Comparison Samples

Two samples of a 3-dimensional reinforced graphite prepared by the Applied Technology Division of the AVCO Corporation were included at the request of AFML in the first series of tests. The material was designated 3-D Mod. 3 graphite and was described as follows (Ref.10). It contains WCA graphite fabric perpendicular to the cylinder axis. Rods containing Thornel 50 fibers were pierced through the fabric parallel to the axis. The material had been densified by multiple impregnation, carbonization and graphitization (to about 2700°C) using a phenolic resin precursor. A furfuryl alcohol impregnant had been used in the final impregnation stages. Two cylinders, taken from AVCO Block 600, were received with 0.631 inch diameter and 1.755 inch length. These had bulk densities of 1.70 g/cc and 1.68 g/cc as received, and the corresponding densities were 1.69 g/cc and 1.67 g/cc after grinding to 0.400-inch diameter cylinders. Note also data in Table II and Figures 14-15.

Microscopic characteristics of this material were studied in order to compare mechanisms of ablation with the other fibrous composites evaluated in the same series of tests. The graphitized phenolic-precursor matrix showed "ductile" fracture, Figure 49. This matrix was very fine-grained, compared with pitch-precursor impregnants, and showed good adherance to both WCA and Thornel 50 filaments (Figure 50). The only gross flaws were cracks around the 0.05-inch diameter rods, Figures 51-52. Regions of glasslike carbon in the larger pores (Figure 53) were not associated with either preferential etching or fracture.

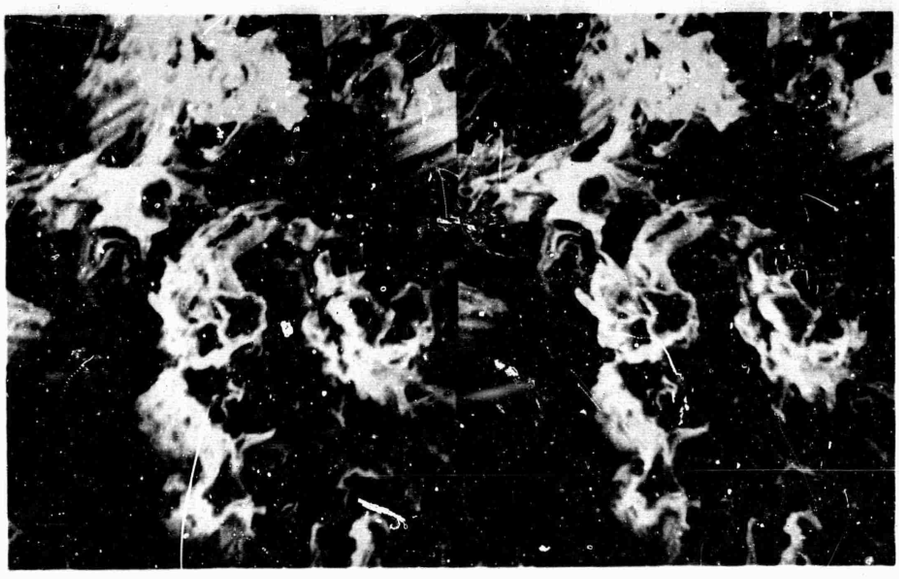

Figure 49 - Fractured surface of 3-D Mod. 3 showing "ductile" fracture of matrix around low-modulus graphite (WCA cloth) fibers. Stereo pair taken by secondary electron emission at 950 X.

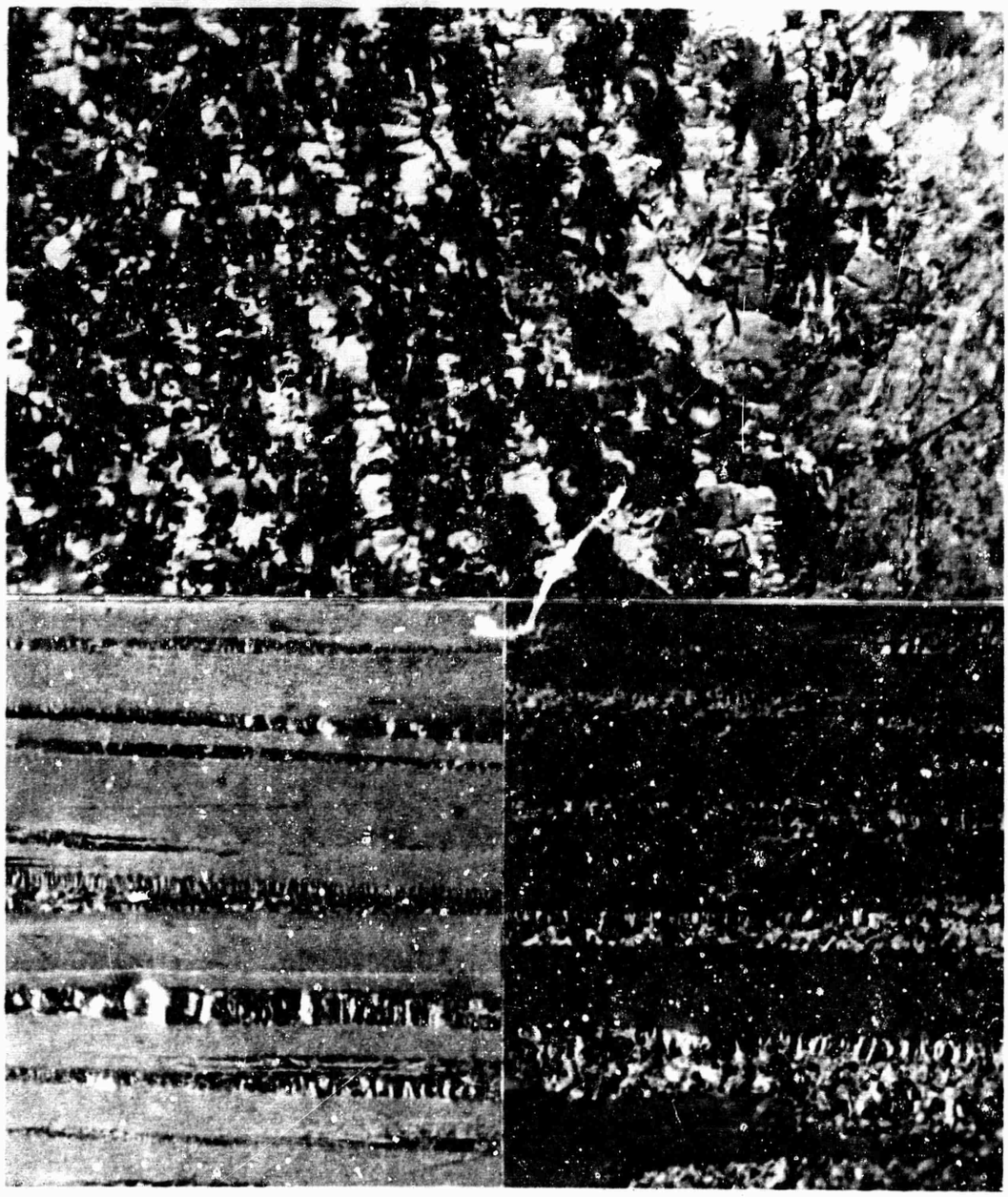

Figure 50 - Polished section of 3-D Mod. 3 in polarized light showing, at top, a crack propagating through the matrix in region of interface between Thornel 50 filaments, at left, and WCA filaments, at right. Bottom views show matrix in regions parallel to filaments of Thornel 50, at left, and WCA at right. 1590 X.

Figure 51 - 3-D Mod. 3 polished section perpendicular to axis.
Polarized light. 50 X.

Figure 52 - 3-D Mod. 3 polished section parallel to axis.
Polarized light. 50 X.

Figure 53 - Microstructure in 3-D Mod. 3 showing mixture of glasslike carbon and graphitized phenolic which filled a large interstice, at top, and fine-grained matrix in WCA bundle at bottom. Polarized light. 1590 X.

5. ABLATION SCREENING IN THE AEDC 5MW ARC

a. Facility Calibration and Test Conditions

The exploratory material developments under this program have required an ablation screening test which is applicable to small samples and provides test conditions relevant to nose tip re-entry. Previous studies (Vol. III) used a 0.222-inch diameter nozzle at the Battelle Aerothermal Research Facility, which provided 1800 BTU/lb at 70 atm. stagnation pressure, but had a relatively small flow field. During 1970, arrangements were made through AFML to explore the applicability of the 5MW Arc Heater Test unit of the Propulsion Wind Tunnel Facility at the Arnold Engineering Development Center (AEDC). This program was very successful. Details of test procedures in the first series of runs, (conducted without facility cost to this program), were reported by Henson in AEDC-TR-70-194; test details of the second series were described in AEDC-TR-71-11. (Ref. 11-12).

The AEDC 5 MW arc is of the Linde type and operates on DC power supplied by an ignition rectifier unit. A contoured nozzle is used to set up a supersonic, underexpanded flow field with a continuous flow of arc-heated air. Five models can be accomodated in each run in a sliding-rack type of injection system. All models in each run (including calorimeters and pressure ports for calibration) are exposed for identical times.

Most previous tests in this facility have used sphere-cone models with 0.25-inch nose radius or (Ref. 8) sphere-cylinders with 0.2-inch radius. An important innovation in the tests conducted here was the use of a 0.125-inch nose radius in the configuration described in Figure 54. This arrangement keeps the model within the rhombus of uniform flow (dotted lines) during most of the test.

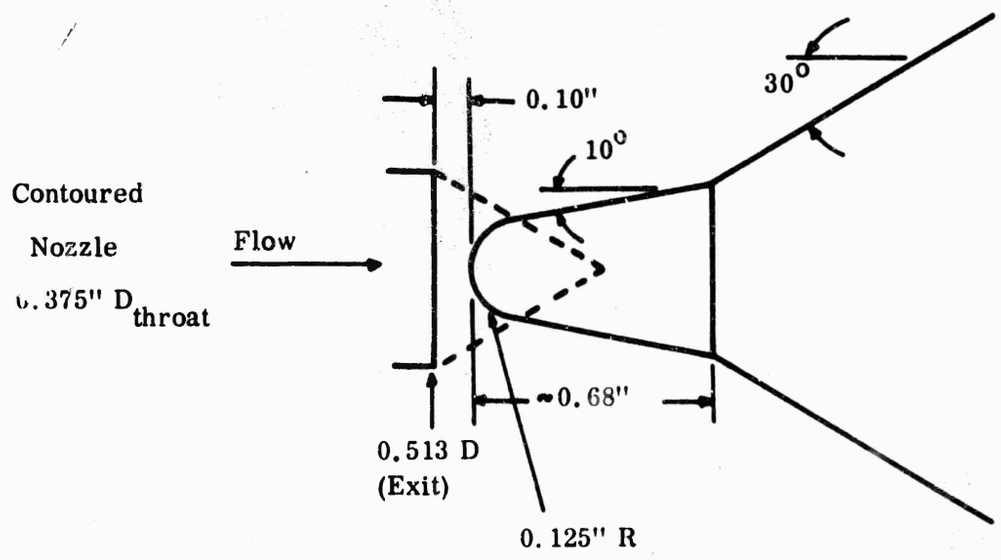

Figure 54 - Test arrangement in the AEDC 5 MW arc.

Figure 55 illustrates the design of the specimen, holder and corresponding pressure calibration model, which was made of ATJ graphite with a steel tube. An estimate of thermal stresses during test was made to determine that the specimen contours were acceptable. The small size of the specimen was particularly useful in this program, since experimental processing was often conducted on small volumes of material.

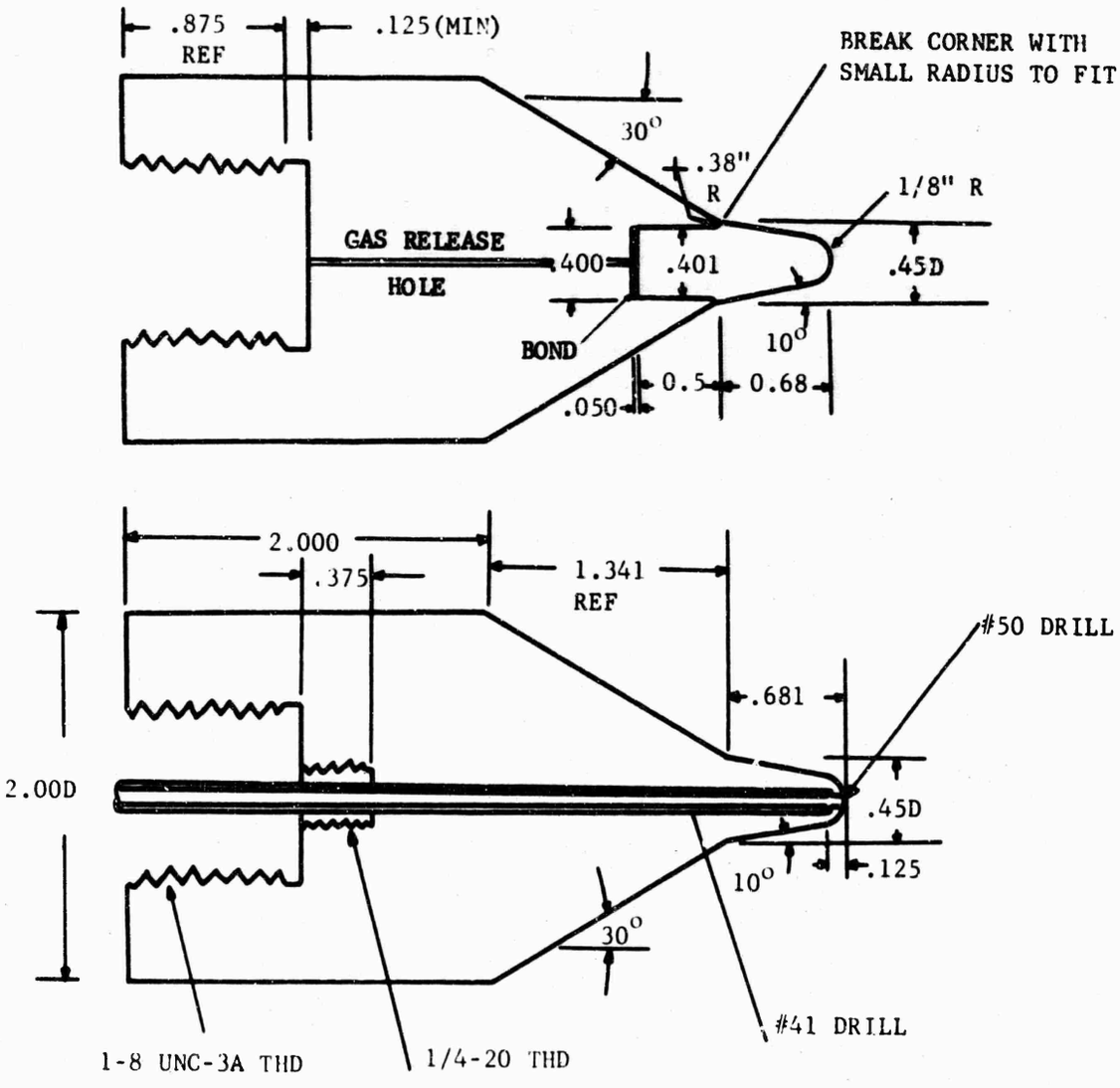

Figure 55 - Design of specimen and pressure port for ablation tests.

During the first tests four pressure-port models were included to determine repeatability of the test conditions from run to run. The first of these was positioned 0.2 inch from the nozzle exit plane, since it was anticipated that the prime ablation data would be obtained after about 0.1 inch recession. However, it was found that comparison of the pressure data with model recession from films, using two cameras at 90°, permitted generation of a pressure-versus-distance curve. Consequently, subsequent models were set at 0.1 inch, as were the specimens. Two pressure models were included in the second series.

Typical pressure calibration data are illustrated in Figure 56. During the first 0.3 seconds the pressure readings were depressed due to outgassing from the tube which changed the shape of the shock in front of the tip (this was visible on the films).

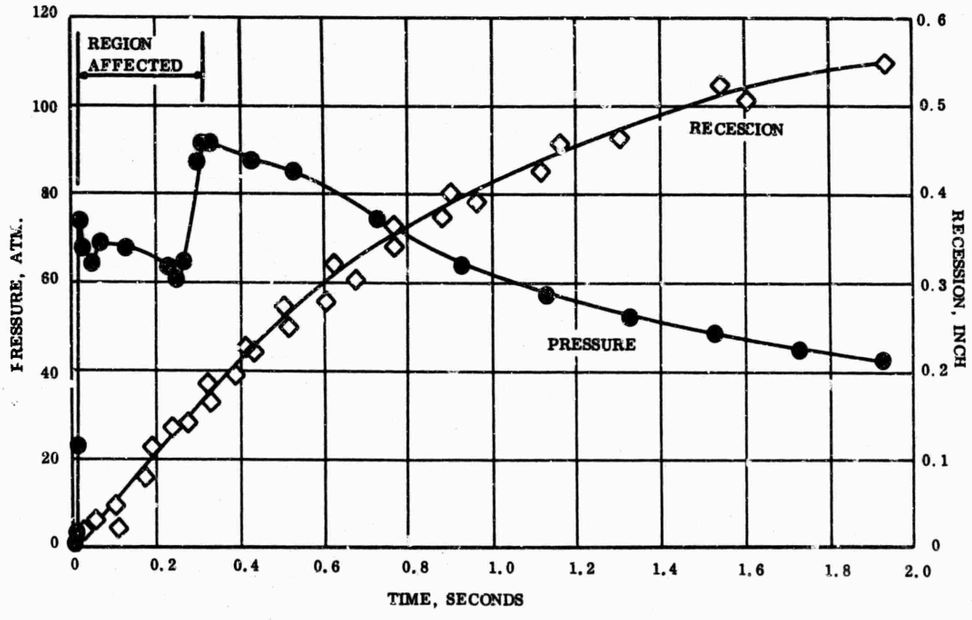

Figure 56 - Measured pressure and recession during a typical run (No. 70-A4).

A summary of all of the pressure data is presented in Figure 57 as a map of pressure versus distance. These results show that a constant pressure field exists on the centerline for at least 0.3 inch from the nozzle exit. Pressure from run to run was within $\pm$ 1 atmosphere with an average of 91 atmospheres.

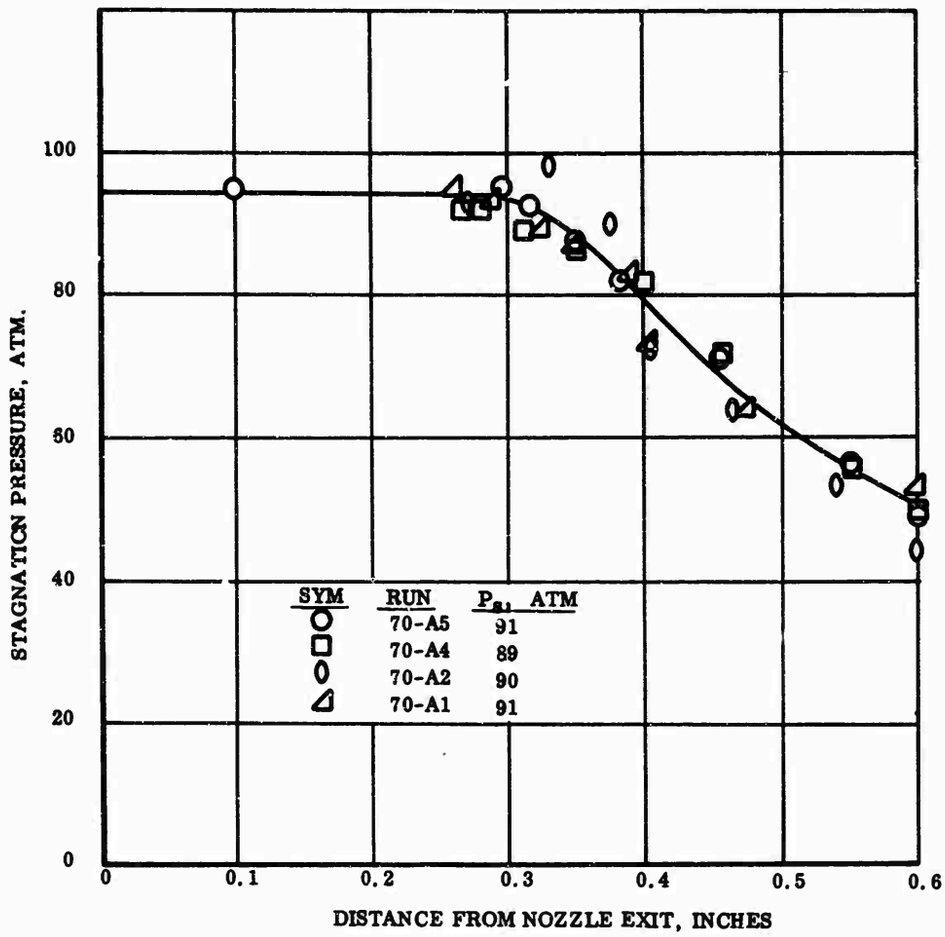

Figure 57 - Results of pressure calibration in the first series.

Three calorimeter models were purchased from AVCO Corporation for calibration of heat flux by procedures consistent with those used with the 50 MW facility at AFFDL. The calorimeters were of copper construction and of the null point type. Two of the models had 1/4 inch nose radius and were identical in design to those which had been used in other facilities. One calorimeter with 1/8 inch nose radius was included to obtain a more reliable measure of the heat flux to the specimens. In the first run a 1/4-inch-radius model fabricated by GE-RESD was used, but this gave a lower response than the others, which had a record of proven reliability. Teflon caps were used in all cases, and these came off after the model was locked on centerline.

The temperature data from the calorimeters was sent to AFML and reduced to heating rates using the same computer program used for the 50 MW arc data. The resulting heat flux histories are shown in Figure 58.

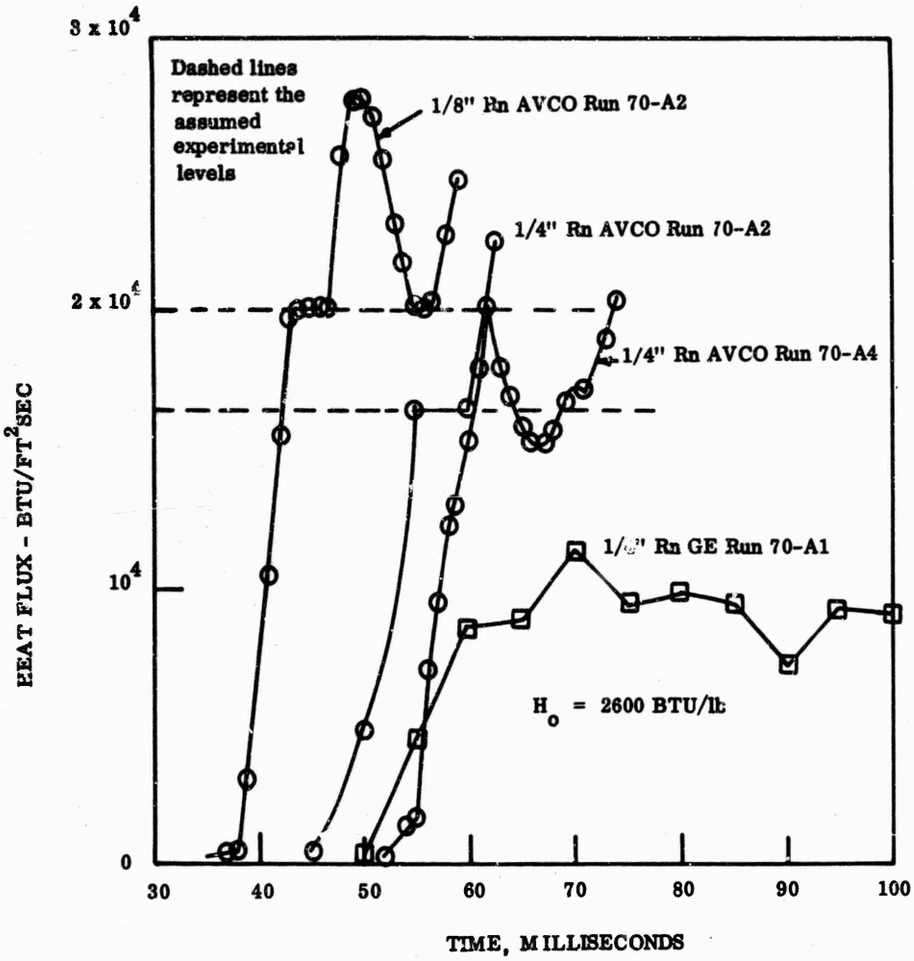

Figure 58 - Results of heat flux calibration.

The two 1/4-inch AVCO calorimeters repeated reasonably well at a level of 16,500 BTU/ft^2 sec. The 1/8-inch model shows a level portion at 20,200 BTU/ft^{2}sec. If the ratio of heat fluxes were proportional to the square root of the radius, 23,300 BTU/ft^{2}sec should have been obtained with the smaller radius model.

A prediction of stagnation heat flux using Lee's equation modified by the reference enthalpy parameter gave a low value, 8500 BTU/ft^{2}sec, for 1/8-inch radius and a wall enthalpy of 550 BTU/lb. Agreement with the measured values would result if total enthalpy used in the calculation were adjusted to 5000 BTU/lb. However, the bulk enthalpy measured is reasonable, assuming 50 % arc efficiency, and it may be that an enthalpy spike associated with this environment is responsible for the discrepancy.

The conditions selected for this screening test were very repetitive and an easy condition for the arc. Table VI describes the test matrix together with the measured plenum pressure, which varied only ± 1.5 atmospheres, and gas enthalpy obtained from the arc heat balance, which was ± 40 BTU/lb, during the first series of tests.

TABLE VI

AEDC 5 MW ARC CONDITIONS AND TEST MATRIX

Run No.	Enthalpy, BTU / lb.	Plenum Pressure, Atmospheres	Model Description in Order of Test
70-A-1	2560	117	(1) GE Calorimeter (1/4 in. R_n) (2) Pressure Port (3) ATJ-S cored billet (4) (Sample lost; retest in 70-A-4) (5) WYF 4-D + PD matrix
70-A-2	2640	118	(1) AVCO Calorimeter (1/4 in. R_n) (2) AVCO Calorimeter (1/8 in. R_n) (3) Pressure Port (4) ATJ-S #2 (5) 3-D Mod. 3 (a)
70-A-3	2630	119	(1) ATJ-S #3 (2) CXH 3-D + CVD matrix, annealed (3) CXH 4-D + CVD matrix (4) CXH 3-D + CVD matrix (5) CXH 4-D + CVD matrix, annealed
70-A-4	2580	118	(1) AVCO Calorimeter (1/4 in. R_n) (2) Pressure Port (3) WYF 4-D + CTP/FA matrix, graph. (4) CXL 4-D + CVD matrix (5) CXH 4-D + CVD, coarse texture.
70-A-5	2610	117	(1) Pressure Port (2) ATJ-S # 4 (3) 3-D Mod. 3 (b) (4) M-II 4-D + CVD matrix (5) ATJ-S # 5

In addition to the five runs listed in Table VI a preliminary facility calibration run was made at a slightly lower enthalpy (2390 BTU/lb.) in which samples of bulk graphite were included to verfy the model design. One of these had a 1/4 inch nose radius, and both the films and appearance of the model after test, Figure 59, showed the effects of the lower ablation rate at the larger diameter. The choice of a 1/8 inch radius for these tests was thus confirmed.

Figure 59 - AXF 9Q, having 1/4-inch initial nose radius, after 2 seconds of test. 1.85 X.

During each test the model was photographed with two Fastex cameras, which were oriented at 90°. Profiles from the camera frames, such as those in Figure 60 were traced, and maximum recession rate was obtained from a plot of peak position as a function of time. Temperature of the side wall of the model was obtained with a continuous recording radiation pyrometer focussed on a spot about 0.1 inch below the tip. The models were moved out of the flow after 2.0 seconds.

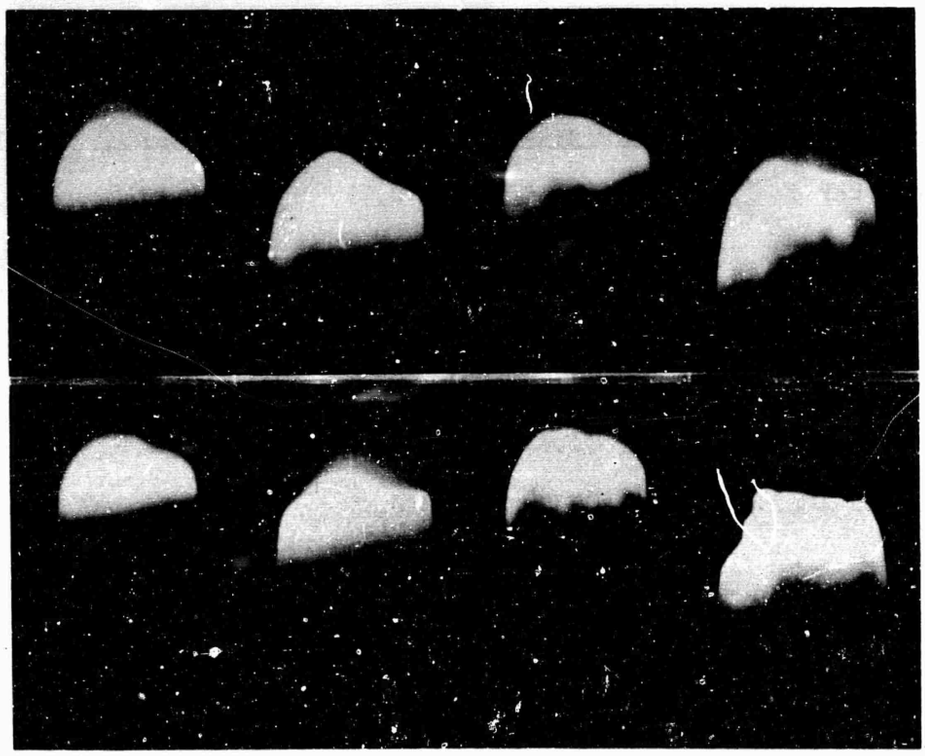

Figure 60 - Photographs of samples during test:

Top:	ATJ-S Model #2 0.285 sec; 0.425 sec.	3-D Mod. 3 (a) 0.200 sec; 0.400 sec.
Bottom:	ATJ-S Model #4 0.200 sec; 0.575 sec.	3-D Mod. 3 (b) 0.200 sec; 0.575 sec.

b. Results of First Series of Tests

One of the purposes of the first series of tests was to establish the utility of the test for reproducible ablation screening of small samples at high stagnation pressure. The results on the ATJ-S standards and 3-D Mod. 3 comparison models indicated that the test was at least as reproducible as the materials themselves. The appearance of these samples after test, the profiles as a function of time in seconds, and the plotted points of peak position are illustrated in Figures 61 through 69. Table VII summarizes the data obtained from the plots: the maximum slope of peak recession (r_{max}), the average rate of loss in 1 second, and the time during the test at which the maximum rate began. Similar data on the experimental samples is on page 80.

TABLE VII

ABLATION DATA ON COMPARISON MATERIALS

Material Description	Run Number	Bulk Density g/cc	Time to Start Maximum Rate, seconds	Tip Recession Rate, inch / sec.	
				r_{max}	$r_{1\ sec.}$
ATJ-S cored	70-A-1-3	1.84	0.45	0.29	0.21
ATJ-S #2	70-A-2-4	1.86	0.55	0.55	0.22
ATJ-S #3	70-A-3-1	1.85	0.35	0.33	0.20
ATJ-S #4	70-A-5-2	1.86	0.35	0.37	0.24
ATJ-S #5	70-A-5-5	1.86	0.35	0.42	0.22
3-D Mod 3-a	70-A-2-5	1.69	0.25	0.36	0.27
3-D Mod 3-b	70-A-5-3	1.67	0.33	0.43	0.31

The curves of tip recession for ATJ-S demonstrate variability resulting from shape change during the test which may have been associated with the formation of tubulent erosion pits (Figure 61.) The increase in heat flux resulting from surface roughening and formation of a biconic shape (110^{o}-120^{o} in most cases) resulted in accelerated ablation until the tip receded from the region of high pressure (about 0.2 inch recession.) Although conditions were less uniform, the average rate $r_{1\ sec}$ showed less variability than r_{max}. Consequently, several comparisons of rate, as in Table VII, plus examination of the profiles during test, are needed for the comparisons of ablation performance between materials.

Note that the two 3-D Mod. 3 samples, which did not show the pitting characteristic of vortex formation, had the same average r_{max} as ATJ-S (0.4).

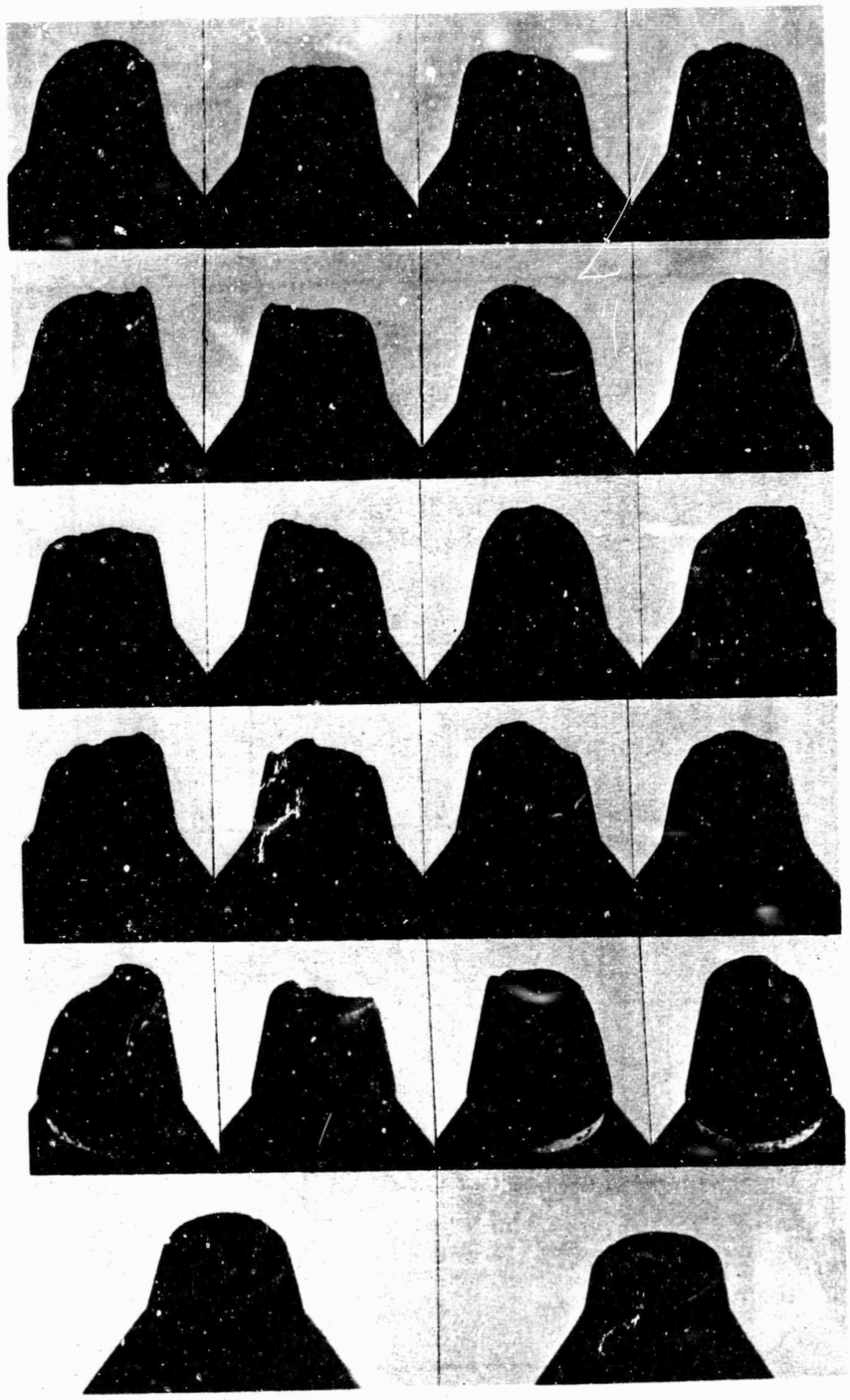

Figure 61 - Appearance of bulk graphite models after test; from top: ATJ-S cored, ATJ-S # 2, # 3, # 4, # 5, ATJ in preliminary run and ATJ pressure port. 1.85 X.

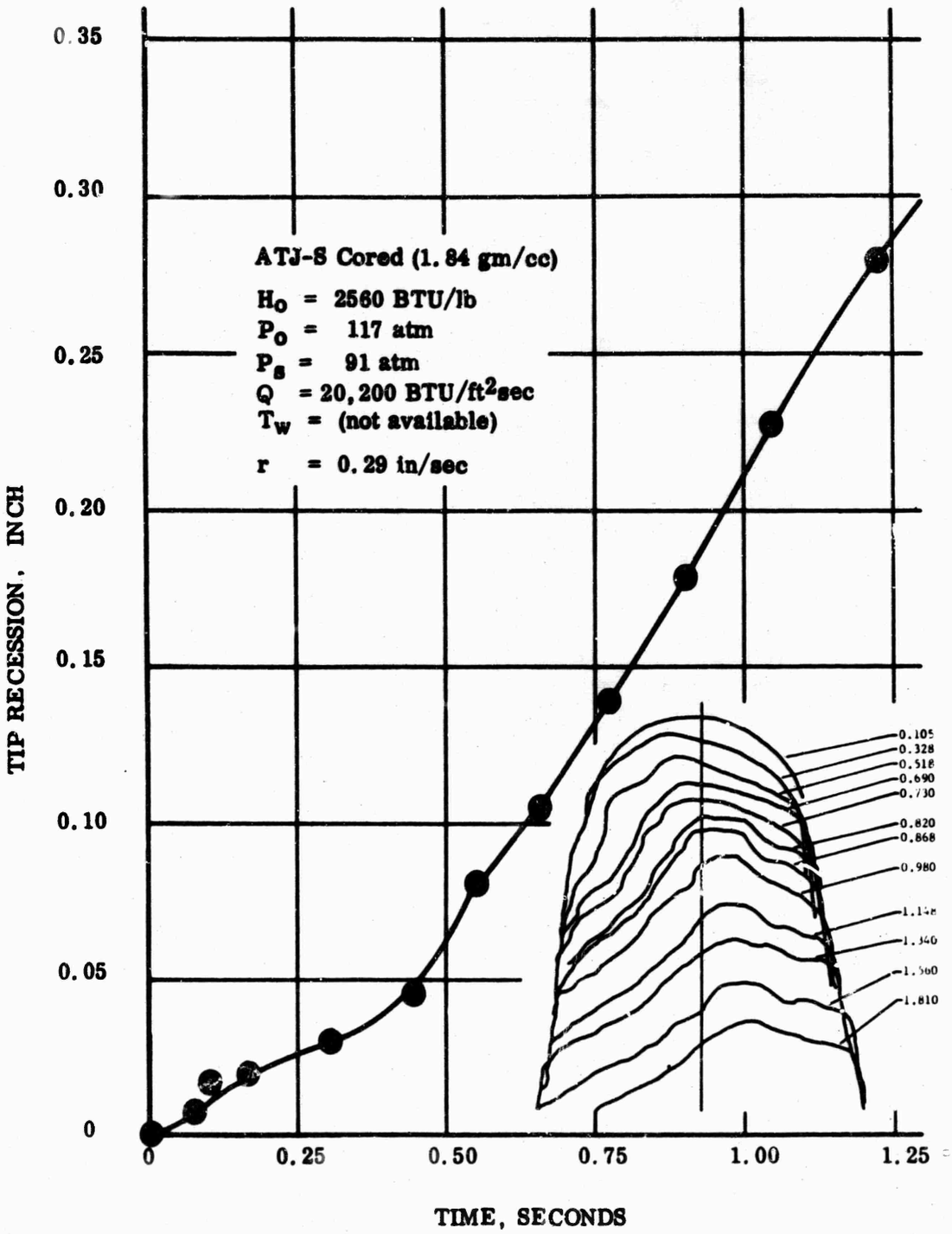

Figure 62 - Ablation of ATJ-S cut from cored billet in across-grain direction; run 70-A-1. Numbers on profiles refer to time in seconds.

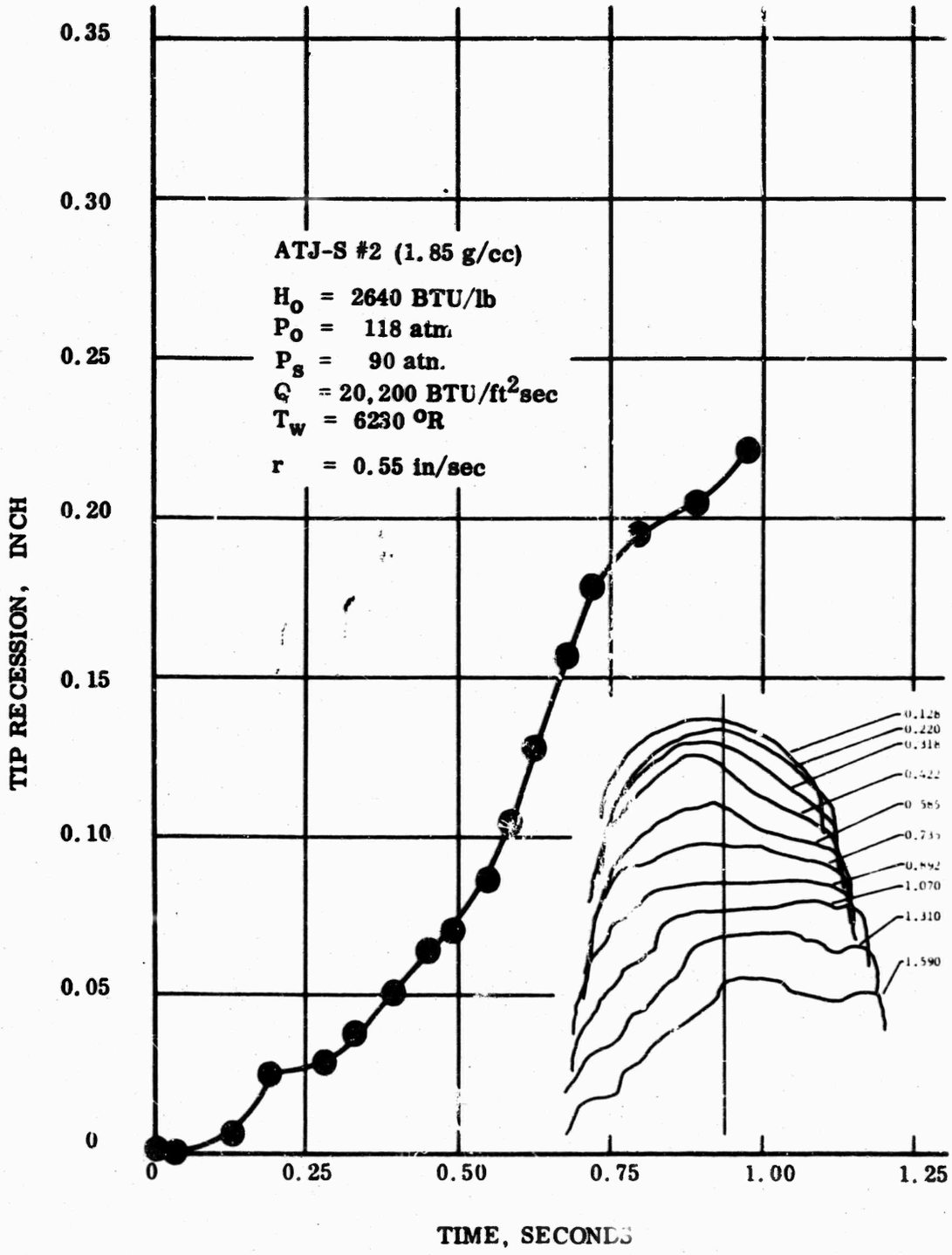

Figure 63 - Ablation of ATJ-S model # 2 in run 70-A-2.

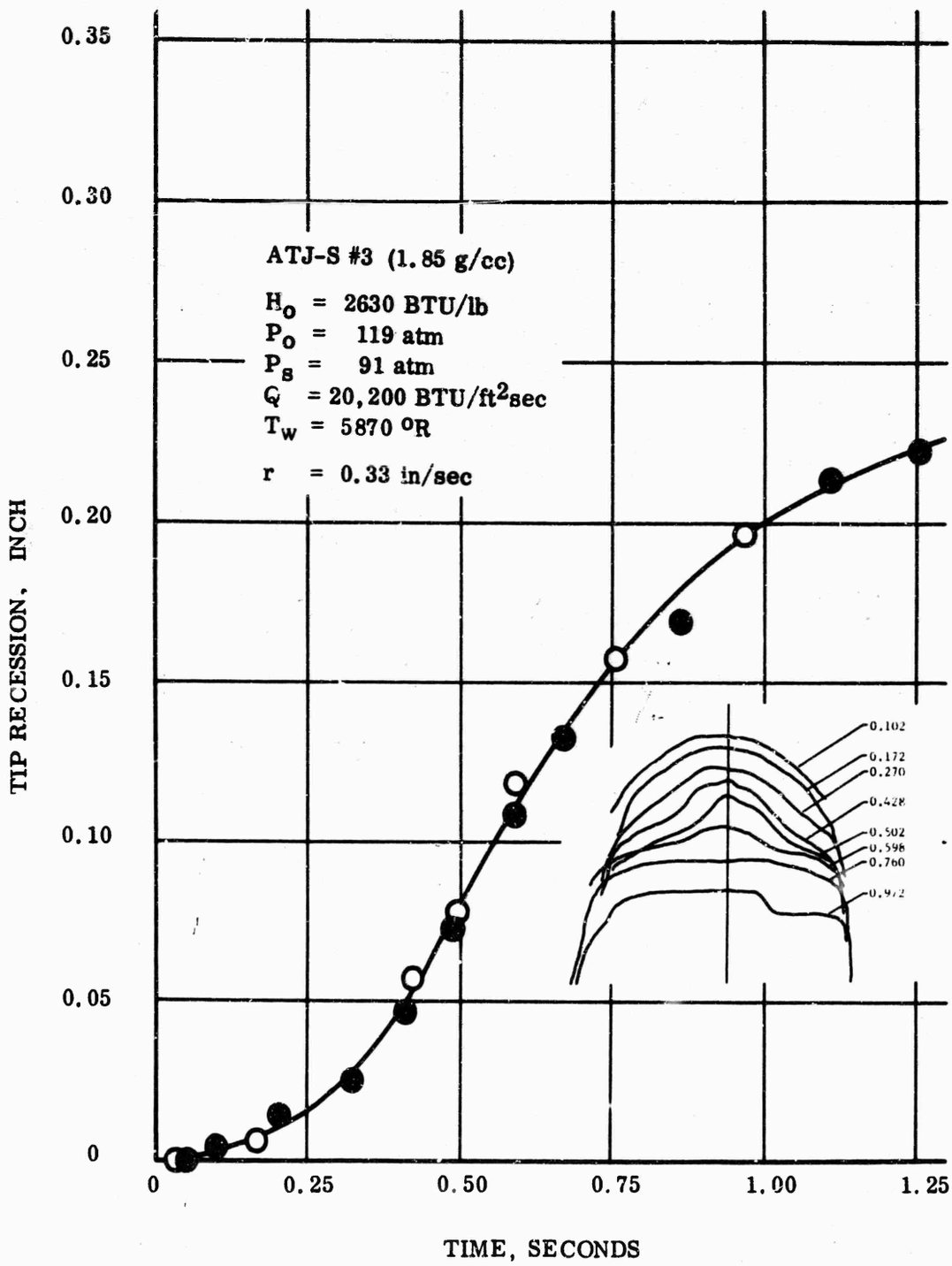

Figure 64 - Ablation of ATJ-S model #3 in run 70-A-3. Open and closed points are taken from films obtained by two cameras.

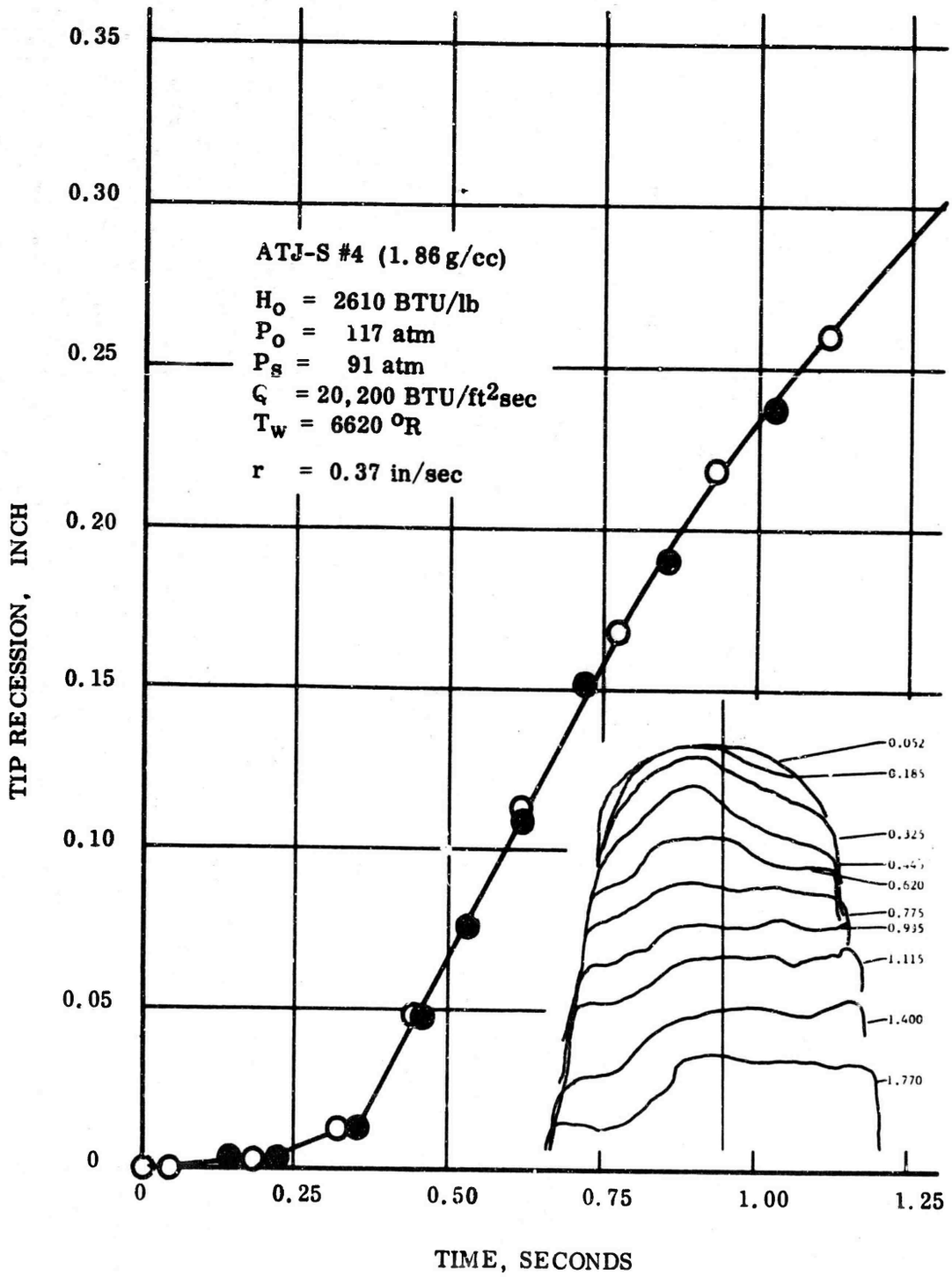

Figure 65 - Ablation of ATJ-S model #4 in run 70-A-5.

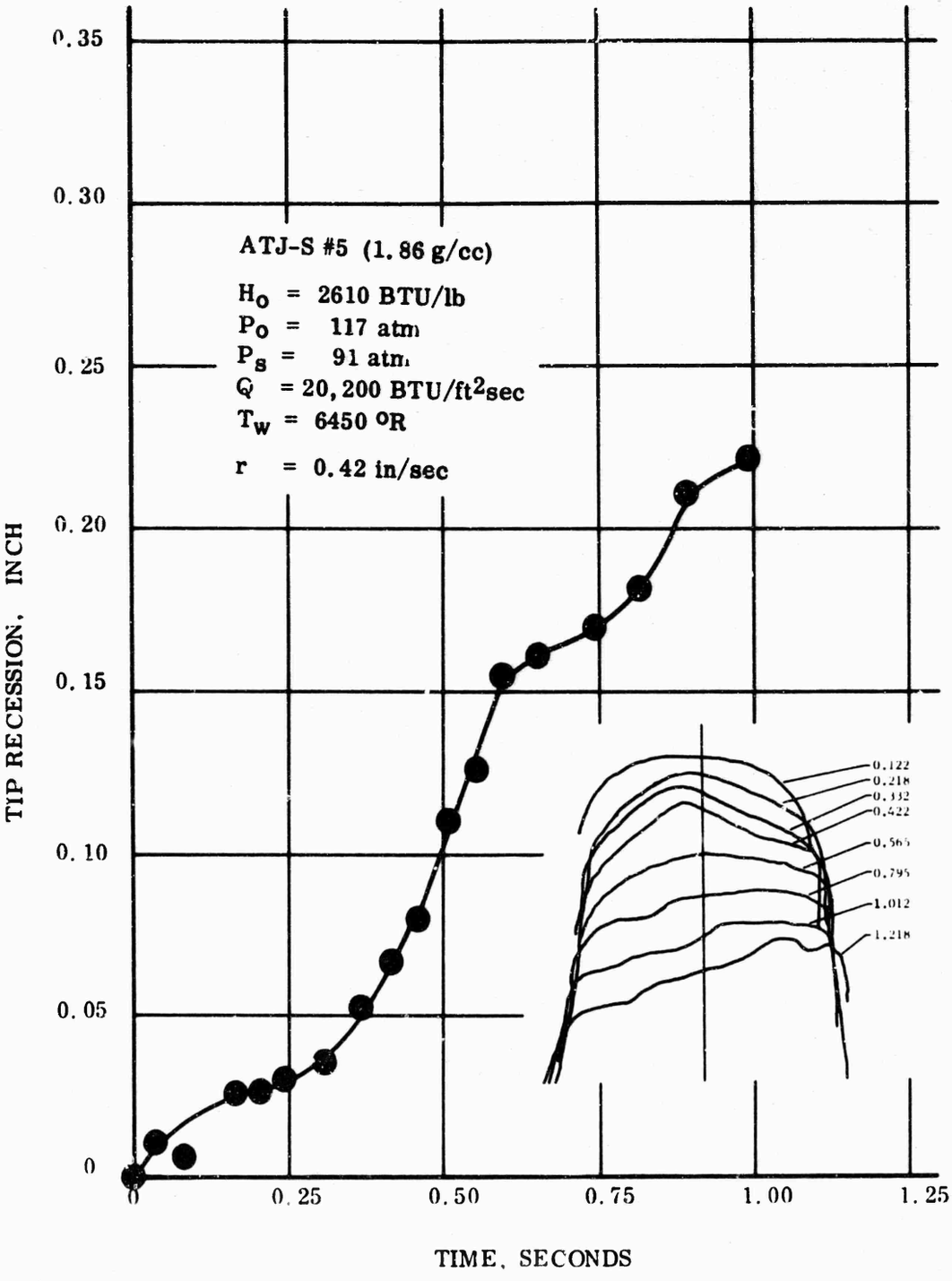

Figure 66 - Ablation of ATJ-S model #5 in run 70-A-5.

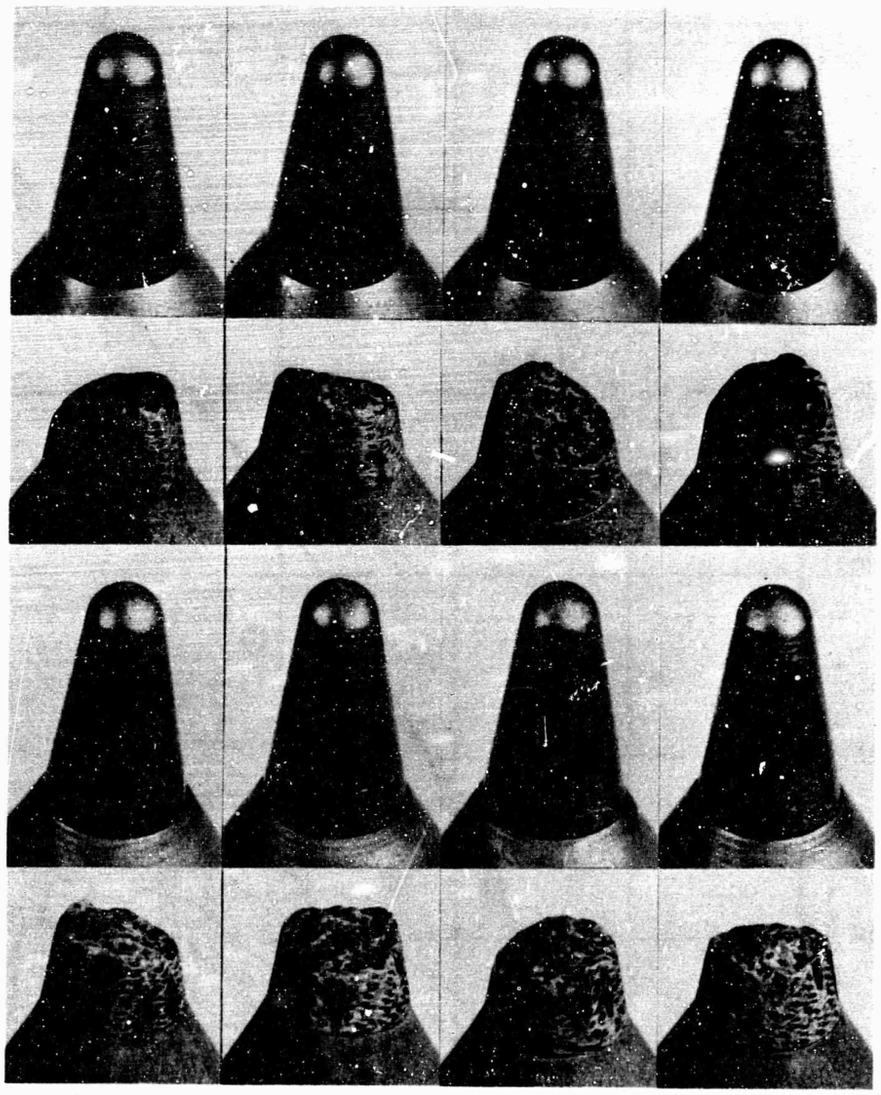

Figure 67 - 3-D Mod. 3 samples before and after test (1.85 X).
Top: Model (a). Bottom: Model (b).

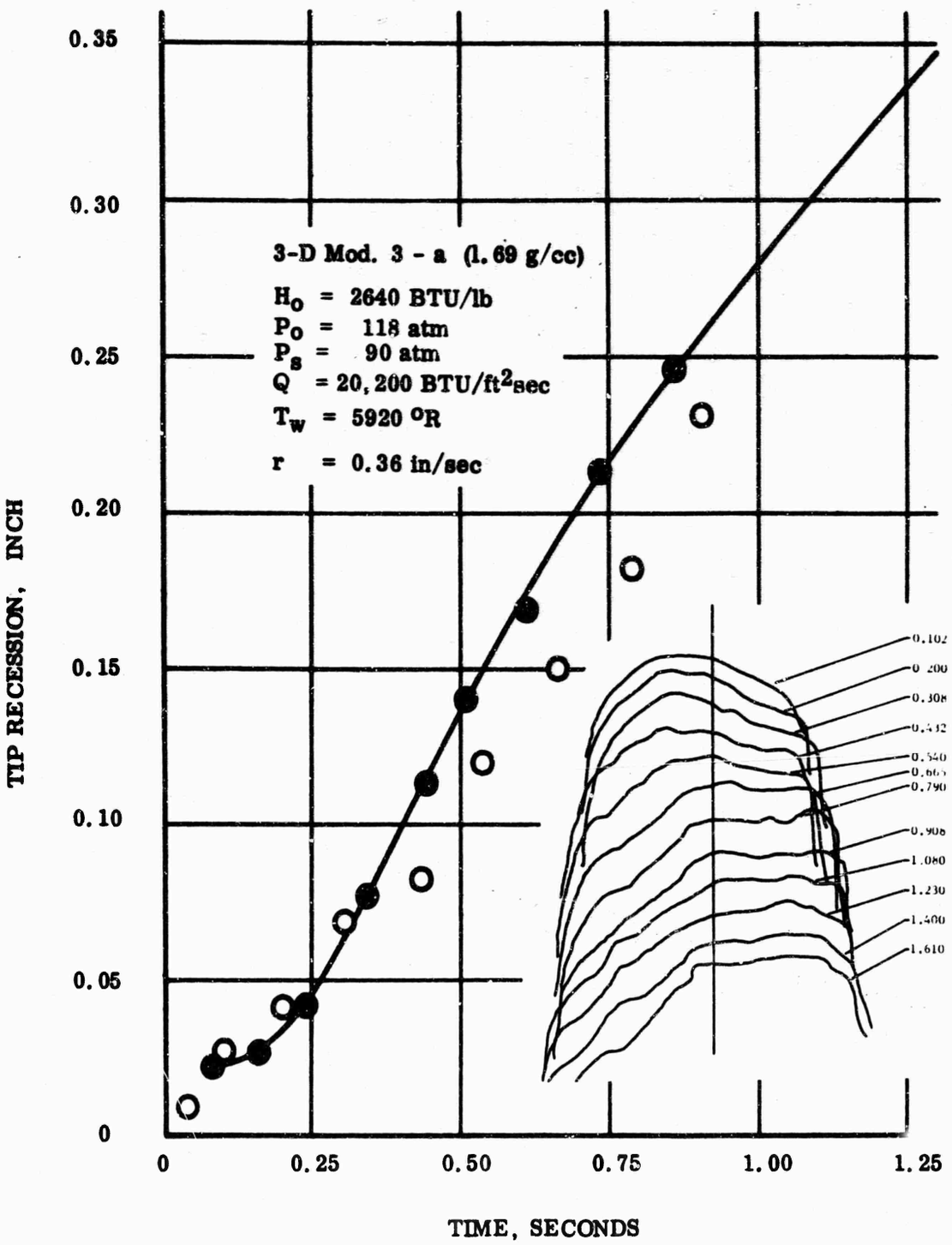

Figure 68 - Ablation of 3-D Mod. 3 model (a) in run 70-A-2.
Open points are from film taken by second camera.

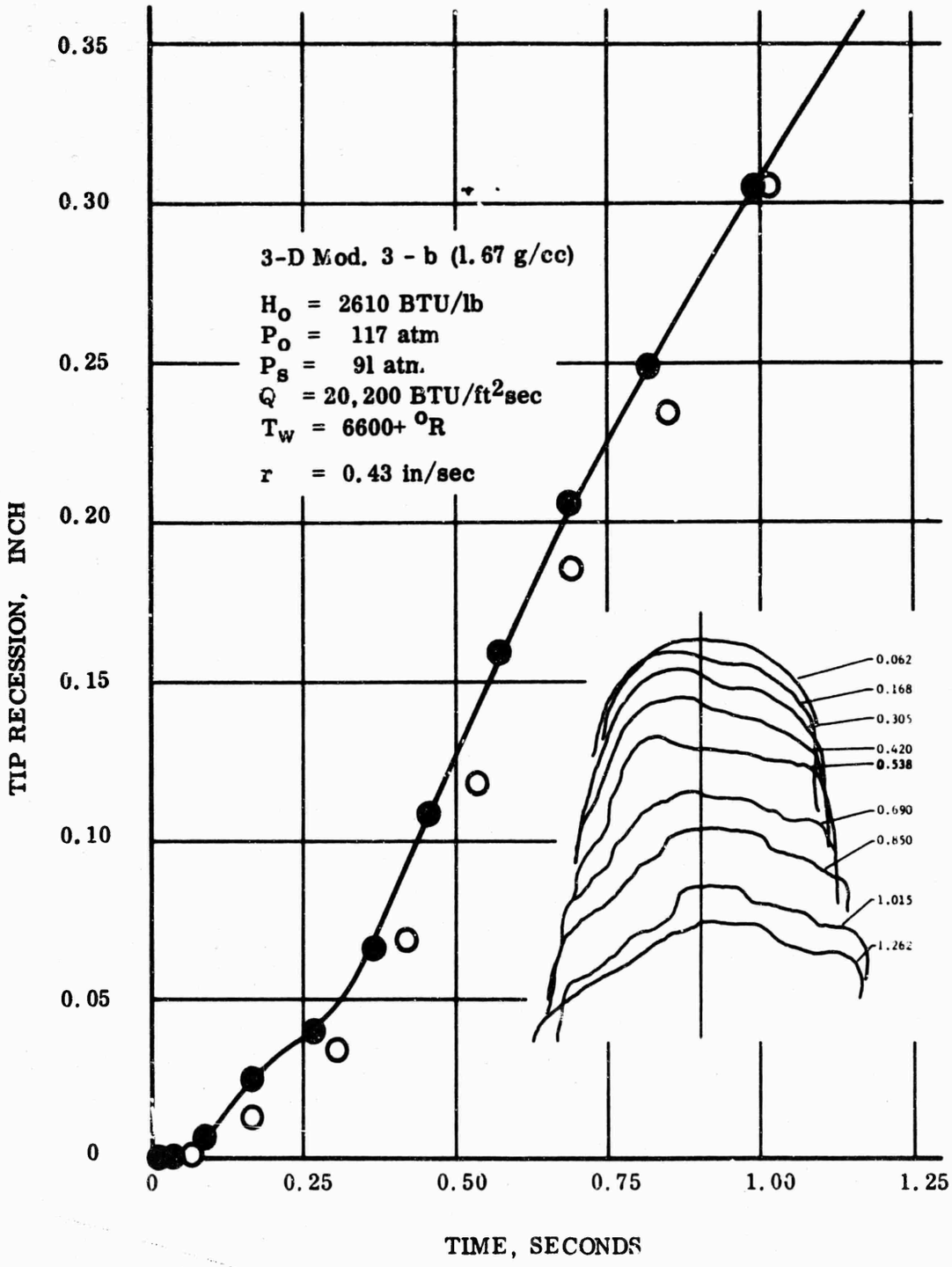

Figure 69 - Ablation of 3-D Mod. 3 model (b) in run 70-A-5.

The results on the experimental composites in the first series of tests are described in Table VIII. Photographs of the samples during test are shown in Figures 70 to 73; the profiles as a function of time in seconds, and the plots of tip recession versus time are given in Figures 74 to 80. Appearance of the models before and after the 2-second tests are shown in Figures 81 to 85.

TABLE VIII

ABLATION DATA ON EXPERIMENTAL MATERIALS IN THE FIRST SERIES

Material Description*	Run Number	Bulk Density g/cc	Time to Start Maximum Rate, seconds	Tip Recession Rate, inch / sec.	
				r_{max}	r1 sec
WYF 4-D + PD matrix	70-A-1-5	1.67	-(Sample failed at 0.15 second)-		
WYF 4-D + CTP + FA	70-A-4-3	1.72	0.15	0.76	0.48
M-II 4-D + CVD	70-A-5-4	1.83	0.15	0.66	0.48
4XH(45-ply)11t11	70-A-4-5	1.55	0.30	0.98	0.50
4XL11t11	70-A-4-4	1.61	-(Sample failed at 0.18 second)-		
4XH11t11	70-A-3-3	1.63	0.30	0.66	0.36
4XH11Gt11	70-A-3-5	1.61	0.25	0.62	0.36
3XH11t11	70-A-3-4	1.55	0.37	0.64	0.36
3XH11Gt11	70-A-3-2	1.57	0.25	0.52	0.36

* See code in Table IV.

The composites with coarse texture, and the pitch-matrix Thornel 40 composite, were significantly worse than the experimental fine-textured samples in ablation. The fine-textured 4-D sample made with impure CXL fibers failed catastrophically (many cracks running through the filaments were observed in the microstructure of the material remaining.)

The samples in run 70-A-3 showed remarkably similar performance, considering the variability observed with ATJ-S. The two geometries, and the effect of heat treatment, did not significantly affect ablation (Figures 70, 77-80,) although maximum slope was slightly lower with the annealing.

Figure 70 - Photographs of CVD infiltrated samples during test:

Top: CXH 3-D (As Dep.) 0.200 sec. 0.575 sec. CXH 3-D (Annealed) 0.200 sec. 0.605 sec.

Bottom: CXH3 4-D (As Dep.) 0.135 sec. 0.595 sec. CXH3 4-D (Annealed) 0.200 sec. 0.575 sec.

Figure 71 - Models with high modulus fibers during test:

WYF 4-D + CTP/FA 0.200 sec.; 0.575 sec. M-II + CVI 0.200 sec.; 0.413 sec.

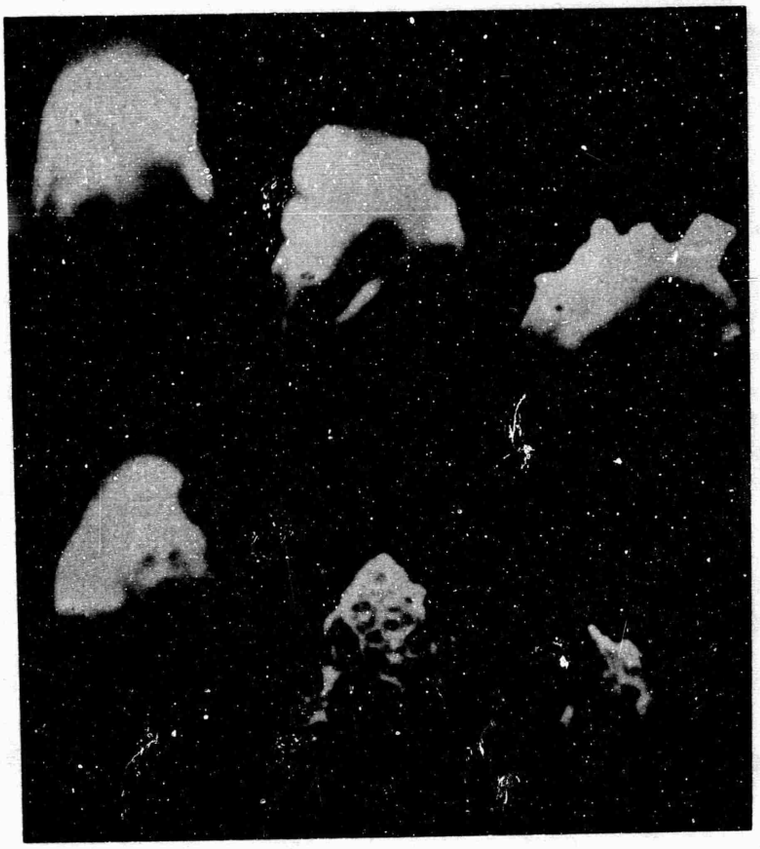

Figure 72 - CVD-infiltrated samples showing higher ablation rates during test:

Top: CXH45 4-D + CVD
0.200 sec.; 0.380 sec.; 0.740 sec.

Bottom: CXL3 4-D + CVD
0.085 sec.; 0.172 sec.; 0.178 sec.

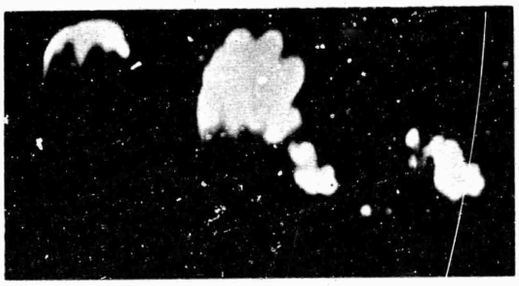

Figure 73- Ablation of WYF 4-D + PD matrix:
0.064 sec.; 0.112 sec.; 0.120 sec.

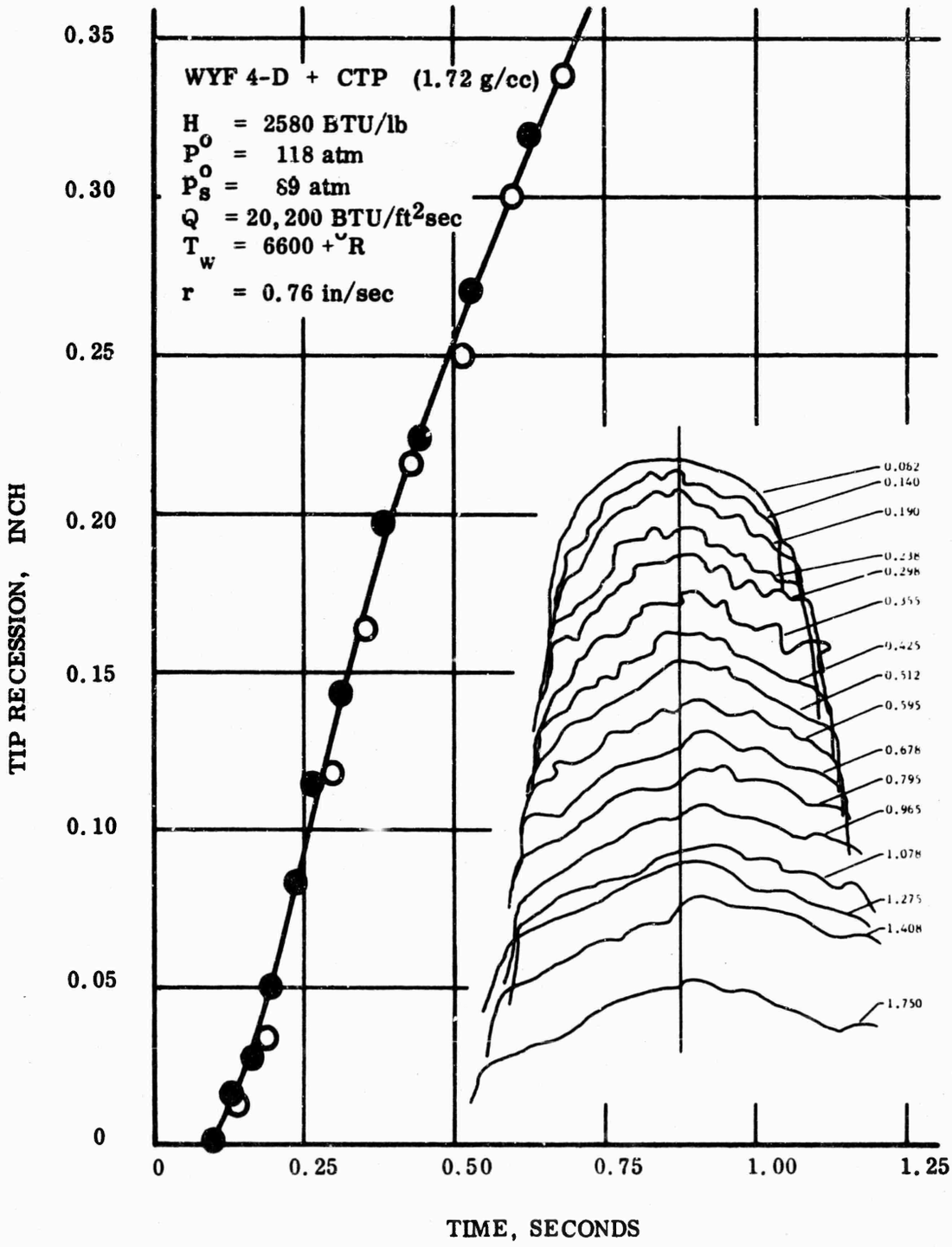

Figure 74 - Ablation of Thornel 40 braid with a graphitized coal tar pitch + furfural resin matrix.

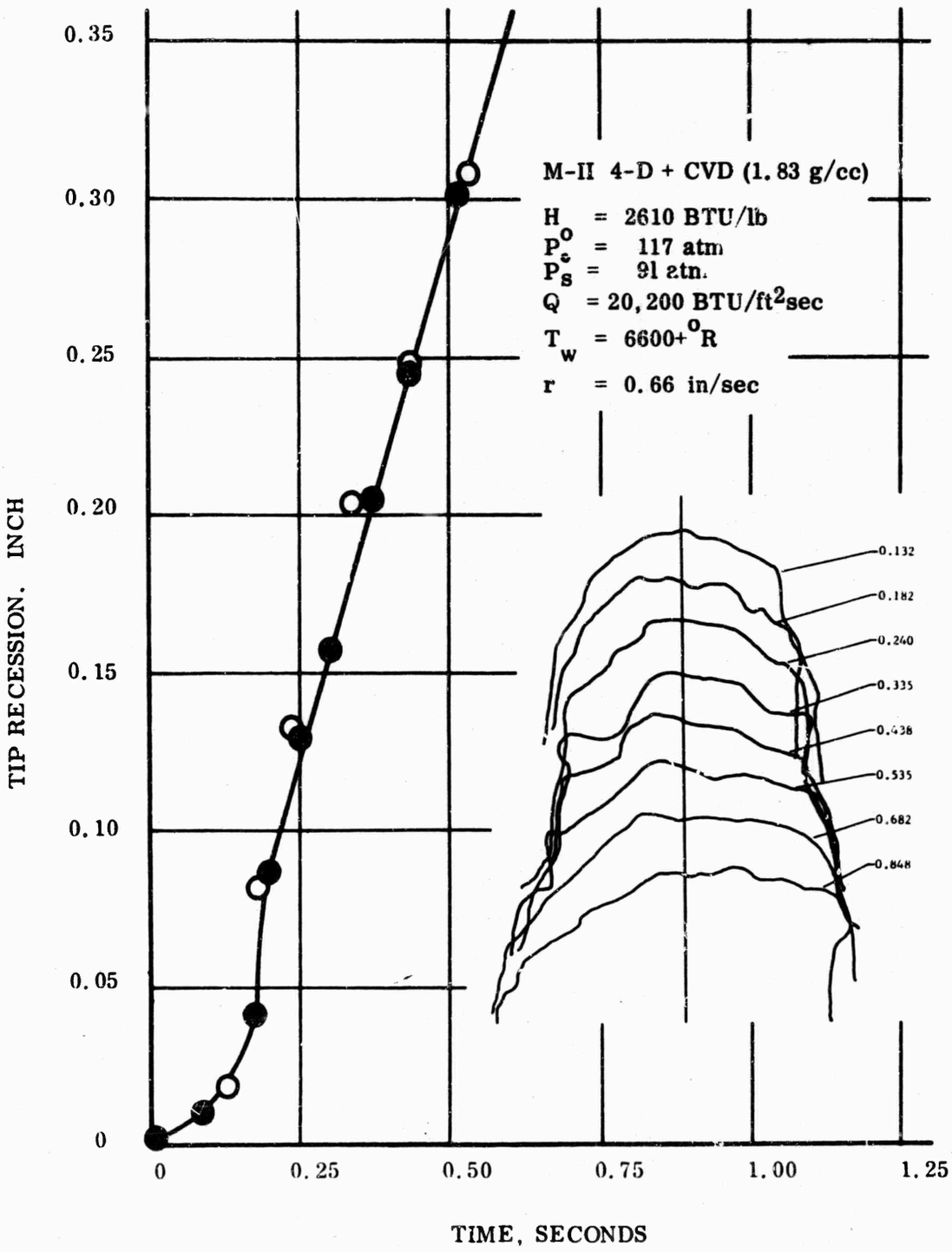

Figure 75 - Ablation of coarse texture, high-modulus carbon Omniweave having an r.f. infiltrated carbon matrix.

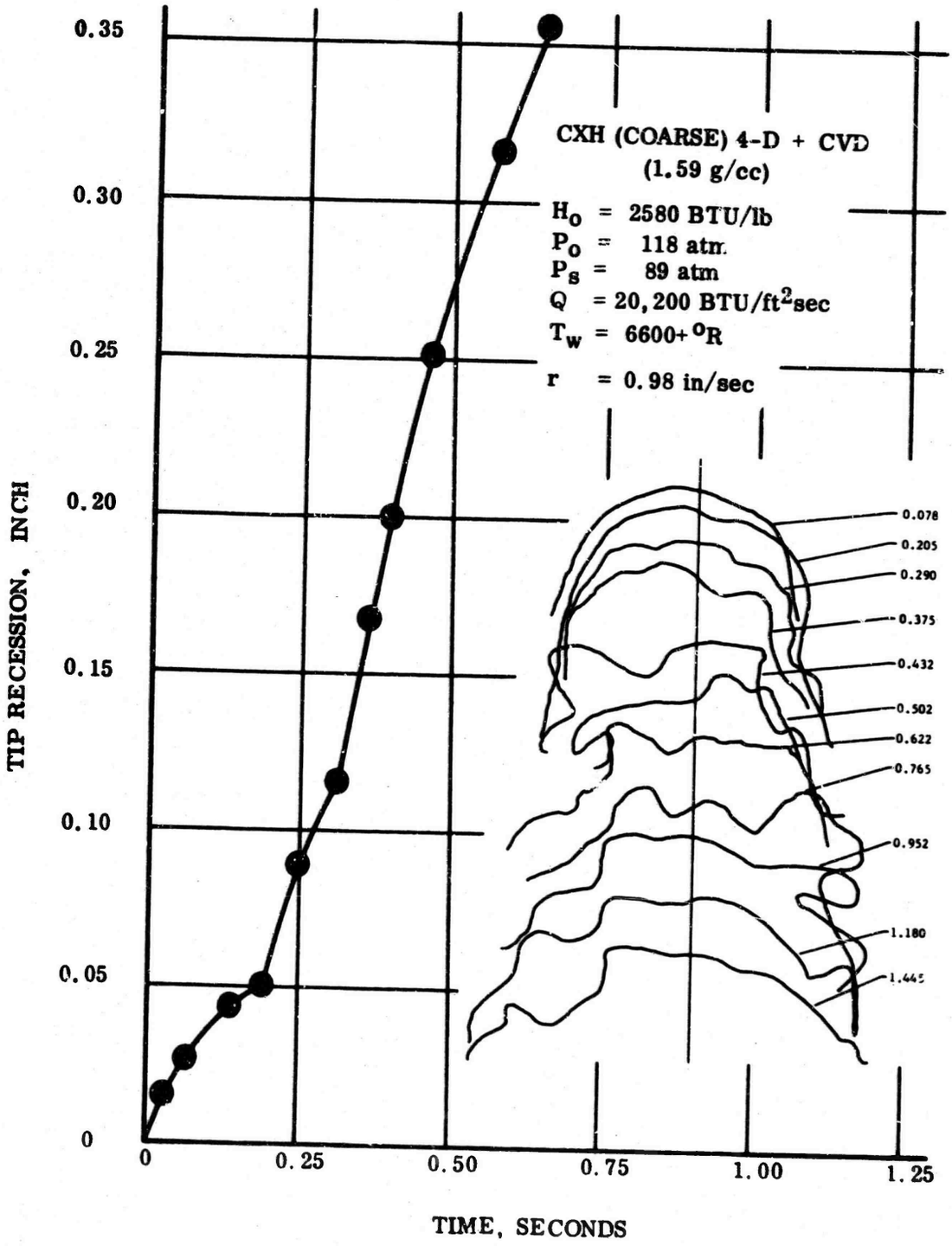

Figure 76 - Ablation of coarse-textured (45 ply) carbon Omniweave with a rapidly infiltrated carbon matrix.

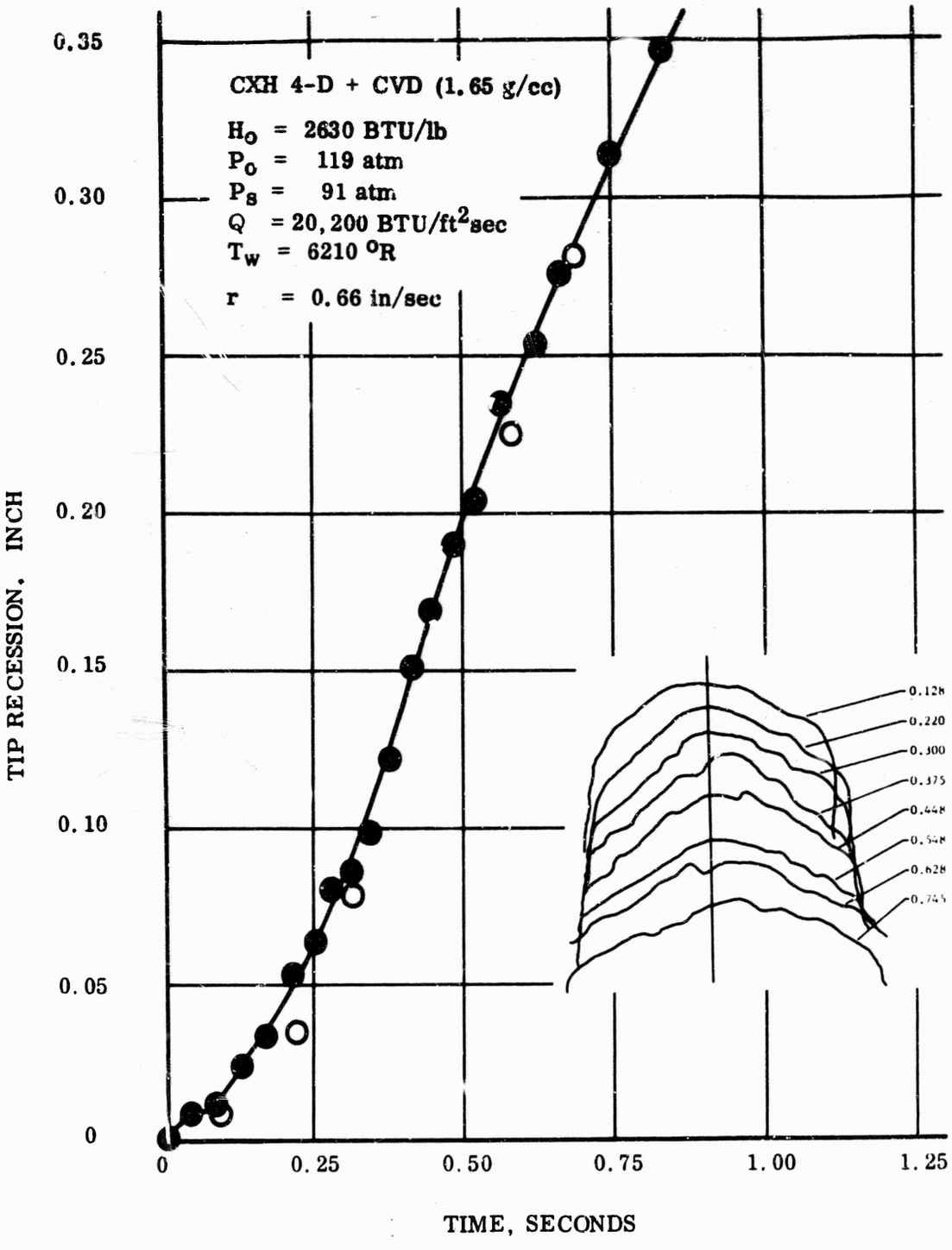

Figure 77 - Ablation of fine textured (3 ply) carbon Omniweave with a rapidly infiltrated carbon matrix.

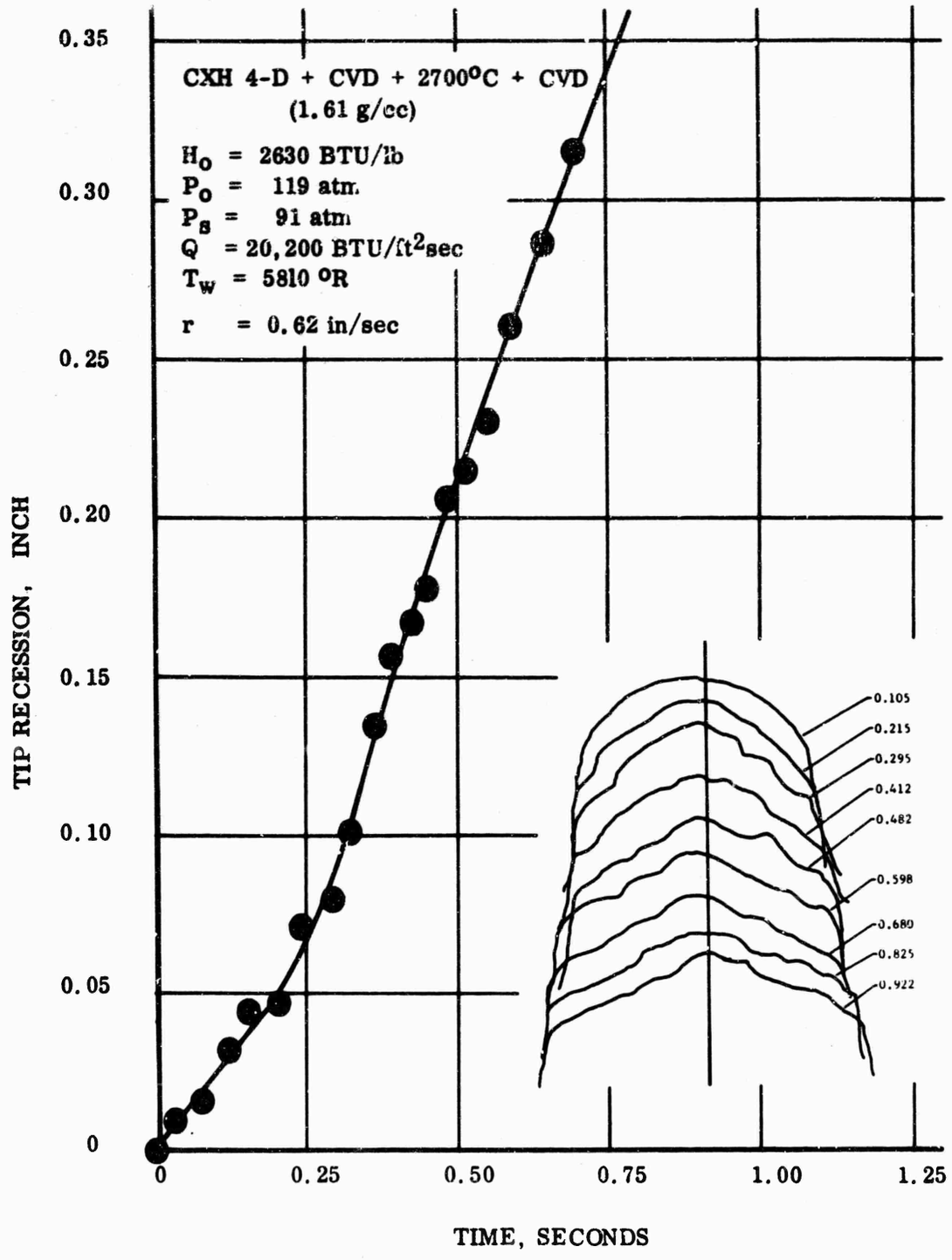

Figure 78 - Ablation of 3-ply carbon Omniweave with a rapidly infiltrated matrix, after heating to 2700°C and re-infiltrating.

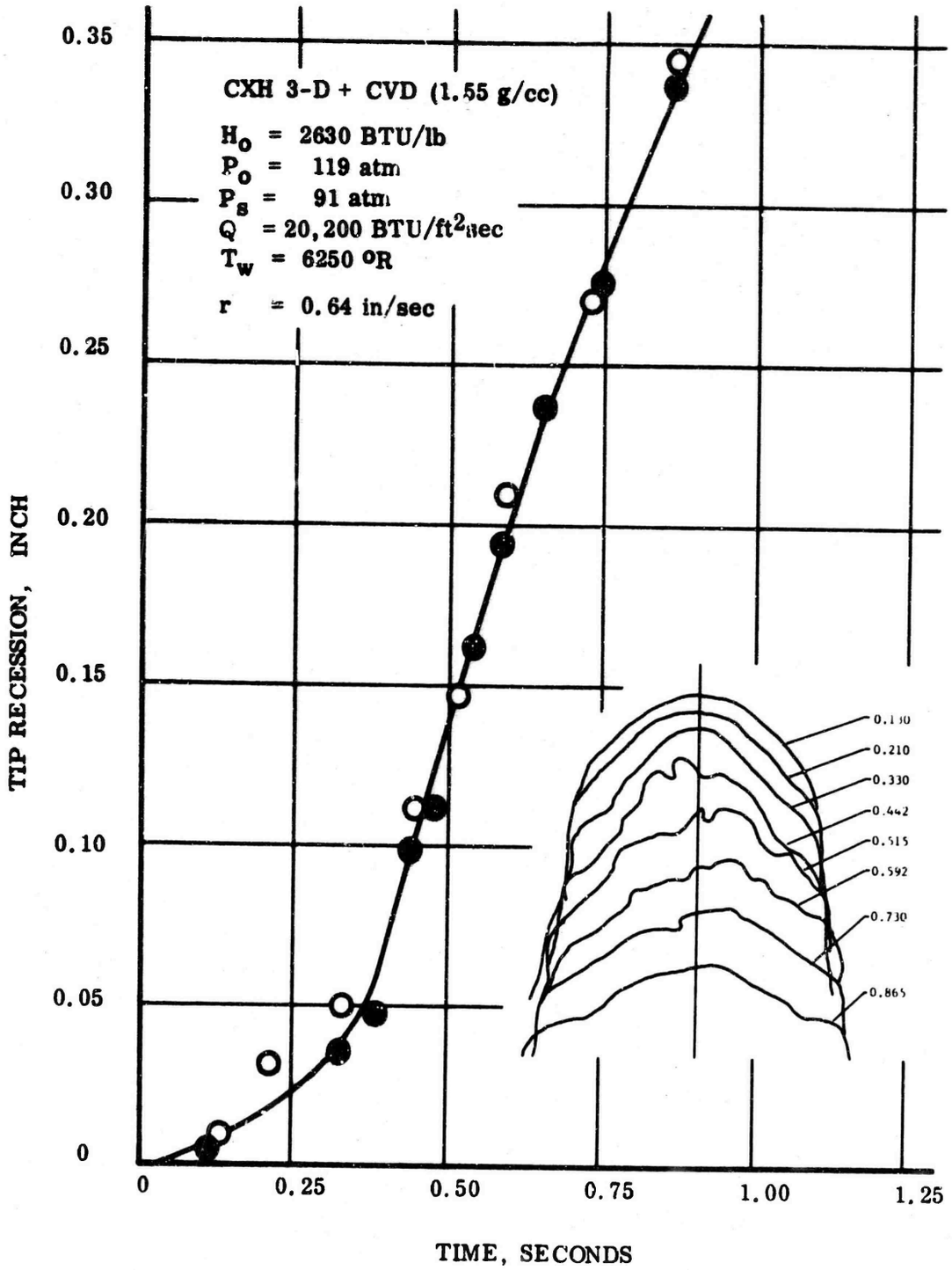

Figure 79 - Ablation of fine textured 3-D orthogonal carbon made by FMI with a rapidly infiltrated carbon matrix.

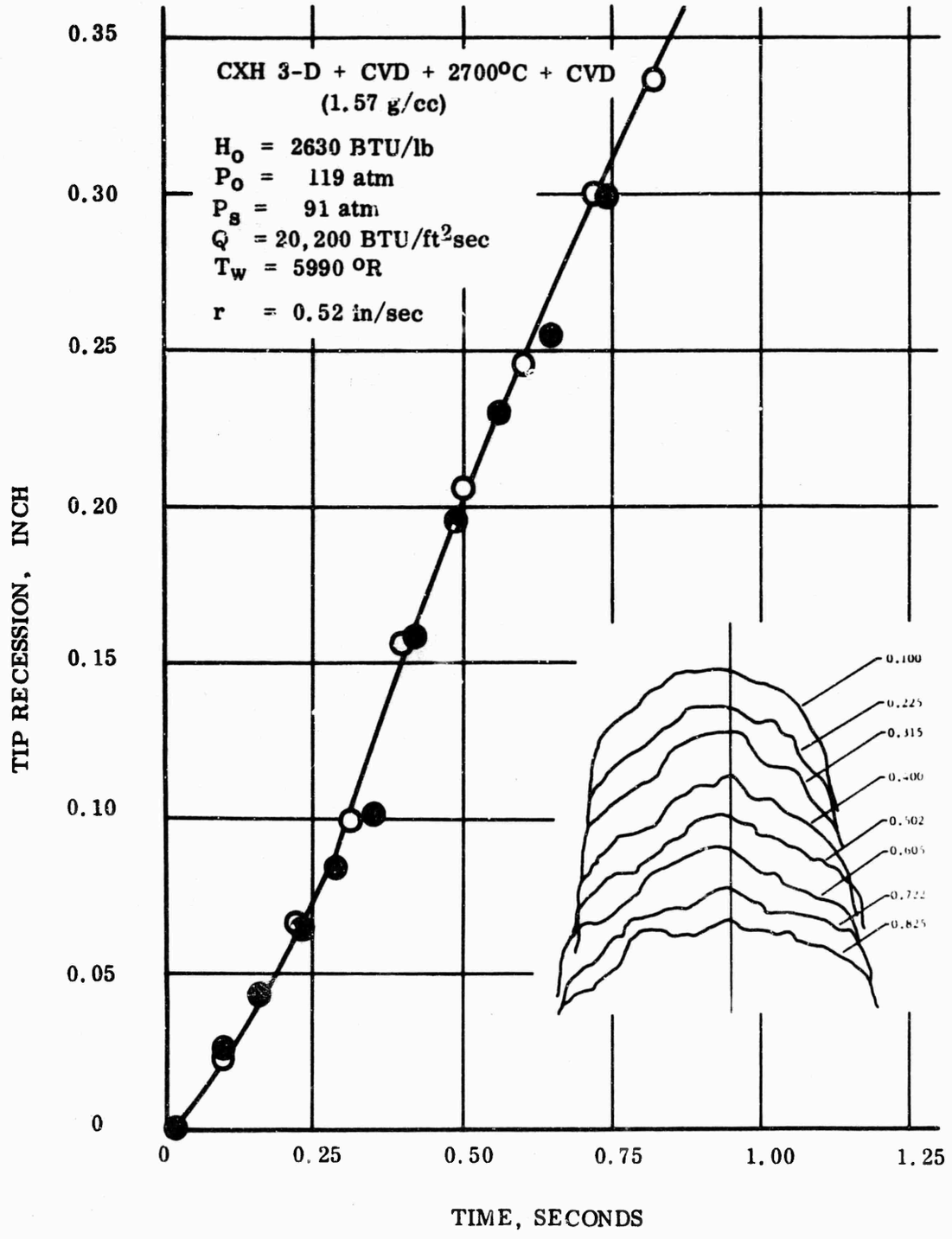

Figure 80 - Ablation of FMI fine 3-D carbon with a rapidly infiltrated matrix, after heating to 2700°C and re-infiltrating.

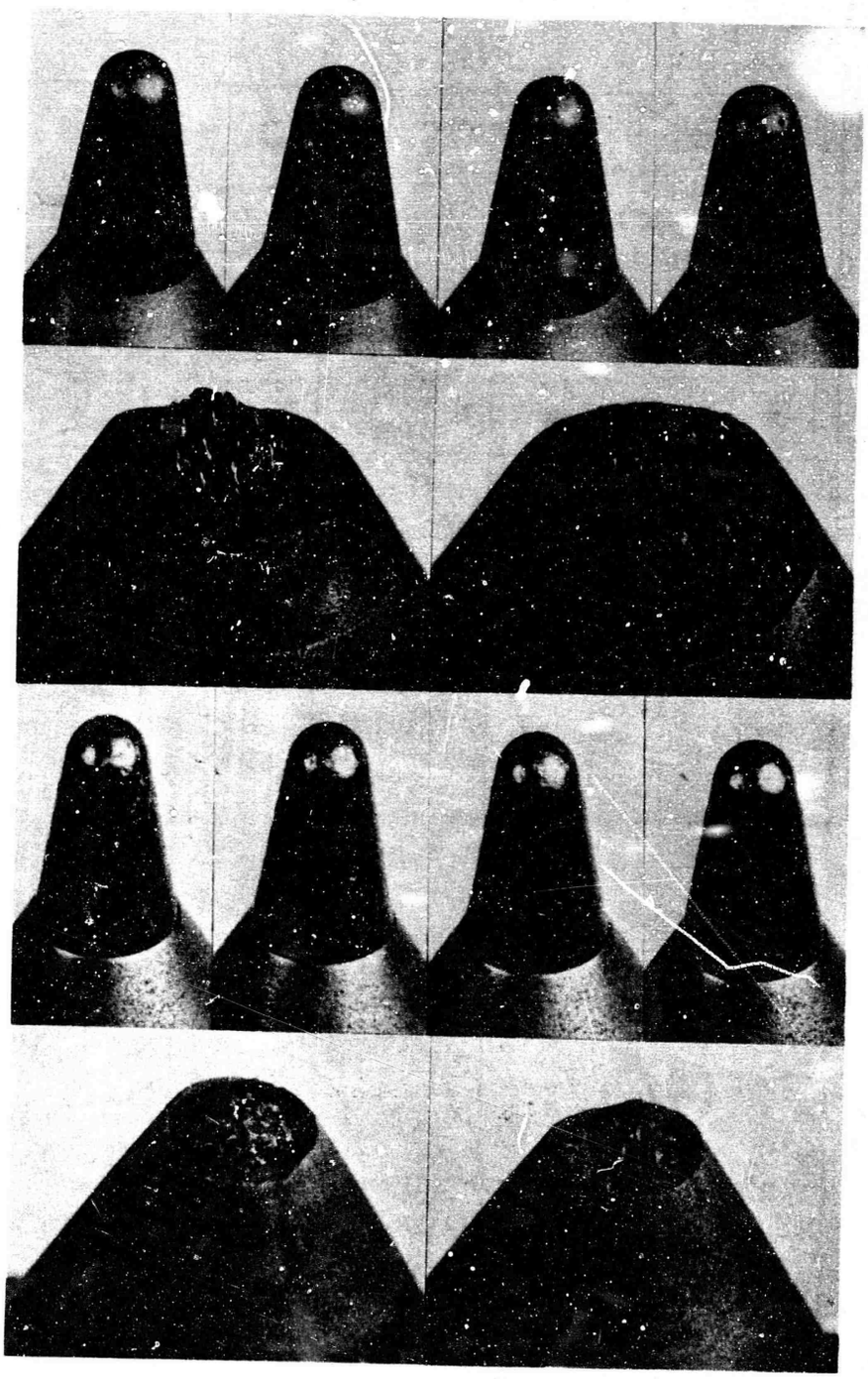

Figure 81 - Thornel 40 braid samples before and after test; "PD" matrix at top (run 70-A-1); graphitized CTP + FA matrix at bottom (run 70-A-4.) 1.85 X.

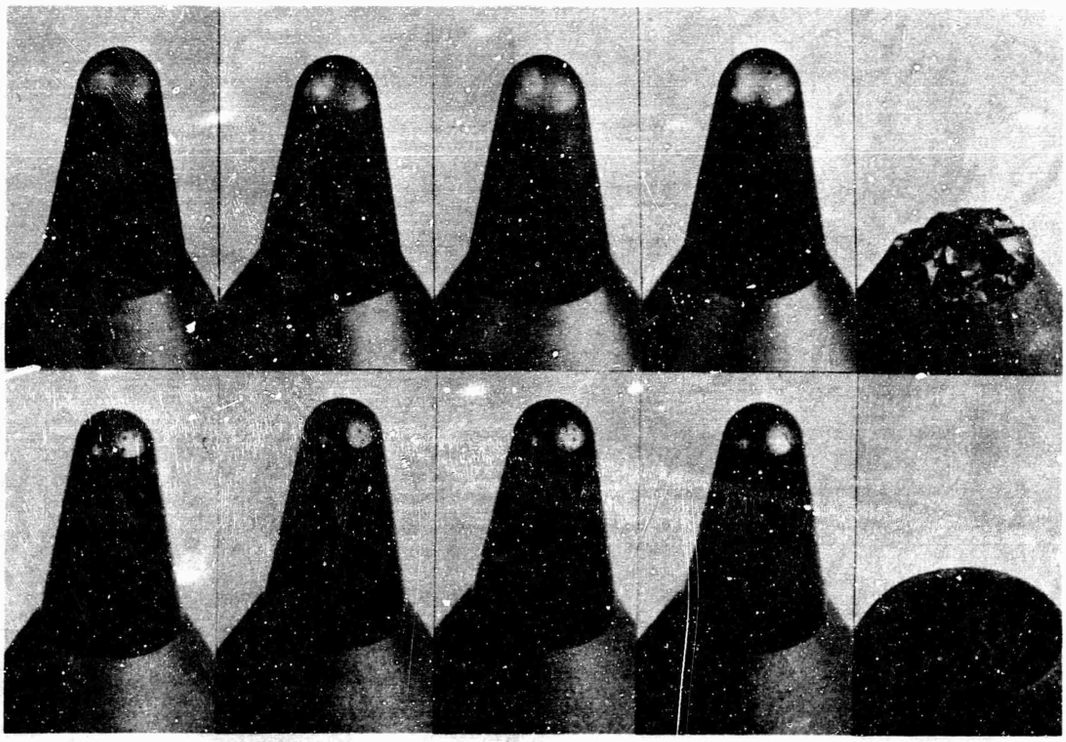

Figure 82 - Rapidly infiltrated 4-D composites before and after test;
top: 45-ply coarse textured sample;
bottom: 3-ply CXL impure fiber (failed after 0.18 sec.)

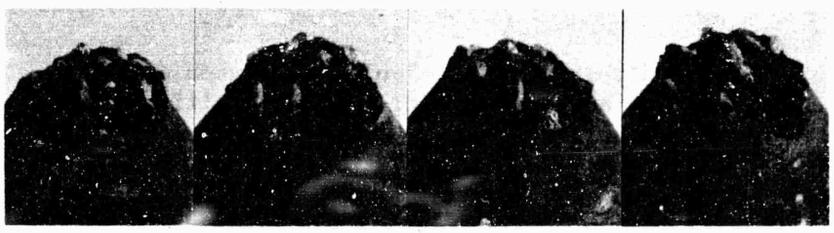

Figure 83 - Rapidly infiltrated M-II 4-D composite after test (material previously tested in 50 MW arc at AFFDL.) 1.85 X

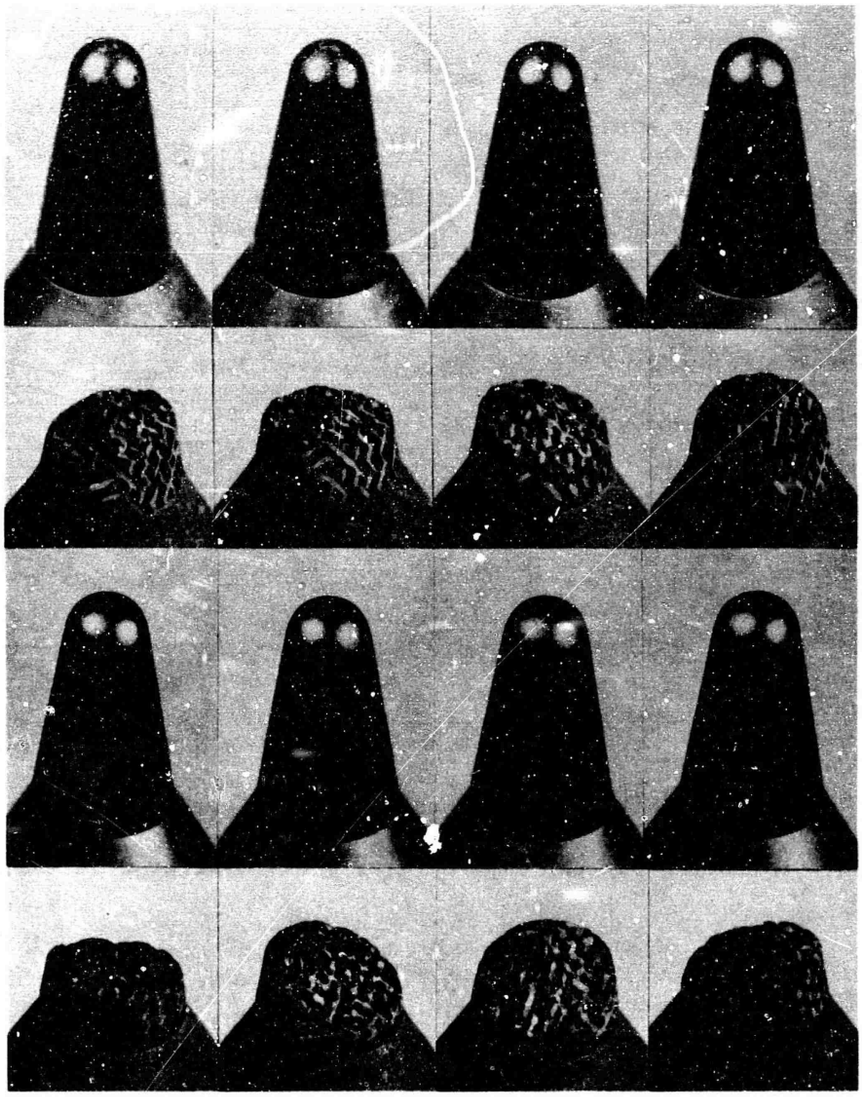

Figure 84 - Rapidly infiltrated 3-ply 4-D carbon samples before and after test; top - graphitized and re-infiltrated; bottom - as deposited. 1.85 X

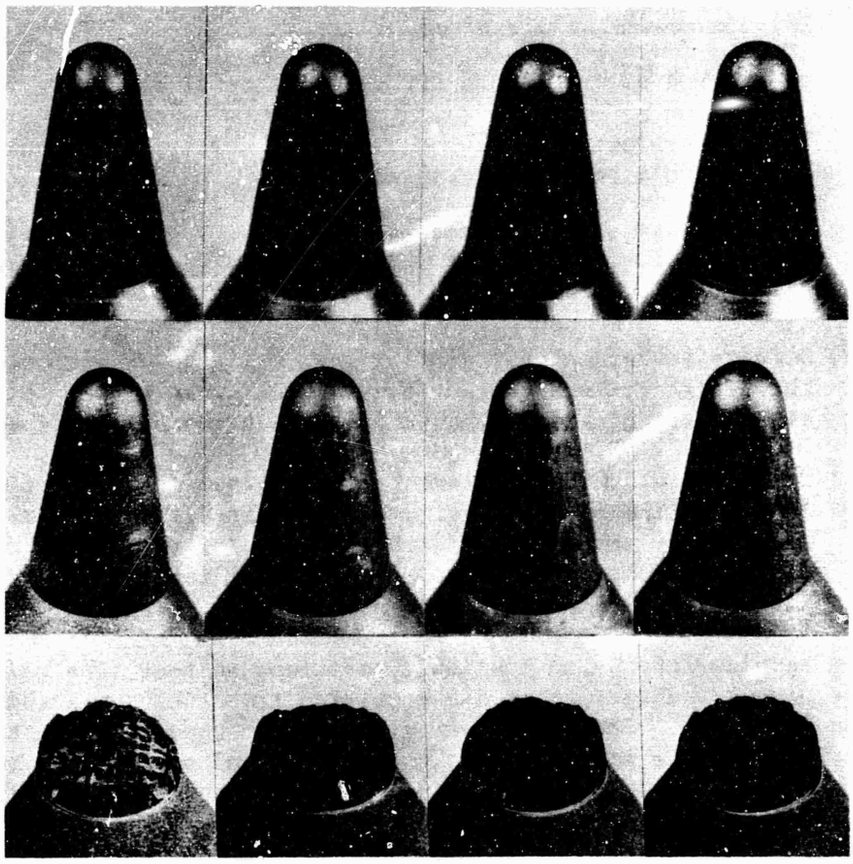

Figure 85 - Rapidly infiltrated 3-D FMI samples ablation tested; top: graphitized and re-infiltrated (sample not recovered); bottom: as-deposited, before and after test.

c. Results of the Second Series of Tests

The objectives of the second series of tests at AEDC were as follows:

(1) Duplicate previous run conditions and verify conditions with two ATJ-S models and two pressure models.

(2) Compare performance of fibrous graphite (IP50 and IP59) at two density levels with ATJ-S and with experimental composites having similar matrix processing.

(3) Compare performance of similar 3-D, 4-D and 7-D composites, having the finest texture currently available, when either low-anisotropy low-density fibers or high-anisotropy high-density fibers are used.

(4) Compare similar reinforcements with either (a) graphitized pitch, (b) glasslike carbon resulting from phenolic resin, (c) CVD carbon followed by impregnation with pitch and/or resin and graphitization, or (a), (b) or (c) followed by final CVD infiltration and graphitization, at similar levels of bulk density.

The samples for the 16 available positions in four runs were selected from the highest density materials resulting from the processing described on pages 31 and 50. Preference was given to 7-D composites instead of 4-D, in order to evaluate more completely the potential of the more isotropic geometry for nose tips. The process history of each specimen was coded as described in Table IV (page 34.)

The four runs at AEDC were intended to duplicate the previous runs, and the measured parameters indicated that this had been accomplished. The pertinant data are given below; these may be compared with Table VI (page 68.)

Run No.	Enthalpy BTU / lb	Plenum Pressure Atmospheres	Stagnation Pressure Atmospheres
70-D-1	2745	117	87
70-D-2	2470	118	--
70-D-3	2560	117	--
70-D-4	2535	116	93

Run times were limited to 1.1 to 1.2 seconds, and it was possible to make meaningful comparisons by measurements of sample weight and length before and after test. The post-test appearances are described in Figures 86 to 94. Profiles and plotted recessions are in Figures 95 to 104. The results are all listed in Table IX, page 112, and sample measurements are compared in Figure 95.

The principal conclusions from this series were:

(1) Acrylic-type precursor fibers, having high density, are preferable to low-density rayon-precursor reinforcements in spite of the cracks resulting from the greater anisotropy.

(2) Fine-textured 7-D reinforced graphites are equivalent to similar 3-D and 4-D reinforced materials.

(3) The samples having three cycles of high pressure pitch impregnation and 3000°C graphitization following CVD infiltration (models 1-3 and 1-5) were significantly more resistant than samples in which this processing sequence was reversed (models 2-1 and 3-5).

(4) The best 3-D composite in this series (model 1-3) showed a rate similar to IP59 in the same run (see Figure 97) up to 0.85 seconds in the test.

(5) Most of the samples suffered accelerated ablation at longer times, probably due to turbulent heating associated with surface roughness; the fine-grained graphites showed localized pitting, as before.

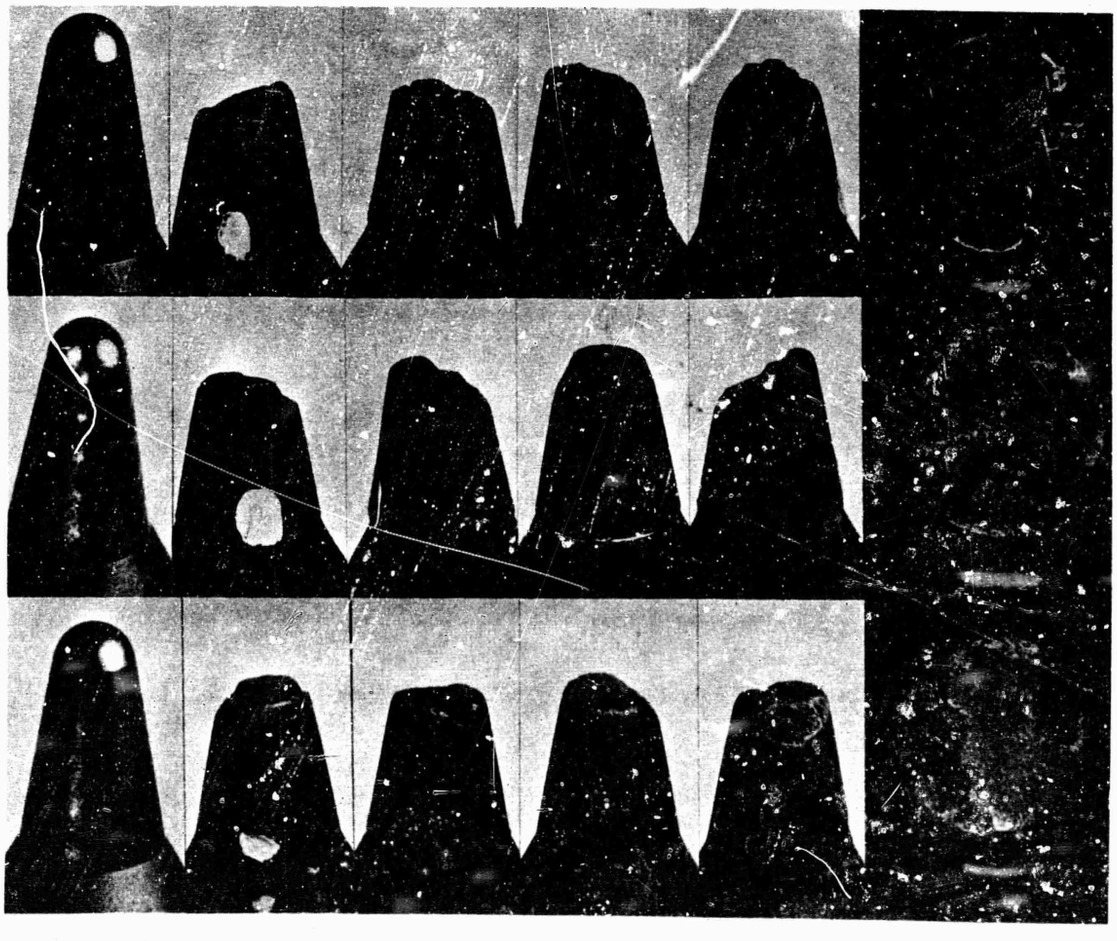

Figure 86 - Models of IP50 and ATJ-S after test; 1.85 X and 3.9 X (right). Top: run 70D3-2 (IP50). Center: run 70D3-1 (ATJ-S #6). Bottom: run 70D4-2 (ATJ-S #7).

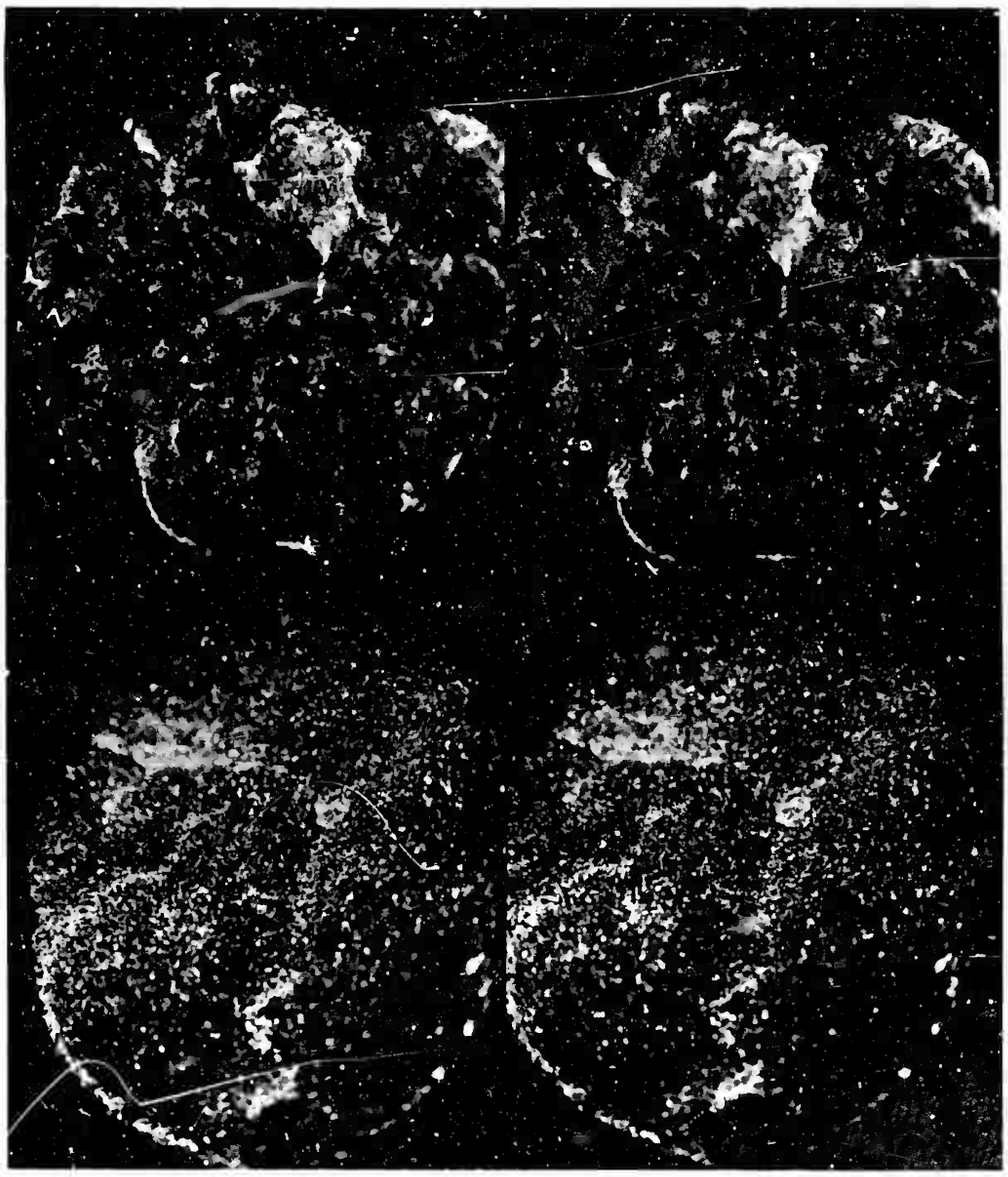

Figure 87 - Stereo pairs of IP50 (top) and ATJ-S #6 (bottom) after test (10X).

Both of the IP59 samples showed a single pit associated with a crack in the material, illustrated in Figures 88 and 89. In the second model tested, the pit had just begun to form at the end of test. Careful examination of pretest radiographs and of the micropolished disc cut from between the two tips (which were machined facing each other in the billet) did not reveal any cracks present in the material before test. There were "lakes" associated with the larger pores, however (see page 55).

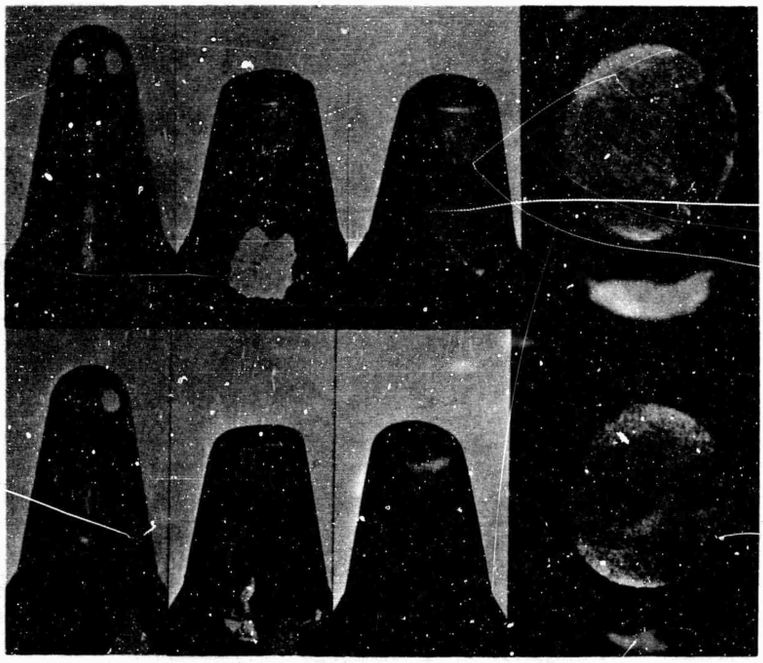

Figure 88 - Models of IP59 before and after test; 1.85 X and 3.9 X (right:)
Top: run 70D1-2. Bottom: run 70D4-5.

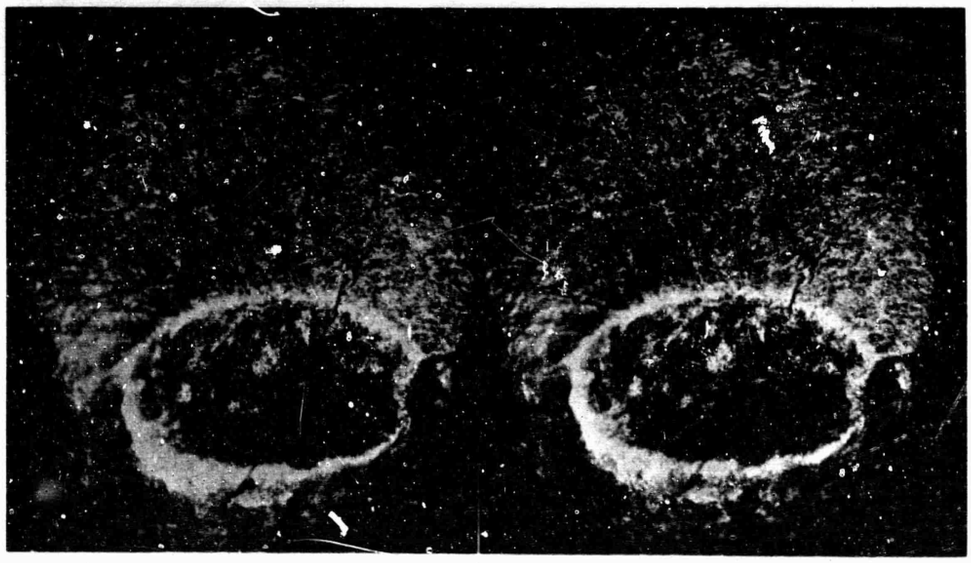

Figure 89 - Stereo pair of ablated surface of IP59C-1 showing concavity associated with a crack in the material. 10 X

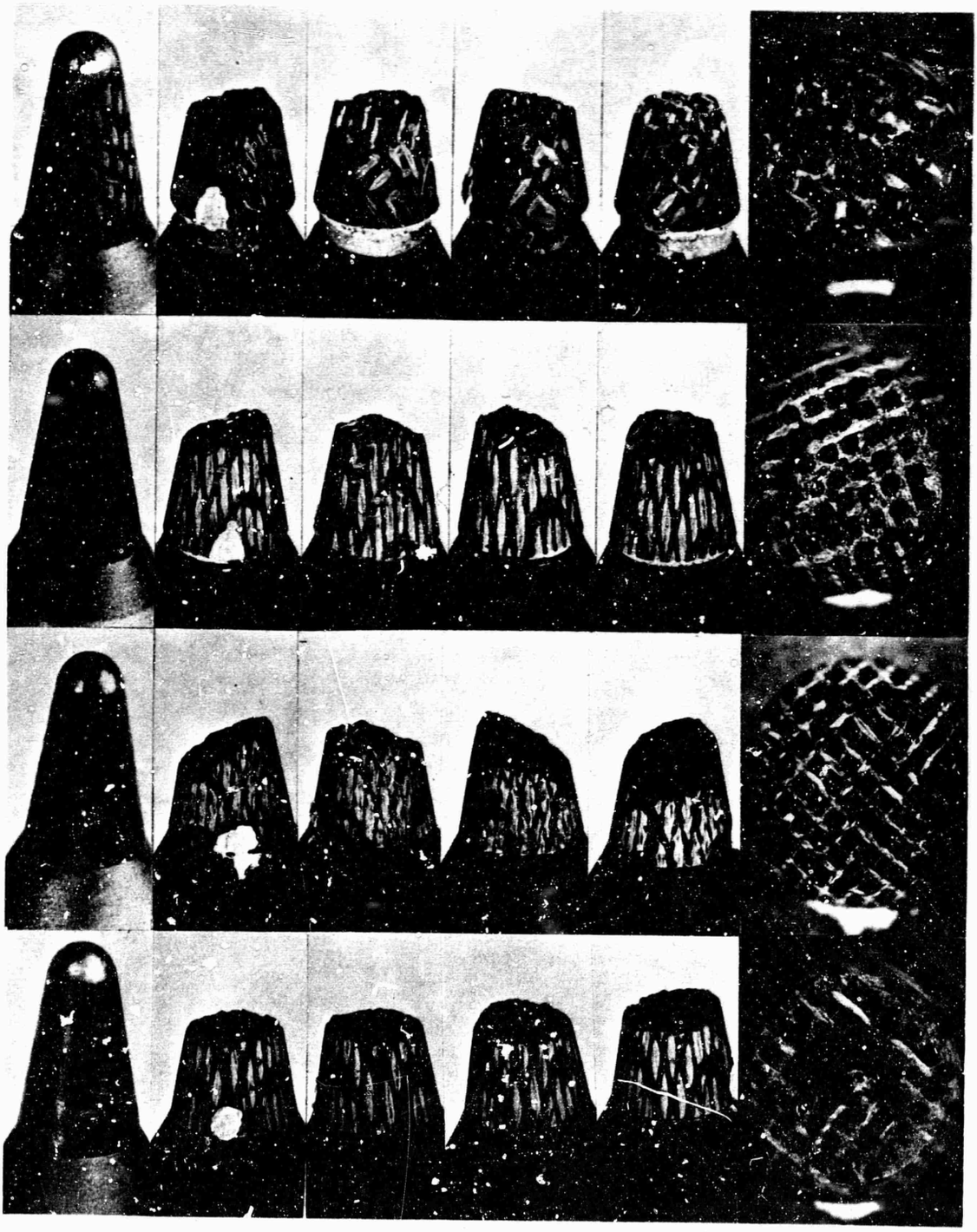

Figure 90 - Models of 4-D (top) and 3-D composites before and after test.
Top: run 70D1-4 (4SS13VYt). Second: run 70D1-3 (3SS11VYt).
Third: run 70D1-5 (3XH11VYt). Bottom: run 70D2-1 (3SSY11Gt).
1.85 X and 3.9 X (right.)

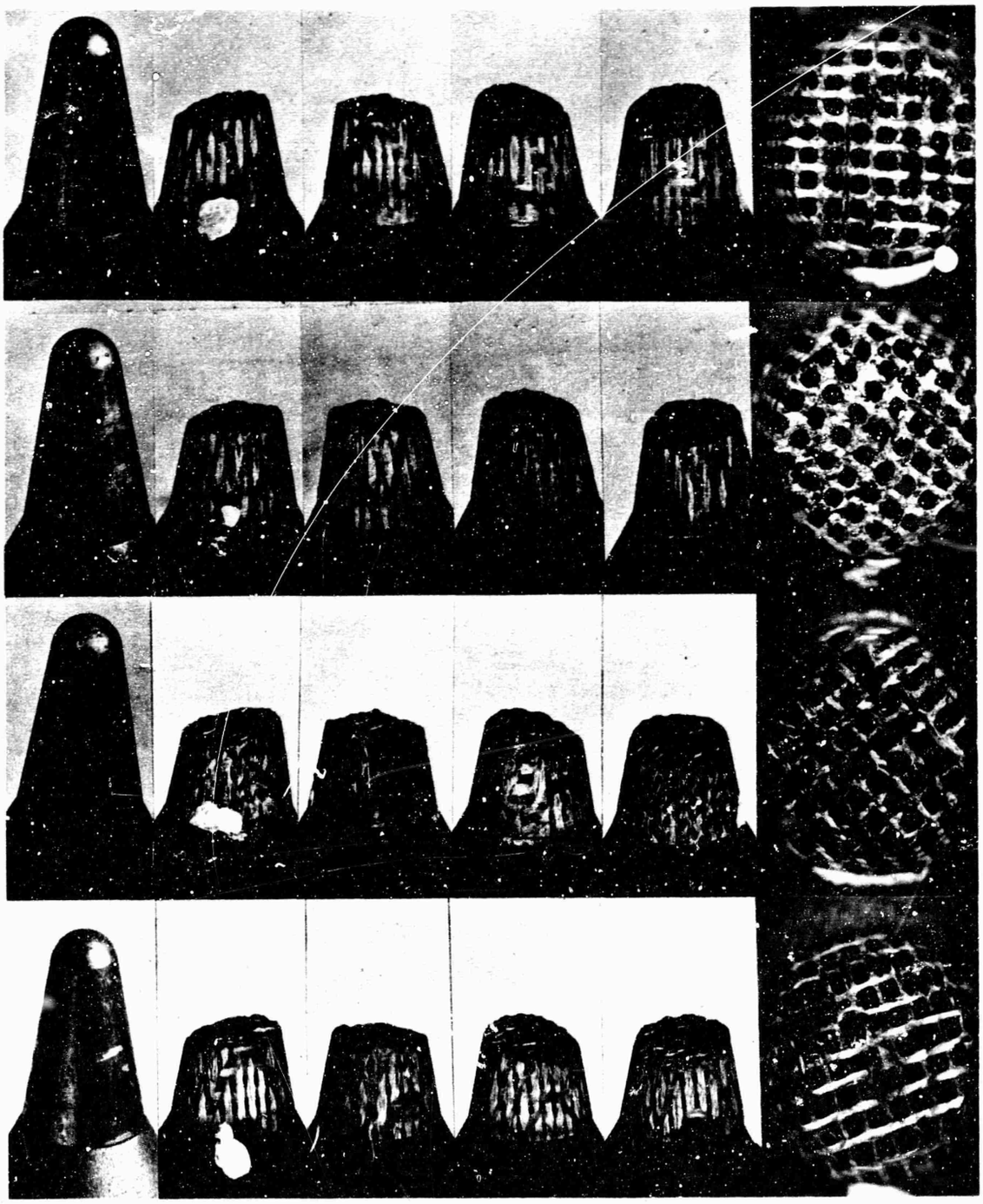

Figure 91 - Models of 3-D composites before and after test; 1.85 X and 3.9 X.
Top: run 70D2-2 (3SS13AYRGt11G).
Second from top: run 70D2-5 (3SS11VRGt11G).
Third from top: run 70D3-4 (3XH13GYRGt11G).
Bottom: run 70D3-5 (3XHYt13G).

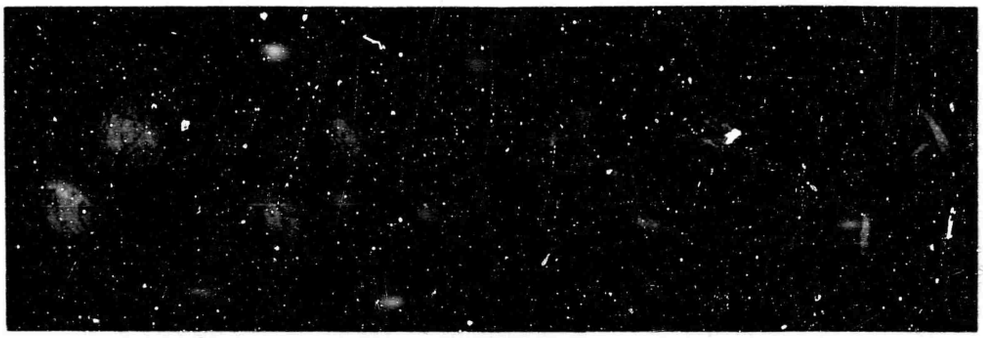

Figure 92 - Tips of 7-directional reinforced models before test at 3.9 X; from left: runs 70D2-3, 70D2-4, 70D3-3, 70D4-3 and 70D4-4.

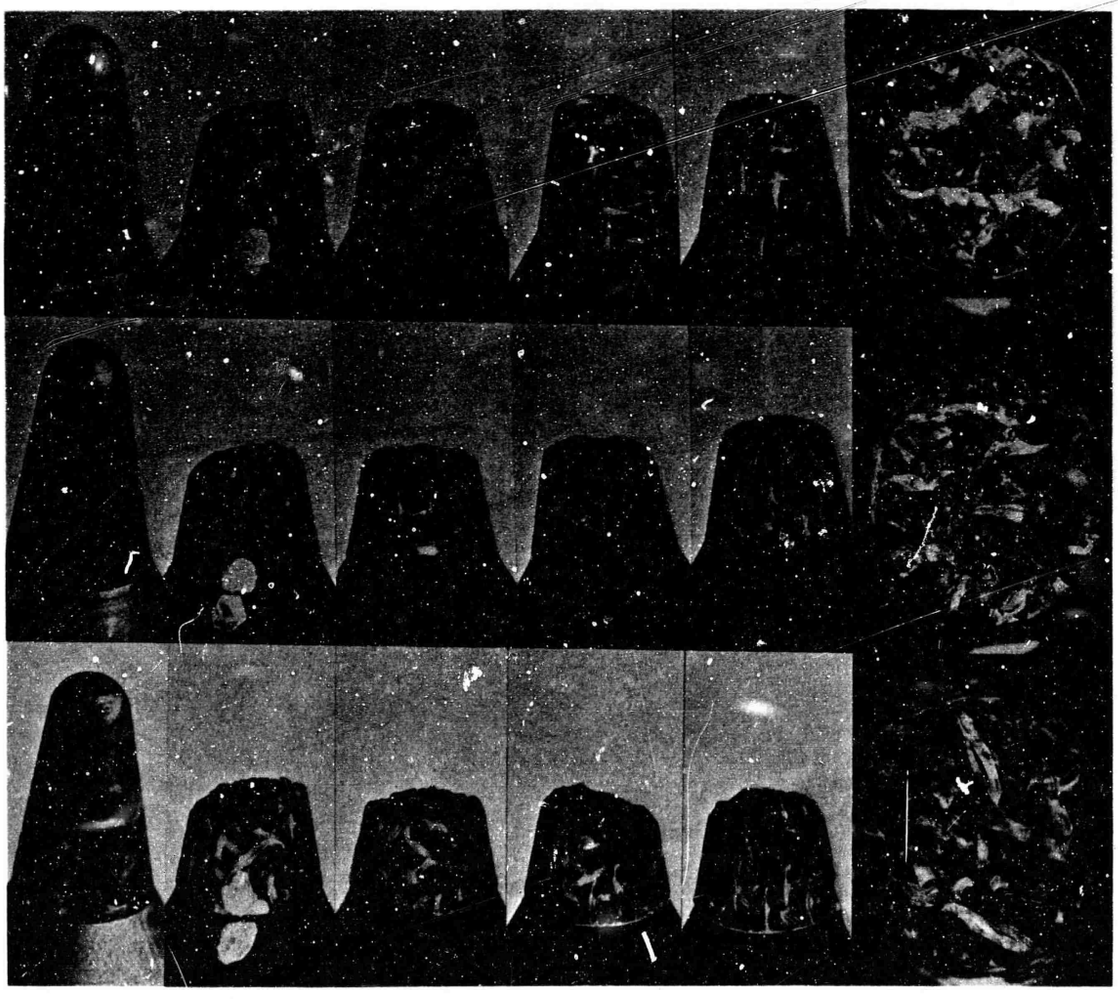

Figure 93 - Models of 7-D composites before and after test; 1.85 X, 3.9 X.
Top: run 70D2-3 (7SS13AYRG11Gt11G).
Center: run 70D2-4 (7XH13AYRG11Gt11G).
Bottom: run 70D3-3 (7XH13AYRG(2)11tG).

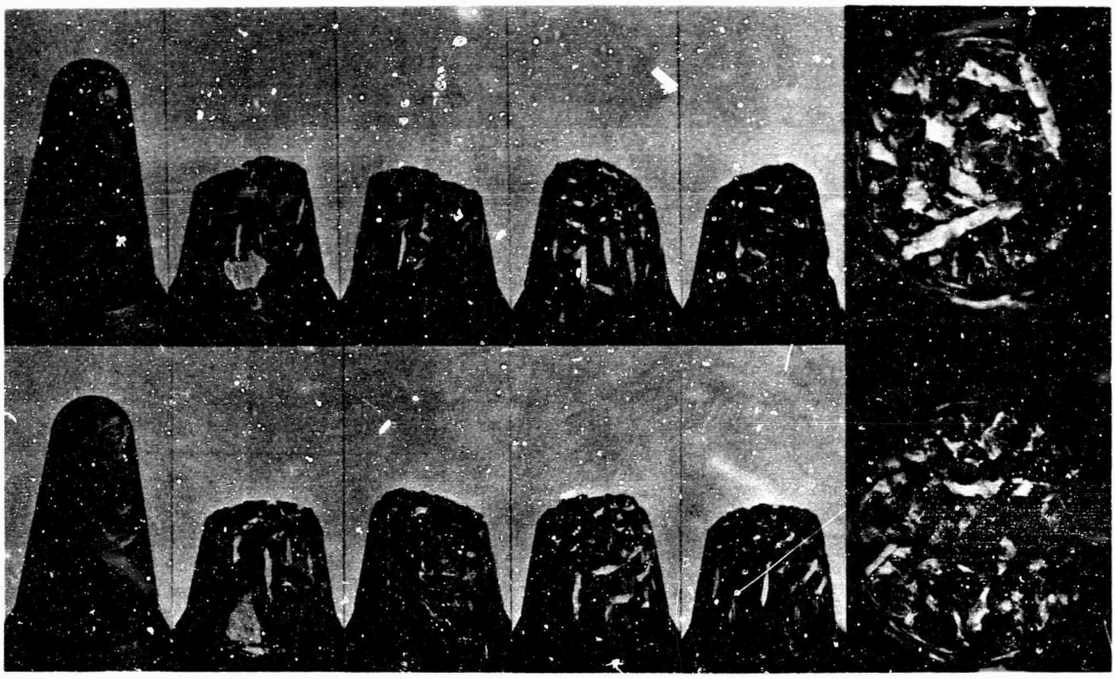

Figure 94 - Models of last 7-D composites before and after test;
1.85 X and 3.9 X (tip view at right.)
Top: run 70D4-3 (7SS13AYRG(2)11tG).
Bottom: run 70F4-4 (7SS13ARG(2)11tG).

The plots of recession versus time and profile changes are presented in the following figures. In each case the point representing measurements on the specimen at the end of test is indicated as a solid symbol following the film measurements. This provides an absolute length vs time reference point (the film data may not start exactly at time zero.)

Note that in most cases the samples sharpened to a point about halfway through the test, and then later became more blunt. The comparison slopes are taken from this region of model biconic shape. The slopes representing maximum recession rate and the time at which this steep rate began are listed in Table IX.

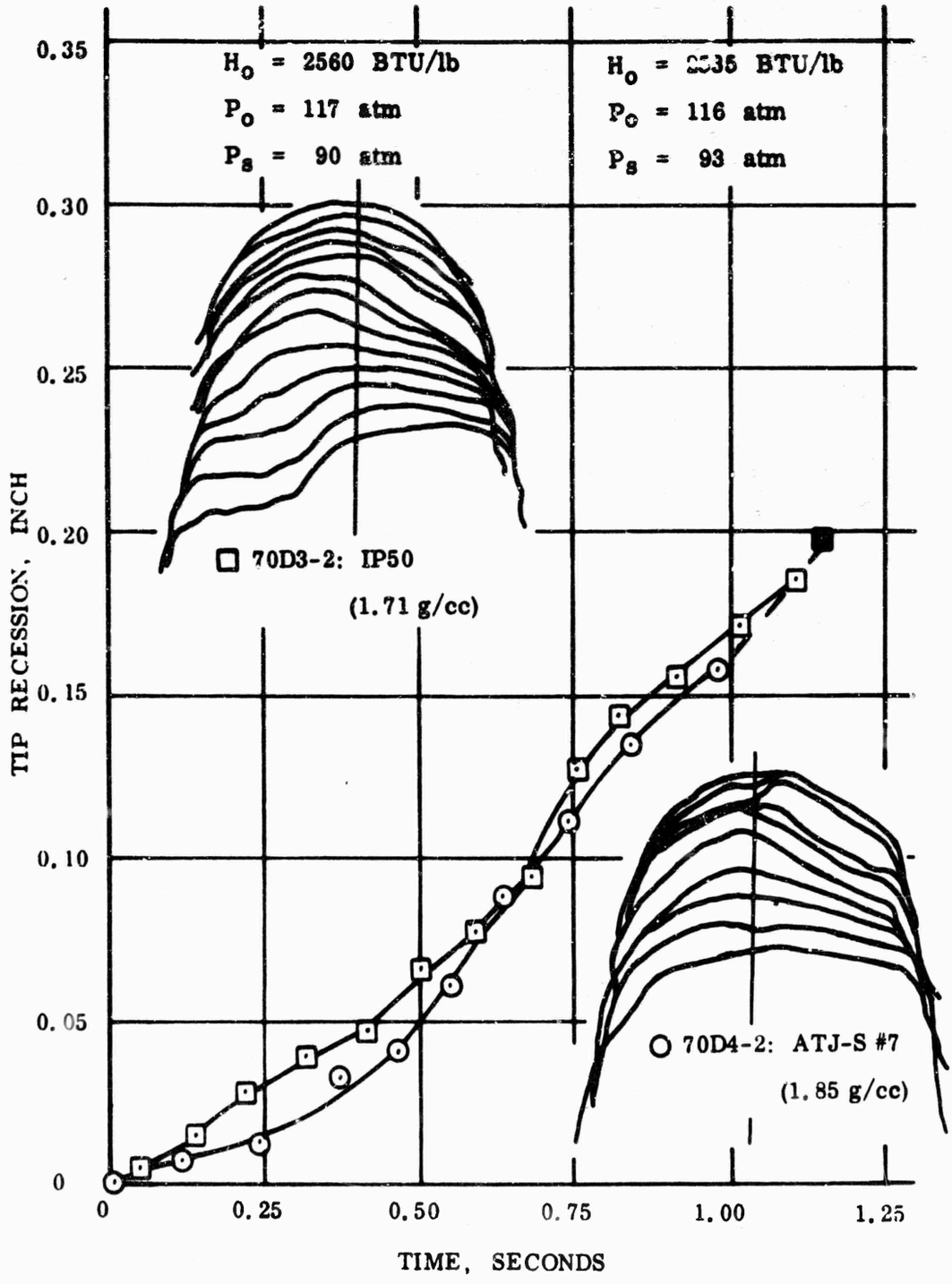

Figure 95 - Ablation of ATJ-S standard compared with low-density IP graphite.

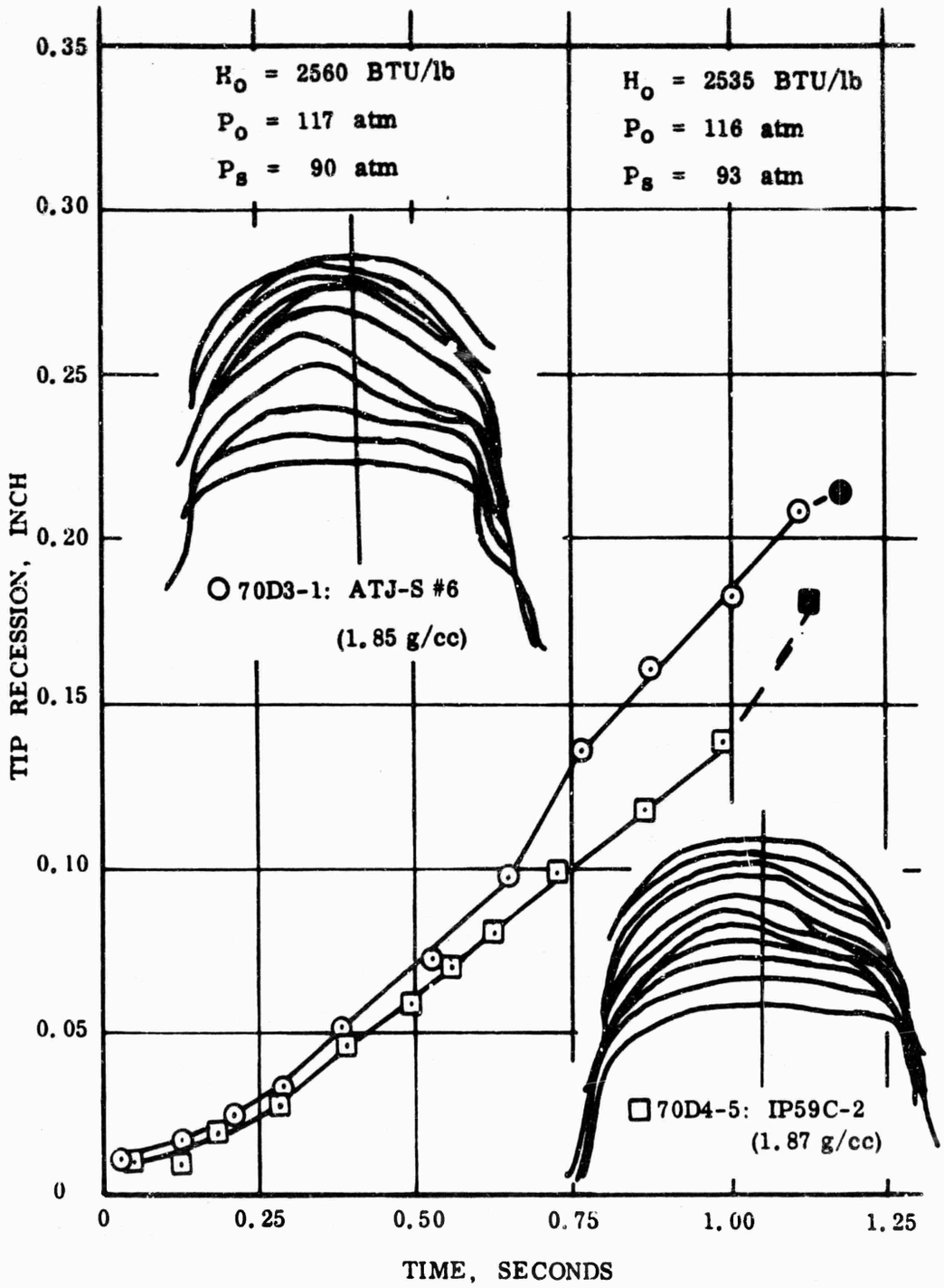

Figure 96 - Ablation of ATJ-S standard compared with high-density IP graphite.

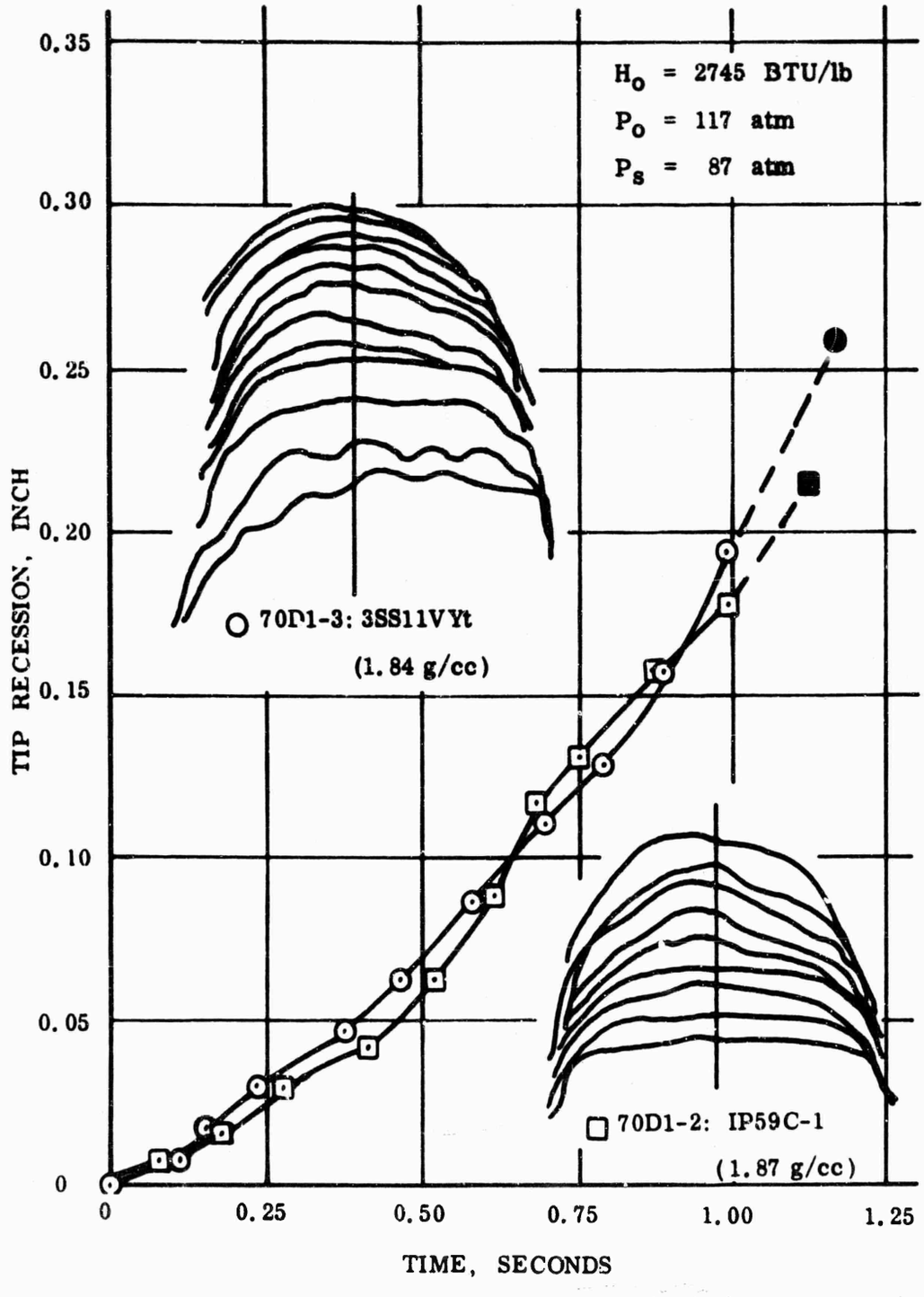

Figure 97 - Ablation of 3-D composite containing acrylic-precursor fibers compared with high-density IP fibrous graphite in the same run.

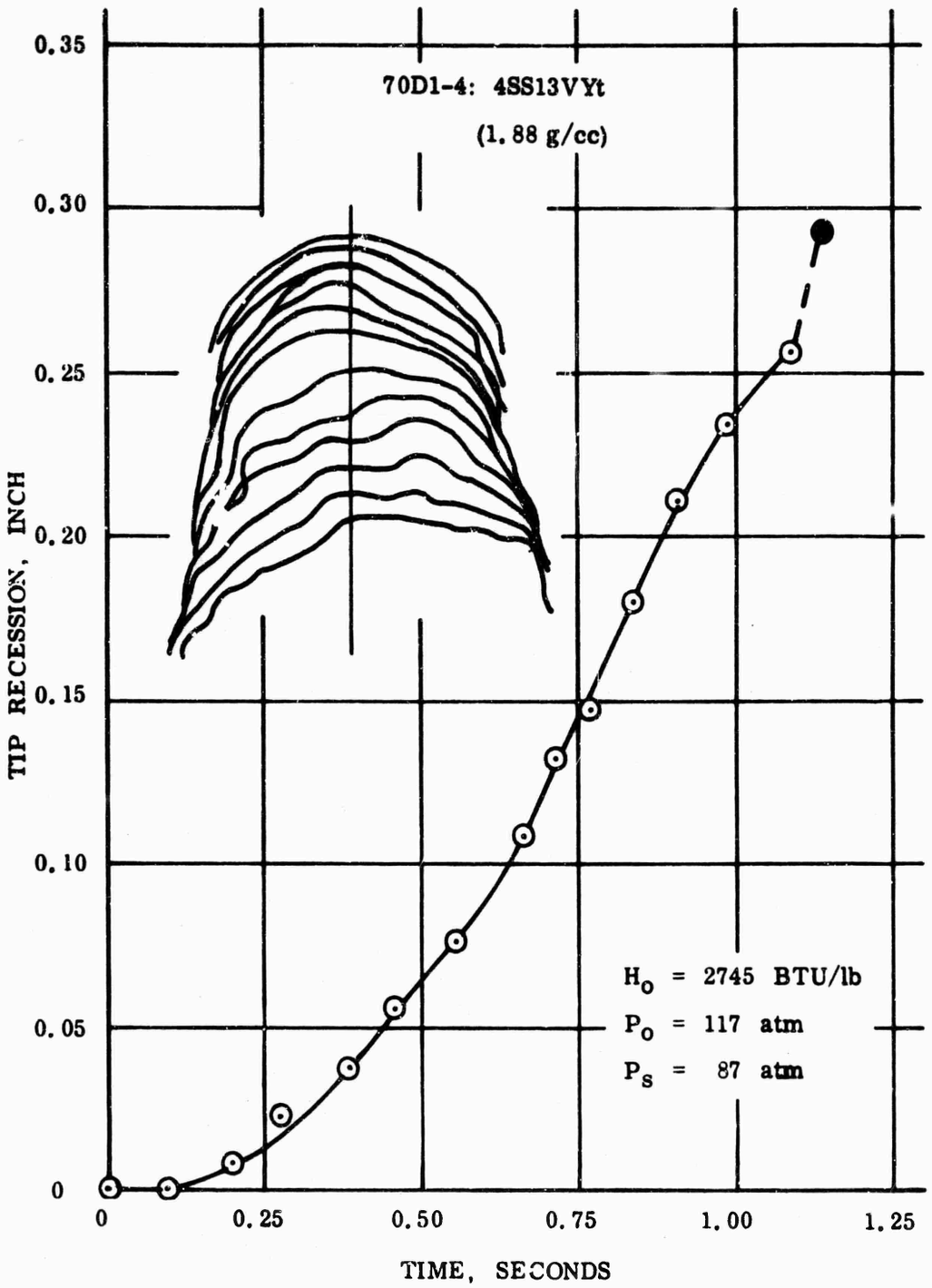

Figure 98 - Ablation of 4-D composite having identical constituents and pitch impregnation used in 3-D composite of preceding figure. Note accelerated rate beyond 0.65 seconds associated with increasing surface roughness.

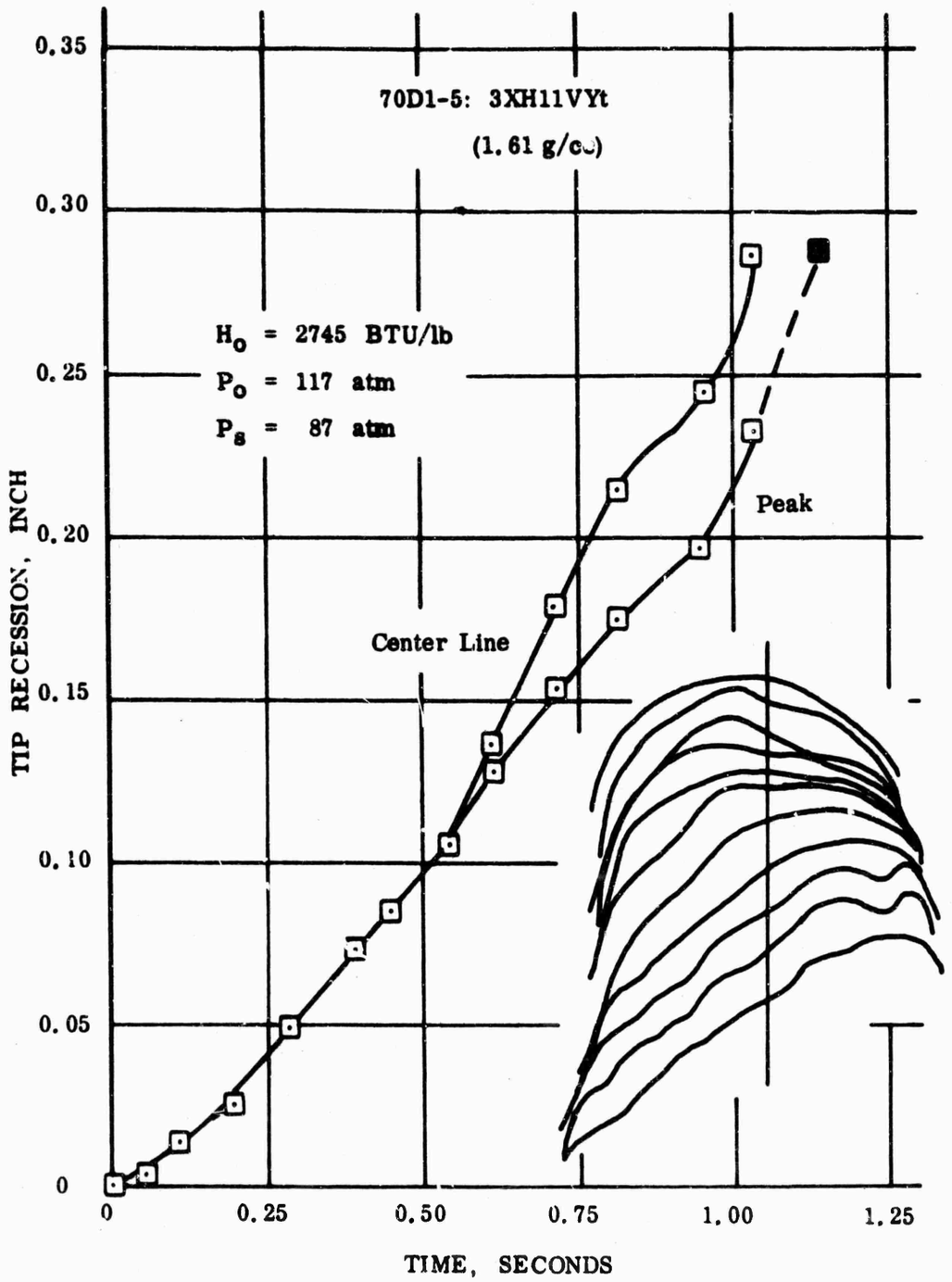

Figure 99 - Ablation of 3-D composite containing rayon-precursor fibers with pitch impregnation following CVD infiltration; compare with previous two figures.

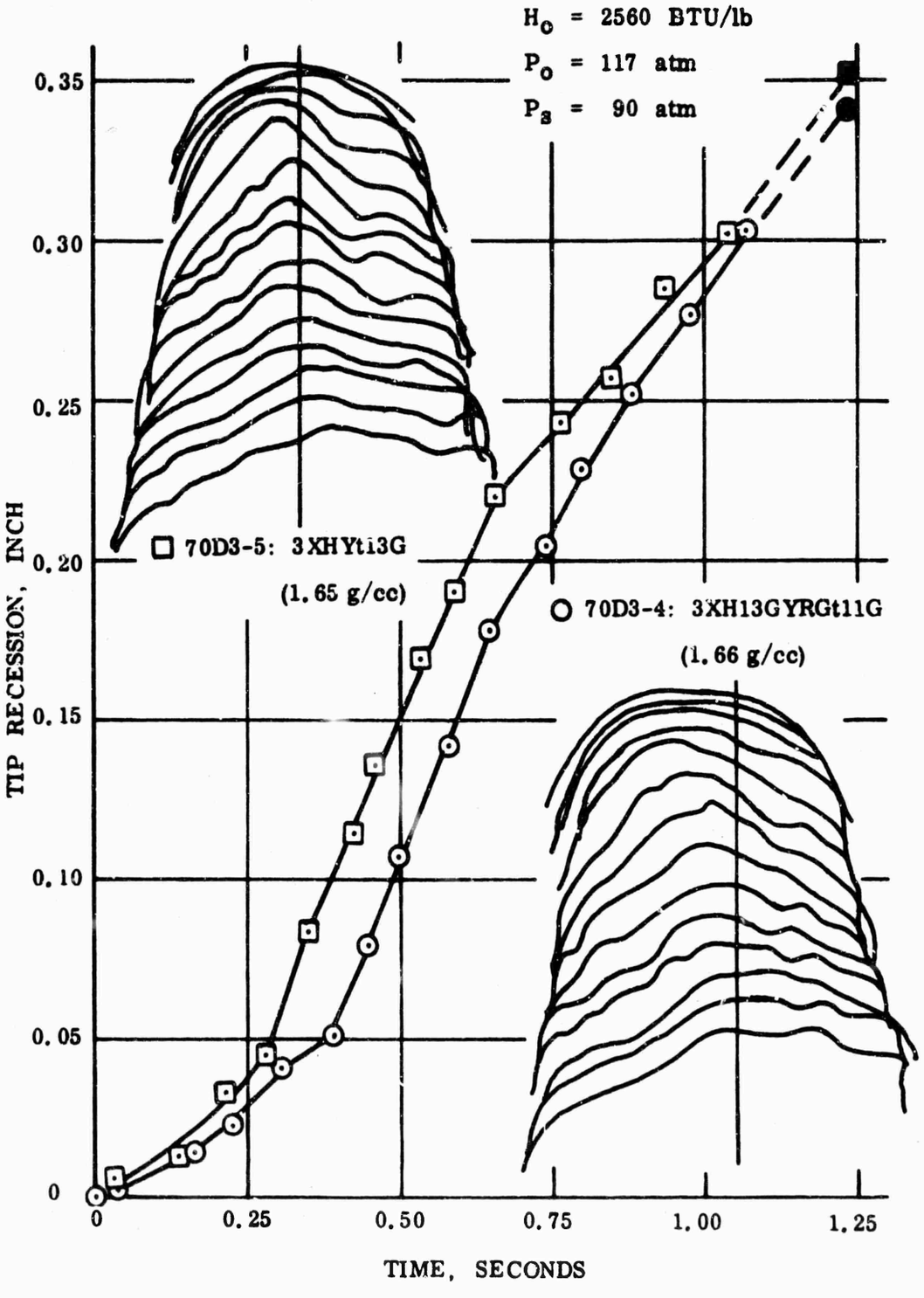

Figure 100 - Ablation of 3-D composites containing rayon-precursor fibers; top - infiltrated following three cycles of pitch impregnation; bottom - infiltrated before one cycle of pitch impregnation, followed by resin impregnation and CVD infiltration.

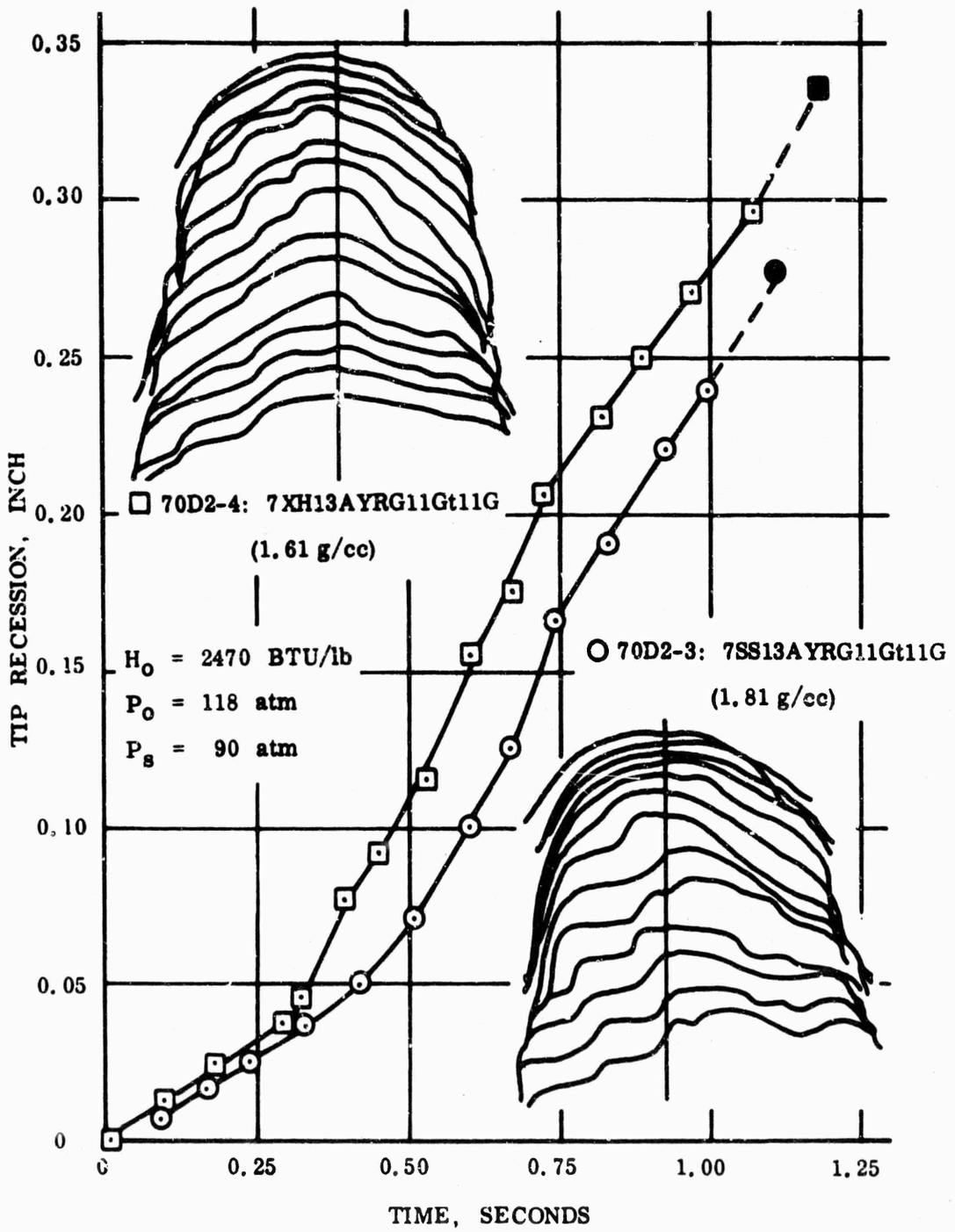

Figure 103 - Ablation of 7-D composites infiltrated after the tip was machined; top: rayon-precursor fibers, bottom: acrylic-precursor fibers.

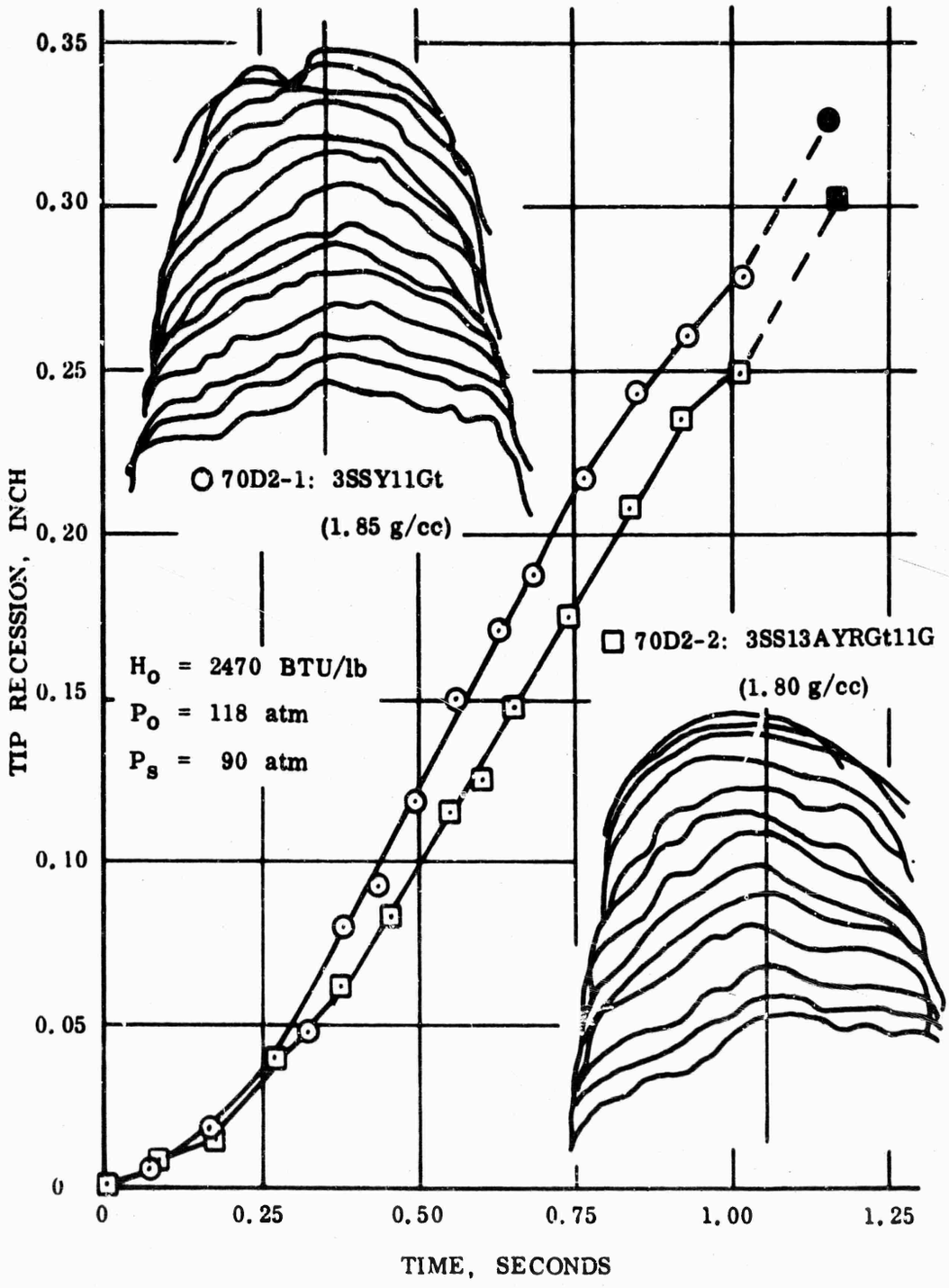

Figure 101 - Ablation of 3-D composites containing acrylic-precursor fibers; top - infiltrated following three cycles of pitch impregnation; bottom - infiltrated before one cycle of pitch impregnation, followed by resin impregnation and CVD infiltration.

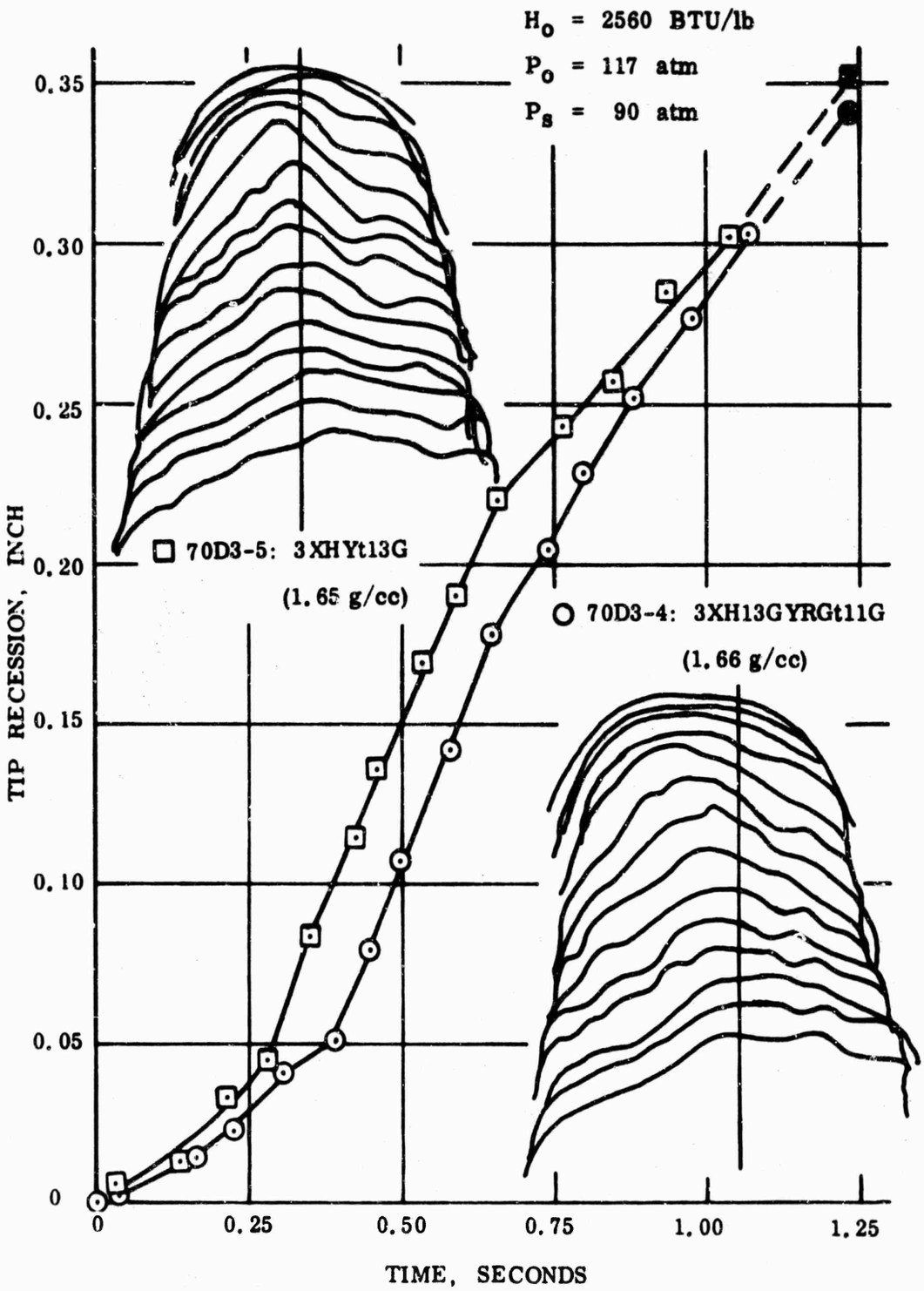

Figure 100 - Ablation of 3-D composites containing rayon-precursor fibers; top - infiltrated following three cycles of pitch impregnation; bottom - infiltrated before one cycle of pitch impregnation, followed by resin impregnation and CVD infiltration.

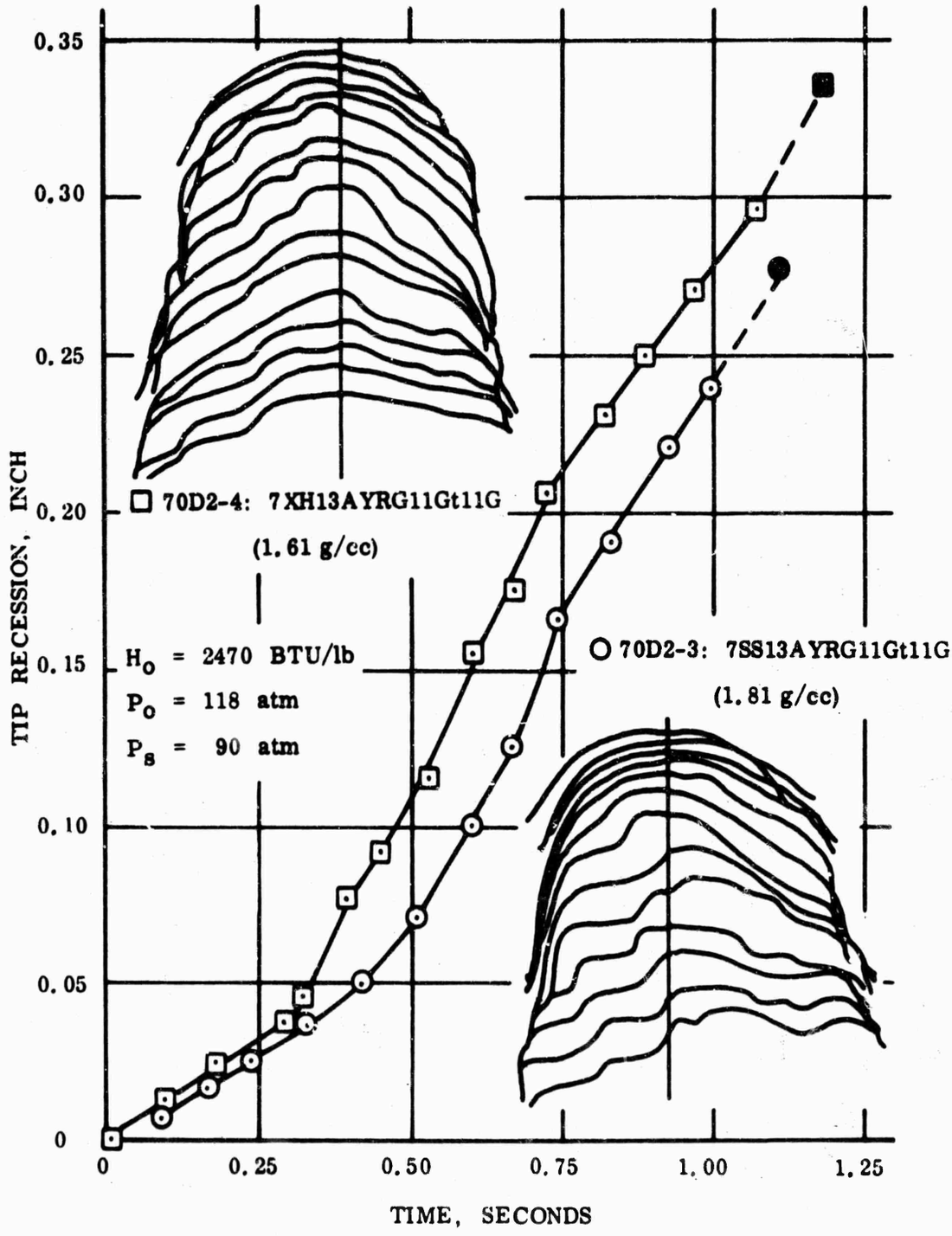

Figure 103 - Ablation of 7-D composites infiltrated after the tip was machined; top: rayon-precursor fibers, bottom: acrylic-precursor fibers.

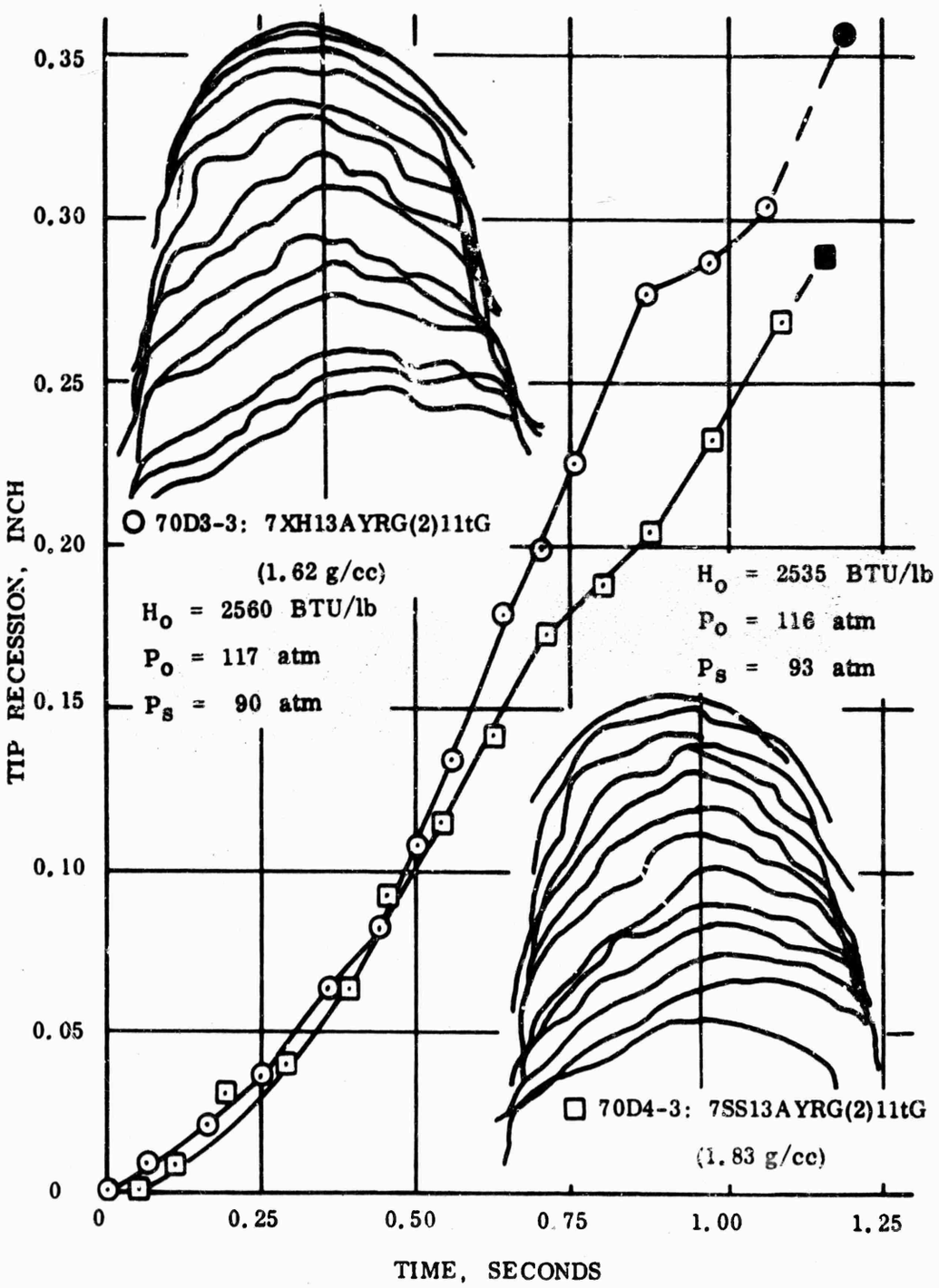

Figure 104 - Ablation of 7-D composites which were not infiltrated after machining; top: rayon-precursor fibers; bottom: acrylic-precursor fibers.

TABLE IX

SUMMARY OF SECOND SERIES OF AEDC TESTS

Model No.	Description	Bulk Dens. g/cc	Run Time sec.	Change in Samples Before-After Test: Weight grams	Length inch	$r_{av.}$ in/sec	Rate From Film: r_{max} in/sec	Time to r_{max} sec.
1-1	Press. #1 (87 atm.)		1.11					
1-2	IP59C-1	1.87	1.12	0.3727	0.213	0.190	0.29	0.50
1-3	3SS11VYt	1.84	1.17	0.5276	0.258	0.221	0.36	0.83
1-4	4SS13VYt	1.88	1.14	0.6141	0.293	0.257	0.41	0.66
1-5	3XH11VYt	1.61	1.14	0.5887	0.288	0.261	0.41	0.54
2-1	3SSY11Gt	1.85	1.16	0.6838	0.326	0.281	0.43	0.32
2-2	3SS13AYRGt11G	1.80	1.17	0.5935	0.302	0.258	0.32	0.37
2-3	7SS13AYRG11Gt11G	1.81	1.12	0.5627	0.276	0.246	0.42	0.47
2-4	7XH13AYRG11Gt11G	1.61	1.19	0.6205	0.336	0.282	0.43	0.31
2-5	3SS11VRGt11G	1.76	1.13	0.6205	0.312	0.276	0.59	0.50
3-1	ATJ-S #6	1.85	1.18	0.4743	0.215	0.182	0.27	0.58
3-2	IP50	1.71	1.15	0.4382	0.219	0.191	0.28	0.68
3-3	7XH13AYRG(2)11tG	1.62	1.19	0.6982	0.356	0.299	0.46	0.43
3-4	3XH13GYRGt11G	1.66	1.22	0.6584	0.342	0.280	0.49	0.39
3-5	3XH?t13G	1.65	1.22	0.6673	0.351	0.288	0.45	0.28
4-1	Press. #2 (93 atm.)		1.15					
4-2	ATJ-S #7	1.85	1.15	0.3788	0.198	0.172	0.25	0.47
4-3	7SS13AYRG(2)11tG	1.83	1.16	0.6291	0.288	0.248	0.34	0.35
4-4	7SS13ARG(2)11tG	1.80	1.13	0.6890	0.328	0.290	0.43	0.41
4-5	IP59C-2	1.87	1.13	0.2989	0.180	0.159	0.17	0.50

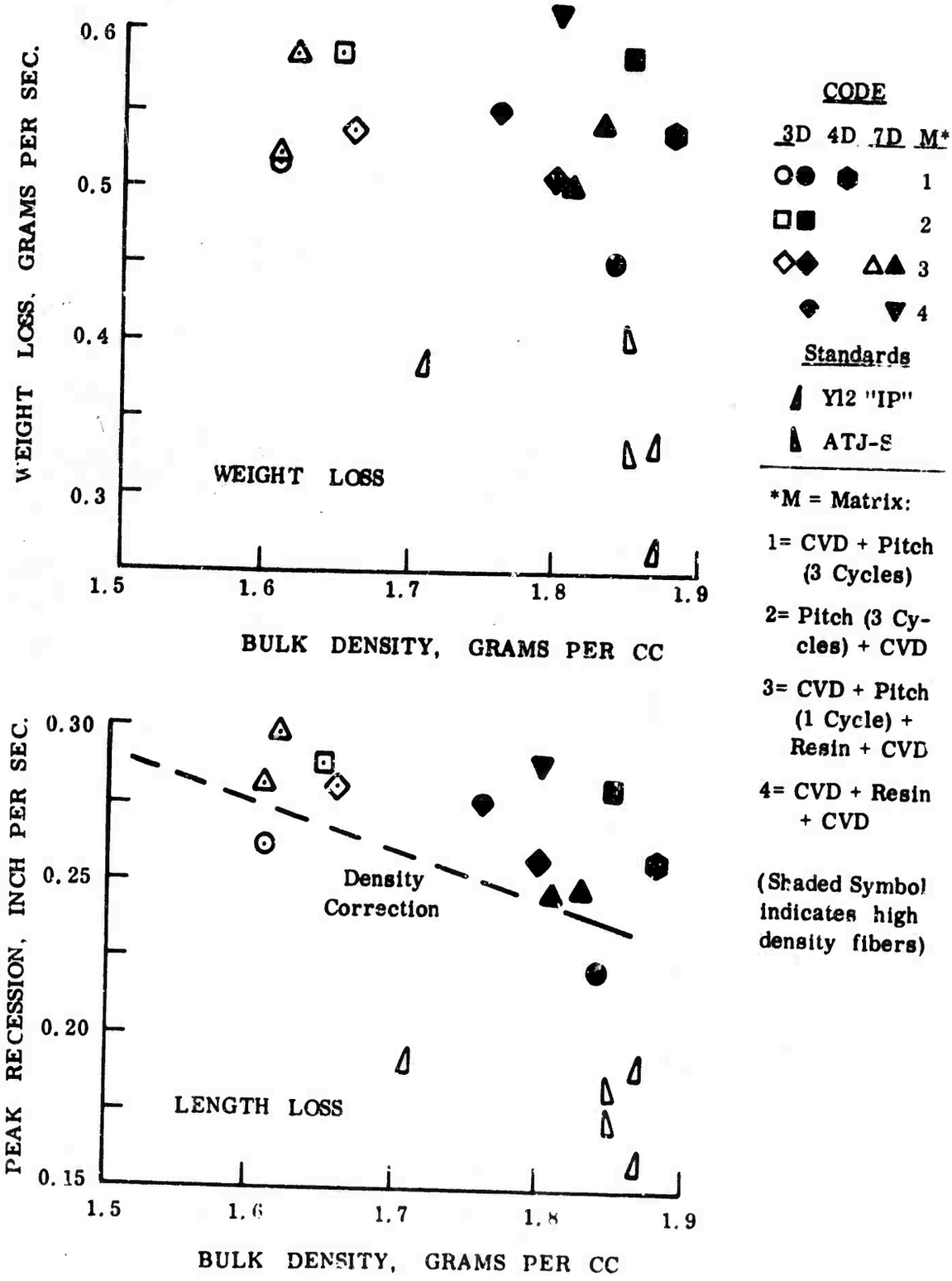

Figure 105- Comparison of average loss rates during 1.1 - 1.2 seconds of test, based on sample measurements before and after test.

d. Apparent Heat of Ablation Comparisons

A comparison between the ablation performance of different samples was made in terms of the "heat of ablation", Q^*, calculated as follows:

$$Q^*_{(apparent)} = \frac{\text{Nominal Heat Transfer Rate (BTU/ft}^2\text{ sec.)}}{5.2 \times \text{Bulk Density (g/cc)} \times \text{Recession Rate (in./sec.)}}$$

Because of the uncertainty in defining the maximum rate of recession, and because of the changes in effective heat transfer to the tip at different times during the run, as shape and surface roughness changed, two values were calculated for each test. In addition to r_{max}, the steepest slope from the film measurements, the average rate from start to 1 second (in the first series) and the total recession in the 1.1 - 1.2 second test time (in the second series) were compared. The latter values, although covering a wider range of conditions during each test, showed less scatter between materials that were nominally the same.

These apparent heats of ablation are illustrated Figure 106. The solid bars represent the calculated Q* corresponding to r_{max}. The actual heat required to remove a given weight of material at the maximum recession rate was, of course, much higher, since the heat transfer at this time in the test was increased by the biconic shape and by the surface roughness. The values of heat transfer rate used for the comparisons are given in the figure; the value from the 1/8 inch R_n calorimeter was used in the first series, and a value of 16,200 BTU/ft^{2}sec was used for the second series simply because the average Q* values for the ATJ-S standards best matched the average in the first series when this value was used. In previous studies under another program, tests by GE-RESD in the 50 MW AF-FDL RENT facility had produced rates for ATJ-S and a composite similar to one tested in the first series, which gave Q* values in good agreement with those in the first series at AEDC. The samples and the calorimeter in the larger facility had 1/4 inch nose radius.

The principal reason for the comparisons in Figure 106 was to assess ablation performance independent of bulk density, since thermochemical removal of carbon should account for linear recession rates inversely proportional to density. The results indicate that such a proportionality exists for these materials, since Q^* is approximately the same when composites are made with either low density (CXH) or high density (C-2000 or C-3000) fibers when processing is similar. Note also the similarity between low-density IP50 and IP59, and the similarity between 3-D Mod. 3 and ATJ-S in the first series. Independent of density, the coarser texture 4-D composites in the first series are significantly inferior to finer textured composites, and samples which were infiltrated initially, and subsequently impregnated and graphitized, performed better than samples in which this process sequence was reversed. With similar texture, there is not a significant difference between 7-D and 3-D reinforced samples, although 4-D samples appeared to be slightly inferior. The differences in Q^* assuming uniform test conditions are associated with differences in porosity accessible to the stream of gas and roughening which can increase the effective heat transfer.

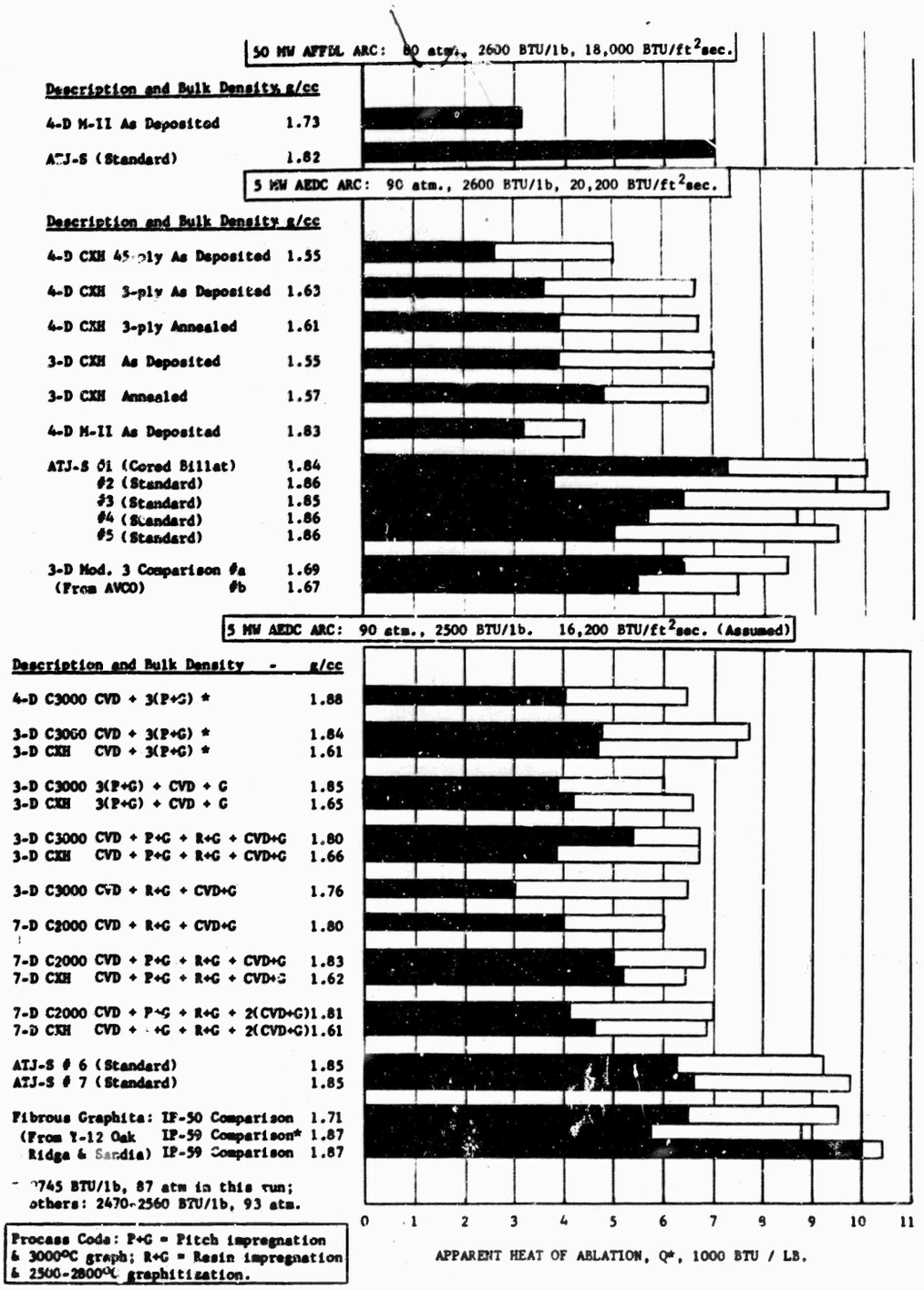

Figure 106- Ablation test comparisons in terms of an apparent heat of ablation, Q*, calculated from maximum rates of tip recession (solid bars) and average recession in 1.1 to 1.2 seconds (open bars).

e. Microscopic Mechanisms Affecting Ablation Performance

After test selected models were sectioned in an axial plane and micro-polished in order to examine cracks, selective etching of constituents, and any other features of structural change resulting from the heating. Figures 107 to 125 illustrate the observations, which included scanning electron microscopy of some of the models from the first series.

The principal features associated with differences in performance were cracks at reinforcement bundle boundaries; these offered paths for pressure build-up within the material, particularly in the 4-D constructions (Figure 107) with low packing angles. Cracks around the rods in 3-D Mod. 3 (Figure 108) were not origins of aggravated erosion and may have been closed at the ablating surface, due to the thermal expansion anisotropy. The longitudinal splits within the 3-D weaves did show opening at the surface indicating that they were open to oxidation during the test (Figures 113, 115, 122.)

At high magnfications, cracks at boundaries of filaments and CVD coatings were often present during ablation, with a consequent oxidation-vaporization etching of the additional free surface exposed. Often the matrix-filament interface was not attacked, however, indicating good adherance, and some of the filament-like projections observed by scanning electron microscopy actually were CVD, resin or pitch precursor material. See Figures 109, 112, 115-118, 123 and 124. There was evidence of constituent density differences, with more rapid attack of glassy carbon versus graphitized resin (Figures 110 and 111) and of low-modulus fibers versus high-density fibers, relative to the high-density CVD carbon or graphitized pitch or resin (Figures 117 and 118, 124.)

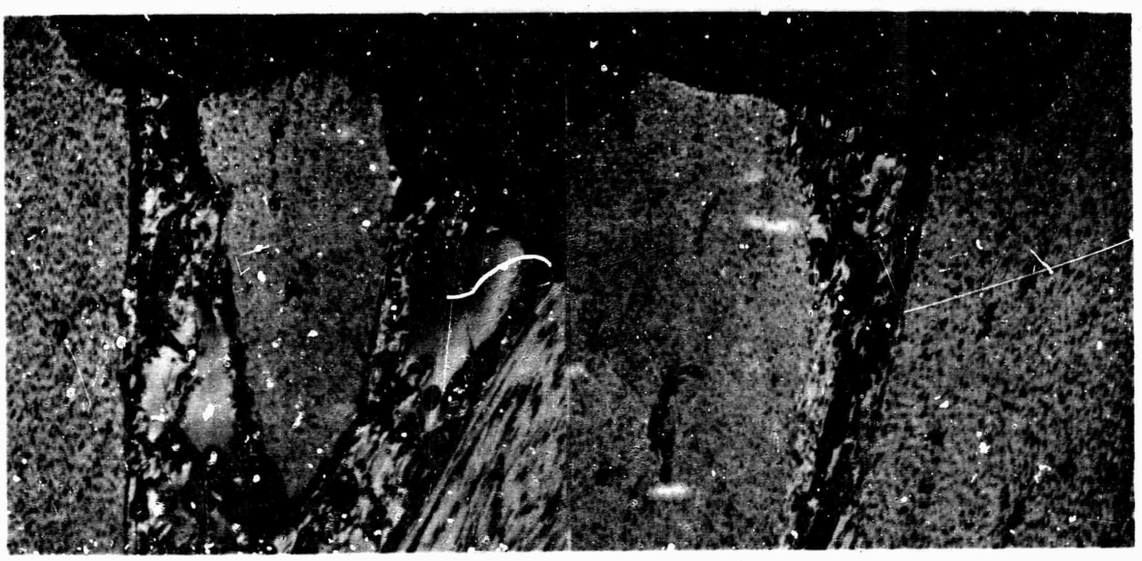

Figure 107 - Sections through Thorrel-40 composites after test showing cracks at matrix-reinforcement boundaries; CTP + FA precursor matrix at left; "PD" matrix at right (see page 23). Polarized light, 50 X.

Figure 108 - 3-D Mod. 3 model (a) after ablation; stereo pairs in electron emission at 20 X (top) and 100 X (bottom) showing cracks at periphery of Thornel 50 rods.

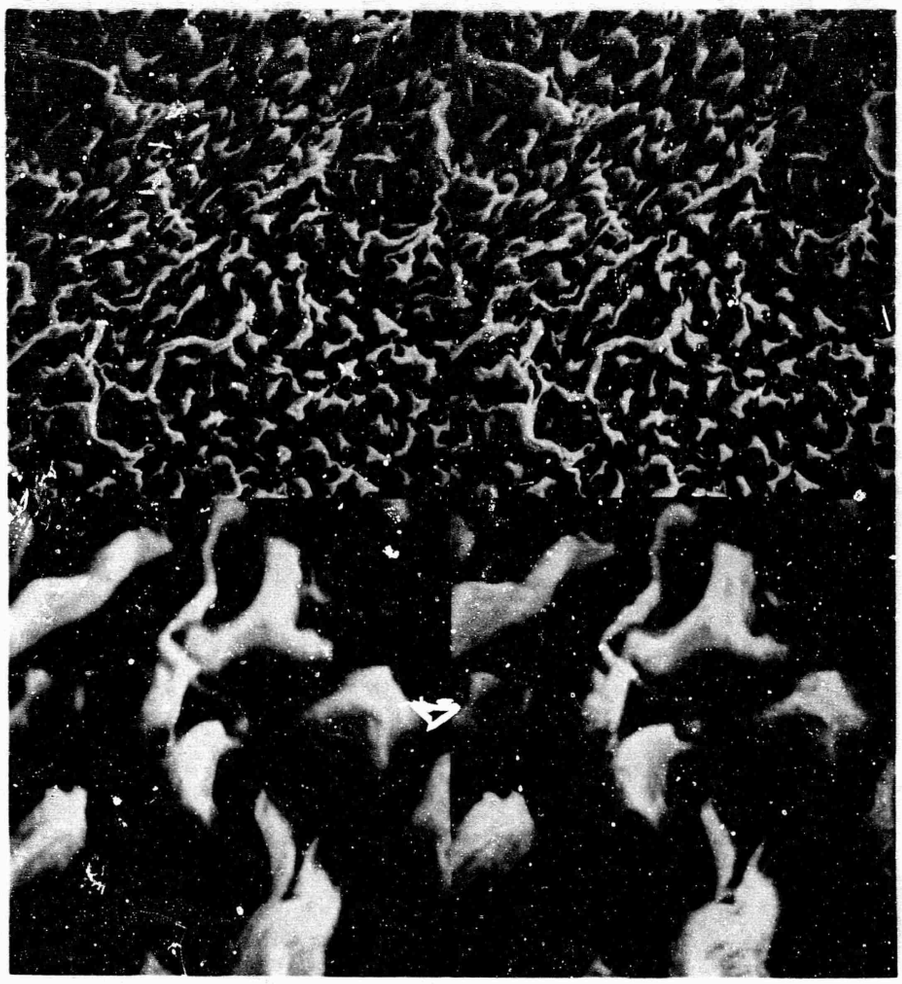

Figure 109 - Ablated surface of 3-D Mod. 3 in region of Thornel 50 bundles (same area as Figure 108) Top: 750 X; Bottom: 3750 X.

The 3-D Mod. 3 had a relatively smooth surface. Shallow pits around the edge of the plateau in the center (Figure 108 top) were not associated with material discontinuities, and probably resulted from transition to turbulent flow. The graphitized resin appeared to be more resistant than the fibers (projecting films in Figure 108 bottom, 109, and 112.)

"Worm holes" drilled into the surface in the region of low-modulus fibers (Figures 111 and 112 at right) were encountered in several materials and are believed to be impurity-catalyzed oxidation during cooling rather than a phenomenon associated with the high-pressure ablation itself.

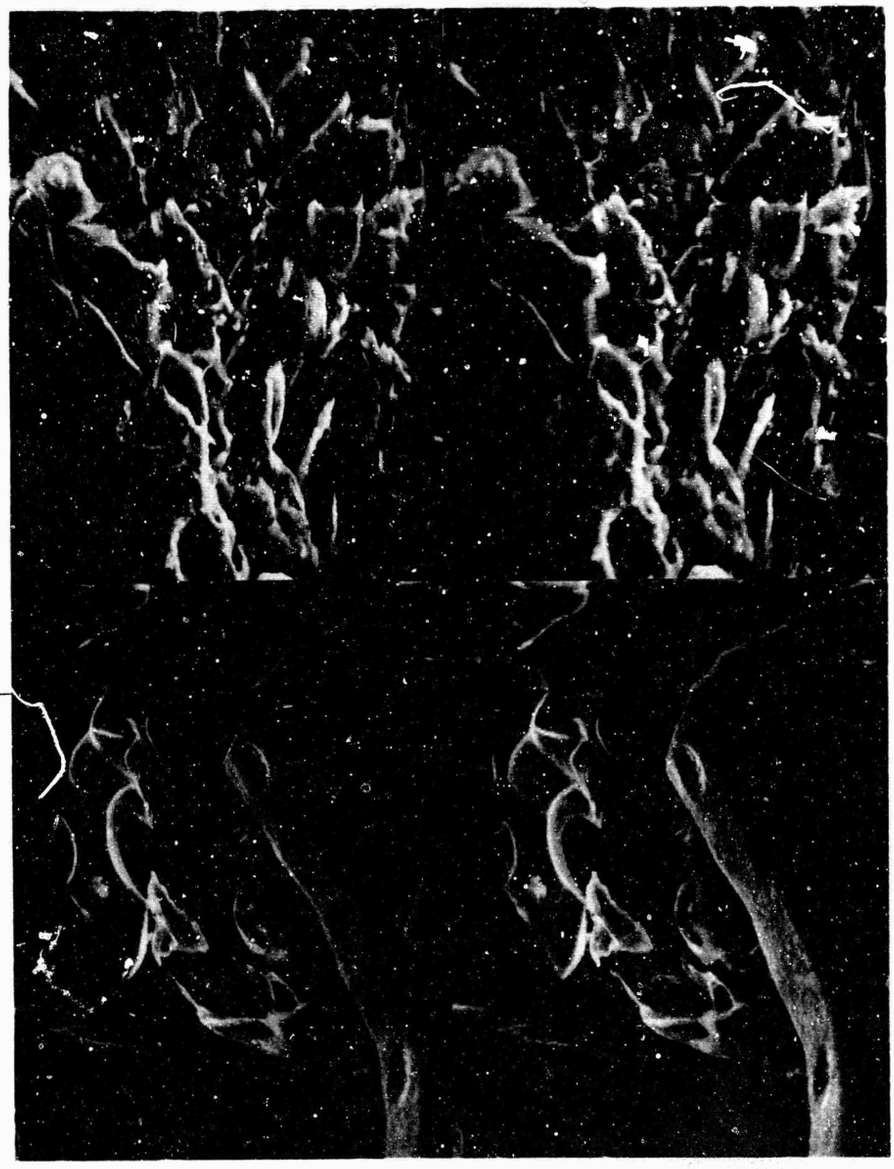

Figure 110 - Ablated surface of 3-D Mod. 3 in areas containing WCA cloth and graphitized resin (top, at 900 X) and glasslike carbon (bottom at 863 X.)

Figure 111 - Polished section through ablation model 3-D Mod. 3 (a) showing region near oxidized surface at 50 X, left, and 1850 X, right, in polarized light.

Figure 112 - Microstructure at oxidized surface of 3-D Mod. 3 (a) showing delaminations in graphitized phenolic filling pores, left, and etching of fibers and graphitized matrix, right. Polarized light, 1850 X.

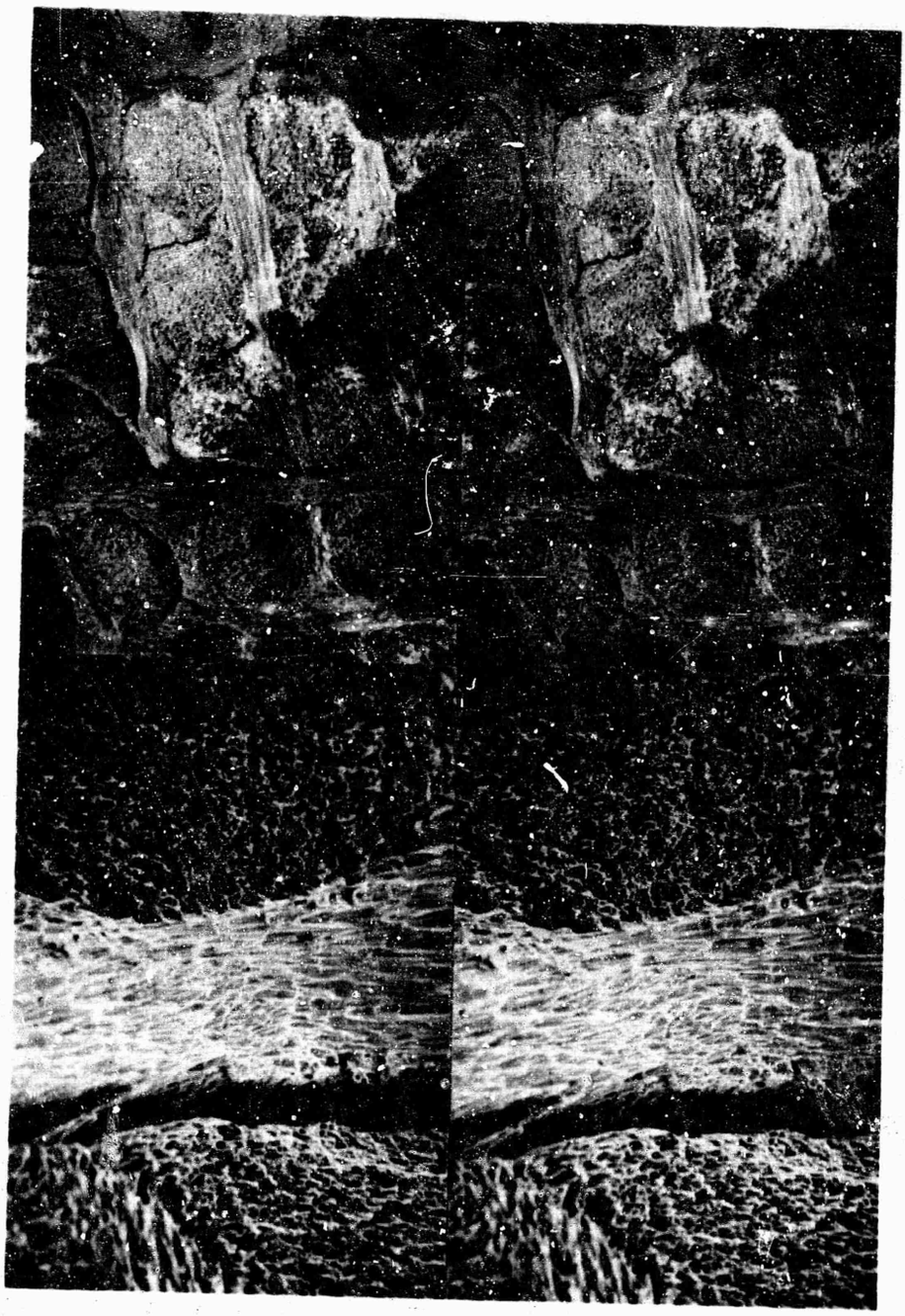

Figure 113 - Scanning electron microscope stereo pairs of surface of 3-D sample after ablation test (5760 filament longitudinal bundles, 1440 filament lateral bundles + CVD)
Top: 20 X; Bottom: 100 X.

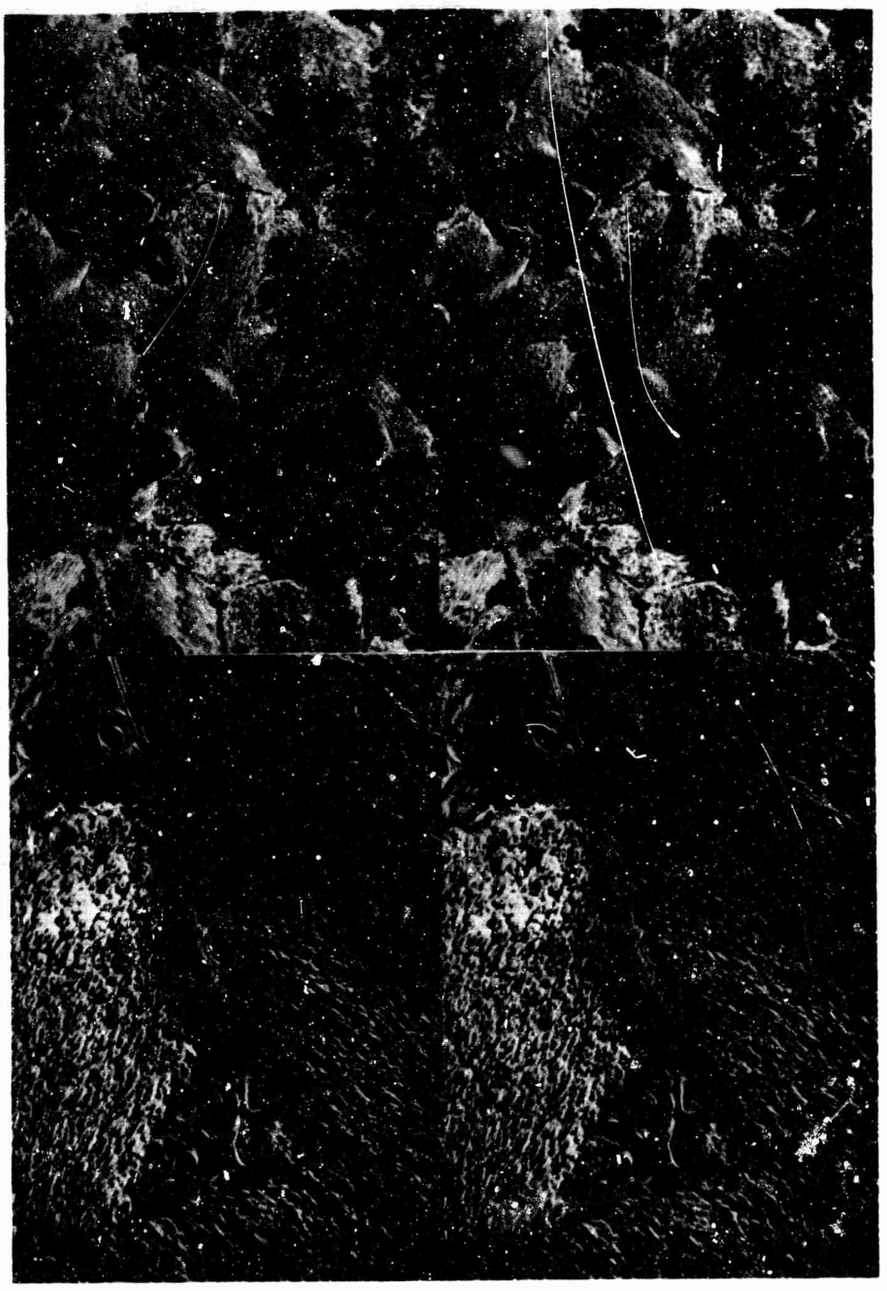

Figure 114 - Scanning electron microscope stereo pairs of surface of 4-D sample after ablation test (2160 filament bundles of CXH fiber + CVD) Top: 19 X; Bottom: 110 X.

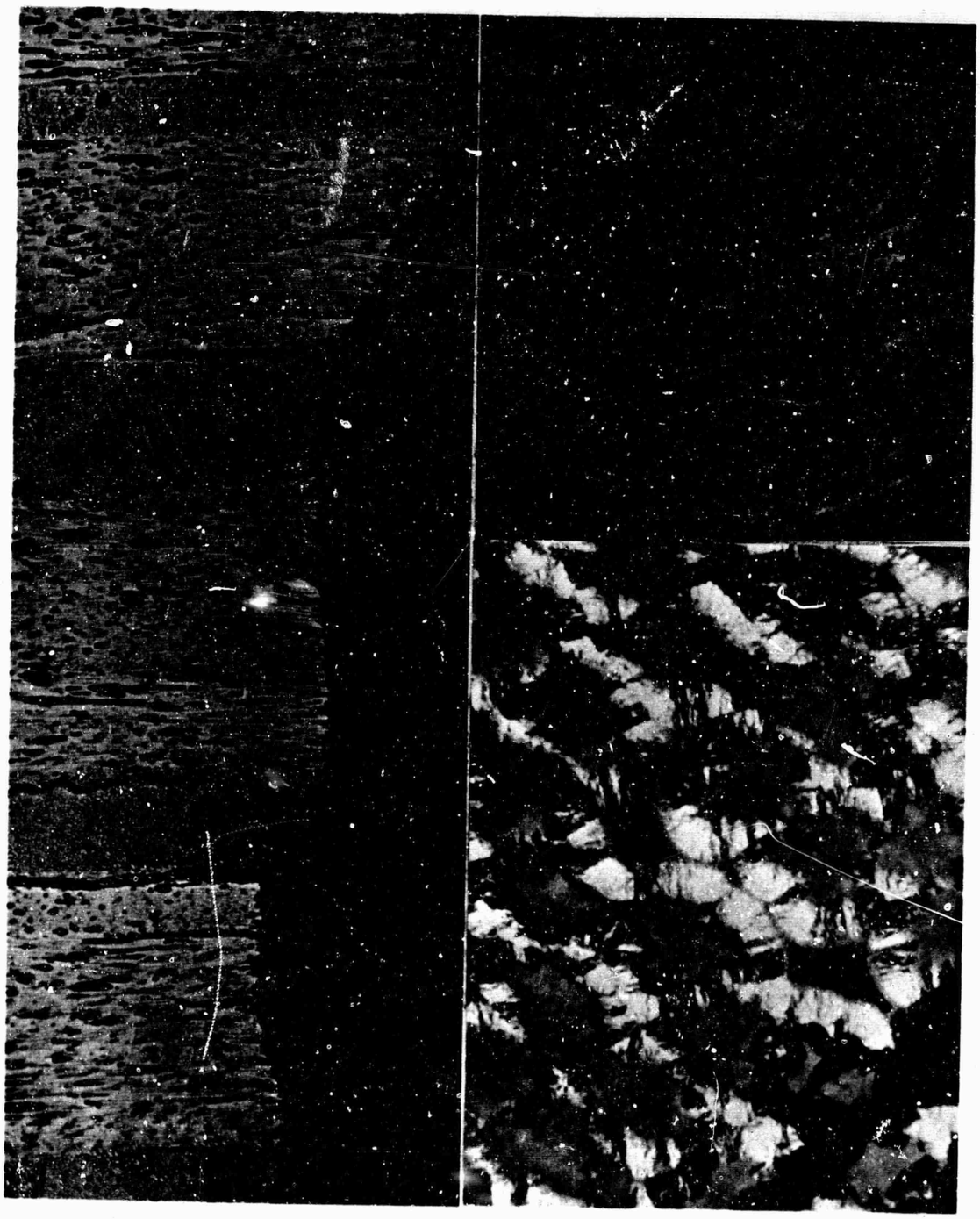

Figure 115 - Section through ablated surface of 3-D CXH + CVD composite showing etching along cracks between bundles (left) at 50 X and etching of constituents at the surface (right) at 1590 X in polarized light.

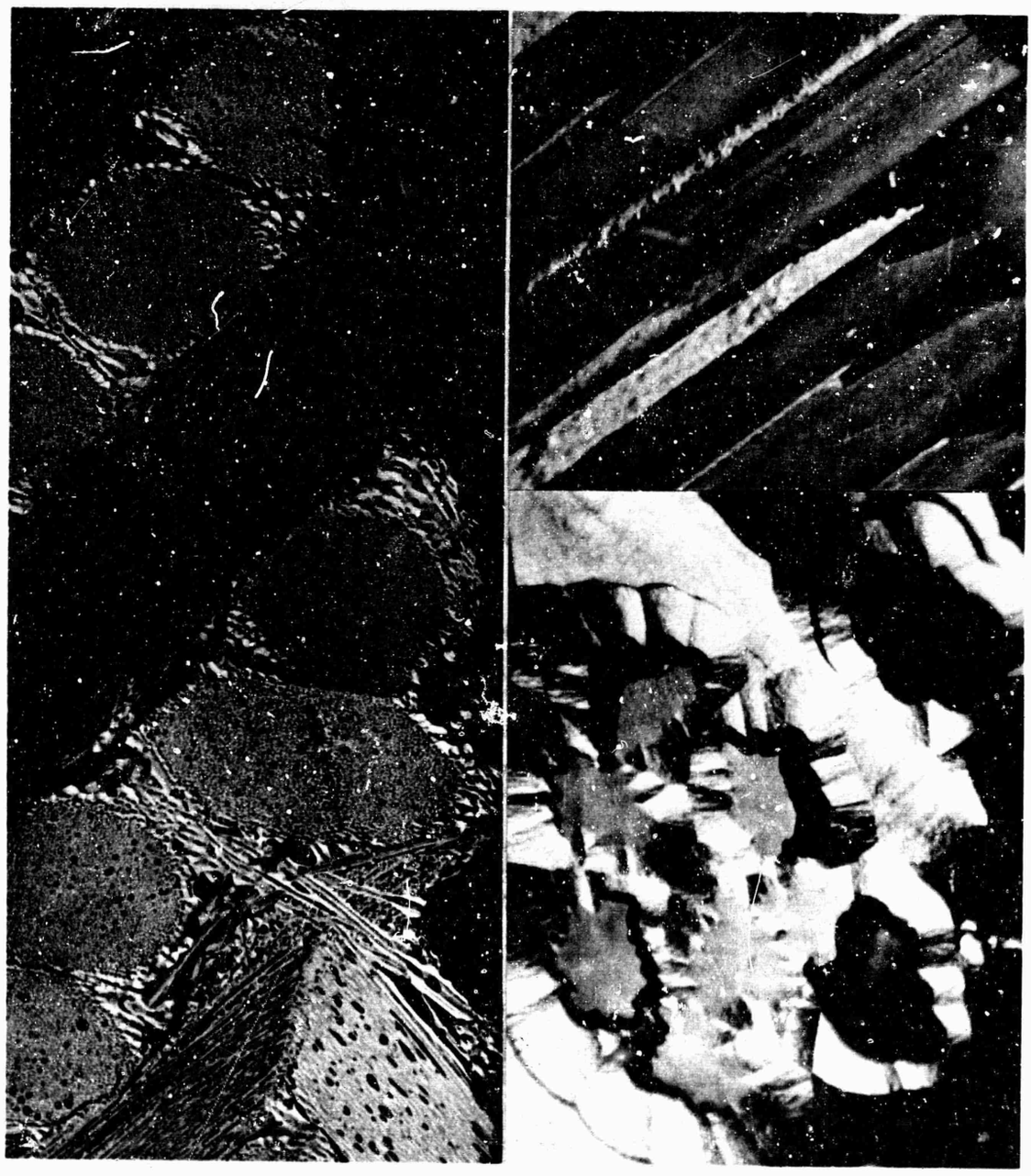

Figure 116- Section through ablated surface of 4-D CXH + CVD composite showing cracks at bundle interfaces (left, 50 X) and etching of constituents at right under polarized light (1590 X.)

Note in Figure 116 the etching at coating-fiber interfaces where the coating has expanded away from the fibers due to transformation during heating (lower right) but absence of etching in more resistant CVD carbon in bundles (upper right.)

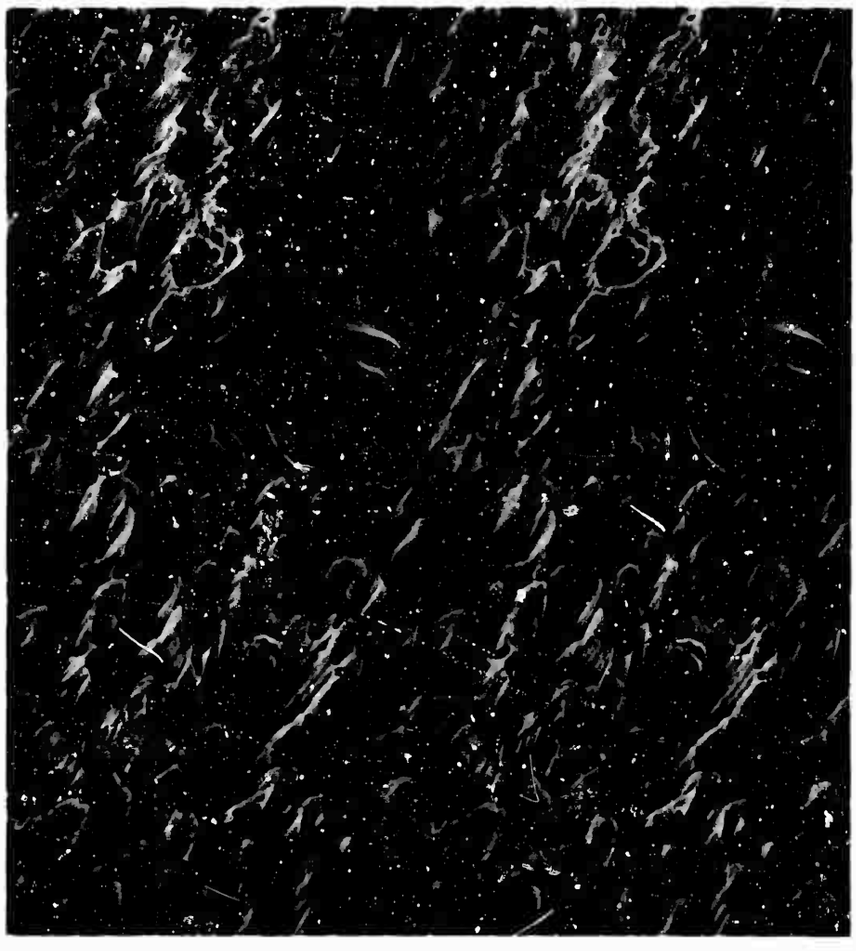

Figure 117 - Ablated surface of 4-D sample made from CKH-3 fibers + CVD (same as Figure 114). 760 X

The r.f. infiltrated matrix was similar in etching characteristics to that produced by the temperature gradient infiltration discussed in Vol. III (pages 111, 123.) Except at cracks, it oxidized with a smooth surface (Figure 117, top.) The low-modulus, low-density fibers were not distinguishable from the pyrolytic carbon on the surface, although high-density Modmore II filaments were clearly defined (Figure 118.)

Figure 118 - Ablated sample prepared by infiltrating Modmore II 4-D Omniweave with pyrolytic carbon by the r.f. method; note filaments within sheaths of CVD carbon. Top: 99 X; Bottom: 985 X.

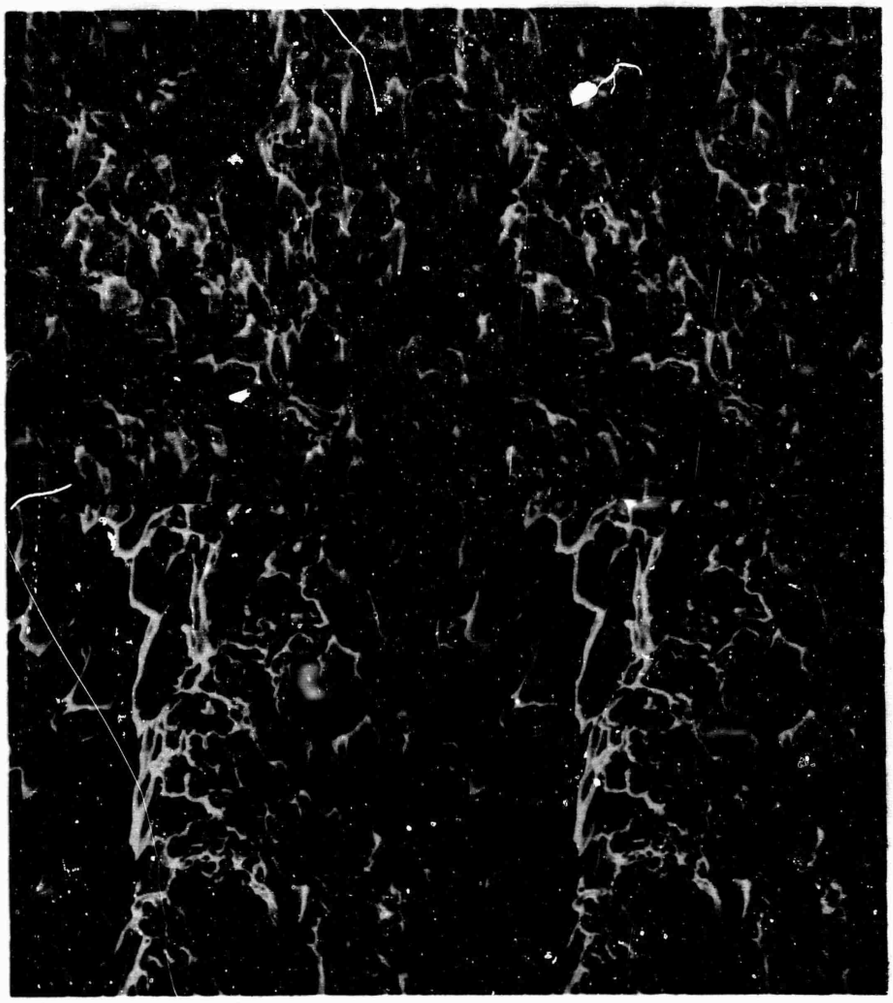

Figure 119 - Ablated surface of 4-D sample made from CKL fibers, showing porous granular matrix; stereo pairs by secondary electron emission. 715 X

Some of the samples in the first series had a relatively porous, sooty deposit which produced a spongey appearance on the ablated surface in the case of the impure-fiber composite, Figure 119 and Figure 120 left. Impurity catalysis may have produced some of the holes, during oxidation on cooling after the test. However, the more rapid ablation of the deposit relative to the fibers was evident.

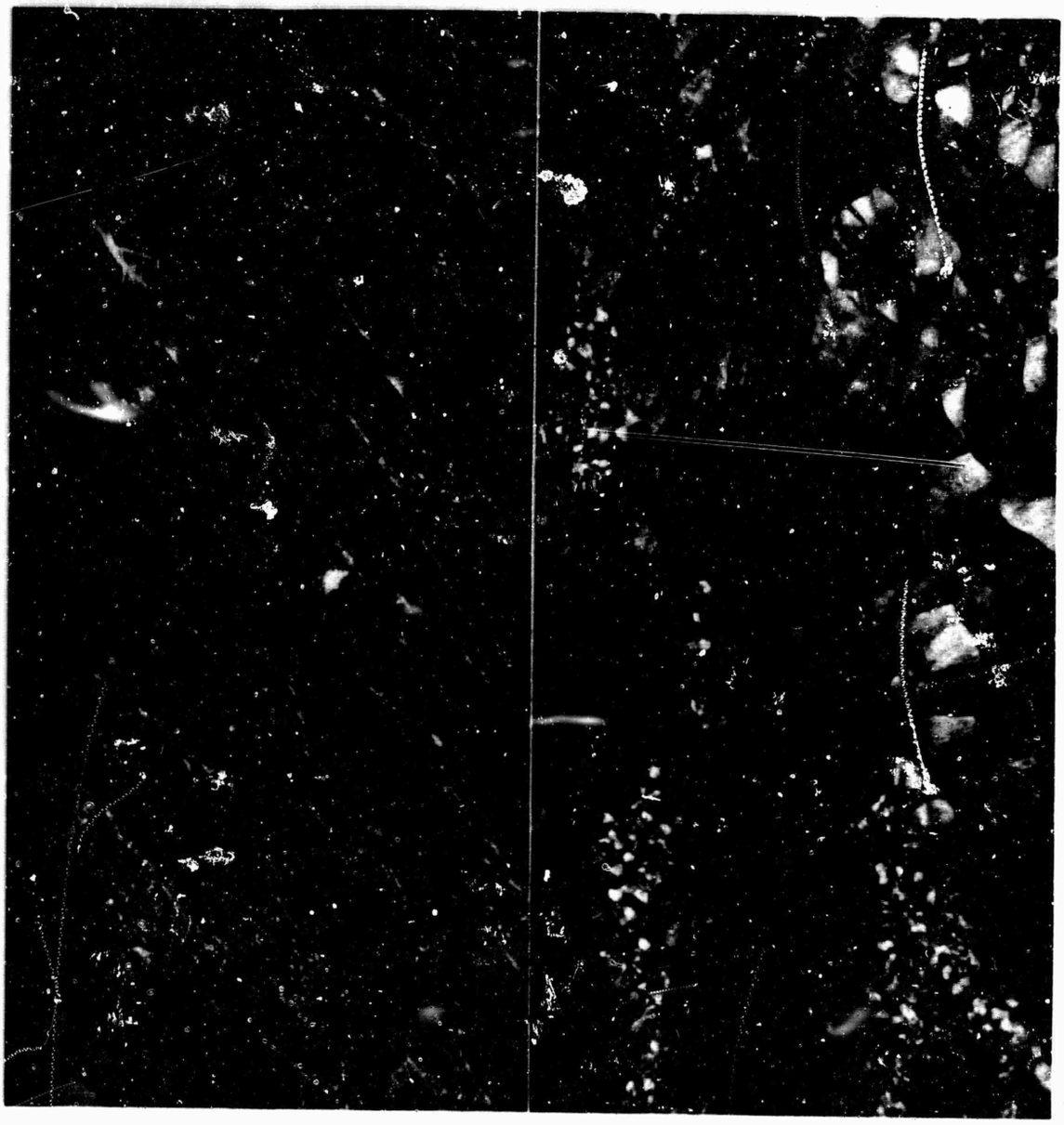

Figure 120- Section through 4-D sample made from impure (CKL) fibers after ablation; etched surface at left and crack through filament bundle within bulk of the material at right; polarized, 1590 X.

Figure 121- Sections through ablated surfaces of models containing high modulus fibers with infiltration followed by three cycles of pitch impregnation and graphitization; top: 4SS13VYt (run 1-2); bottom: 3SS11VYt (run 1-3). Polarized light, 50 X.

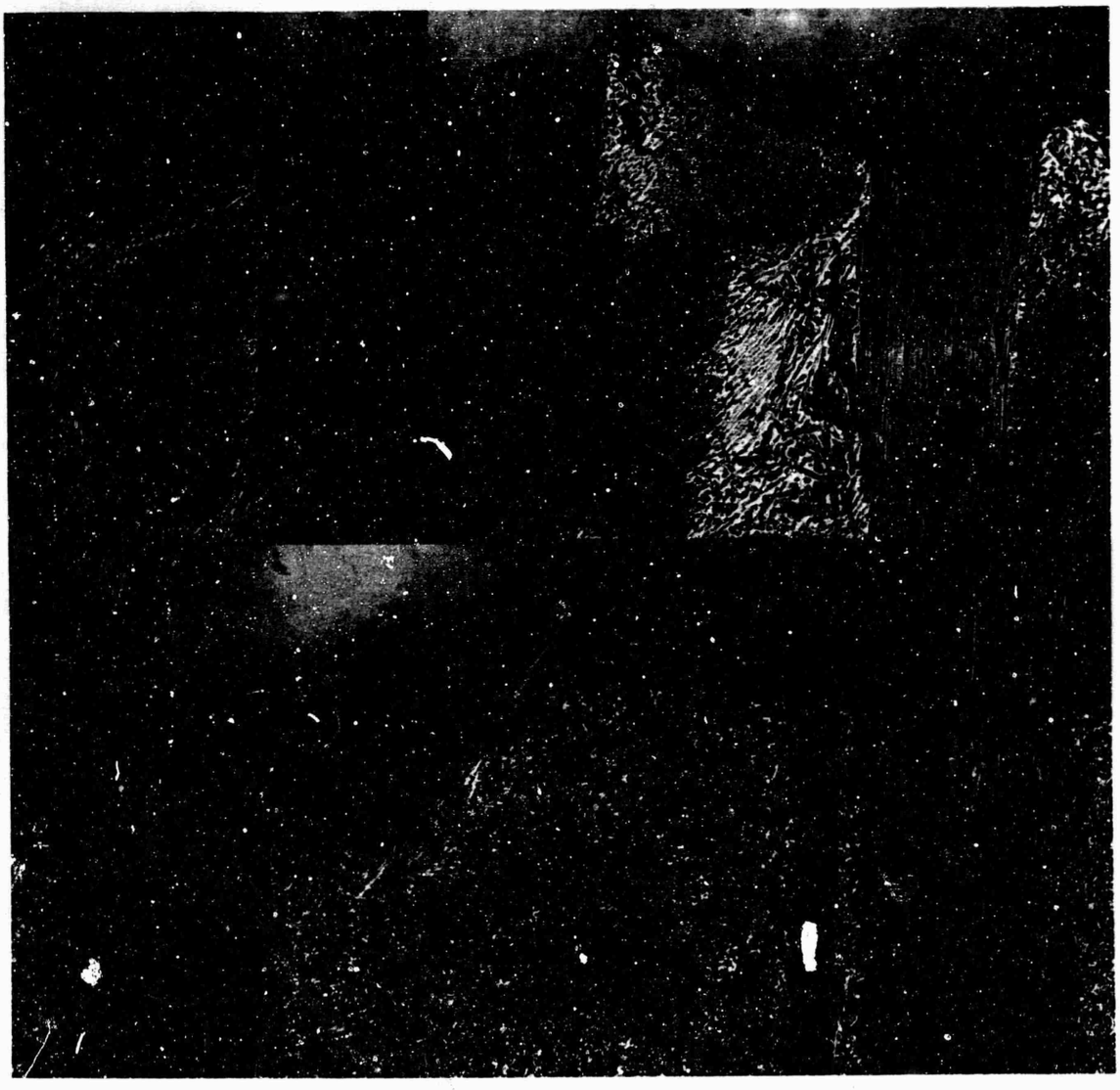

Figure 122 - Sections through ablated surfaces of models containing low modulus fibers (3XH13GYRGt11G) at top, and containing high modulus fibers with pitch impregnation before infiltration (3SSYG11G) at bottom. Polarized light, 50 X.

Figure 123- Section through etched surface of high modulus fiber bundle in 3SS11VYt, showing preferential attack along filament/CVD carbon interfaces. Polarized light, 1390 X.

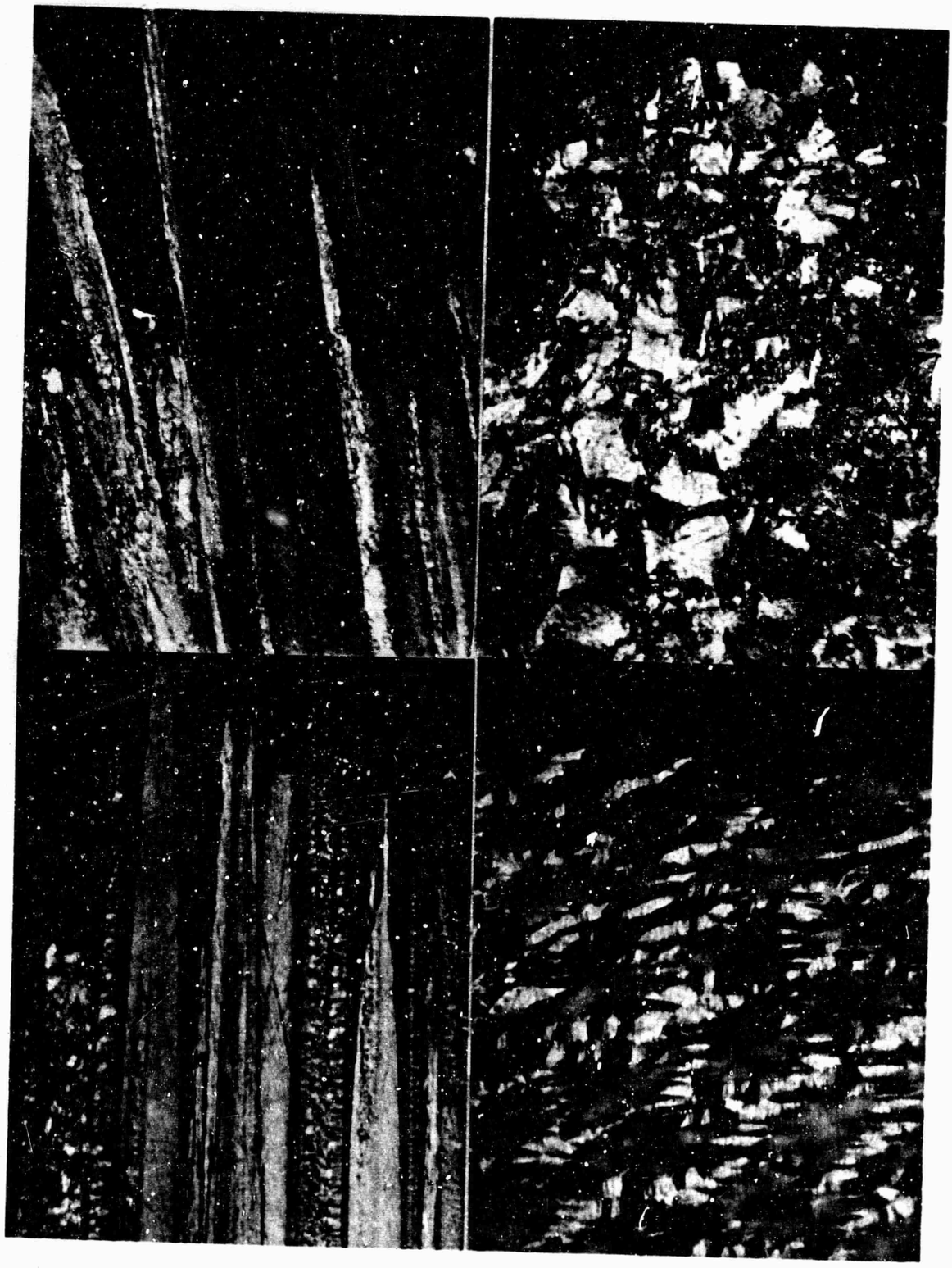

Figure 124 - Sections through ablated surfaces of 3SSY11G (top) and 3SS13AYRG11Gt11G (bottom). Polarized light, 1390 X.

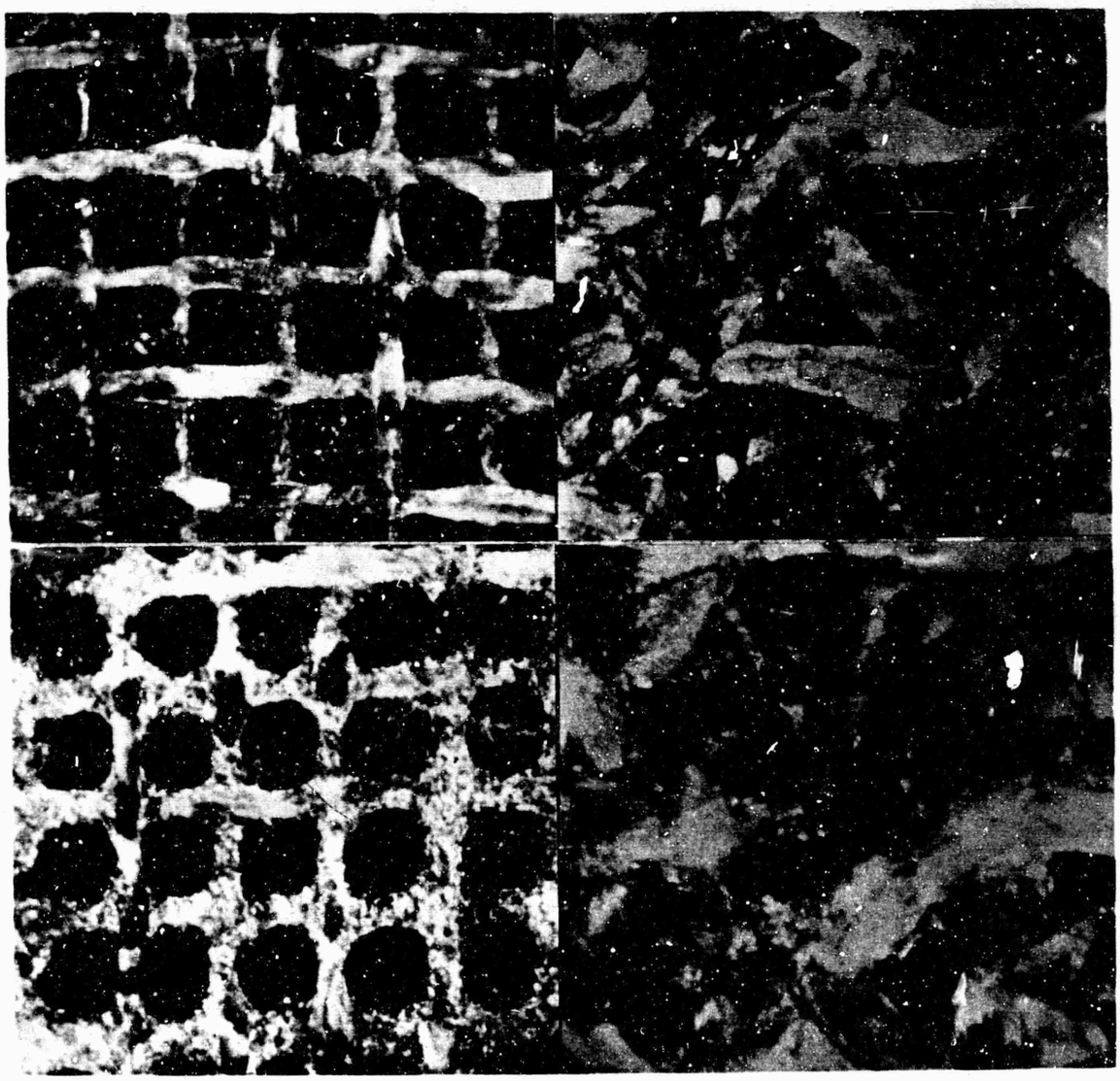

Figure 125 - Comparison of ablation-etched composites with different fibers;
top: rayon precursor (CX) filaments; bottom, acrylic type precursor filaments (C-2000 or C-3000;)
left: 3-D weave with 0.04 inch centers; right: 7-D weave. 15.15 X

SECTION III

DEVELOPMENT OF 4-DIRECTIONAL REINFORCED HEAT SHIELD MATERIALS

1. COMPOSITE FABRICATION

a. Fiber Selection and Bundle Preparation

As discussed in AFML-TR-70-283 (Ref. 13) a C-C candidate heat shield material was prepared during 1970 as an addition to this contract. The evaluation of this material required cylinders 9 inches outside diameter and 8.1-inch inside diameter, and it was proposed to fabricate a 4-directional Omniweave cylinder having tight packing and approximately cubic symmetry, which would then be infiltrated using the temperature-gradient technique described by Gebhardt (Ref. 2.) Because the Omniweave fabrication apparatus has weaving elements arranged in 240 radial rows and 32 circumferential layers, of which at least 6 layers were required for the cylinder, it was calculated that the reinforcements should be yarn bundles approximately 0.08-inch packed diameter, if the required cylinder dimensions were to be met. (Each cubic unit cell would be $8.1\pi/120$ inch on the inside of the cylinder, and the width of hexagonal elements is $\sqrt{2}/4$ times unit cell dimensions, as shown in Figure 1.)

The previous work had shown that ablation performance was degraded by coarse texture, and consideration of the anisotropy-induced thermal stresses resulting from cooling indicated that mechanical strength would also be lower than in composites with smaller reinforcement dimensions. The practical aspects of fabricating large frusta by the Omniweaving method requires 0.1 to 0.4-inch unit cells however, with cubic symmetry maintained by grading bundle diameter as frustum diameter changes. As discussed in AFML-TR-69-67 Vol. III, the unit cell may be distorted to provide more circumferential strength, relative to axial strength, at the larger diameters thus reducing the bundle size requirement. However, the data obtained on the distorted pitch-impregnated composite previously showed that the change in properties would be too great without some bundle size grading. Thus, the thermal shield concept requires a combination of bundle diameter change and fiber angle change with changing frustum diameter, with fiber angle used to tailor the properties in different directions as required along the length. The cubic packing, with 0.21 to 0.23 inch unit cell dimensions in the cylinders required for evaluation, was considered to be a realistic reinforcement construction for comparing properties resulting from using different fibers and process variations.

Consequently, an objective of the basic study contract was identified as exploration of the material variables relative to the 4-D C-C frustum concept. Development of a fiber reinforcement construction which permits diameter grading and reduces the deleterious effects of large diameter was critical. Also, the trade-off between high anisotropy and high strength in high-modulus fibers, and low anisotropy but lower strength in low-modulus fibers required study. The effects of different fibers and fiber combinations on tensile stress-strain, plate-slap spall and thermal expansion of CVD-infiltrated composites of identical geometry were selected as the focus of the initial exploration of this class of composites.

The technique of wrapping a fiber core with other fiber bundles oriented at an angle to the core was selected as a means of grading anisotropy across the bundle diameter, thus reducing thermal expansion mismatch at reinforcement interfaces, and as a means of grading bundle diameter by permitting the inclusion of varying numbers of fiber strands within the core. A series of experiments was conducted by Prodesco, Inc., Perkasie Pennsylvania, for this program. Fiber Technology acrylic-type precursor yarn (C-3000) and cellulose precursor yarn (CX-2 and CX-3) were used primarily as wrapping materials. Several strands of the same yarns were used as core, and 10,000 filament acrylic-type precursor tow (Modmore II) was also used as core in some of the trials. Most of the composites were overwrapped with 20 denier nylon to compact the bundles and reduce fraying. The best wrapping technique was found to be tubular braiding, with 8 to 12 ends around the core and with controlled tension on the feeding core material. The 12-end braid was finally selected for the composite fabrication because of a steeper fiber angle to the core and the tendency to form hexagonal bundles. Examples are illustrated in Figure 126. Yarn length in the braid was 6 per cent longer than the core.

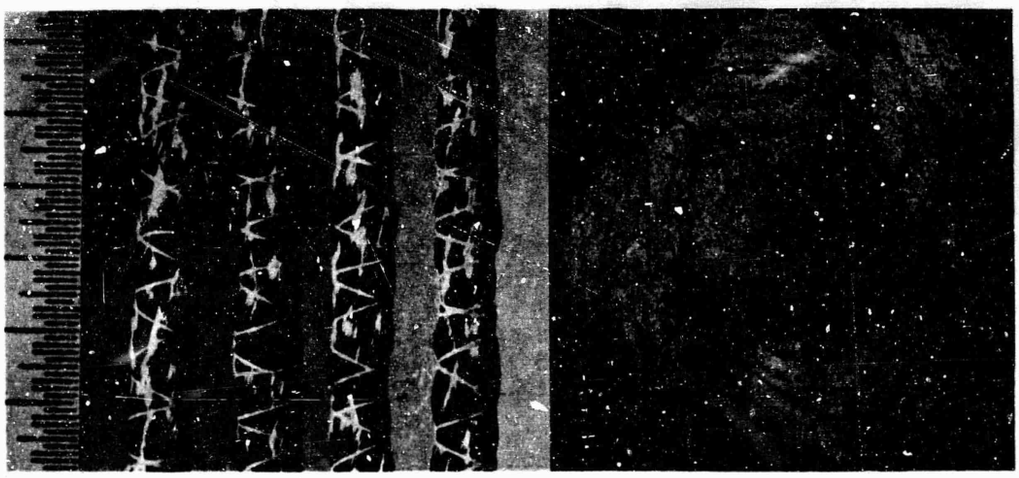

Figure 126 - Examples of 12-end braid overwrapped fiber bundles; yarns used in Omniweaves 237 and 238 (left) at 3.9 X; cross-section of C-3000 / M-II (weave 235) at 27 X.

Four different fiber combinations were selected for different weaves, as described below; all fibers except the CX-2 were coated with 3 to 5 % teflon by Fiber Technology Inc. before fabrication:

Weave:	Braided Overwrap Fibers (12 Ends)	Core Fibers (Total)
235	C-3000 high-modulus (3000 filaments)	/ Modmore II (10,000 filaments)
236	CX-3 low-modulus (2160 filaments)	/ 3 ends CX-3 (6,480 filaments)
237	CX-2 low-modulus (1440 filaments)	/ Modmore II (10,000 filaments)
238	CX-2 low-modulus (1440 filaments)	/ Modmore II (10,000 filaments) + Hitco HMG-15 (1440 filaments)

The fibers were the same as those used in preparing the fine-textured nose tip composites, and are described in Table I in the 7th TMR. The C-3000 had an average strength of 330,000 psi and a modulus of 49 x 10^6 psi, as reported by the vendor, which was similar to Modmore II, although slightly lower strength and higher modulus indicated a higher process temperature. The CK-2 and CK-3 both had the standard high-temperature treatment which resulted in a carbon content of 99 per cent, a strength of about 160,000 psi, and a modulus of 5.4 x 10^6 psi. In one of the weaves a strand of HMG-15 was included between the high-modulus core and the wrap in a further attempt to grade properties through the bundle; this fiber is reported by HITCO to have a modulus of 12.7 x 10^6 psi, a strength of 153,000 psi, and a density of 1.51 g/cc.

In order to distinguish the 4-directional composites made with the graded-anisotropy bundles from those made with plied yarns, the term 4-D* ("four-D-star") was applied to this class of reinforcements.

b. Omniweave Fabrication

The apparatus used to prepare the experimental strips had six layers of yarn guides, with up to 72 yarns in each layer. The first two weaves, numbers 235 and 236, were set up in this apparatus with 33 guides filled in each of the six layers for each weave. Subsequently, weave 237 was prepared utilizing 55 guides per layer, and weave 238 was woven with 17 guides across the width. A final weave, which was infiltrated but not tested, number 240, was identical to 237 but packed more tightly and used the full 72 element width of the apparatus. In all of these weaves a similar fabrication technique was used; the elements were displaced to carry the yarns along diagonal rows, and the resulting cross-overs were combed and packed into position by hand, with tension applied to the bundles to produce the tightly packed cubic geometry. Further details of the technique are described in AFML-TR-70-283.

After weaving the strips were heated in vacuum (~1 torr) to 1750°C estimated true temperature (1700°C measured) to remove the nylon and coating materials. Then the surface which would be exposed to the infiltrating gas was slit with a razor blade to a depth of 1/8 inch or less, and the fibers were compacted with a fork using a kneading action to produce a felted surface. The objective was to open the porosity which is closed by the cross-over yarns on the surface of the weave. Results of this treatment are shown in photographs of some of the weaves, Figures 126 - 133 (weave 238 was not slit or felted as a comparison.)

Weave 235, with all high-modulus fibers, had a thickness of 0.56 inch, approximately 0.21 inch unit cell across width, and a bulk density of 0.87 g/cc after the vacuum heat treatment (it lost 4.5 % by weight.) The surface slitting and felting, which resulted in 1 % weight loss, resulted in thickness increasing to 0.62 inch and a reduction in density to 0.74 g/cc.

Similar results were found with weave 236 (all low-modulus fibers.) The thicknesses before and after felting were the same as 235 within 0.01 inch; weight loss was 4.04 % on vacuum heating and 0.6 % as a result of felting. Bulk density changed from 0.68 g/cc as heated to 0.59 g/cc as felted; considering the filament densities (1.4 g/cc for 236 and 1.8 g/cc for 235) the packing densities of the two weaves were similar (about 40 % after felting.)

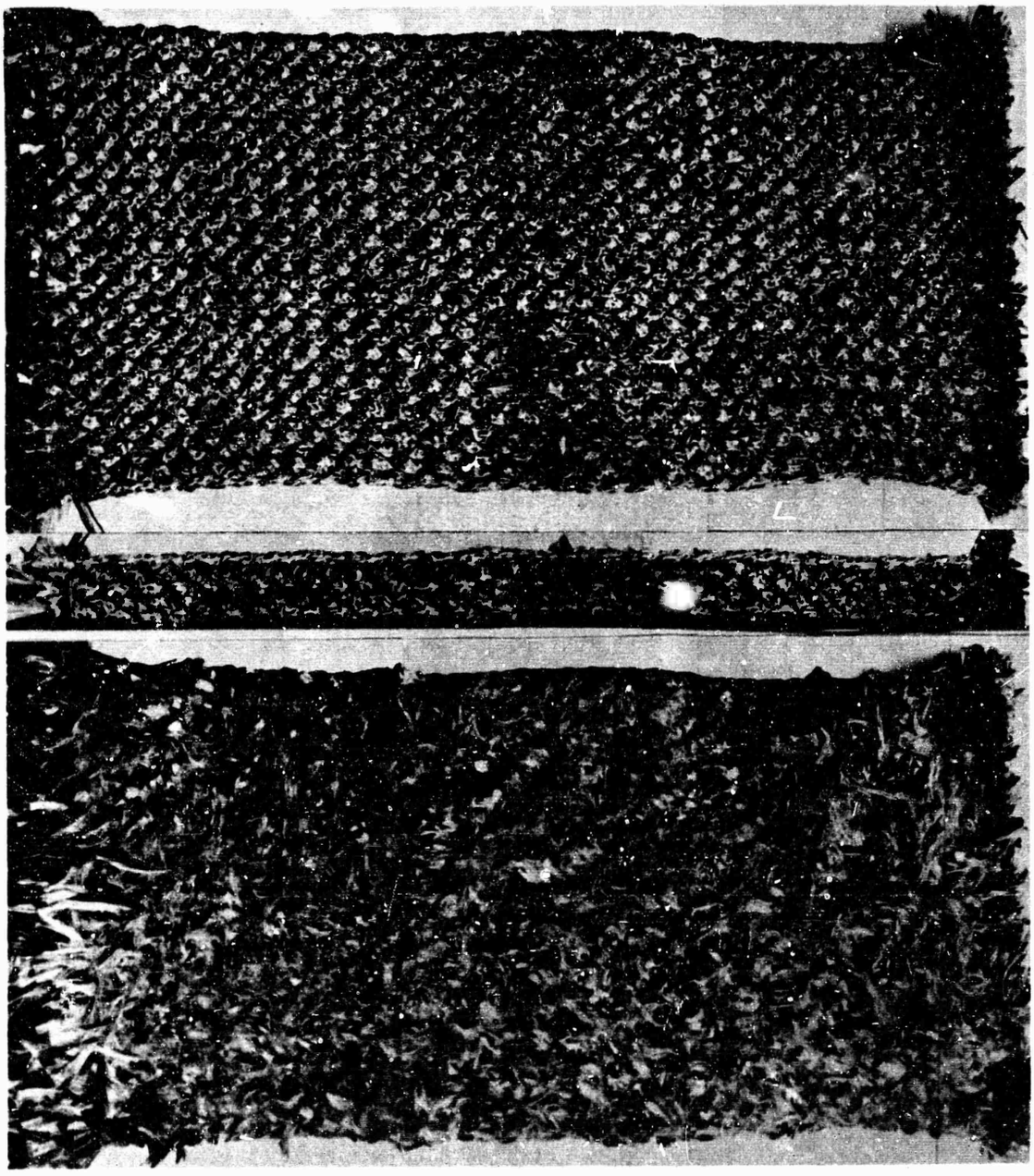

Figure 127 - Omniweave 235 (all high-modulus fibers) as woven (top) and after vacuum heat treatment and surface felting (bottom). 0.75 X.

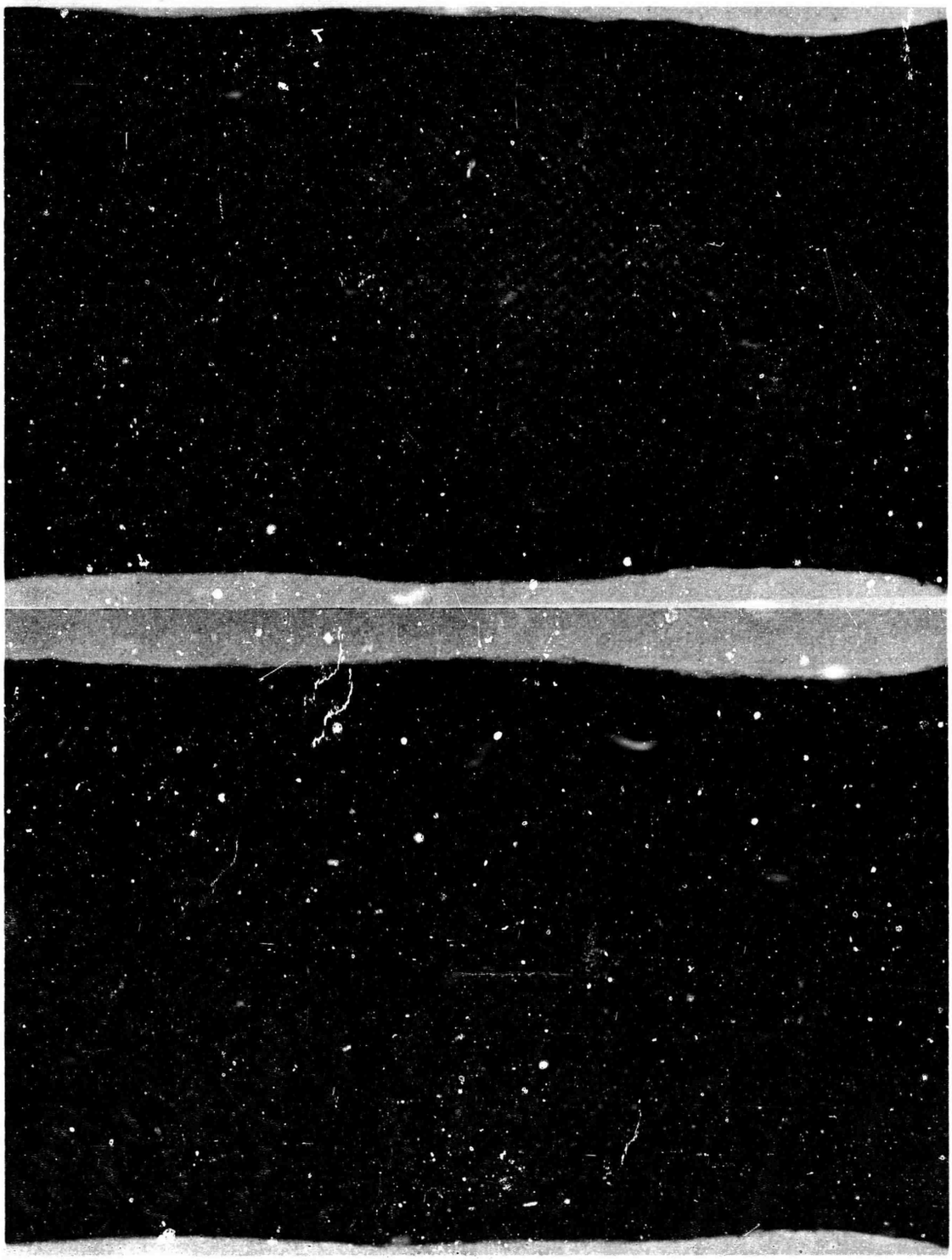

Figure 128 - Radiographs of weave 235 as woven (top) and after slitting and felting the outer surface prior to infiltration (bottom.) 1 X.

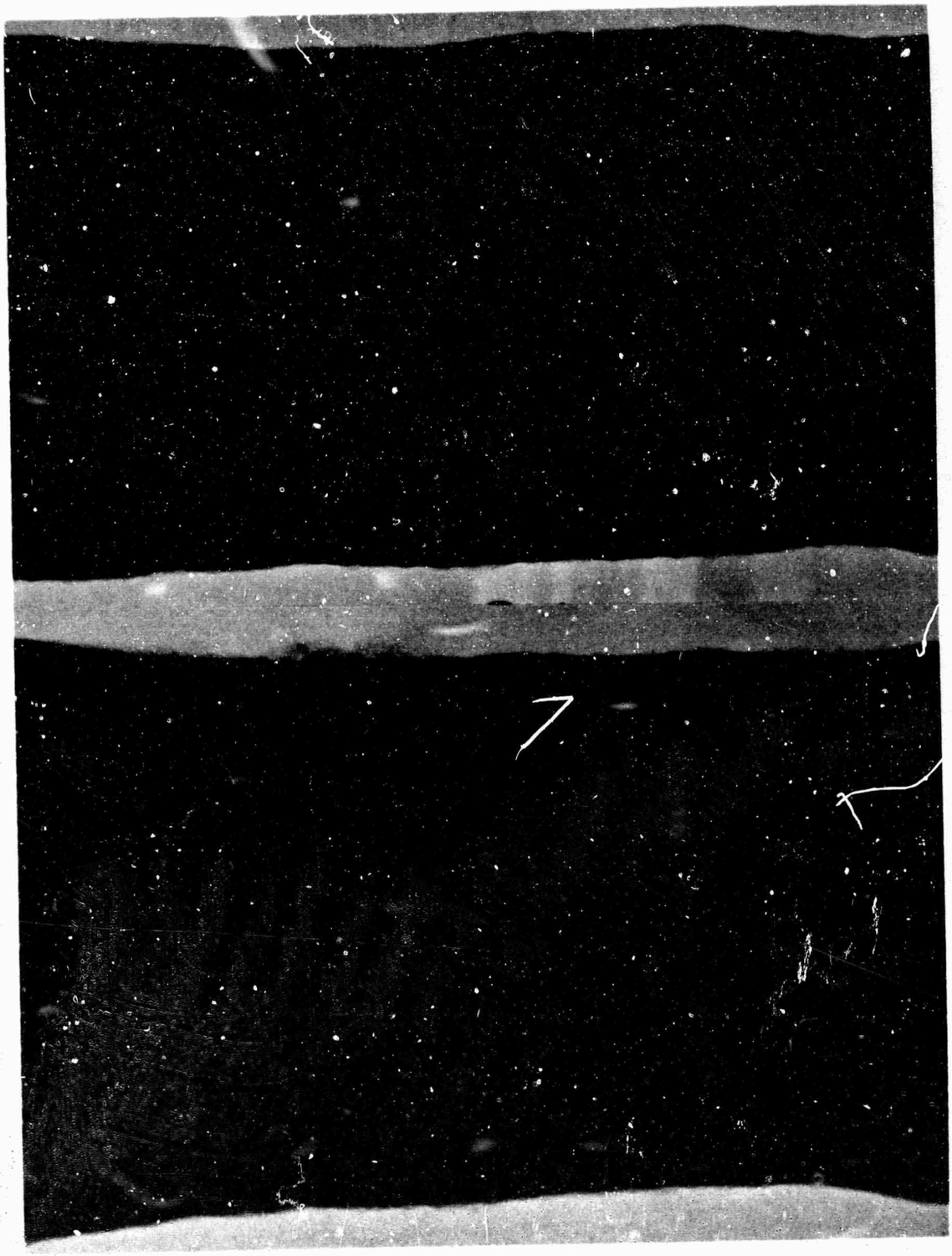

Figure 129 - Radiographs of weave 236 (low-modulus fibers) as woven (top) and after slitting and felting (bottom.) 1 X.

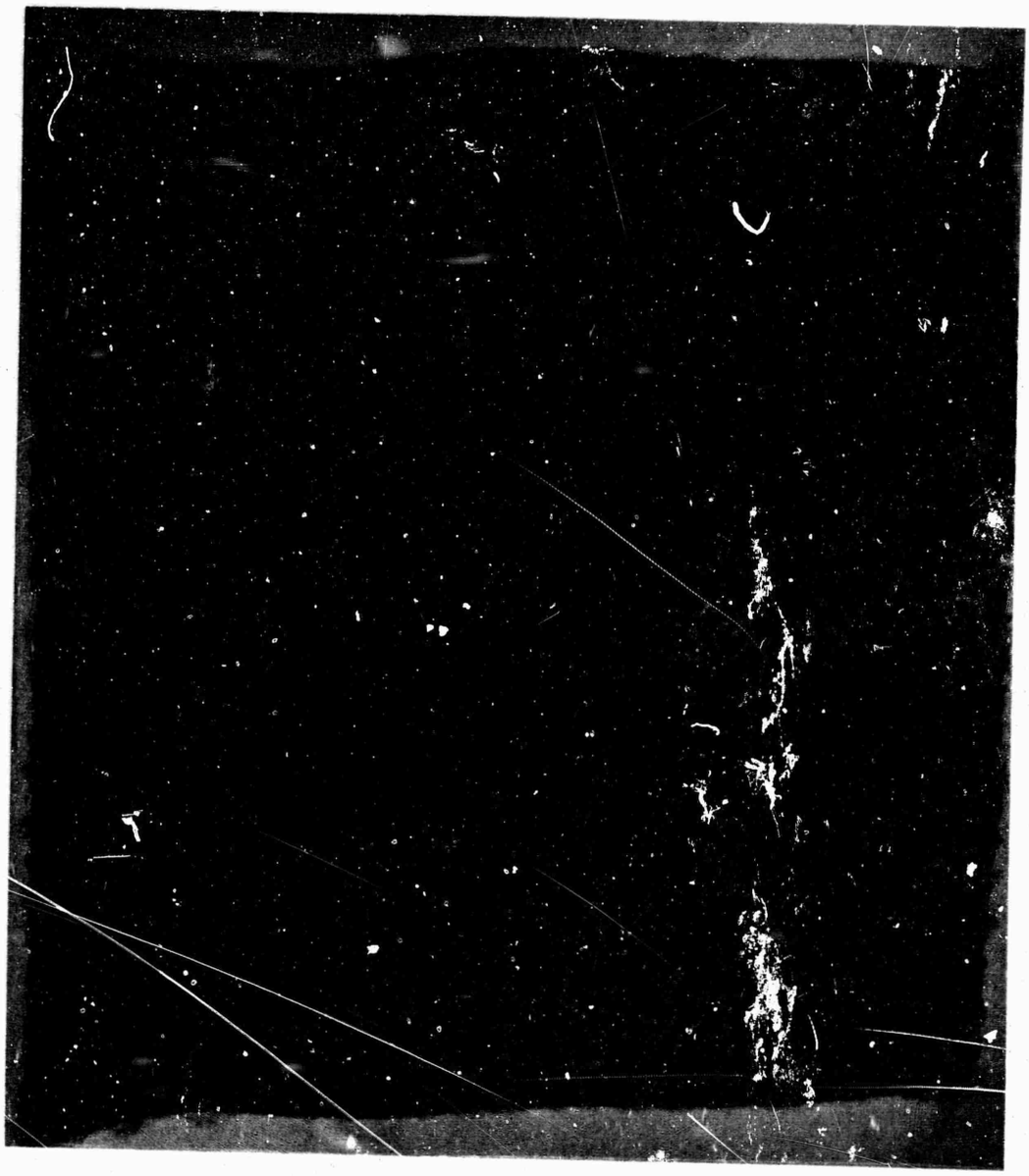

Figure 130. Weave 237 (low-modulus wrap / high-modulus core) as woven. Radiograph at 1X.

Weave 237 was prepared with smaller fiber bundles resulting from CX-2 instead of CX-3 in the braid. Packing density was also lower, and the weave could be compacted to 87 % of the original area; it was expanded again 120 % during final treatment, which included strapping onto a 1-inch wide curved portion of the hexagonal graphite susceptor for infiltration. This weave was not slit, but the outer loops were loosened and dry chopped felt was forced into the pores using a 1/16-inch diameter rod. Packing density was about 33 % of the average fiber density after this treatment.

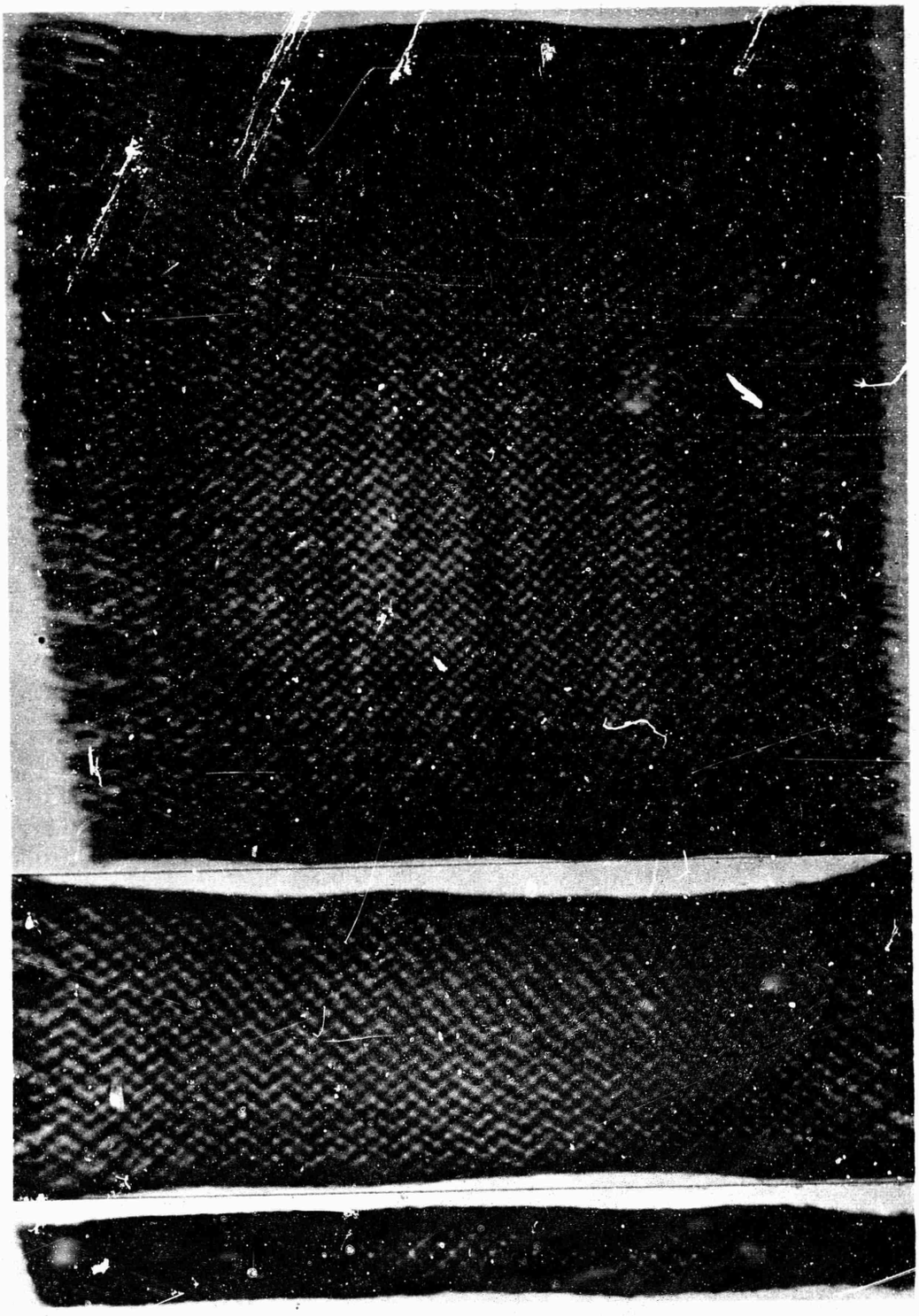

Figure 131- Radiographs of weave 237 compacted to high density (top) and weave 238 (two orthogonal views at bottom.) 1 X.

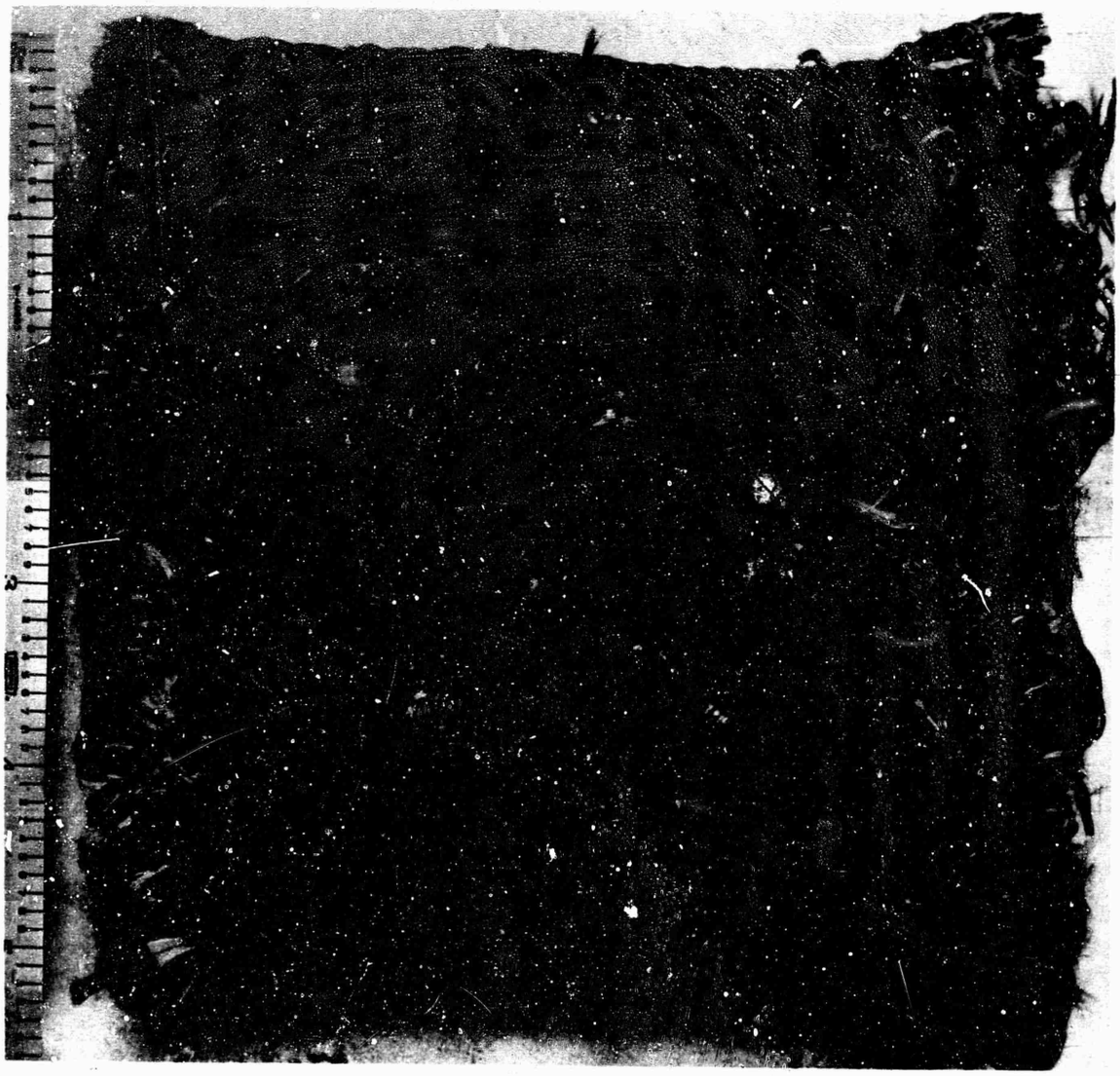

Figure 132- Felted surface of weave 237, prior to CVD infiltration. 1 X.

Weave 240 used the same bundles as 237 but was packed to higher density (about 10 % smaller unit cell) as woven. This was slit in the same manner as 235 and 236, but an improved technique of adding fibers to the pores was used. Chopped Union Carbide VFA fiber was passed through a micropulverizer, dispersed in water and poured over the slit surface while a vacuum was applied through a perforated plate on the opposite side of the weave. The filtrate was put through the weave twice and the finest fibers were finally poured over the surface. After drying, excess fibers were removed and the weave was heated 20 minutes at 750°F to burn off residual dispersing agent (weight loss was 41 % in the excess fibers and 3.4 % for the weave.) Final bulk density was 0.58 g/cc, or about 38 % of the average fiber density.

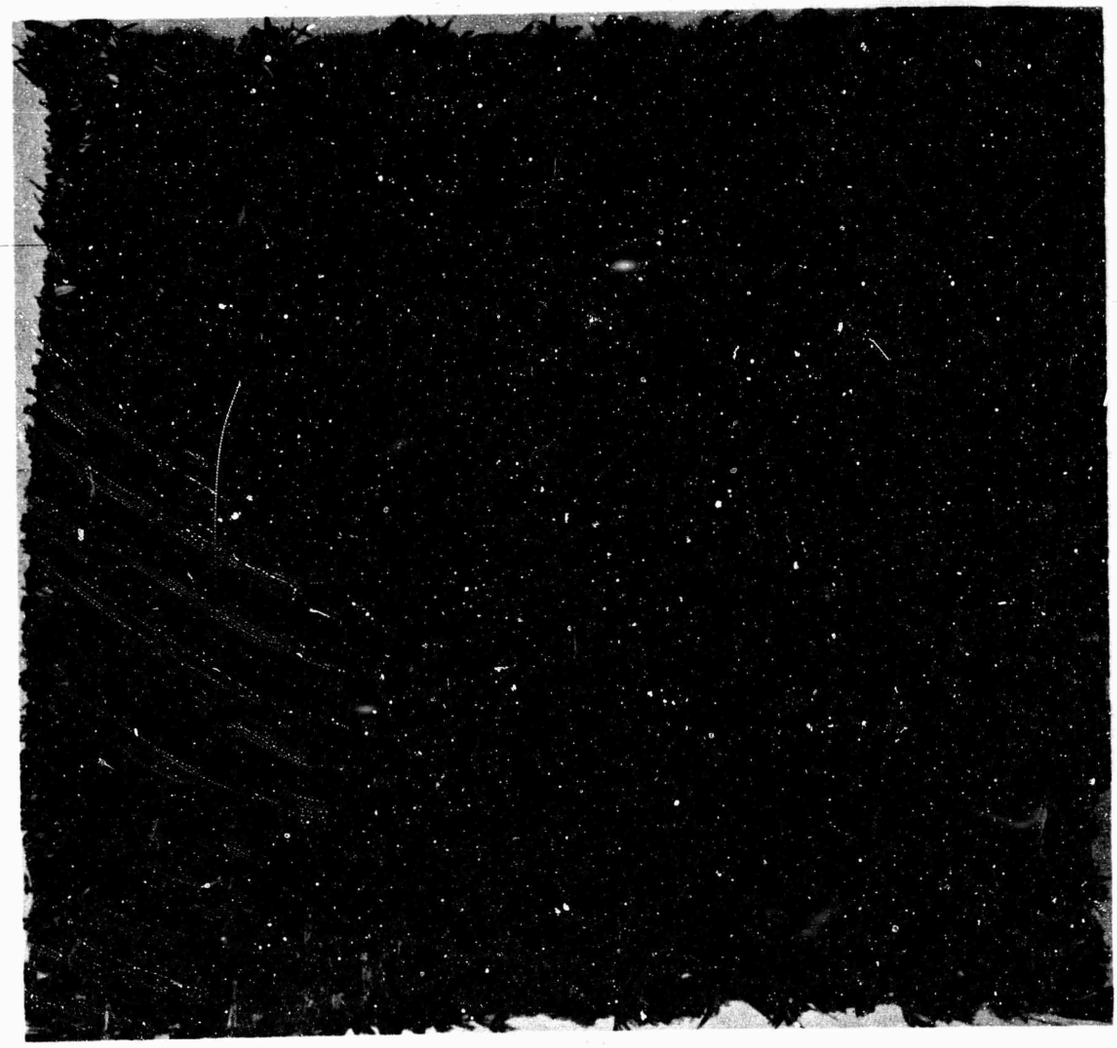

Figure 133- Surface of weave 240 after felting and impregnating with a fibrous slurry. 0.75 X.

The data indicate that about 2.1 to 2.3 % of the final material in weave 240 had been added from the suspension. This would correspond to the packing in a low-density felt (~0.04 g/cc) assuming 25 to 30 % of the weave volume consists of interstitial porosity as in the model of Figure 1. The same technique of felting and fibrous addition was applied to the cylinder (weave 239) described in AFML-TR-70-283; the plate 240 was more tightly packed, however.

c. CVD Infiltration and Sample Preparation

The woven samples were infiltrated with pyrolytic carbon using a standard thermal gradient infiltration technique previously described (Ref. 2). The samples were mounted on the upper half of the 12-inch long x 6-inch wide faces of a hexagonal graphite susceptor to insure uniform temperatures and to allow the gas to be sufficiently pre-heated prior to reaching the samples. Either carbon cloth or sections of "Grafoil" were placed between the samples and the susceptor to reduced sooting and to reduce the adherence of the sample to the susceptor as a result of the infiltration. Layers of carbon felt were used to separate the samples on the susceptor faces and to present a relatively uniform surface to the gas flow to reduce localized turbulence. Carbon yarn was wrapped around the susceptor to hold the samples and the carbon felt in place during assembly into the furnace and during initial infiltration.

The furnace was flushed with nitrogen, heated in hydrogen to 1000°C measured temperature and held for one-half hour. Then, city gas, which was sometimes mixed with methane to obtain the required flow, was passed through the assembly at 1 atm and 950°C measured temperature on the top of the susceptor. Previous calibration had shown that this procedure yielded an infiltration temperature of 1050-1070°C (nominally the 1100°C PCTG condition). All of the plates were infiltrated under the same conditions, with a sequence of furnace runs used to follow the increase in density. Table X indicates the approximate values of bulk density obtained on the different samples after different infiltration times.

TABLE X

BULK DENSITY CHANGES DURING TEMPERATURE GRADIENT INFILTRATION

Run No.	Infiltration Time, Hours	Density, g/cc, for Weaves Listed: 235	236	237	238	240
	0	0.65	0.58	0.51	0.51	0.61
310-51	97.5	1.65	1.57	--	--	--
310-52	44.5	1.86 1.73m	1.69 1.58m	--	--	--
310-57	102	1.77m	1.63m	1.62m	1.53m	--
310-60	65	--	--	1.67m	1.59m	--
310-61-2	167	--	--	--	--	1.7

Note: m = machined to specimen blank

The first two weaves, 235 and 236, were cut to 5-inch lengths and infiltrated simultaneously. After the first two runs, the blocks were sectioned and ground to remove any outer deposit which might block the pores, and the blocks were then given a final infiltration. The blocks were sectioned to provide two tensile specimen bars in the weaving direction and three 1.5-inch square blocks for plate slap (one of these was too close to the end of the weave and was used for short-beam flexure instead, after grinding to 1-inch width.) A thin slab was removed between the tensile and plate-slap blanks and was micropolished and radiographed in order to evaluate uniformity; these slabs are illustrated in Figure 134. The weave containing high modulus fibers showed a region of inter-bundle separation and porosity in the center of the block.

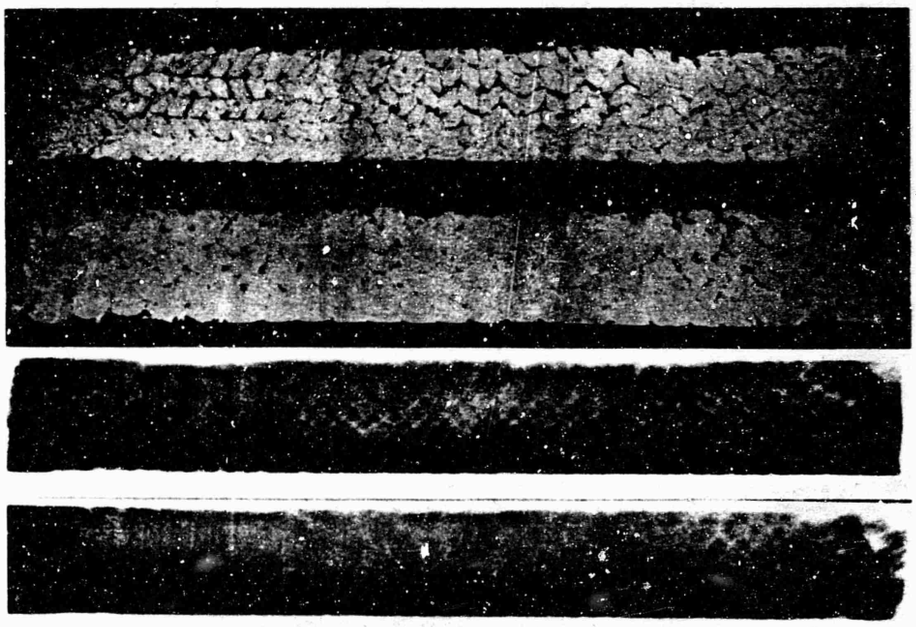

Figure 134- Polished sections and radiographs of thin slabs cut from plates 235 (top) and 236 (bottom) after infiltration. 1 X.

Weaves 237 and 238 were also processed in the same run. The width of 237 required wrapping around a corner, as illustrated in Figure 135. After the first 102 hours of infiltration, this was sectioned, a tensile blank was removed from the 1-inch wide flat portion (sample 237-a), an ablation specimen was ground from the curved portion, and the remaining 3.25-inch wide plate was re-infiltrated and ground to tensile and plate slap specimens identical to those of plates 235 and 236.

Weave 240 was cut into sections suitable for tensile specimens in both weaving and lateral directions and infiltrated for the same time as the other weaves. A 5-inch bar of unidirectional bundles of the composite yarn was also included for property comparisons.

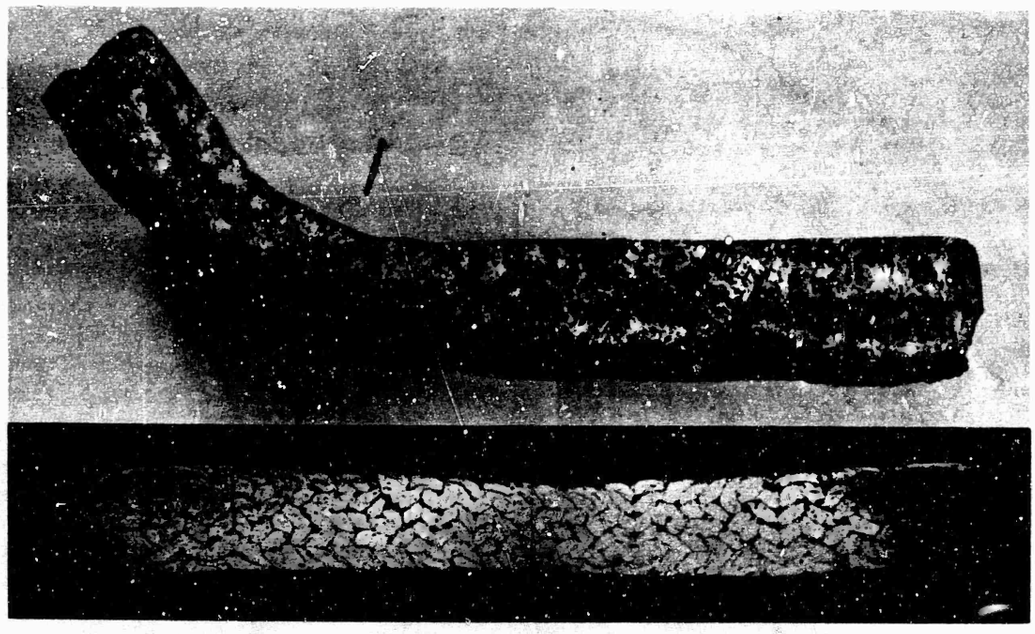

Figure 135- Curved plate 237 and polished section cut from plane in region of curvature, after 102 hours infiltration. 1 X.

d. Microstructure

Studies of the polished sections indicated that the weave containing all low-modulus fibers was relatively free of cracks (Figure 136) while the 235 and 237 weaves had significant separations between some of the major composite bundles. The composites with high-modulus core material also contained cracks within the core, or at core-wrap interfaces, but these cracks were not continuous across the bundle or completely around the core-wrap interface. The location of these cracks, which resulted from anisotropic shrinkage from the infiltration temperature (1000° to 1100° C), indicated that the "graded anisotropy" approach had resulted in bundles having a better match at reinforcement boundaries (Figures 137 and 138).

Figure 136 - Polished section of 236 showing "felted" surface at left and surface next to susceptor at right. Polarized light, 10 X.

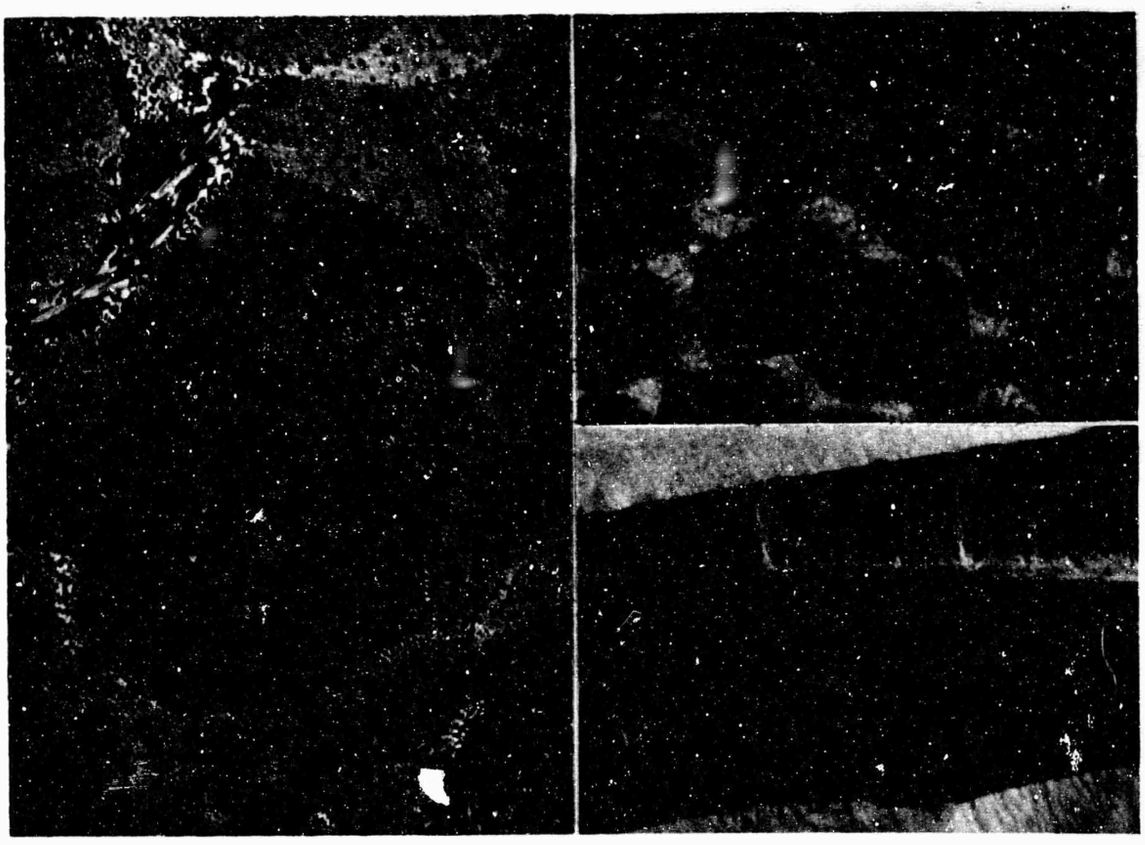

Figure 137- Microstructures of 4-D* composite 237 (high-modulus core, low-modulus wrap;) left view shows crack in core bundle at 50 X; right view shows CVD matrix at 1850 X (polarized light.)

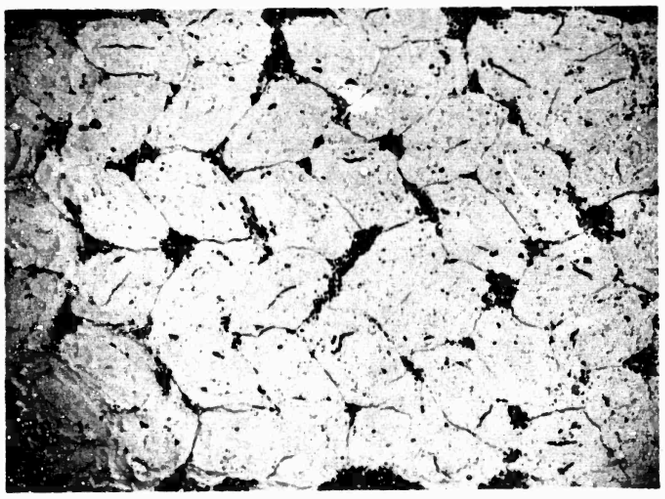

Figure 138- Section of curved portion of 237 showing residual pores and cracks within bundles. Bright field, 4.6 X.

2. THERMAL AND MECHANICAL PROPERTIES

a. Thermal Expansion

Thermal expansion was measured on two of the composites having a high modulus core in the bundle in order to compare the effects of the fiber anisotropy in the wrap. Two samples (cut from the grip end of a tensile specimen after test) were ground to 2.00 inch long bars, 0.25 inch square, from both 235 and 237. Data were taken in the Brinkman dilatometer, but the samples were heated in steps, permitting thermal equilibration, instead of continuous heating, as described in previous reports. One of the samples was run twice as a check of reproducibility. The results are shown in Figure 139; the instantaneous expansion coefficients at 1500°F are 2.2 x 10^{-6}/°F (237) and 1.3 x 10^{-6}/°F (235,) compared with 1.0-1.1 x 10^{-6}/°F for unidirectional M°-II infiltrated (Vol. III.)

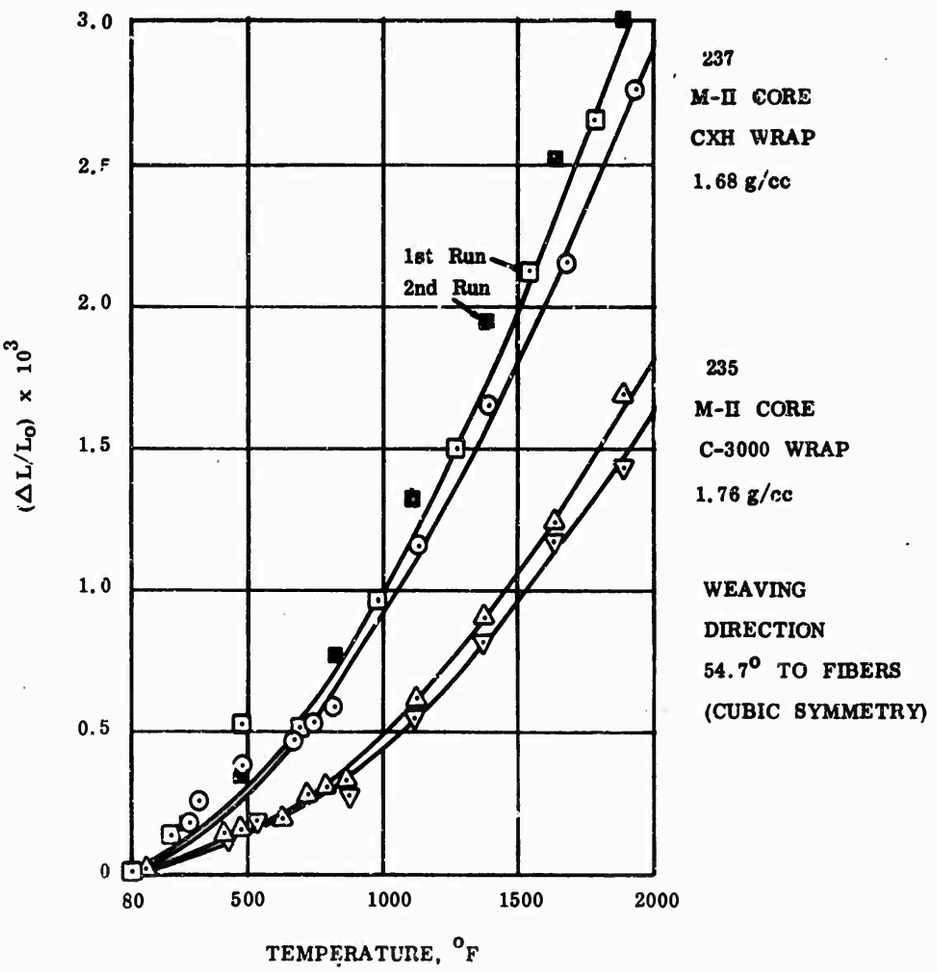

Figure 139- Expansion on heating two 1100°C PCTG infiltrated cubic 4-D* C/C composites, having different core/wrap fiber combinations.

b. Tensile Stress-Strain Properties

Tensile tests were conducted on the largest bars which could be obtained from the plates. These were 4.5 to 5 inches long, 0.375 inch thick, and up to 0.75 inch wide (0.67 inch was minimum.) This cross section thus contained 5 or 6 unit cells (about 0.2 inch square), as illustrated by the texture on the surface of the ground bars, Figure 140.

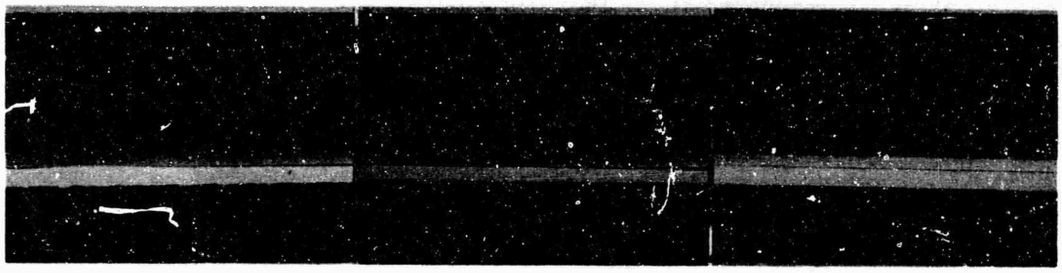

Figure 140. Uniformity of composite textures with different fibers; Left: 235 (all high modulus); Center: 236 (all low modulus); Right: 237 (high modulus core, low modulus overwrap.) 1 X.

Fiberglass plates were ground to a 7° taper for 0.5 to 1.0 inch length, leaving 0.75 inch flat for gripping, and cemeted with epoxy to all four sides of each end of each bar. These tabs were held in jaw grips of an Instron universal testing machine. Automation Industries C6-141 strain gages were bonded to the gage with Eastman 910 adhesive, and elastic modulus (plus Poisson's ratios on two bars) was obtained by cycling to low loads (300 to 500 psi.). Then a 1-inch gage-length Instron extensometer was attached, the modulus was checked with that obtained from the strain gages, and finally the sample was pulled to failure, with intermediate load cycling in some cases. The load versus extensometer deflection was recorded on an X-Y recorder, and an Instron chart record of load versus time was also obtained. All tests were run at 0.02 inch per minute. The results are presented in Table XI

As shown by the data in the table, strain measurements from the extensometer did not always agree with those from the strain gages, which were recorded both as averaged and, in the later tests, by independent measurement on each gage. Although the size of the gage relative to the material unit cell may have caused some of the difference, the principal difficulty appeared to be the attachment of the extensometer to the specimen. Consequently, in the later tests on 237 and 238, improved attachment was made with an intermediate layer of emery paper bonded to the specimen beneath the extensometer attachment points. In some cases a good approximation of total failure strain was obtained from independent measurements between paper fiducial marks bonded to the gage length and by length measurements between the cemented grips before and after failure. Consequently, the high strains to failure exhibited by these materials were confirmed, although some of the earlier strain measurements were not as precise as those in the later tests.

Figures 141 and 142 illustrate the most significant stress-strain curves. In order to check the effect of the gage and grip design, comparison samples

TABLE XI

TENSILE TEST DATA ON GRADIENT-INFILTRATED 4-D* COMPOSITES

Code	Bulk Density g/cc	Elastic Modulus 10^6 psi: Strain Gage	Elastic Modulus 10^6 psi: Extensometer	Elastic Limit psi	End of Cycle or End of Test: Stress psi	End of Cycle or End of Test: Strain %	Ultimate Tensile Stress psi	Strain at Max. Load %
235-1	1.76	1.22			492			
			1.86	1,500	1,096	2.06	5,370	1.33
235-2	1.76	1.39		-	394			
			(0.5)[a]	-	1,459	(2.11)	4,852	(2.00)
236-1	1.63	1.76	1.60		537			
			1.67	1,200	0		3,718[b]	0.75[b]
236-2	1.6	1.27	0.86		423			
			1.1	800	4,230	1.20[c]		
			0.4		0		4,270	1.10
237-a	1.64	0.75	0.46		300			
			0.51	1,200	3,320	0.94[c]		
			0.41	3,300	200	1.6	4,000	1.14
237-1	1.69	1.04[e]	1.02	710	1,424	0.02[d]		
			0.79	1,424	2,545	0.21[d]		
			0.37	2,563	1,400	2.7p[d]	3,079	2.23
237-2	1.69	1.19[e]	1.24[e]	740	1,500	0.02[d]		
			0.75	1,500	2,539	0.25[d]		
			0.37	2,240	2,200	2.5p[d]	2,856	2.3
238-1	1.67	1.83			360			
			1.42	1,200	0		3,980	1.30
238-2	1.67	1.02			360			
			0.86	800	650	1.9	3,080	1.28

NOTES:

a - Sample 235-2: Slip in extensometer caused questionable strain.

b - Sample 236-1: Fracture at edge of grip.

c - Samples 236-2 and 237-a: Slippage in grip; load released.

d - Samples 237-1 and 2: Strain at end of cycle after load released. Permanent strain (p) on sample after test.

e - Poisson Ratios:

	237-1	237-2
V_1 (width):	0.22	0.25
V_2 (thickness):	0.33	0.32

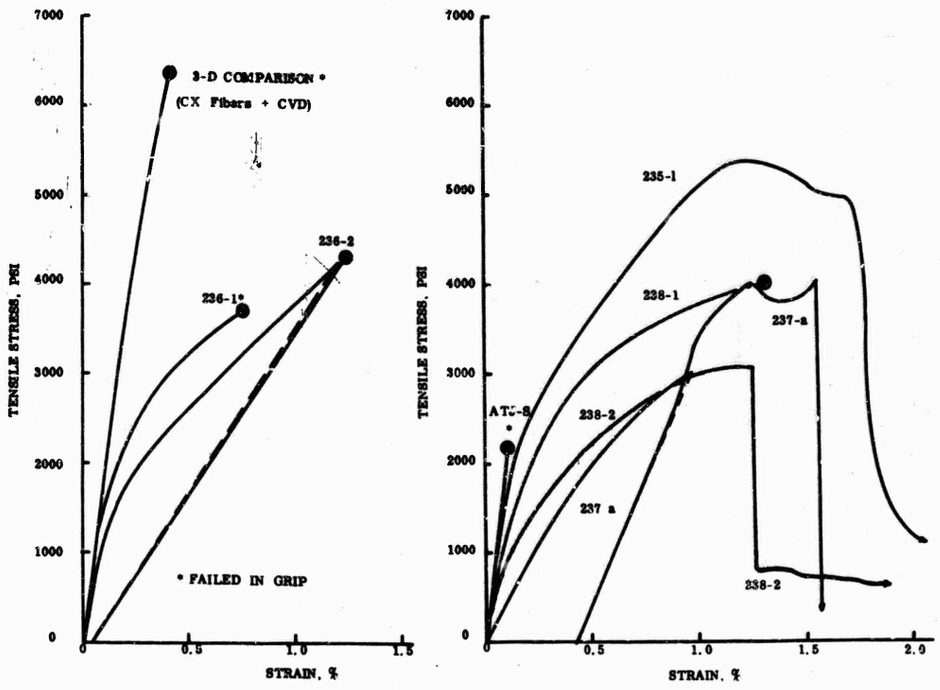

Figure 141 - Tensile stress-strain curves of CVD-infiltrated composites; all-low-modulus fibers (block 236) at left is compared with a test on a 3-D composite with same fibers and processing; samples with high-modulus fibers are compared with a test on ATJ-S in same sample configuration, which broke in grip, at right.

of ATJ-S and a 3-D woven composite having the same fibers and process history as 236 were also tested. Both of these samples, and 236-1, failed at the edge of the tapered fiberglass plates, indicating premature fracture due to the stress concentrations in that area. The ATJ-S (across-grain) showed a modulus of 1.1 x 10^6 psi by both strain gage and extensometer, but ultimate strength and strain to failure were only 2,154 psi and 0.19 %, compared with average values of 3,590 psi and 0.44 % for the billet from which the bar was ground. The fact that all but one of the 4-D* composites failed in the gage, in spite of the stress concentrations due to the specimen design, suggests that these composites are less sensitive to such stress concentration. Figures 143 to 146 illustrate the fractured specimens in comparison with the original structure as shown by radiographs before and after test.

Samples 236-2 and 237-a (which was removed before the final infiltration) were cycled because of slippage in the grips during the initial loading. The decrease in modulus upon reloading, and return to the original stress-strain curve suggested significant damage in the material associated with the "pseudo-plastic" behavior. A radiograph of 237-a after the first cycle revealed no

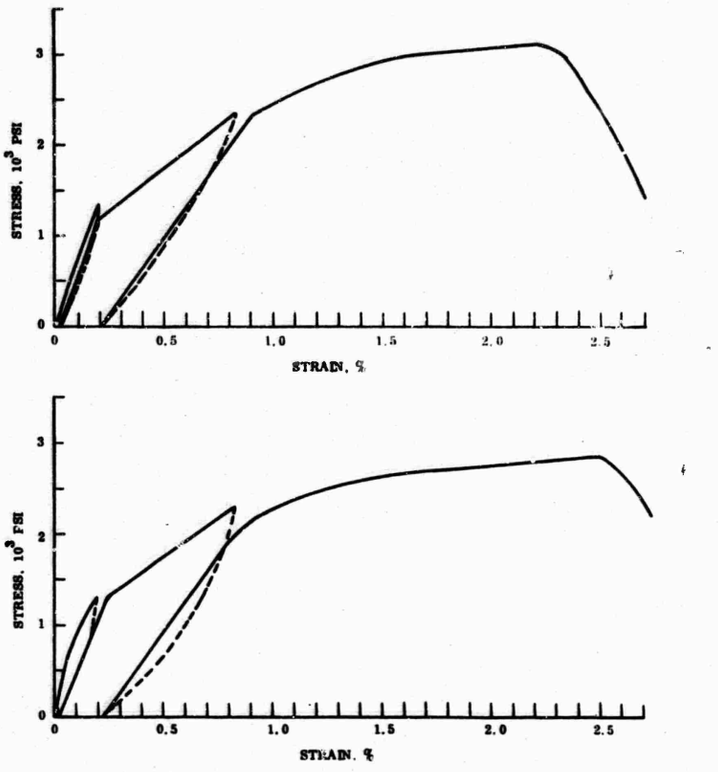

Figure 142- Stress-strain curves on samples 237-1 (top) and 237-2 (bottom) showing reproducibility in cycling.

visible damage, although material cracking had been audible during test at loads above the elastic limit, as was the case in all of the tests. The reproducibility of the change in stress-strain behavior upon cycling to increasing loads was then checked with samples 237-1 and 237-2. The change in modulus by similar prior strain was approximately the same in both tests. Although initial modulus was higher than in the lower-density 237-a, strength was lower, with a higher strain at maximum load.

The final two specimens tested were pulled directly to fracture in the expectation that this material would be similar to 237. However, the 238 bars showed different stress-strain curves, possibly because of the density variations (probably bands of soot during infiltration) visible in the radiographs of the gage sections. The stronger of the two failed completely in one of the dense bands. The fracture was examined by scanning electron microscopy after test and showed a typical low-temperature CVD carbon around the fibers, as illustrated in Figure 147.

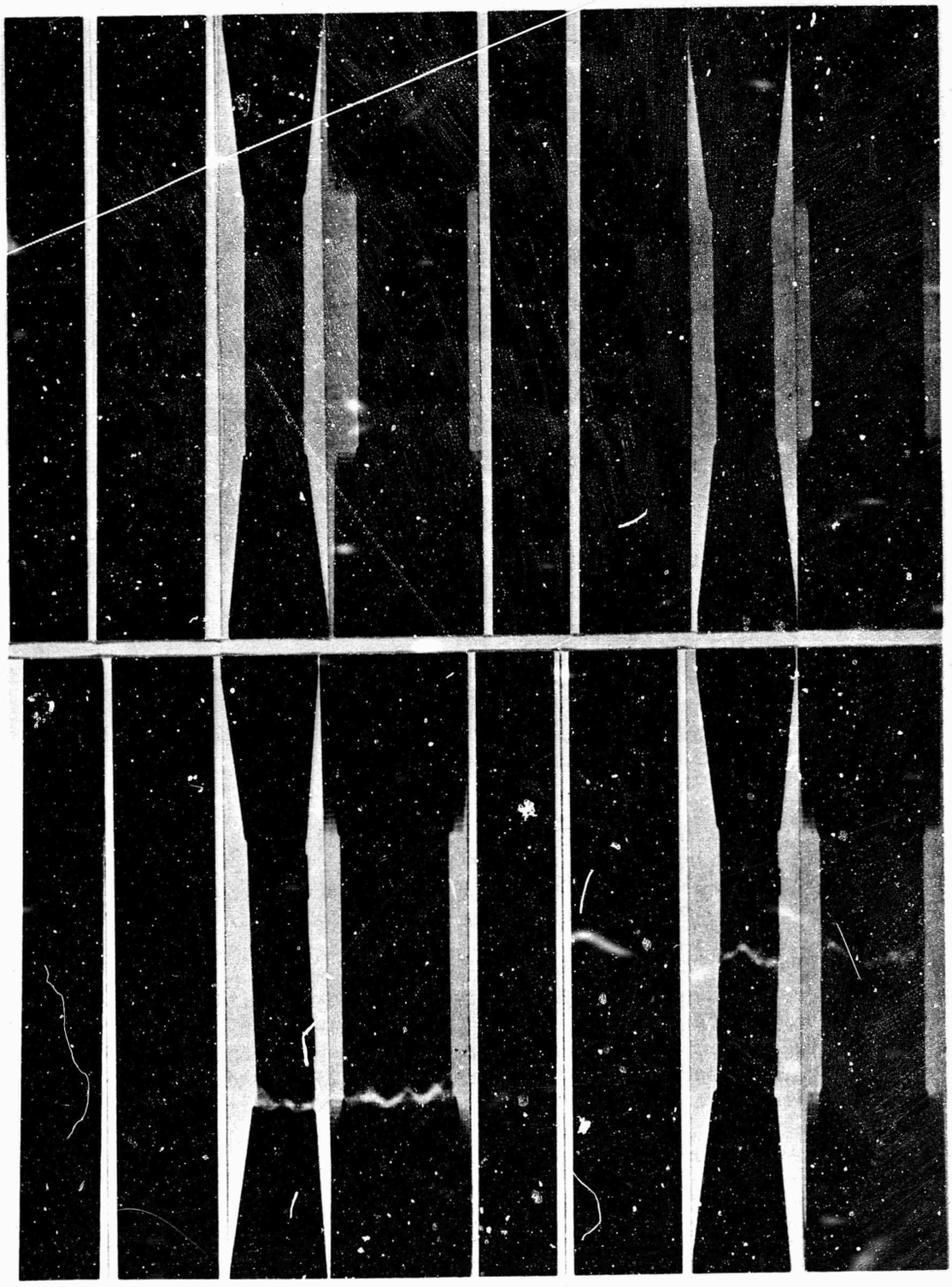

Figure 143- Radiographs of ground bars and samples after test; 235-1 and 2 at top; 236-1 and 2 at bottom. 1 X.

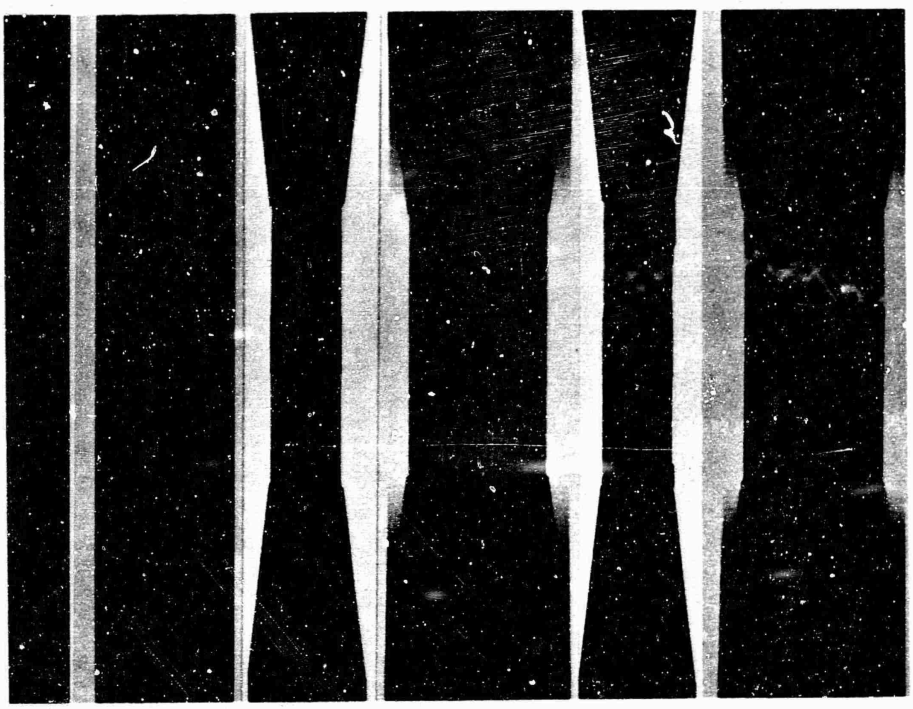

Figure 144- Radiographs of 237-a as ground, after stressing to 3,320 psi (center), and after fracture at 4,000 psi (right.) 1 X.

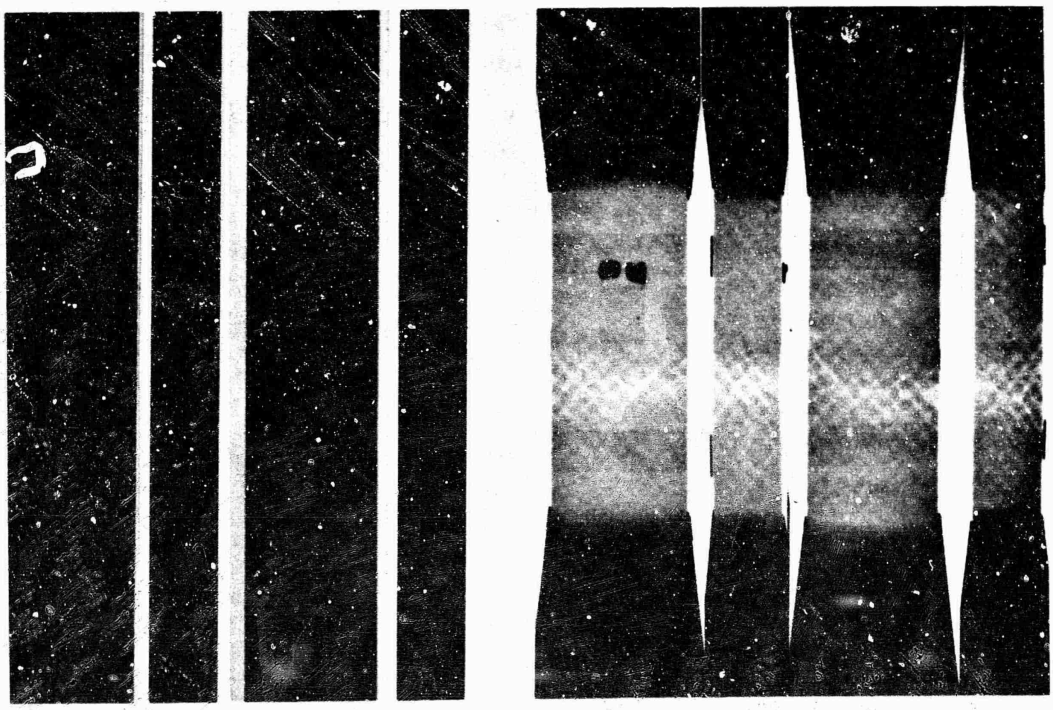

Figure 145- Radiographs of 237-1 and 237-2 as ground and after test. 1X.

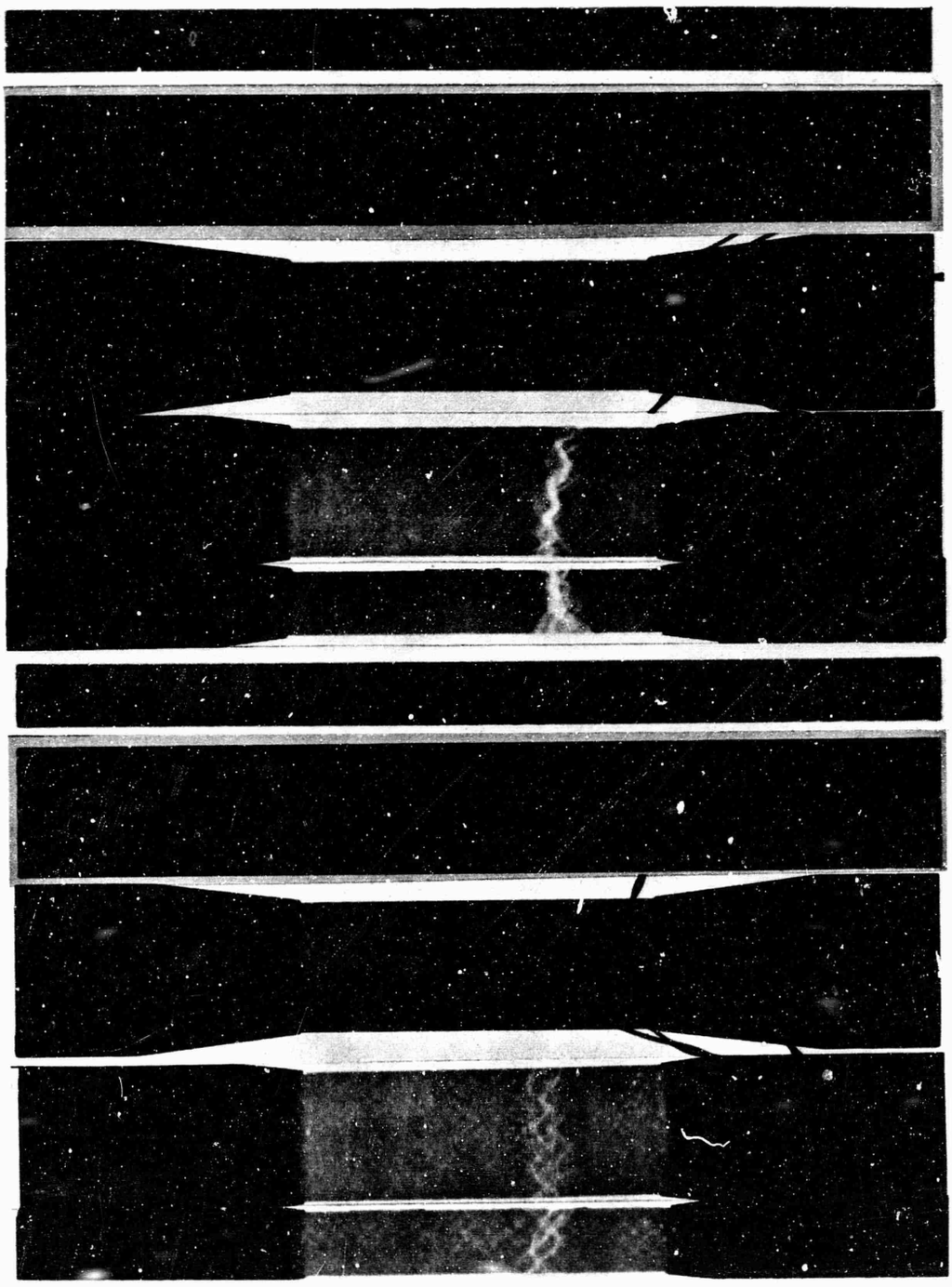

Figure 146 - Radiographs of samples 238-1 (top) and 238-2 before and after test; note position of strain gages in 238-2, which resulted in modulus values of 1.02×10^6 psi, 1.18×10^6 psi, and 0.86×10^6 psi when measured separately.

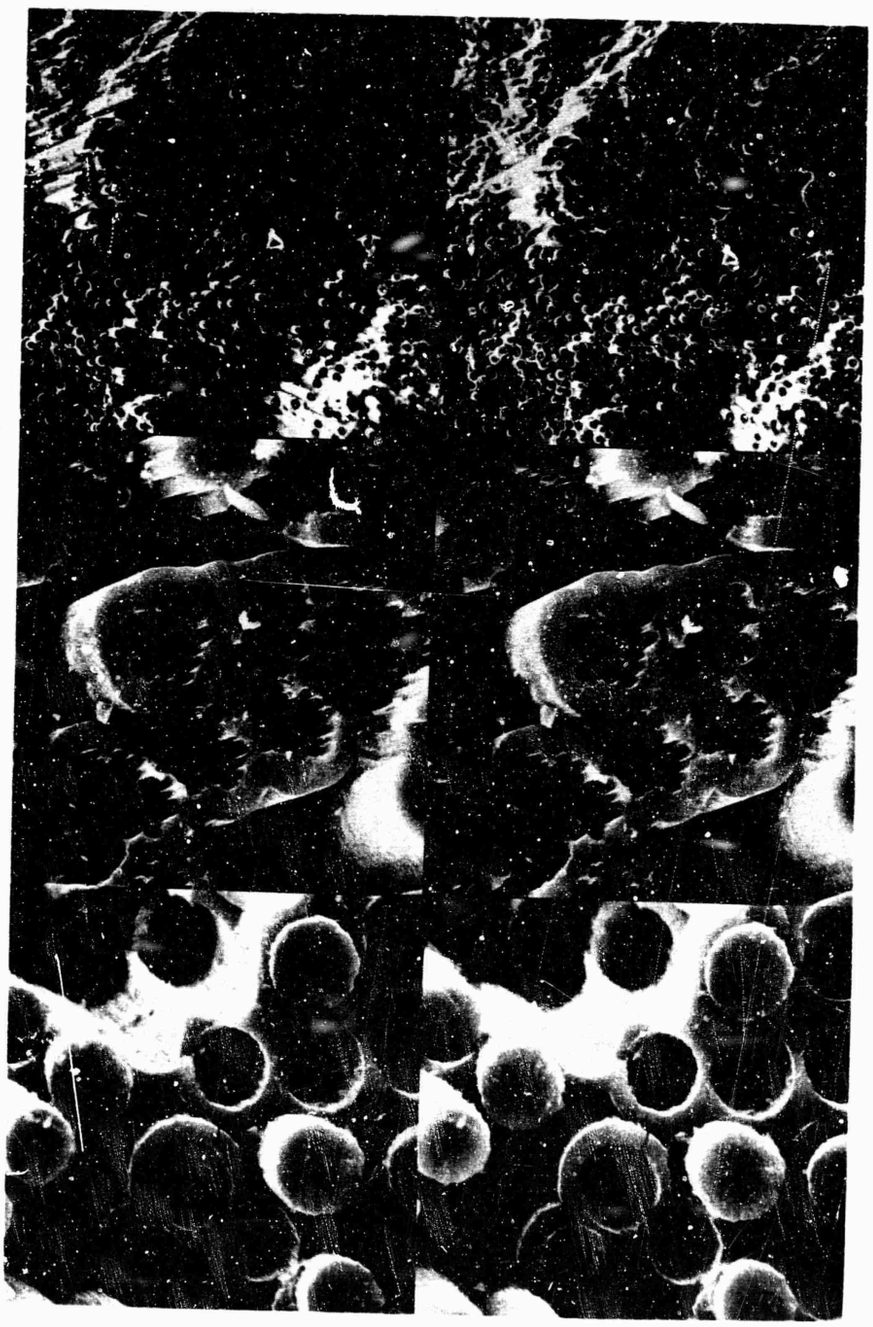

Figure 147 - Fractured surface of tensile specimen 238-1 after test; top: 145 X showing region between CX fibers (at top) and M-II fibers (at bottom;) center and bottom, 1450 X views of CX and M-II regions, respectively.

c. Mechanical Behavior in Flexure

Table XII presents 3-point flexure results on bars made from either the 1x1.5 inch residual blocks or reground ends of tensile specimens. In the latter case the flexure bars were broken in regions previously enclosed by the cemented fiberglass doublers within the tensile grips. 4-D* bars with L/h = 3 were 0.45 in. thick x 0.90 in. wide; these were undamaged material.

Comparison with the tensile data shows about 2X ratio of flexure/tensile strength in the 4-D* materials. All samples broke in tension on the surface without any visible evidence of damage from the maximum shear stress in bending. Apparent elastic modulus (from calibrated change in distance between the loading points in the direction of load) followed the usual extrapolation with h/L ratio in good agreement with the E from strain gages in the tensile tests, (h/L = 0). The load-deflection curves for 4-D* showed the same characteristic toughness described in Vol. III, p-70. Typical samples are illustrated in Figure 148.

TABLE XII

FLEXURE TEST DATA ON GRADIENT-INFILTRATED COMPOSITES

Code	Bulk Density gm/cc	Ratio: Length to Thickness	Apparent Modulus 10^6 psi	Flexure Strength psi	Shear Stress psi
235-2	1.76	5.6	0.90	11,500	1040
235-5	1.77	3.0	0.34	12,030 (9,760)*	2027
237-5	1.70	3.0	0.26	7,480 (6,980)*	1230
236-1	1.63	5.4	0.77	9,100	838
236-5	1.66	3.0	0.34	6,490 (5,900)*	1070

* First Break.

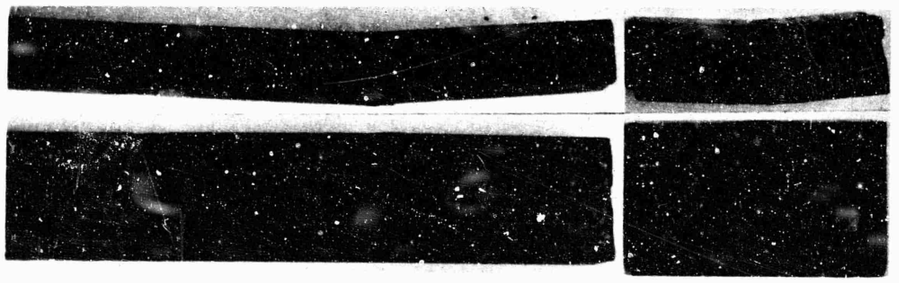

Figure 148- Typical flexure specimens after test (235-2 and 235-5.) 1 X.

3. PERFORMANCE IN PLATE SLAP AND ULTRASONIC PROPERTIES

a. Plate Slap Tests

A series of magnetically driven flyer impulse tests were performed to evaluate the relative damage threshold and damage extent of the three different "4-D"* C/C composites. The 7-D sample discussed in the 7th TMR, and a 3-D weave left from the previous year of work were also tested in this series. It was necessary to use only two different impulse levels, 3.0 and 3.5 kilotaps, because of the limited material available.

The tests were conducted in the manner described in AFML-TR-69-67, Vol. III, p. 77, except that higher levels of impulse were applied by using 0.012 inch thick (1100) Aluminum flyers. The RESD 43 kilojoule capacitor-bank facility was used. This bank, Maxwell Model 50E38HR consists of twenty canister-type low-inductance capacitors with a total capacity of 35 microfarads and a working voltage of 50 kilovolts, plus a Maxwell Laboratories developed dielectric type switch. The bank is designed to be as low in inductance as is practical and has a short circuit ringing frequency of 345 kilohertz. Instrumentation of the facility consists of coaxial electrical probe pins for determining time of arrival and velocity, a coil pick up for recording the shape of the current pulse and a Barr & Stroud high speed framing camera for observing the flyer motion. Electrical signals are recorded on fast response oscilloscopes.

For the sixteen-capacitor configuration used for these tests, (29.7 microfarad capacity) the flyer-impulse charge relationship is shown in Figure 149. The curve was determined by extrapolation of calibrated data measured with the bank in a 33.5 microfarad configuration at the charge levels used, (39.5 and 42.5 KV.). No evidence of flyer melting in the specimen impact area was observed, although the flyer edges occasionally welded to the aluminum surrounds on impact with the 42.5 KV charge.

Each 1.5 inch square specimen was surrounded by four 0.5 x 0.5 x 1.75 inch Aluminum blocks clamped in close contact by a tight rubber band. These surrounds were designed to reduce the small sized specimen edge effects by

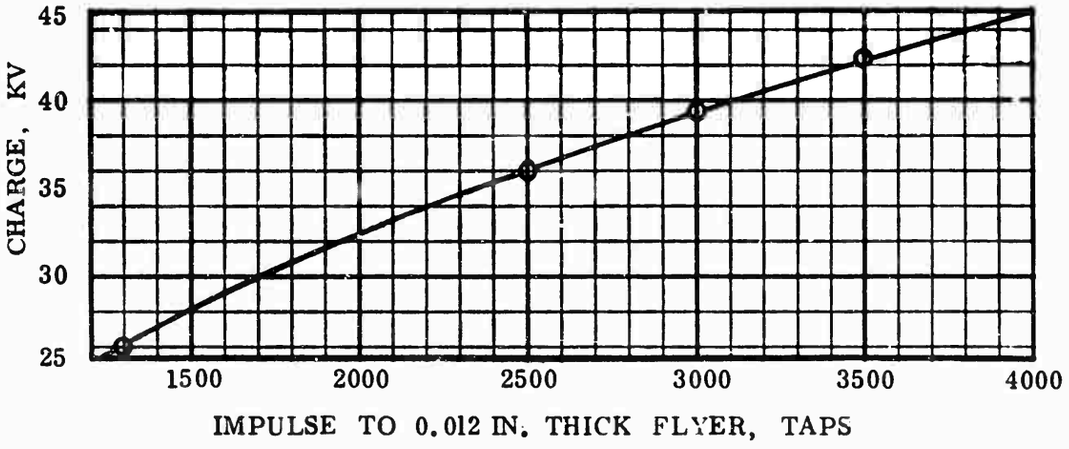

Figure 149- Capacitor bank charge voltage for flyer impulse values.

providing a one-way (outward compression) interface for the lateral stress waves. The effectiveness of the surrounds in absorbing the outward shock wave was evidenced by the full edge weave pattern of the specimen imprinted on the blocks after each test. Each specimen with surround (2.5 inch square) was aligned to the center area of the 2.25 x 4.25 inch flyer and positioned for impact with the surface corresponding to the outside of a heat shield (cold surface during infiltration) 0.100 inch above and parallel to the aluminum flyer.

After impact, the specimens were softly decelerated in a catcher box filled with increasing density foam layers backed by plywood and lead. The imbedded specimens and flyers were carefully removed from the foam without further damage. All identifiable back face spall and edge chips were gathered. Specimen post-test thickness was measured and compared to the pre-test value, and ultrasonic data was obtained on samples without spall.

Radiographs of the blocks before test, Figure 150 showed some porosity but no significant defects. Appearance of the samples after test is shown in Figures 151 through 156. The first set of specimens, including a 3-D weave comparison, were impacted at 3500 taps and the second set, which included the 7-D sample described in Section II, were impacted at 3000 taps. Table XIII summarizes the results on the 4-D* composites.

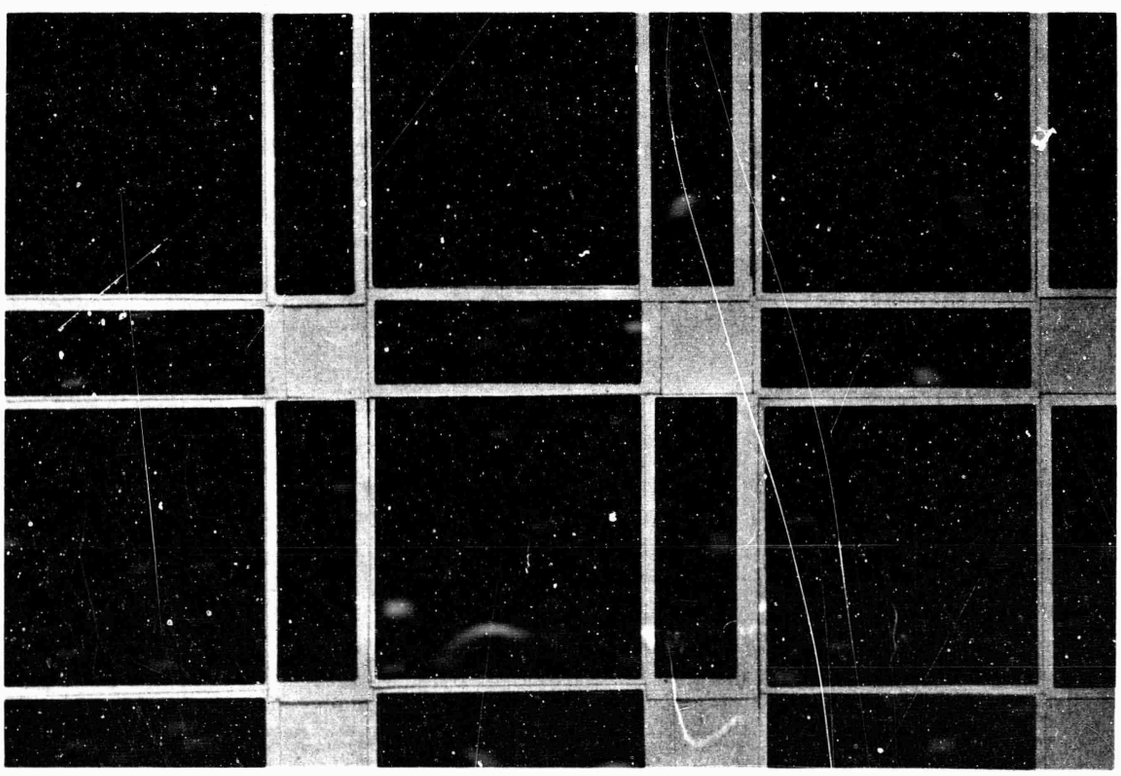

Figure 150 - Radiographs of plate-slap specimens before test (1 X): Top: 235-1, 236-1 and 237-3; Bottom: 235-2, 236-2 and 237-4.

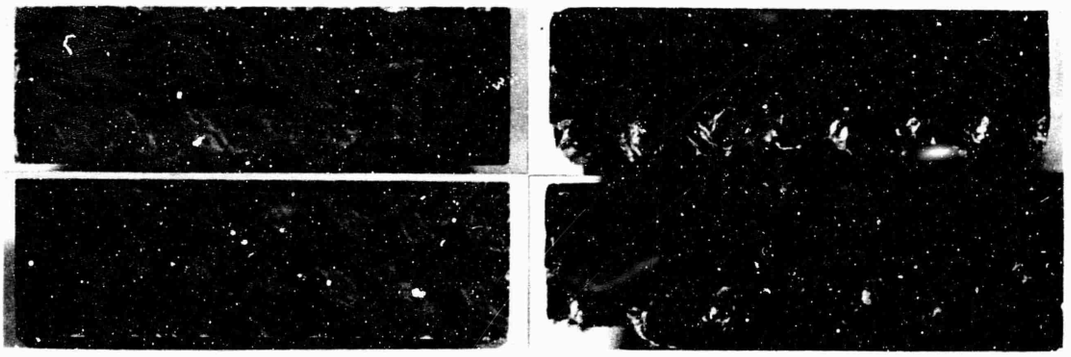

Figure 151 - Edge views of samples 236-1, before and after impact at 3500 taps (top) and 236-2, before and after impact at 3000 taps (bottom.) This all-low-modulus fiber composite spalled completely at both levels close to the back face. 1.85 X.

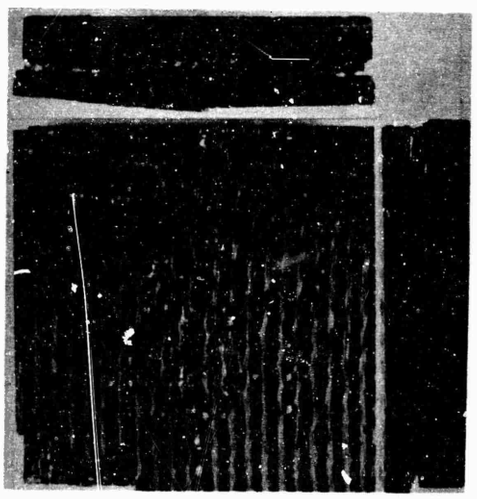

Figure 152 - 3-D Angle-Interlocked comparison sample WC'-1 showing complete spall of back face after impact at 3500 taps with all-low-modulus fibers. 1 X.

The comparison sample was part of the series described in Vol. II, and was tested because material of the same type showed no spall at 1720 taps with 5-mil aluminum flyers (Vol. III, page 84.) This material had VYB fibers with 2/3 oriented at 50° to the thickness and 1/3 (fill yarn) parallel to the surface. It had been impregnated repeatedly with coal tar pitch and graphitized to 2500°C. A final CVD infiltration was used to bring density to 1.60 g/cc. The 2-inch square, 0.375-inch thick block spalled completely at 3500 taps.

The all-low-modulus fiber composite 236 (1.63-1.62 g/cc) spalled at both 3500 and 3000 taps. The composite 237 with low-modulus braid over the high-modulus core (1.66-1.67 g/cc) showed back face chipping at 3000 taps.

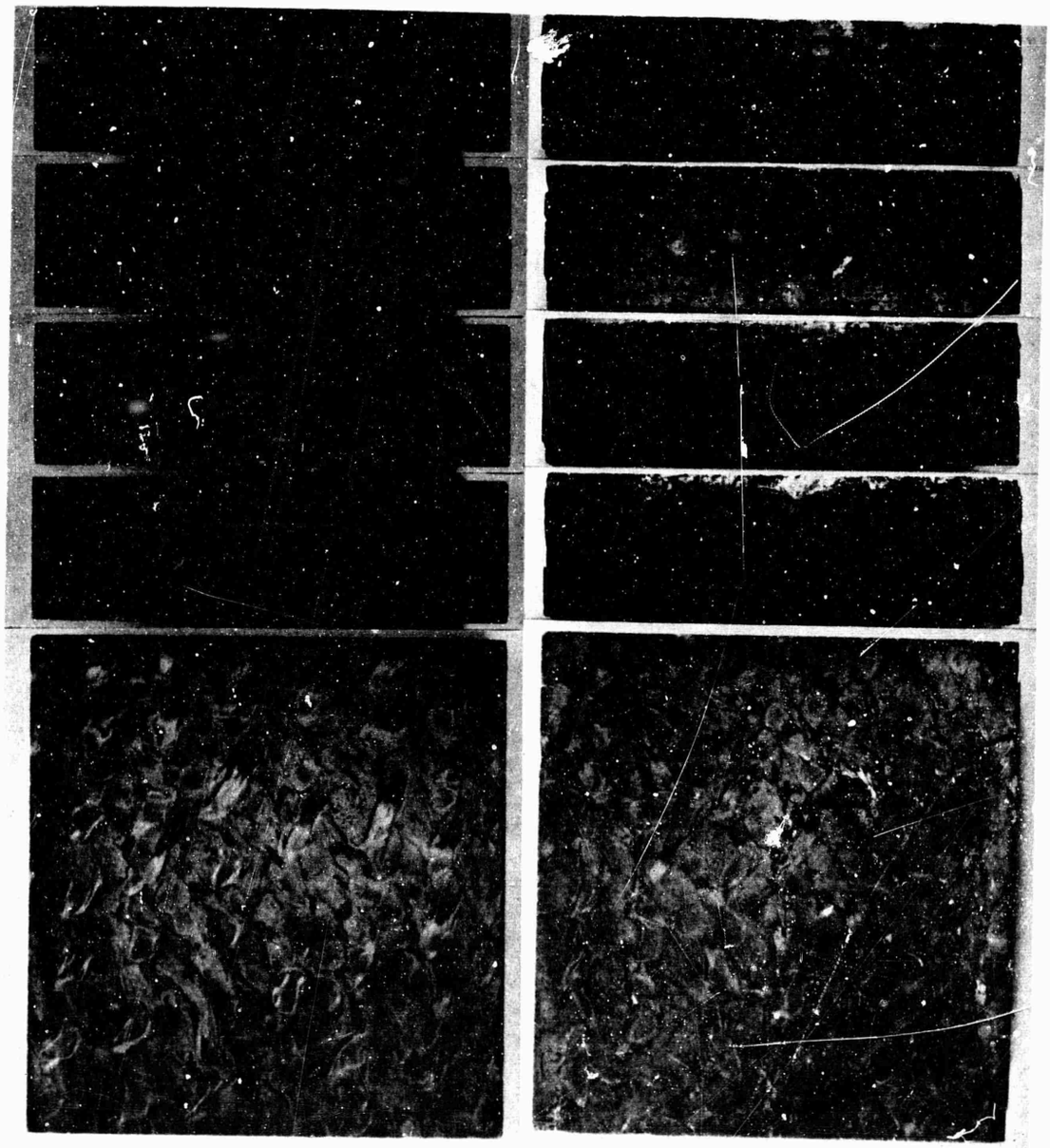

Figure 153 - Omniweave composite 237-3 before (left) and after (right) impact at a nominal level of 3500 taps; in this test a portion of the bank energy was lost in a small arc discharge through the flyer insulation layer (note aluminum deposited on the front face at top of the edge views at right.) A small amount of backface spall is evident at lower right. 1.85 X.

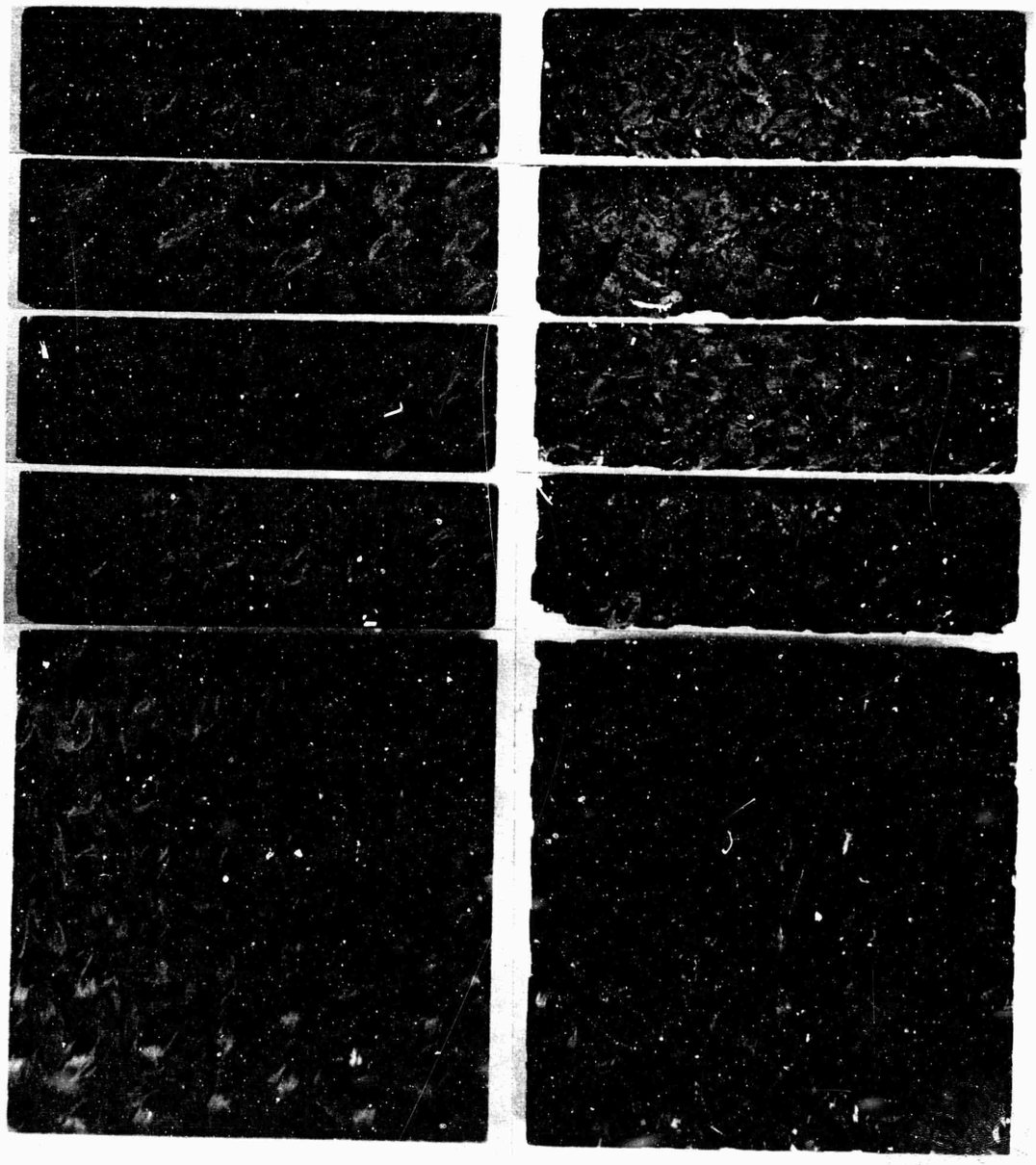

Figure 154. Omniweave composite 237-4 before (left) and after (right) impact at 3000 taps. Note cracks between bundles, which account for 2.1 % increase in thickness, and backface edge removal of some bundles which do not pass into the block. 1.85 X.

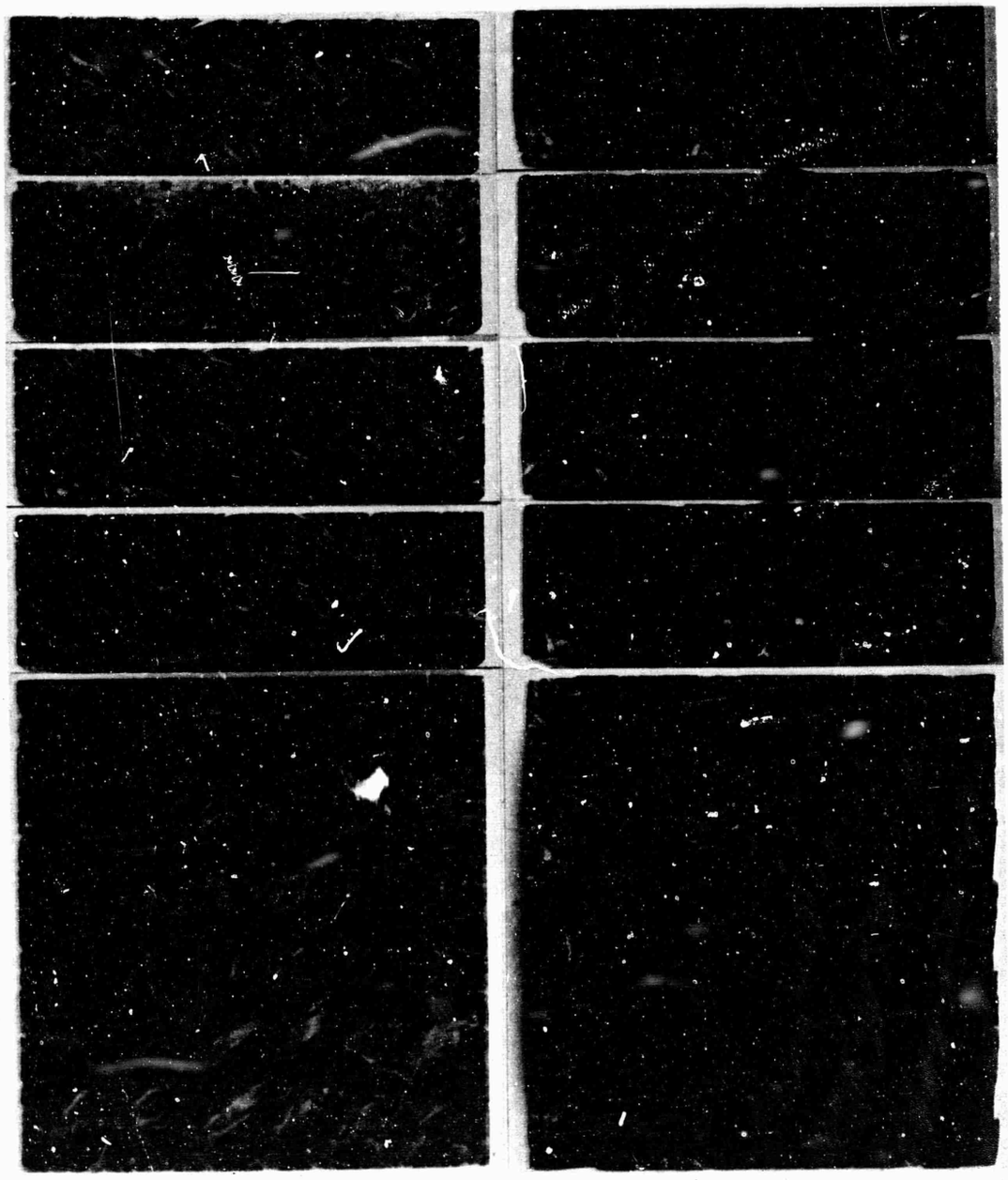

Figure 155- Omniweave composite 235-1 before test (left) and after impact with 0.012-inch thick aluminum at 3500 taps; four sides and the back face are shown at 1.85 X.

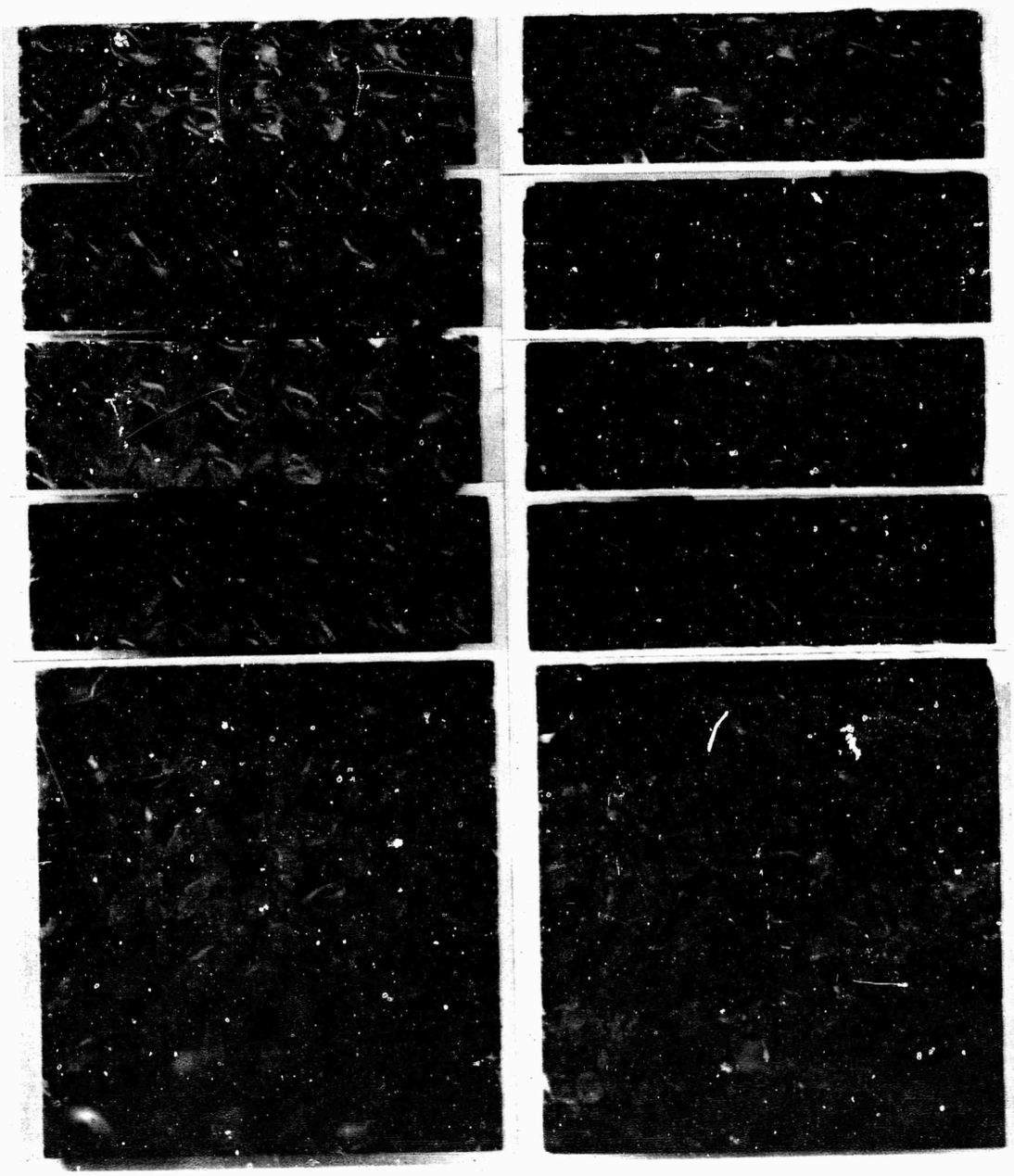

Figure 156 - Omniweave composite 235-2 before test (left) and after impact at 3000 taps (right) showing sides and back face at 1.85 X.

TABLE XIII

SUMMARY OF PERFORMANCE OF 4-D* COMPOSITES IN PLATE SLAP TESTS

Impulse	Property[a]	Fiber Modulus In Core/Wrap of Bundles Low/Low	High/Low	High/High
	Sample No.	236-1	237-3[b]	235-1
3500 Taps	Spall	Complete	Incipient	No
	Sound Velocity	--	--	-13%
	Attenuation	--	--	+45%
	Thickness	--	+2.7%	+ 0.6%
	Sample No.	236-2	237-4	235-2
3000 Taps	Spall	Complete	Incipient	No
	Sound Velocity	--	-11%	-11%
	Attenuation	--	- 2%	+ 5%
	Thickness	--	+ 2.1%	+ 0.5%

Notes: a = Samples 1.50 in. x 1.50 in. x 0.43-0.45 in. thick.

b - Partial energy loss in this test due to arc discharge through the flyer insulation layer.

The composite with all high-modulus fibers (235, 1.79-1.77 g/cc) had no spall at either level, although some damage occurred, including rear edge chipping and cracks between bundles at the higher level. Note that thickness increase was less than in 237, indicating less damage.

b. Ultrasonic Characteristics Before and After Test[1]

Ultrasonic velocity and attenuation measurements were made on the 4-D* composites before and after plate slap, with the changes shown in Table XIII. The types of signals and material characteristics which they indicate are discussed below, and the velocity and attenuation data are shown in Table XIV.

The technique involved use of an aluminum buffer block, as described in Vol. III page 64 and Vol. II pages 107-122. All-high-modulus 235 had

1. Section prepared by J. A. Roetling.

TABLE XIV

ULTRASONIC VELOCITY AND ATTENUATION DATA

Block	Bulk Density g/cc	BEFORE TEST 0.71-0.73 MHz V_1	α	0.76 MHz V_1	α	0.95-1.00 MHz V_1	α	AFTER TEST 0.70 MHz V_1	α
235-1	1.79	5.01	33	-	--	-	--	4.34	48
235-2	1.77	4.98	36	-	--	-	--	4.43	38
235-3	1.77	-	--	4.80	44 (38&31)	4.93	39	-	--
236-1	1.63	4.05	22	-	--	-	--	-	--
236-2	1.62	4.21	12	-	--	-	--	-	--
236-3	1.66	-	--	3.92	18	3.92	27	-	--
237-3	1.66	4.17	42 (27)	-	--	4.24	45 (41)	-	--
237-4	1.67	4.10	42 (29)	-	--	4.17	44 (41)	3.65	41
237-5	1.70	-	--	3.95	39 (31)	3.92	43 (38)	-	--

NOTES:

V_1 = Longitudinal Wave Velocity, mm / microsecond.

α = Attenuation, decibels / cm. (Numbers in parentheses are based on stronger trailing signals.)

Samples 235-3, 236-3 and 237-5 are narrow (1-inch) specimens later tested in flexure, and boundary effects are possible.

the highest velocity, corresponding to a uniaxial strain modulus of 6.5 X 10^6 psi through the thickness. All-low-modulus 236 had the lowest velocity, which indicates 4.0 x 10^6 psi uniaxial strain modulus; 237 with mixed fibers had almost as low a modulus, 4.1 x 10^6 psi (or 4.3 x 10^6 psi using data taken at the higher frequency.) The signals received through 236 was similar to that observed with homogenous materials, whereas the signals observed with the other two materials were typical of those which result from scattering in inhomogeneous materials.

Further information about the types of signals is presented in Figures 157 and 158. First, consider the response illustrated in Figure 157. The signal received through an aluminum buffer block is compared with the signal received through the buffer plus a specimen of composite 237. Note that with the buffer alone the first pulse to arrive was the strongest and the trailing signals (reflections) were weaker. With materials like 237 which tend to scatter the

NOT REPRODUCIBLE

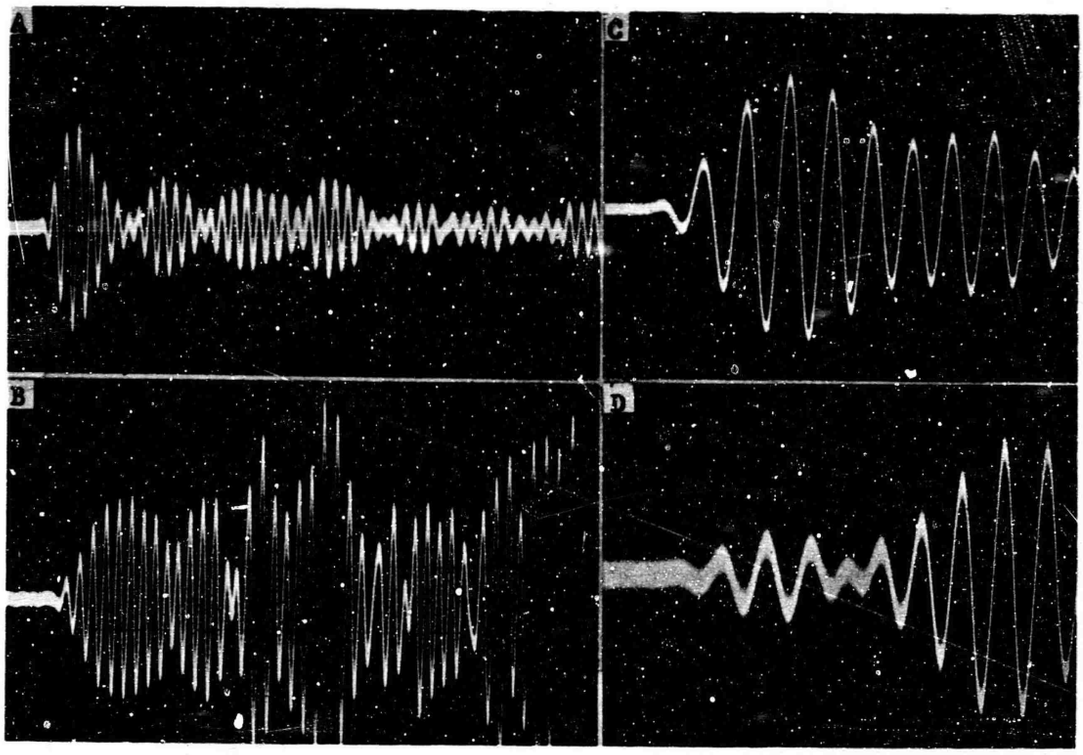

Figure 157 - Ultrasonic signals through aluminum buffer blocks (A and C at top) and through specimen 237-5 (B, left) and 237-3 (D, right.) Conditions for A and B are 1.0 MHz frequency and 5 microsec./cm sweep speed; for C and D they are 0.71 MHz and 2 microsec./cm.

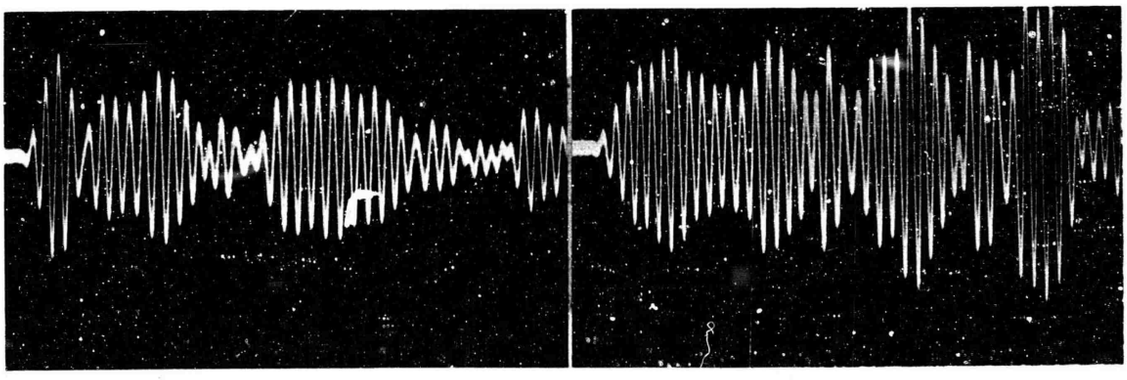

NOT REPRODUCIBLE

Figure 158- Ultrasonic signals received through specimen 236-3, at left, and through 235-3 at right (before test); 1MHz frequency and 5 microsecond/cm sweep speed.

signals, it is frequently observed that trailing signals occur which are stronger than the first arrival. In general, meaningful velocity and attenuation measurements are possible only on the first arrival. However, where stronger trailing signals occured and these were not too far behind the first arrival, an attempt was made to indicate their amplitude. The "attenuation" based on these trailing signals is indicated in parenthesis in Table XIV.

The signals on 236 indicated not only the lowest velocity, due to the lower modulus of the CX-3 fibers, but a homogeneous material, so far as the transmitted ultrasonic signal is concerned. This is illustrated in Figure 158 (left) where it will be noted that the first signal to arrive was the strongest and had essentially retained the shape and short duration of the incident signal through the buffer block. The lower attenuations observed for this material were probably the result of less scattering, which in turn was probably due to a greater similarity of the fiber and matrix materials.

Sample 235, with all high modulus fibers, showed the highest wave velocity but otherwise was very similar in behavior to 237. At the lower frequencies (0.71-0.76 MHz) both showed a distinct, weak leading pulse (35 to 45 db/cm attenuation) followed by a somewhat stronger signal (approximately 29 db/cm). The trailing signal was roughly 6 microseconds behind for 0.45 inch thick specimens, thus corresponding to a velocity of only 1.3 to 1.4 mm/microsecond, if it is assumed to be straight-through transmission. At the higher frequency (0.95 to 1.0 MHz) these two signals appeared to have run together, producing a single pulse which increased more gradually in amplitude than the signal seen through the buffer block only. Figure 157B is a typical example of this. Note that the apparent pulse width of this first signal is considerably greater than that seen in Figure 157A. Sometimes there appeared to be an inflection in the amplitude, suggesting the presence of two pulses. Figure 158 shows, at right, a representative example.

For samples 235 and 237, the received signal of maximum amplitude often arrived far behind the initial signal. For specimen 235-3, for example, the peak signal at 0176 MHz was roughly 27 microseconds after the first arrival. For 237-3, at 0.71 MHz, the peak occurred after 20 microseconds. This tendency for late occurrance of the peak signal seems to be typical when measurements are made on materials which scatter the energy (as opposed to a true absorption of the energy).

After test, all of the 4D* specimens showed a significant decrease in velocity of propagation. Of these, 235-1 showed a significant increase in attenuation, but the other two showed no change. Specimen 235-1 appeared to have suffered the most damage. However, the back-face of this specimen seemed to be rougher and the larger attenuation may have resulted from poorer contact. Internal damage to 235-2 and 237-4 would appear to be very minor. As discussed in Section II, Specimen 7D1, which was measured at the same time as the 4D*, appeared to be undamaged and showed no significant change in velocity of propagation after 3000 taps.

4. CHANNEL FLOW ABLATION TEST OF 4D* MATERIAL

The region from plate 237 which had a 2.5 inch radius of curvature was ground to a 0.40-inch thick plate, 1.13 x 4 inches, and ablation tested in subsonic flow in the channel mode of the GE Hyperthermal Arc Facility, which was described in AFML-TR-69-67 Vol. III, pp 100-109. The plate was held in an ATJ graphite block against a 1-inch wide rectangular channel while arc-heated air was passed through at 0.1015 lb/sec., with an enthalpy (calculated from power and water temperature of the arc) of 7505 BTU/lb. Plenum pressure was 69.5 psia, and pressure in the chamber was measured by a port opposite the sample as 57.8 psia. Two slug calorimeters in the wall opposite the sample provided heat flux data of 1567 and 1550 BTU/ft^{2}sec, about 50 % higher than in the tests reported in Vol. III. The results are shown in Figures 159-160.

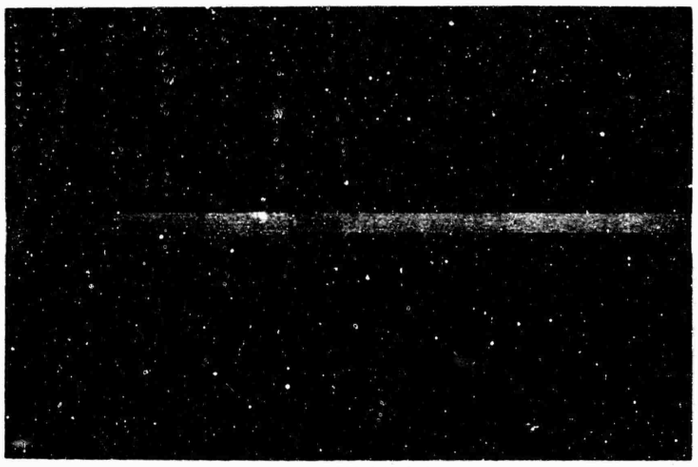

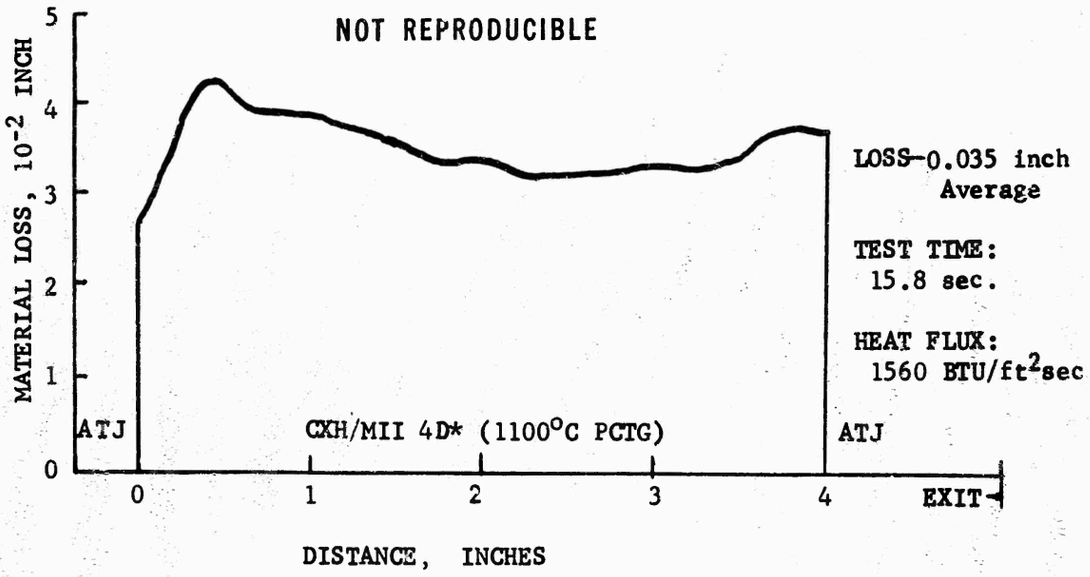

Figure 159- Radiograph and surface of sample before test, compared with center-line recession profile after subsonic channel flow ablation test.

Figure 160 - Appearance of 4-D* sample after ablation, at forward end of chamber, showing uniformity in ablation with absence of any turbulent pitting associated with the coarse texture.
Top: 1.8 X; Bottom: 5 X.

The purpose of this test was to determine if the coarse weave texture created a surface roughness during ablation, and the test showed that this was not the case. The technique of adding fibers to the interstices after weaving also resulted in sufficient density uniformity in the infiltrated material that cavitation in these locations did not occur.

Although thermocouples could not be imbedded in the material because of difficulty in drilling the holes, two thermocouples at the back face showed the following:

2 sec.	4 sec.	6 sec.	8 sec.	11 sec.	15 sec.
550°R	900°R	1510°R	2070°R	2700°R	3400°R

Instrumented ablation tests of this type provide a comparison of the thermal characteristics of ablative materials, although the heat flow is not sufficiently controlled to obtain accurate conductivity data. A value of thermal diffusivity was calculated as $8 \pm 1 \times 10^{-6}$ ft^2/sec from the back face temperature rise, assuming the front face was instantly heated to 4500° to 5800°F and a linear change in thickness with time. The corresponding conductivity for 1.64 g/cc density, 3×10^{-4} BTU/ft-sec-°F, is lower by about 5 times than steady-state data on similar materials (e.g. Vol. III, page 53.) (Note: the ablation test was conducted without cost to the contract.)

5. COMPARISON WITH OTHER CARBON-CARBON COMPOSITES

The 4-D* C-C type of material is unique among the fiber-reinforced carbon composites in the type of reinforcement geometry. Properties on cylinder material similar to composite 237 discussed in this report have been determined under a separate Air Force program by Southern Research Institute, and will be reported separately. It should be noted that this material was prepared before the properties in this report were available; use of all high-modulus fibers in the construction should have resulted in higher strength.

The principal advantages of 4-D* C-C are high through-thickness strength, compared with filament-wound or cloth-laminate composites, and a high strain-to failure combined with low yield strength, which impart greater toughness and should reduce sensitivity to stress concentrations in comparison with 3-D composites, particularly those with hard carbon matrices. A relatively high resistance to failure from thermal stress should also result. Figure 161 compares the strength and strain to failure of these composites, compared with data on pyrolytic graphite, ATJ-S, AXF 9Q and other reinforced C-C materials. Data on candidate fiber reinforcement materials (with strength-to-modulus ratio taken as strain to failure) are included for comparison. The advantages of the 4-D* C-C materials developed here would be in applications where the quasi-ductility is more important than high in-plane strength.

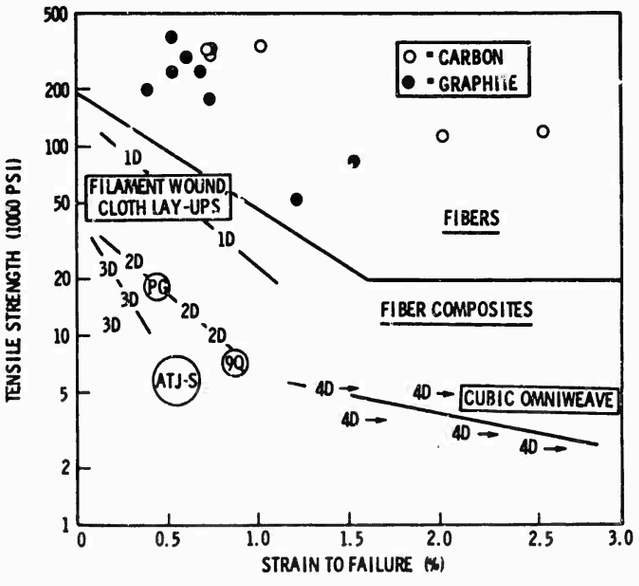

Figure 161- Comparison of tensile strength and strain to failure of 4-D* C-C (cubic omniweave) with fibers and other C-C composites.

SECTION IV

SUMMARY AND RECOMMENDATIONS

The thermal-shield material development described in this report has resulted in preliminary data needed to evaluate feasibility of a unique C-C frustum concept. It is proposed that a frustum fibrous reinforcement may be prepared by constructing tapered fiber bundles, several feet in length, which contain varying numbers of strands or filaments of a core fiber along the length, covered with an overwrapping braid. A 12-end braid wrapped under tension to control packing and fiber angle, and a double overwrap in opposite directions of 20 denier nylon were used in the samples prepared here. High-strength acrylic-type precursor carbon, at least 10,000 filaments in the core if 3,000 filament ends are used in the braid, are preferred to low-modulus, cellulosic-type precursor carbon in both core and wrap. Superior tensile strength and spall resistance in plate slap were obtained with this combination in comparison with all-low-modulus fiber bundles or low-modulus braid wrapped over high-modulus acrylic-type core material. This improvement occurred even though the all-high-modulus fiber bundles were not packed to as high a density and showed more separation between bundles in the final samples. Future development should evaluate smaller bundles (e.g. 1,000 filament acrylic-type fiber bundles) in the braid. The advantages of such a composite fiber reinforcement are (1) gradation in anisotropy and thermal expansion coefficient between the straight fibers in the core, through the braid, to braid and core of an adjacent bundle oriented at an angle to the first and (2) reduction in size of thermal cracks to the dimensions of the core or braid bundles instead of the dimensions of the entire reinforcement.

The composite "graded anisotropy" reinforcements are arranged in a three-dimensional, four-directional construction in which each bundle parallels the diagonal of a cube. The General Electric Co. "Omniweave" apparatus is particularly suited to preparing such a geometry. Tight packing is important to minimize porosity and obtain more contact area between reinforcements. In frusta the geometry may be deformed to provide fibers with lower angles to one of the three orthogonal directions requiring higher strength or modulus relative to the other directions (or, one direction such as thickness may be reduced in strength by steeper fiber angles in order to strengthen the other two.) This type of geometry, using composite bundles, has been given a brief designation of "4-D*" (four-D-star,) for convenience in discussion. A frustum should contain a combination of bundle taper and geometric distortion to give the desired combinations of properties at different positions along the length.

The matrix employed to hold the reinforcements together in these studies was a low-temperature, 1-atmosphere-pressure deposition from methane, using the heated substrate technique developed previously. The fibers were heated to about 1750°C after weaving to develop some improved thermal stability, but the composite was not heated above 1100°C during deposition of CVD carbon. This technique provided a hard, strong matrix material and a minimum internal stress due to cooling from process temperature. An ablation test described in this report demonstrated the suitability of such a material for a thermal shield, in spite of the low process temperatures.

The nose-tip oriented work described in this report has shown effects of reinforcement geometry, fiber characteristics and type of matrix processing on high-pressure ablation performance (90 atmospheres) in the AEDC 5MW arc. By using 1/8-inch radius nose-tip specimens, ablation characterization for exposure times up to about 1 second was comparable with results on similar materials in the 50MW AFFDL facility (using larger specimens and longer times) thus establishing the validity of the test for small-sample screening. The utility of the arc could be improved if feed-in apparatus were added to the model holders, since in-depth, time-dependent thermal degradation (graphitization growth phenomena and cracking) could occur in some of these materials. This facility is a valuable complement to the facilities with larger flow field because of the need to survey economically many material variables in optimization.

The most important result of the material comparisons was the demonstration that the higher-density acrylic-type precursor fibers can be used successfully in woven-reinforced nose tips. These showed lower recession rates in similar geometries and with similar matrices than did samples with low-density, low-anisotropy cellulosic-type precursor fibers in spite of what appeared to be more severe microscopic cracking. The cracks are inevitable in this class of materials because of the inherent anisotropy between radial and length directions of the fiber bundles comprising the reinforcement elements, and this anisotropy is greater with high-modulus filaments. Partly because of these cracks, which tend to close on heating, thermal expansion is lower, approximately that of the reinforcement bundles themselves, even in multi-directional reinforcements. The cracks also function as crack-stoppers, thus contributing to toughness when stress is applied in certain directions. The roll which the microcracks play in determining orientation-dependent properties and resistance to thermal stress should be studied further in optimizing these materials.

The deformed 4-directional geometry (as in the Thornel-40 composites described in this report) appears to give poorer ablation performance, although high strength and toughness in flexure (axial-equivalent direction) was demonstrated. A petroleum-derivative impregnant gave best mechanical properties, although residual porosity was severe and probably was the cause of failure at 90 atmospheres stagnation pressure. The close-to-cubic (tightly packed) 4-D reinforcements, 3-D reinforcements with a high axial component of fibers, and cubic 7-D reinforcements, all having similar bundle sizes, showed similar ablation performance, when good pore-filling was accomplished in processing. CVD infiltration to produce a transformation-resistant matrix around the fibers gave results superior to initial impregnation with pitch in these tests. In addition, the phenolic-resin-originating matrix (which was the filament bond in 3-D Mod. 3 samples tested) also provided good ablation performance and microscopic evidence of the required characteristics. Further studies of impregnants which give well-bonded transformation-resistant, high-density structures around the fibers, and techniques of completing the filling of residual pores should lead to further improvements in ablation performance and properties.

The 7-directional reinforced graphite has been demonstrated to have good potential as a tough material, based on preliminary plate-slap and flexure tests, and ablation performance with high-modulus fibers in fine texture has been demonstrated. Mechanical properties as a function of orientation should be obtained on a scaled-up fine-textured billet to determine the advantages which this close-to-isotropic reinforcement provides over other C-C composites.

REFERENCES

1. E.R. Stover, "Evaluation of Structural Characteristics of Carbon/Carbon Composites", Proceedings of the 10th Annual Symposium of the New Mexico Section of ASME and University of New Mexico College of Engineering, University of New Mexico, Albuquerque NM, January 29-30, 1970, pp. 55-87.

2. J. J. Gebhardt, "Optimization and Process Improvement of "Omniweave" Carbon-Carbon Composite Materials", in Graphite Materials for Advanced Re-Entry Vehicles Part III, AFML TR-70-133, Part III, ed. by D. M. Forney, Jr., August 1970, pp. 171-239.

3. J. P. Sterry, Fiber Technology Inc., North Hollywood California, personal communications, 1970.

4. D. H. Petersen, LTV Research Center, Dallas Texas, personal communications, 1970.

5. F. Lambdin, J. L. Cook and G. B. Marrow, Fiber-Reinforced Graphite Composite Fabrication and Evaluation, AEC Research and Development Report Y-1684 (TID-4500), Oak Ridge, Tennessee, September 4, 1969.

6. J. L. Cook, F. Lambdin and P. E. Trent, Discontinuous Carbon-Carbon Composite Fabrication, AEC Research and Development Report Y-1719 (TID-4500) Oak Ridge, Tennessee, May 20, 1970. Also published in Carbon Composite Technology, Proceedings of the 10th Annual Symposium (Ref. 1 above) pp 143-171.

7. J. L. Cook, Y-12 Plant, Union Carbide Nuclear Corp., Oak Ridge, Tennessee, personal communications, 1970.

8. D. F. McVey, I. Auerbach and D. D. McBride,"Some Observations on the Influence of Graphite Microstructure on Ablation Performance", AIAA Paper No. 70-155, AIAA 8th Aerospace Sciences Meeting, New York, New York, January 18-21, 1970.

9. I. Auerbach, Sandia Laboratories, Albuquerque, New Mexico, personal communications, 1970.

10. L. E. McAllister, Applied Technology Division, AVCO Corporation, personal communication, 1970.

11. J. R. Henson, Ablation Tests of Sphere-Cone Models in the AEDC 5MW Facility, AEDC TR-70-194, August, 1970.

12. J. R. Henson, AFML Materials Ablation Tests in the AEDC 5-MW Facility Series II, AEDC-TR-71-11, January, 1971.

13. E. R. Stover, W. C. Marx, L. Markowitz and W. Mueller, Preparation of an Omniweave-Reinforced Carbon/Carbon Cylinder as a Candidate for Evaluation in the Advanced Heat Shield Screening Program, AFML-TR-70-283, April, 1971